



Novel Respiratory Flavocytochromes of *Shewanella oneidensis* MR-1

Morag Bilsland

**Thesis presented for the degree of Doctor of Philosophy
The University of Edinburgh
2003**



Dedicated with love to Mum, Dad, Lewis and Kirsty

And

For Richard, from me to you

Acknowledgements

I first of all thank my supervisors Professor Graeme Reid and Professor Malcolm Walkinshaw for their constant enthusiasm and support throughout my PhD. I also thank Professor Stephen Chapman and past and present members of the Reid, Walkinshaw and Chapman research groups for all their help, advice and encouragement, particularly, Dr. Caroline Miles, Dr. Doina Atanasiu, Dr. Lisa McIver, Pauline Cuthbertson, Dr. Chris Mowat, Dr. Carsten Schwalb, Nic Corcionvoschi, Dr. Jacqueline Dornan, Dr. Paul Taylor, Sandra Bruce, Dr. Iain McNae and Dr. Violet Warwick. I also give many thanks to my mentor Dr. Karen Chapman for giving me lots of invaluable career advice and guidance and I thank Dr. Lindsay Sawyer for being my committee chairperson and my mentor during my work as lab demonstrator. I also thank Dr. Andy Cronshaw, Hannah Florance, Caroline Johnstone, Sally Shirran, and Helen Williamson for protein and DNA analyses.

I thank Karen Brown, Louise Adamson, and Dr. Nicola McEwen, for being wonderful flatmates and friends and always being there during my time in Edinburgh. I also thank all my family, including the Mathers for their constant support and good laughs and most of all I thank Richard for giving me so much encouragement especially in the last year during my write up.

Abstract

Shewanella oneidensis MR-1 is a Gram-negative bacterium isolated from anaerobic freshwater lake sediments of Oneida Lake that exhibits remarkable respiratory versatility. In the absence of molecular oxygen, *S. oneidensis* MR-1 couples anaerobic growth to the reduction of various substrates, including ferric iron (FeIII), thiosulfate ($\text{S}_2\text{O}_3^{2-}$), sulfite (SO_3^{2-}), trimethylamine *N*-oxide (TMAO), nitrate (NO_3^-), nitrite (NO_2^-) and organic substrates such as fumarate. The metabolic flexibility of *S. oneidensis* MR-1 is coupled to a complex and branched anaerobic respiratory chain. The respiratory enzymes of the fumarate reduction pathway have been extensively studied in *S. oneidensis* MR-1 and the related marine bacterium, *S. frigidimarina* NCIMB 400. The terminal fumarate reductase of *Shewanella* species is a soluble periplasmic flavocytochrome c_3 (Fcc₃) that catalyses the unidirectional production of succinate. The X-ray crystal structure of Fcc₃ solved to high resolution provided the first detailed insight into the catalytic mechanism of fumarate reduction.

In this work, the Fcc₃ X-ray crystal structure provided a structural template to construct homology models of related flavoenzymes of unknown structure and function. The novel flavoenzymes were identified by sequence analysis of the *S. oneidensis* MR-1 genome and were shown to comprise separately encoded flavin (FccA54, FccA56 and FccA342) and cytochrome subunits (FccB54, FccB56 and FccB342), respectively, that were related by sequence to the corresponding domains in Fcc₃. Molecular modelling of the catalytic flavin-binding subunits led to the suggestion that these related enzymes catalyse the reduction of acrylate substrates.

Several biologically relevant plant metabolites, including phenylacrylates incorporated into lignin, were identified as potential substrates of the Fcc₃-like enzymes. An *fccA54* and *fccB54* knockout strain of *S. oneidensis* MR-1 (*S. oneidensis* MB5415) was constructed and grown anaerobically with each of the candidate acrylates to ascertain the biological function of FccA54. Complementary to these studies, the genes encoding the novel flavoenzymes were PCR amplified from the *S. oneidensis* MR-1 genome and cloned into appropriate expression plasmids for protein overexpression in *Escherichia coli* or *Shewanella* strains. The FccA54 flavin subunit was overexpressed and purified but was found to be unstable in the absence of the FccB54 partner cytochrome subunit.

Abbreviations

ADP	Adenosine 5'-diphosphate
APS	Ammonium persulfate
ATCC	American Type Culture Collection
ATP	Adenosine 5'-triphosphate
bp	Base pair
BSA	Bovine serum albumin
Da	Dalton
dATP	Deoxyadenosine triphosphate
dCTP	Deoxycytidine triphosphate
dGTP	Deoxyguanosine triphosphate
dITP	Deoxyinosine triphosphate
dTTP	Deoxythymidine triphosphate
dH ₂ O	Distilled water
HCC	Hexamminecobalt chloride
DMSO	Dimethylsulfoxide
DNA	Deoxyribonucleic acid
dNTP	Mixture of dATP, dCTP, dGTP and dTTP
E°	Standard redox potential at a defined pH
E_m	Mid-point potential at a defined pH
EDTA	Ethylenediaminetetraacetic acid
FAD	Flavin adenine dinucleotide
Fcc ₃	Flavocytochrome <i>c</i> ₃
FNR	Fumarate nitrate reductase regulator
FRD	Fumarate reductase
IPTG	Isopropylthiogalactoside
kb	Kilo base pair
kDa	Kilo Dalton
l	litre
LB	Luria Bertani Broth
M	Molar
MR	Manganese reducing
NAD ⁺	Nicotinamide adenine dinucleotide
NCIMB	National Collection of Industrial and Marine Bacteria
OD	Optical density
ORF	Open reading frame
PAGE	Polyacrylamide gel electrophoresis
PCR	Polymerase Chain Reaction
PEG	Polyethylene glycol
Pi	Inorganic phosphate
pI	Isoelectric point
PVDF	Polyvinylidene fluoride
rpm	Revolutions per minute
Sdh	Succinate dehydrogenase
SDS	Sodium dodecyl sulfate
TAE	Tris-acetate EDTA
Tat	Twin arginine translocation

TE	Tris-EDTA
TEMED	N,N,N',N'-tetramethylethylene diamine
TIGR	The Institute for Genomic Research
T _m	Melting temperature
UV	Ultraviolet radiation
Xgal	5-bromo-4-chloro-3-indolyl- β -D-galactoside
Δ	Gene deletion

Antibiotic Abbreviations

Ap	Ampicillin
Cm	Chloramphenicol
Km	Kanamycin
Rm	Rifampicin
Sm	Streptomycin

Protein Abbreviations

Amino acid	3-letter code	1-letter code
Alanine	Ala	A
Arginine	Arg	R
Asparagine	Asn	N
Aspartate	Asp	D
Cysteine	Cys	C
Glycine	Gly	G
Glutamate	Glu	E
Glutamine	Gln	Q
Histidine	His	H
Isoleucine	Ile	I
Leucine	Leu	L
Lysine	Lys	K
Methionine	Met	M
Phenylalanine	Phe	F
Proline	Pro	P
Serine	Ser	S
Threonine	Thr	T
Tryptophan	Trp	W
Tyrosine	Tyr	Y
Valine	Val	V

Nucleic acid abbreviations

A	adenine
C	cytosine
G	guanine
T	thymine
U	uracil

List of Contents		Page
	Declaration	i
	Dedication	ii
	Acknowledgements	iii
	Abstract	iv
	Abbreviations	vi
	List of Contents	viii
	List of Figures	xiii
	List of Tables	xix
1	Introduction	1
1.1:	The generation of energy in the form of ATP	2
1.1.1:	Electron transport in the mitochondrial inner membrane	3
1.1.2:	Bacterial anaerobic electron transport chains	6
1.1.3:	Fermentation	7
1.2:	Anaerobic metabolism of <i>Shewanella</i> species	9
1.3:	Regulation of genes encoding proteins for anaerobic respiration	12
1.4:	Unusual anaerobic-induced distribution of cytochromes	14
1.5:	Anaerobic electron transfer pathways	18
1.6:	Cytoplasmic membrane-bound fumarate reductases	21
1.6.1:	The flavoprotein catalytic subunit	23
1.6.2:	The iron-sulphur electron transfer subunit	23
1.6.3:	The hydrophobic membrane anchor	24
1.6.4:	Electron transfer in membrane-bound fumarate reductases	27
1.6.5:	Bidirectional fumarate reductase activity	29
1.7:	Soluble fumarate reductases related to Fcc ₃	31
1.7.1:	Flavocytochrome <i>c</i> ₃ of <i>S. frigidimarina</i> NCIMB 400	33
1.7.2:	Fcc ₃ is a unidirectional fumarate reductase	38
1.8:	Novel flavocytochromes of <i>S. oneidensis</i> MR-1	39
1.8.1:	Identification of novel <i>S. oneidensis</i> MR-1 genes	39
1.8.2:	Arrangement of the novel <i>S. oneidensis</i> MR-1 genes	43
1.8.3:	Novel <i>S. oneidensis</i> MR-1 periplasmic flavocytochromes	47
1.8.4:	FAD-dependent tetrahaem flavocytochromes	50
1.8.5:	Putative function of the novel periplasmic flavocytochromes	53
1.9:	Aims of project	55
2	Materials and Methods	56
2.1.1:	Luria-Bertani (LB) medium	57
2.1.2:	Small-scale aerobic growth of <i>Shewanella</i> species	57
2.1.3:	Small-scale aerobic growth of <i>E. coli</i>	58
2.1.4:	Large-scale aerobic growth of <i>S. frigidimarina</i> EG301	58
2.1.5:	Large-scale aerobic growth of <i>E. coli</i>	59
2.1.6:	Preparation of <i>E. coli</i> cells for purification of FccA54	59
2.1.7:	Preparation of <i>S. frigidimarina</i> EG301 cells for protein purification	60

2	Materials and Methods	Page
2.1.8:	Anaerobic growth of <i>Shewanella</i> species	60
2.1.9:	Colony counts of <i>Shewanella</i> strains	62
2.1.10:	Single colonies of transformants	63
2.1.11:	Preparation of liquid culture –80 °C stocks	63
2.1.12:	Optical density measurements	63
2.2:	Isolation and preparation of DNA	64
2.2.1:	Preparation of plasmid DNA (QIAprep Spin Miniprep)	64
2.2.2:	Preparation of plasmid DNA by alkaline lysis and PEG treatment	64
2.2.3:	Preparation and isolation of genomic DNA	65
2.2.4:	Preparation of single-stranded DNA for automated sequencing	66
2.3:	Restriction enzyme digests	67
2.4:	Ligation reactions	67
2.5:	Preparation of calcium competent cells	68
2.6:	Transformation and selection of transformants	69
2.7:	Conjugative transfer of DNA from <i>E. coli</i> to <i>Shewanella</i> species	70
2.8:	The Polymerase Chain Reaction	71
2.8.1:	PCR amplification using <i>PfuTurbo</i>	71
2.8.2:	PCR amplification using <i>Taq</i> DNA polymerase	73
2.9:	Preparation of samples for automated sequencing	77
2.10:	Purification of PCR products and restriction fragments	78
2.11:	Detection and analysis of DNA samples	78
2.12:	IPTG induction experiments	79
2.13:	Tris-glycine SDS polyacrylamide gel electrophoresis	80
2.14:	Staining of SDS-PAGE gels	82
2.14.1:	Coomassie Blue staining of SDS-PAGE gels	82
2.14.2:	Silver staining of SDS-PAGE gels	83
2.14.3:	Cytochrome haem staining	83
2.15:	Periplasmic extraction	84
2.16:	Purification of FccA54 from <i>E. coli</i> TG1 (pMB3)	84
2.17:	Protein concentration	85
2.18:	Co-purification of FccA54 and FccB54	85
2.19:	Fumarate reduction assay	86
2.20:	Succinate oxidation assay	86
2.21:	Preparation of samples for N-terminal Sequencing	87
2.22:	Preparation of samples for mass spectrometry	87
2.23:	Homology modelling	88
2.24:	Plasmids, bacterial strains and primers	90
2.25:	Preparation of antibiotics	96
2.26:	Sterilisation	96
2.27:	Restriction enzymes	97

	List of Contents	Page
3	Molecular modelling of <i>Shewanella oneidensis</i> MR-1 flavoproteins	98
3.1:	INTRODUCTION	99
3.1.1:	The catalytic mechanism of Fcc ₃	99
3.2:	RESULTS AND DISCUSSION	104
3.2.1:	Sequence analyses of <i>S. oneidensis</i> MR-1 flavoproteins	104
3.2.2:	Molecular models of the novel <i>S. oneidensis</i> MR-1 flavoproteins	114
3.2.2.1:	Structural details of the molecular models	115
3.2.2.2:	Molecular model of the FccA54 enzyme active site	120
3.2.2.3:	Molecular model of the FccA56 enzyme active site	125
3.2.2.4:	Molecular model of the FccA342 enzyme active site	129
3.2.3:	Acrylate substrates modelled in the enzyme active sites	134
3.2.3.1:	Molecular modelling of the acrylate substrates	137
3.3:	Conclusions derived from molecular modelling	140
4	Gene replacement of <i>fccA54</i> and <i>fccB54</i> in <i>Shewanella oneidensis</i> MR-1 and phenotypic analysis of the deletion strain	142
4.1:	INTRODUCTION	143
4.1.1:	Mechanisms of genetic change	143
4.1.2:	The generation of gene disruptions in <i>S. oneidensis</i> MR-1	145
4.1.3:	Constructing an <i>fccA54</i> and <i>fccB54</i> gene replacement	146
4.1.4:	A novel gene replacement strategy	147
4.2:	RESULTS AND DISCUSSION	147
4.2.1:	Fusion PCR amplification and primer design	147
4.2.2:	Synthesis of the homologous template DNA by fusion PCR	150
4.2.3:	Cloning the homologous template DNA in plasmid pUC19	153
4.2.4:	Sequencing of the PCR product cloned in pMBGK9	156
4.2.5:	Construction of the gene replacement fragment	157
4.2.6:	Construction of a recombinant mobilisable plasmid	158
4.2.7:	Conjugative DNA transfer and antibiotic screening	162
4.2.8:	PCR screening of transconjugants from conjugation II	164
4.2.9:	Identification of an <i>fccA54</i> and <i>fccB54</i> null mutant	166
4.2.10:	Phenotype analyses	174
4.2.10.1:	Anaerobic growth on acrylate substrates	174
4.2.10.2:	Anaerobic growth of <i>S. oneidensis</i> MB5415	179
4.3:	CONCLUSION	188

	List of Contents	Page
5	Over-expression and Purification of a <i>Shewanella oneidensis</i> MR-1 Flavoprotein	190
5.1:	INTRODUCTION	191
5.1.1:	Putative interaction of flavin and cytochrome subunits	191
5.1.2:	A strategy to overexpress and purify the FccA54 flavoprotein	192
5.2:	RESULTS AND DISCUSSION	193
5.2.1:	PCR amplification of <i>fccA54</i> from the <i>S. oneidensis</i> MR-1 genome	193
5.2.2:	Cloning of the <i>fccA54</i> 54FMRA PCR product in pGEM-T	196
5.2.3:	Sequencing the <i>fccA54</i> 54FMRA PCR product of pMB3-4	199
5.2.4:	Cloning of the <i>fccA54</i> 54FMRA PCR product in pMMB503EH	199
5.2.5:	Cloning of the <i>fccA54</i> 54FMRA PCR product in pJF118	201
5.2.6:	Modification of pMB1 expression plasmid by fusion PCR	206
5.2.6.1:	Primer design and fusion PCR amplification	206
5.2.6.2:	Sequencing of the FccA54 overexpression fragment	211
5.2.6.3:	Cloning of the FccA54 overexpression fragment	215
5.2.6.4:	Formation of the FccA54 overexpression plasmid	217
5.2.7:	Cytoplasmic overexpression of FccA54 in <i>E. coli</i> TG1	219
5.2.8:	FccA54 protein purification	223
5.2.9:	Characterisation of the FccA54 flavoprotein	226
5.3:	CONCLUSION	227
6	Overexpression and purification trials of novel <i>Shewanella oneidensis</i> MR-1 flavocytochromes	230
6.1:	INTRODUCTION	231
6.2:	RESULTS AND DISCUSSION	232
6.2.1:	Primer design and PCR amplification of <i>fccAB54</i>	232
6.2.2:	Cloning of the <i>fccAB54</i> 54FRB PCR product in pGEM-T	235
6.2.3:	Sequencing of the <i>fccAB54</i> 54FRB PCR product in pMB2-1	236
6.2.4:	FccA54 and FccB54 co-expression in <i>S. frigidimarina</i> EG301	239
6.2.5:	Insertion of the <i>fccAB54</i> 54FRB PCR product in pMB3	240
6.2.6:	Insertion of the <i>fccAB54</i> overexpression fragment in pMMB503EH	241
6.2.7:	Overexpression of FccA54 and FccB54 in <i>S. frigidimarina</i> EG301	244
6.2.8:	Characterisation of the putative overexpressed FccB54 protein	248
6.2.9:	Purification trials of the FccA54 and FccB54 subunits	250
6.2.10:	Overexpression and purification of FccA54 and FccB54	256

6	Overexpression and purification trials of novel <i>Shewanella oneidensis</i> MR-1 flavocytochromes	Page
6.2.11:	Primer design and PCR amplification of <i>fccAB342</i>	257
6.2.12:	Cloning of the <i>fccAB342</i> 342FRB PCR product in pGEM-T	260
6.2.13:	Sequencing of the <i>fccAB342</i> PCR product in pMB6-14	261
6.2.14:	Cloning of the <i>fccAB342</i> PCR product in pMB5	262
6.2.15:	Flavocytochrome overexpression in <i>S. frigidimarina</i> EG301	264
7	PCR amplification constructs for flavoprotein overexpression	267
7.1:	INTRODUCTION	268
7.2:	RESULTS AND DISCUSSION	269
7.2.1:	PCR amplification of the <i>fccA54</i> preprotein coding sequence	269
7.2.2:	PCR amplification of an <i>fccAB54</i> co-expression fragment	271
7.2.3:	Cloning of the PCR products in pGEM-T	273
7.2.4:	Sequencing of the <i>fccA54</i> and <i>fccAB54</i> PCR products	274
7.2.5:	Future cloning of the <i>fccA54</i> and <i>fccAB54</i> PCR products	275
7.2.6:	PCR amplification of the <i>fccA342</i> flavoprotein encoding sequence	277
7.2.7:	Cloning of the <i>fccA342</i> PCR products in pGEM-T	279
7.2.8:	PCR amplification of <i>fccAB342</i> from <i>S. oneidensis</i> MR-1	280
7.2.9:	Cloning of the <i>fccAB342</i> PCR product in pGEM-T	282
7.2.10:	Sequencing of the <i>fccAB342</i> PCR product of pMB8-3	283
7.2.11:	Future overexpression work of FccA342	284
7.2.12:	Future co-expression work of FccA342 and FccB342	285
7.2.13:	A putative iron-induced flavocytochrome of <i>S. oneidensis</i> MR-1	286
7.2.14:	PCR amplification and cloning of <i>ifcA-1</i>	290
7.2.15:	Future overexpression work of IfcA-1	292
7.2.16:	Summary	293
8	Conclusion	294
8.1:	Molecular modelling	295
8.2:	A mutant strain of <i>S. oneidensis</i> MR-1	296
8.3:	Protein overexpression and purification	299
	Bibliography	302
	Appendix 1	314

List of Figures			Page
1 Introduction			
1.1.1	Figure 1.1:	Enzymes of the mitochondrion involved in oxidative phosphorylation	4
1.1.2	Figure 1.2:	Fumarate reduction	7
1.1.3	Figure 1.3:	Proposed model for the fermentation process of <i>A. globiformis</i>	8
1.4	Figure 1.4:	Anaerobic respiratory network of <i>S. oneidensis</i> MR-1	17
1.6	Figure 1.5:	<i>E. coli</i> membrane-bound fumarate reductase	25
1.6	Figure 1.6:	<i>W. succinogenes</i> membrane-bound fumarate reductase	26
1.6.4	Figure 1.7:	Electron transfer in fumarate reductases	29
1.6.5	Figure 1.8:	The putative FAD binding site of fumarate reductases	30
1.7.1	Figure 1.9:	Map of the <i>fccA</i> gene	33
1.7.1	Figure 1.10:	X-ray crystal structure of Fcc ₃ solved to 1.8 Å resolution	35
1.8.2	Figure 1.11:	Gene arrangement of the novel <i>S. oneidensis</i> MR-1 genes	46
1.8.3	Figure 1.12:	N-terminal Tat signal peptide alignment of the novel flavoproteins	49
1.8.4	Figure 1.13:	Non-covalent attachment of FAD	51
1.8.4	Figure 1.14:	Tetrahaem <i>c</i> -type cytochrome proteins	52
1.8.5	Figure 1.15:	Potential acrylate substrates	54
2 Materials and Methods			
2.24	Figure 2.1	Selected plasmid maps	91
3 Molecular modelling of <i>Shewanella oneidensis</i> MR-1 flavoproteins			
3.1.1	Figure 3.1:	The active site of Fcc ₃ solved to 1.8 Å resolution	100
3.1.1	Figure 3.2:	Fcc ₃ catalytic mechanism involves a proton delivery pathway for fumarate reduction	101
3.1.1	Figure 3.3:	Position of the Arg402 side chain	103
3.2.1	Figure 3.4:	'ClustalW' multiple sequence alignment of Fcc ₃ and the novel flavoenzymes	105
3.2.1	Figure 3.5:	Schematic diagram of the novel flavoprotein active sites compared to Fcc ₃	107

List of Figures

3 Molecular modelling of <i>Shewanella oneidensis</i> MR-1 flavoproteins			Page
3.2.1	Figure 3.6:	‘ClustalW’ multiple sequence alignment of FccA and the novel flavoenzymes	109
3.2.1	Figure 3.7:	Pair-wise sequence alignment of Fcc ₃ and FccA54	111
3.2.1	Figure 3.8:	Pair-wise sequence alignment of Fcc ₃ and FccA56	112
3.2.1	Figure 3.9:	Pair-wise sequence alignment of Fcc ₃ and FccA342	113
3.2.2.1	Figure 3.10:	Overlay of the molecular models with Fcc ₃	116
3.2.2.2	Figure 3.11:	An overlay of the FccA54 molecular model with the Fcc ₃ active site	121
3.2.2.2	Figure 3.12:	An alternative proton delivery pathway for FccA54	124
3.2.2.3	Figure 3.13:	An overlay of the FccA56 molecular model with the Fcc ₃ active site	126
3.2.2.3	Figure 3.14:	An alternative proton delivery pathway for FccA56	128
3.2.2.4	Figure 3.15:	An overlay of the FccA342 molecular model with the Fcc ₃ active site	131
3.2.2.4	Figure 3.16:	An alternative proton delivery pathway for FccA342	133
3.2.3	Figure 3.17:	Acrylate substrates of the novel flavoproteins	136
3.2.3.1	Figure 3.18:	FccA56 complexed with cinnamate	138
3.2.3.1	Figure 3.19:	FccA54 complexed with crotonate	139
4 Gene replacement of <i>fccA54</i> and <i>fccB54</i> in <i>Shewanella oneidensis</i> MR-1 and phenotypic analysis of the deletion strain			
4.2.1	Figure 4.1:	A schematic diagram of the fusion PCR procedure	148
4.2.1	Figure 4.2:	Engineering of the proximal primers to optimise fusion PCR	150
4.2.2	Figure 4.3:	PCR amplification of genomic DNA upstream of <i>fccA54</i>	151
4.2.2	Figure 4.4:	PCR amplification of genomic DNA downstream of <i>fccB54</i>	152
4.2.2	Figure 4.5:	PCR amplification of the homologous template DNA	153
4.2.3	Figure 4.6:	A map of the <i>E. coli</i> pUC19 cloning plasmid	154

List of Figures

4 Gene replacement of <i>fccA54</i> and <i>fccB54</i> in <i>Shewanella oneidensis</i> MR-1 and phenotypic analysis of the deletion strain			Page
4.2.3	Figure 4.7:	Restriction digests to identify recombinant pUC19 plasmid	156
4.2.5	Figure 4.8:	Restriction digests to identify formation of the gene replacement fragment	158
4.2.6	Figure 4.9:	Map of pEP185.2 mobilisable plasmid	159
4.2.6	Figure 4.10:	Restriction digests to verify construction of pMBGK15	160
4.2.6	Figure 4.11:	Plasmids constructed to generate the null mutant	161
4.2.8	Figure 4.12:	A schematic diagram to show PCR screening of transconjugants	165
4.2.9	Figure 4.13:	PCR screening of <i>S. oneidensis</i> MB5413	167
4.2.9	Figure 4.14:	PCR screening of <i>S. oneidensis</i> MB5415	168
4.2.9	Figure 4.15:	PCR screening of <i>S. oneidensis</i> MB5413 and <i>S. oneidensis</i> MB5415	170
4.2.9	Figure 4.16:	Schematic diagram to show PCR screening of <i>S. oneidensis</i> MB5415	171
4.2.9	Figure 4.17:	PCR screening of <i>S. oneidensis</i> MB5415	173
5 Overexpression and purification of a <i>Shewanella oneidensis</i> MR-1 flavoprotein			
5.2.1	Figure 5.1:	A schematic diagram to show PCR amplification of <i>fccA54</i>	194
5.2.1	Figure 5.2:	PCR amplification of <i>fccA54</i> mature coding sequence	196
5.2.2	Figure 5.3:	Map of pGEM-T (Promega) high copy number cloning plasmid	197
5.2.2	Figure 5.4:	Cloning of the <i>fccA54</i> <i>Bam</i> HI/ <i>Pst</i> I PCR product in pGEM-T	198
5.2.4	Figure 5.5:	Construction of a plasmid for FccA54 overexpression in <i>Shewanella</i> species	200
5.2.5	Figure 5.6:	Construction of a modified pJF118 plasmid for FccA54 overexpression in <i>E. coli</i>	204
5.2.5	Figure 5.7:	Cloning of <i>fccA54</i> in pJF118 <i>E. coli</i> expression plasmid	205
5.2.6.1	Figure 5.8:	A schematic diagram of the fusion PCR procedure	208

List of Figures

5 Overexpression and purification of a <i>Shewanella oneidensis</i> MR-1 flavoprotein			Page
5.2.6.1	Figure 5.9:	PCR amplification of modified pMB1 plasmid DNA	209
5.2.6.1	Figure 5.10:	PCR amplification of modified pJF118 plasmid DNA	210
5.2.6.1	Figure 5.11:	Fusion PCR amplification of the FccA54 overexpression fragment	211
5.2.6.2	Figure 5.12:	Cloning of the fusion PCR product in pGEM-T	212
5.2.6.3	Figure 5.13:	Cloning of the FccA54 overexpression fragment in pMB1	216
5.2.6.4	Figure 5.14:	Correction of the <i>fccA54</i> mutated sequence in pMB2	218
5.2.7	Figure 5.15:	Time course of FccA54 overexpression in <i>E. coli</i> TG1	220
5.2.7	Figure 5.16:	FccA54 flavoprotein is located in the soluble cell fraction	221
5.2.7	Figure 5.17:	Mass spectrometry of FccA54	222
5.2.8	Figure 5.18a:	UV absorption spectra of FccA54 column fractions	224
5.2.8	Figure 5.18b:	UV absorption spectra of FccA54 column fractions	224
5.2.8	Figure 5.19a:	FccA54 protein purification	225
5.2.8	Figure 5.19b:	FccA54 protein purification	225
5.2.8	Figure 5.20:	UV/visible absorbance spectrum of the purified FccA54 flavoprotein	226
6 Overexpression and purification trials of novel <i>Shewanella oneidensis</i> MR-1 flavocytochromes			
6.2.1	Figure 6.1:	A schematic diagram of the <i>fccAB54</i> PCR amplification	234
6.2.1	Figure 6.2:	PCR amplification of the <i>fccAB54</i> 54FRB fragment	235
6.2.3	Figure 6.3:	Correction of the mutated <i>fccAB54</i> 54FRB DNA sequence	238
6.2.5	Figure 6.4:	Restriction digests to confirm insertion of <i>fccAB54</i> in pMB3 to form pMB4	241
6.2.6	Figure 6.5:	Construction of the recombinant pMB5 expression plasmid	243
6.2.7	Figure 6.6a:	Time course overexpression of FccB54	245

List of Figures

6 Overexpression and purification trials of novel <i>Shewanella oneidensis</i> MR-1 flavocytochromes			Page
6.2.7	Figure 6.6b:	Time course overexpression of FccB54	245
6.2.7	Figure 6.7:	Periplasmic extraction to identify FccA54 overexpression	247
6.2.7	Figure 6.8:	Periplasmic extraction to identify FccB54	248
6.2.8	Figure 6.9:	Mass spectrometry of FccB54	249
6.2.8	Figure 6.10:	Mass spectrometry of the 'lower protein'	250
6.2.9	Figure 6.11:	Isolation of FccB54 from the soluble cell fraction	251
6.2.9	Figure 6.12:	A chromatogram of the HS cation exchanger fractions	253
6.2.9	Figure 6.13:	Haem staining analysis of fractions collected from the HS cation exchanger	254
6.2.9	Figure 6.14:	Silver staining analysis of fractions collected from the HS cation exchanger	255
6.2.11	Figure 6.15:	PCR amplification of <i>fccAB342</i>	258
6.2.11	Figure 6.16:	PCR amplification of <i>fccAB342</i>	259
6.2.12	Figure 6.17:	Restriction digests to show isolation of recombinant pGEM-T	261
6.2.14	Figure 6.18:	Construction of the pMB6 expression plasmid	263
6.2.15	Figure 6.19:	Time course overexpression of FccB342	265
 7 PCR amplification constructs for flavoprotein overexpression			
7.2.1	Figure 7.1:	PCR amplification of the <i>fccA54</i> preprotein coding sequence	270
7.2.2	Figure 7.2:	A schematic diagram of <i>fccAB54</i> PCR amplification	272
7.2.2	Figure 7.3:	PCR amplification of <i>fccA54</i> and <i>fccB54</i> as a single product	273
7.2.3	Figure 7.4:	Cloning of the alternative <i>fccA54</i> and <i>fccAB54</i> PCR products in pGEM-T	274
7.2.6	Figure 7.5:	A schematic diagram of <i>fccA342</i> PCR amplification	278

List of Figures

7 PCR amplification constructs for flavoprotein overexpression			Page
7.2.6	Figure 7.6:	PCR amplification of <i>fccA342</i> from the <i>S. oneidensis</i> MR-1 genome	279
7.2.7	Figure 7.7:	Cloning of the <i>fccA342</i> PCR products in pGEM-T	280
7.2.8	Figure 7.8:	PCR amplification of <i>fccA342</i> and <i>fccB342</i>	281
7.2.8	Figure 7.9:	PCR amplification of <i>fccAB342</i> from <i>S. oneidensis</i> MR-1	282
7.2.9	Figure 7.10:	Cloning of the <i>fccAB342</i> PCR product in pGEM-T	283
7.2.13	Figure 7.11:	‘ClustalW’ multiple sequence alignment of IfcA-1 and related proteins	288
7.2.14	Figure 7.12:	PCR amplification of <i>ifcA-1</i> from <i>S. oneidensis</i> MR-1	290
7.2.14	Figure 7.13:	PCR amplification of <i>ifcA-1</i> from the <i>S. oneidensis</i> MR-1 genome	291
7.2.14	Figure 7.14:	Cloning of the <i>ifcA-1</i> PCR product in pGEM-T	292

List of Tables

1 Introduction			Page
1.8.1	Table 1.1:	Predicted properties of the novel flavoproteins related to Fcc ₃	41
1.8.1	Table 1.2:	Flavoprotein amino acid sequence identities	42
1.8.1	Table 1.3:	Cytochrome protein amino acid sequence identities	42
1.8.3	Table 1.4:	Tat transfer peptide lengths	48
2 Materials and Methods			
2.8.1	Table 2.1:	PCR cycling parameters when using <i>PfuTurbo</i> DNA polymerase	72
2.8.2	Table 2.2:	PCR cycling parameters when using <i>Taq</i> DNA polymerase	73
2.8.2	Table 2.3:	PCR cycling parameters when using <i>Taq</i> DNA polymerase	74
2.8.2	Table 2.4:	PCR cycling parameters when using <i>Taq</i> DNA polymerase	75
2.8.2	Table 2.5:	PCR cycling parameters when using <i>Taq</i> DNA polymerase	76
2.24	Table 2.6:	Bacterial strains used and constructed	90
2.24	Table 2.7:	Plasmids for construction of the <i>fccA54</i> and <i>fccB54</i> gene knockout	91
2.24	Table 2.8:	Plasmids used for overexpression of FccA54, FccB54, FccA342, FccB342 and IfcA-1	92
2.24	Table 2.9:	Primers used in construction of the <i>fccA54</i> and <i>fccB54</i> gene-knockout	93
2.24	Table 2.10:	Primers used for PCR amplification and sequencing of <i>fccA54</i> and <i>fccB54</i>	94
2.24	Table 2.11:	Primers used for PCR amplification and sequencing of <i>fccA342</i> , <i>fccB342</i> and <i>IfcA-1</i>	95
2.25	Table 2.12:	Antibiotic preparation	96
2.27	Table 2.13:	Restriction enzymes	97
3 Molecular modelling of <i>Shewanella oneidensis</i> MR-1 flavoproteins			
3.2.2.1	Table 3.1:	Structural data of molecular models	117
3.2.2.1	Table 3.2:	Close contacts between the Fcc ₃ substrate and protein atoms	119

List of Tables

4	Gene replacement of <i>fccA54</i> and <i>fccB54</i> in <i>Shewanella oneidensis</i> MR-1 and phenotypic analysis of the deletion strain	Page
4.2.10.1	Table 4.1: Growth of wild-type <i>S. oneidensis</i> MR-1 on acrylate electron acceptors	177
4.2.10.2	Table 4.2: Anaerobic growth of <i>S. oneidensis</i> MB5415 and <i>S. oneidensis</i> MR-1 on acrylates	182
7	PCR amplification constructs for flavoprotein overexpression	
7.2.13	Table 7.1: Predicted properties of a putative iron-induced flavocytochrome	287

Chapter 1

Introduction

INTRODUCTION

1.1 The generation of energy in the form of ATP

The production of adenosine 5'-triphosphate (ATP), by the process of oxidative phosphorylation in prokaryotic cells is localised to the 'energy-transducing' plasma membrane that is functionally related to the chloroplast thylakoid membrane and the mitochondrial inner membrane of eukaryotic cells. Mitochondria and the cytoplasmic membrane of respiring bacteria are associated with a common ATP synthesis mechanism comprising the transfer of electrons 'downhill' along an electron transport chain to a terminal electron acceptor (Nicholls and Ferguson, 2002). The electrons are generated from the oxidation of high-energy nutrients such as glucose and are ultimately transferred to molecular oxygen that serves as the terminal oxidant in the aerobic respiratory chain of animal and bacterial cells. The electrons are transferred along membrane-bound enzyme complexes and the energy released by the constituent redox reactions is coupled to the generation of a proton gradient across the membrane (Nicholls and Ferguson, 2002). The membrane-bound enzyme complexes of the respiratory chain have chemi-osmotic coupling (Mitchell, 1961), where the energy conserved in the resulting proton motive force (Δp) is used to drive various energy-dependent membrane reactions, including ATP synthesis from adenosine 5'-diphosphate (ADP) and inorganic phosphate (Pi). The chemiosmotic coupling mechanism (Mitchell, 1961) is also observed in membranes of photosynthetic bacteria and plant chloroplast thylakoid membranes where the energy derived from absorption of visible light generates a proton gradient that drives the synthesis of ATP by photosynthetic phosphorylation (Nicholls and Ferguson, 2002).

1.1.1 Electron transport in the mitochondrial inner membrane

The electron transport chain of the mitochondrial inner membrane (Figure 1.1) is composed of four membrane-integrated multisubunit complexes comprising various redox active cofactors with increasing reduction potentials. Complex I (NADH: ubiquinone oxidoreductase) represents the largest protein component of the mitochondrial inner membrane and contains an FMN redox cofactor and iron-sulfur clusters that transfer electrons from NADH to ubiquinone (Nicholls and Ferguson, 2002). The mobile ubiquinone electron carrier shuttles electrons between the membrane-bound complexes I, II and III. Succinate dehydrogenase (SDH) of the citric acid cycle is a flavoprotein subunit of Complex II (Succinate-ubiquinone reductase) and catalyses the oxidation of succinate coupled to reduction of ubiquinone. The electrons released from oxidation of succinate are transferred from the flavoprotein subunit to the iron-sulfur subunit toward the membrane anchor, located in close proximity to ubiquinone (Nicholls and Ferguson, 2002). Ubiquinol is subsequently oxidised by respiratory Complex III (ubiquinol: cytochrome *c* oxidoreductase; cytochrome *bc*₁), which comprises a dihaem cytochrome *b*, cytochrome *c*₁ and a Rieske protein containing a [2Fe:2S] cluster. Domain movement of the intermediate iron-sulfur protein mediates interdomain electron transfer between cytochrome *b* and cytochrome *c*₁ for subsequent transfer to cytochrome *c* (Zhang *et al.*, 1998). The peripheral membrane-bound cytochrome *c* protein alternatively binds to cytochrome *c* of Complex III and components of Complex IV (cytochrome *c* oxidase) and shuttles electrons between the membrane-bound complexes.

Complex IV of the aerobic respiratory chain accepts electrons from cytochrome *c* and catalyses the reduction of O_2 to H_2O that is subsequently released through a putative water channel to the cytosolic surface of the membrane (Tsukihara *et al.*, 1996). Complexes I, III and IV catalyse oxidation-reduction reactions that are coupled to proton translocation across the membrane. A protonmotive Q-cycle operates in Complex III in which a two-cycle re-oxidation of ubiquinol is coupled to proton translocation across the membrane (Nicholls and Ferguson, 2002; Figure 1.1). The free energy sequestered by the resulting protonmotive force across the energy transducing membrane powers the proton translocating ATP synthase (Complex V) to generate ATP.

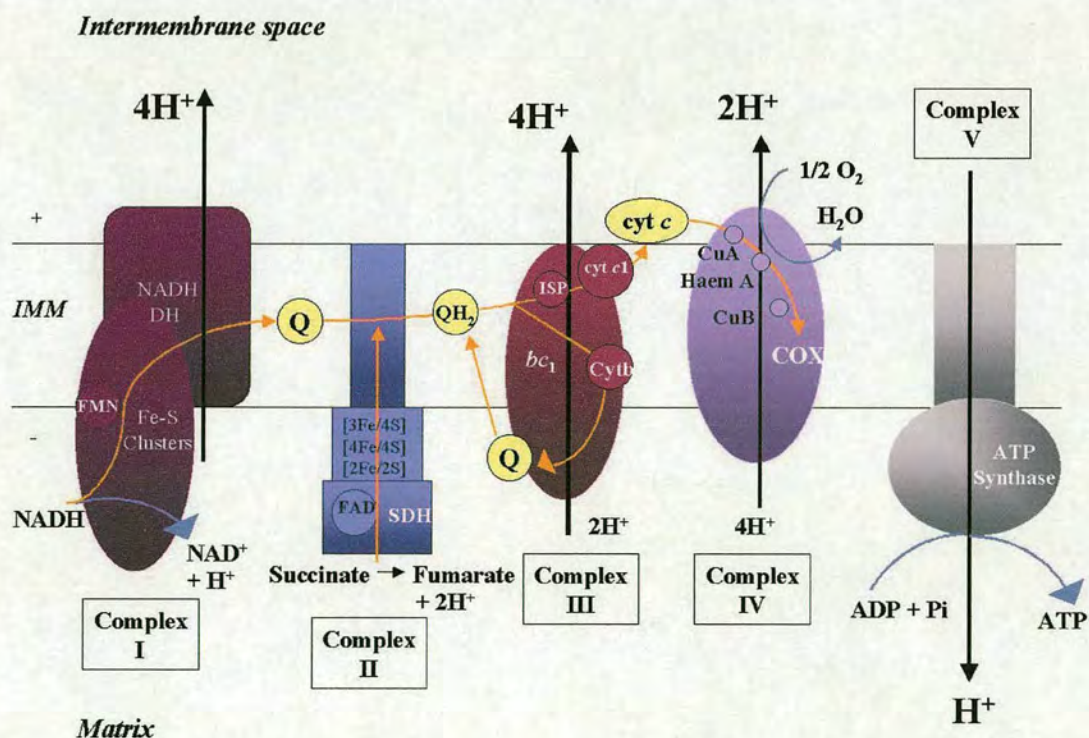


Figure 1.1: Enzymes of the mitochondrion involved in oxidative phosphorylation

The four respiratory complexes of the mitochondrial inner membrane involved in electron transfer (orange arrow) and the proton translocating ATP synthase are shown. Three of the complexes are involved in proton translocation (black arrow) across the energy transducing membrane. The mobile electron carrier, ubiquinone (Q) is shown to shuttle electrons between Complex I, II and III. The redox cofactors of each complex are shown, where ISP is the iron sulfur Rieske protein of Complex III.

The amount of energy that is released during electron transfer in the mitochondrion is determined by the difference between the redox potential of the donor couple (NADH/NAD⁺) and acceptor couple ($\frac{1}{2}\text{O}_2/\text{H}_2\text{O}$; Jones, 1988). The actual redox potential at pH 7.0 ($E_{\text{h},7}$) of the NADH/NAD⁺ couple (-280 mV) and the $\frac{1}{2}\text{O}_2/\text{H}_2\text{O}$ couple (780 mV) results in a large redox potential difference ($\Delta E_{\text{h},7}=1.06\text{ V}$) coupled to the release of a large amount of free energy ($\Delta G -205\text{ kJ mol}^{-1}$; Nicholls and Ferguson, 2002), which is sufficient to power synthesis of ATP.

The electron transport chain of the mitochondrial inner membrane (Figure 1.1) is provided as a key example of oxidative phosphorylation, where the underlying mechanism is analogous to electron transport and the generation of ATP in prokaryotes. However, different integral membrane components involved in electron transfer are expressed in energy-transducing membranes of different organisms in response to the presence of alternative primary electron donors and terminal acceptors (Nicholls and Ferguson, 2002). This is particularly apparent in prokaryotes that can respire in the absence of oxygen and couple the oxidation of an energy rich substrate to the terminal reduction of an alternate terminal electron acceptor (Jones, 1988).

1.1.2 Bacterial anaerobic electron transport chains

In its simplest form, the anaerobic respiratory chain of prokaryotes comprises a primary dehydrogenase that catalyses electron transfer via oxidation-reduction reactions to a terminal reductase that functions in place of a terminal oxidase (Jones, 1988). Nitrate (NO_3^-) respiration of *Escherichia coli* with formate as the electron donor induces expression of the cytoplasmic membrane-bound formate dehydrogenase-N that transfers electrons via menaquinol to the terminal nitrate reductase. The two proteins can form a redox loop coupled by menaquinol, which leads to generation of a proton motive force across the membrane (Jormakka *et al.*, 2002). In addition to nitrate/nitrite ($E'^\circ = 420 \text{ mV}$), prokaryotes utilise other substrates of widely differing redox potentials, such as the fumarate/succinate couple ($E'^\circ = 30 \text{ mV}$), sulfite/sulfide ($E'^\circ = -116 \text{ mV}$) and Fe(III)/Fe(II) ($E'^\circ = 760 \text{ mV}$) as terminal oxidants during anaerobic respiration. The diverse redox potentials are characterised by wide variations in the amount of free energy released, which is considerably lower compared to aerobic respiration. However, the use of these alternative electron acceptors permits non-fermentative microorganisms to respire and survive in anaerobic environments. Phosphorylative fumarate reduction to succinate (Figure 1.2) is the most commonly occurring type of anaerobic respiration amongst non-fermentative facultative and strictly anaerobic bacteria. This is probably due to the prevalence of fumarate from the breakdown of protein and carbohydrate readily available in the environment (Hamilton, 1988).

The reduction of fumarate ($E'^{\circ} = 30$ mV) is typically coupled to the oxidation of substrates with more negative redox potentials, such as formate/ HCO_3^- ($E'^{\circ} = -416$ mV; Myers and Myers, 1993), which generates an efficient respiratory system in the absence of molecular oxygen.

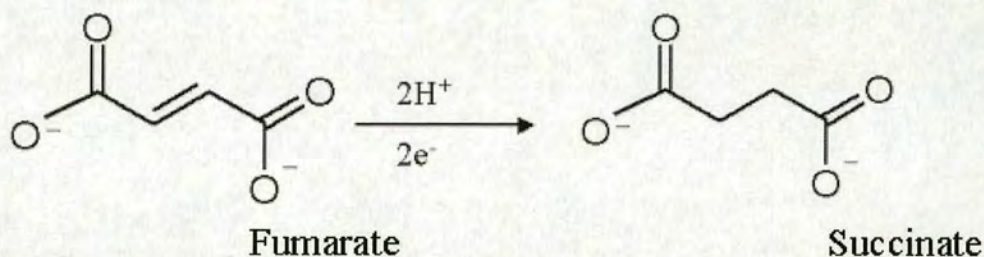


Figure 1.2: Fumarate reduction

The terminal fumarate reductase of the electron transport chain accepts two electrons for reduction of fumarate across the double bond to produce succinate as the end-product.

1.1.3 Fermentation

Some yeasts and prokaryotes are also able to obtain ATP by fermentation in which an organic substrate such as pyruvate formed by glycolysis is converted to a reduced end product with the concomitant generation of NAD^+ . The energy released from conversion of pyruvate to end products, such as ethanol and CO_2 during alcoholic fermentation in yeast is used to synthesise 2 molecules of ATP per molecule of glucose oxidised. Soil bacteria of the species *Arthrobacter globiformis* are able to survive in anaerobic layers of the soil by respiring anaerobically with nitrate or by fermentation. Anaerobic growth of *A. globiformis* in the presence of glucose and pyruvate leads to the formation of acetate, lactate and ethanol in a mixed fermentation process (Eschbach *et al.*, 2003; Figure 1.3).

A. globiformis preferentially respire anaerobically with nitrate as terminal electron acceptor and when the source of nitrate is exhausted, the bacterium obtains energy by fermentation of pyruvate and glucose (Eschbach *et al.*, 2003).

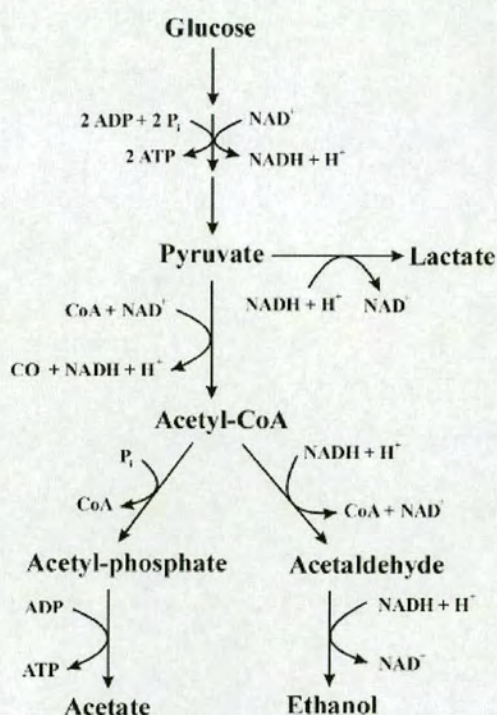


Figure 1.3: Proposed model for the fermentation process of *A. globiformis*

A. globiformis obtains energy from the process of a mixed fermentation. The carbon sources, pyruvate and glucose are converted to reduced end products, lactate, acetate and ethanol and the energy released is used to generate ATP. The figure is taken from Figure 2 of Eschbach *et al.*, 2003.

1.2 Anaerobic metabolism of *Shewanella* species

The wide range of substrates that are available to bacterial species to support anaerobic growth leads to the generation of many different redox reactions and expression of different redox proteins in bacteria (Nicholls and Ferguson, 2002). This is particularly apparent in the Gram-negative γ -proteobacteria of the genus *Shewanella* that are notable for their unique metabolic properties involving anaerobic reduction of many unusual substrates in addition to fumarate. The respiratory versatility is linked to the diverse range of environments inhabited by *Shewanella* species, including, marine (Lee *et al.*, 1977) and freshwater sediments (Myers and Nealson, 1988), the deep sea (Nogi and Kato, 1999), activated sludge (Barberio *et al.*, 2001), butter (Derby and Hammer, 1931; Murray *et al.*, 2001) and oil fields (Semple and Westlake, 1987). Some species such as *Shewanella algae* are opportunistic pathogens (Khashe and Janda, 1998; Venkateswaran *et al.*, 1999) and others are associated with fish spoilage and the production of trimethylamine (Jørgensen and Huss, 1989). Novel species of the genus include the recently discovered non-fermentative luminous species, *Shewanella woodyi* (Makemson *et al.*, 1997), the metal-reducing species, *Shewanella amazonensis*, isolated from Amazonian shelf coastal muds (Venkateswaran *et al.*, 1998), *Shewanella frigidimarina* (Bowman *et al.*, 1997), including *S. frigidimarina* NCIMB 400 (formerly *S. putrefaciens*; Reid and Gordon, 1999), *Shewanella gelidimarina* from Antarctic sea ice (Bowman *et al.*, 1997) and *Shewanella oneidensis* (Venkateswaran *et al.*, 1999).

All known *Shewanella* strains are capable of reducing trimethylamine *N*-oxide (TMAO) and nitrate (NO_3^-) during anaerobic growth and the majority of strains produce hydrogen sulfide (H_2S) from thiosulfate ($\text{S}_2\text{O}_3^{2-}$) reduction. However, only a select group of *Shewanella* species, including, *S. algae*, *S. amazonensis* and *S. oneidensis* are able to reduce elemental sulfur (S^0), iron oxides and manganese oxides (Venkateswaran *et al.*, 1999).

S. oneidensis MR-1 (formerly *S. putrefaciens* MR-1; Venkateswaran *et al.*, 1999) was originally isolated from anaerobic sediments of Oneida Lake, New York, for its remarkable ability to couple respiratory-linked proton translocation and anaerobic growth to the reduction of insoluble manganese (IV) oxides (Myers and Nealson, 1988; Myers and Nealson, 1990). *S. oneidensis* MR-1 (deposited as ATCC 700550; Venkateswaran *et al.*, 1999) is a non-fermentative facultative aerobe (Myers and Nealson, 1988) most closely related to *S. oneidensis* DLM7, isolated from Lower Green Bay sediments of Lake Michigan (Murray *et al.*, 2001; Venkateswaran *et al.*, 1999). *S. oneidensis* MR-1 is now identified with the anaerobic respiratory-linked reduction of many other electron acceptors, including, nitrate (NO_3^- ; Myers and Nealson, 1988), thiosulfate ($\text{S}_2\text{O}_3^{2-}$; Myers and Nealson, 1988 and Myers and Nealson, 1990), nitrite (NO_2^-), tetrathionate ($\text{S}_4\text{O}_6^{2-}$; Myers and Nealson, 1988), elemental sulfur (S^0 ; Moser and Nealson, 1996), sulfite (SO_3^{2-}), TMAO, fumarate, ferric iron, glycine and dimethylsulfoxide (DMSO; Myers and Nealson, 1988). *S. oneidensis* MR-1 couples the oxidation of primary electron donors such as succinate, acetate, lactate and fumarate to reduction of the numerous electron acceptors (Myers and Nealson, 1988; Venkateswaran *et al.*, 1999).

Toxic environmental substrates such as Chromium (CrVI) are readily reduced by *S. oneidensis* MR-1 and may also serve as terminal electron acceptors during anaerobic respiration (Myers *et al.*, 2000). The electron acceptors utilised by *S. oneidensis* MR-1, including, nitrate, nitrite, Mn(IV), Fe(III) and sulfite occur in redox clines of the sedimentary environment, where the substrates are preferentially metabolised by *S. oneidensis* MR-1 in order of their oxidative energy (Nealson *et al.*, 1995). The motility of the rod-shaped bacterium is likely to enable *S. oneidensis* MR-1 to seek-out the preferred substrate enriched zones of the anaerobic sedimentary environment (Myers and Nealson, 1988). Indeed, *S. oneidensis* MR-1 demonstrates chemotactic behaviour to nitrate and nitrite, which occurs at a greater propensity than chemotaxis to fumarate, DMSO, TMAO and thiosulfate. Furthermore, the presence of oxygen, nitrate and nitrite inhibit chemotaxis of *S. oneidensis* MR-1 to other electron acceptors (e.g. fumarate), which exhibit lower reduction potentials. The chemotactic response of *S. oneidensis* MR-1 to electron acceptors is postulated to involve a receptor and substrate-specific sensory mechanism that is independent of electron transfer to the preferred substrate (Nealson *et al.*, 1995).

1.3 Regulation of genes encoding proteins for anaerobic respiration

The remarkable respiratory versatility of *S. oneidensis* MR-1 is coupled to a branched anaerobic respiratory chain comprising many redox proteins, including, flavoprotein reductases, iron-sulfur proteins, quinones and 39 *c*-type cytochromes [The Institute of Genomic Research (TIGR); <http://www.tigr.org>; Heidelberg *et al.*, 2002]. Anaerobic expression of these redox proteins is tightly controlled by an oxygen-responsive regulatory system in *S. oneidensis* MR-1 that has evolved to exclusively express proteins required for growth on a particular substrate. This system is predicted to contain multiple regulatory transcription factors (Maier and Myers, 2001; Saffarini and Nealson, 1993), including the *electron transport regulator* protein, EtrA that shares 73.6 % sequence identity to the fumarate nitrate reductase regulator (FNR) of *E. coli* (Saffarini and Nealson, 1993). FNR is responsible for positively regulating expression of terminal reductase genes of *E. coli* including the *frdABCD* operon encoding the fumarate reductase (Jones and Gunsalus, 1987). The *frdABCD* operon of *E. coli* is induced by anaerobiosis and is regulated at the transcriptional level by FNR in response to the cellular availability of nitrate, oxygen and fumarate (Jones and Gunsalus, 1985). *E. coli* preferentially utilises oxygen and nitrate as terminal electron acceptor during oxidative phosphorylation and the prevalence of these substrates inhibits the expression of the *frdABCD* operon (Jones and Gunsalus, 1985). The presence of fumarate as sole terminal electron acceptor activates the *frdABCD* operon and induces expression of the encoded fumarate reductase enzyme (Jones and Gunsalus, 1985). The FNR protein enables *E. coli* to conserve energy by positively regulating expression of specific genes encoding proteins required for anaerobic respiration on a particular substrate.

The FNR protein regulates gene expression by specifically binding to FNR-dependent promoters comprising a 22 bp inverted repeat sequence located approximately 30 nucleotides upstream of the target gene transcription start site. This recognition sequence is represented by a consensus nonamer sequence, AAA-TTGAT that is separated by four nucleotides from a second complementary consensus sequence, ATCAA-TTT (Eiglmeier *et al.*, 1989). The activity of the FNR regulator protein is regulated by the stability of a $[4\text{Fe}:4\text{S}]^{2+}$ cluster oxygen sensing mechanism. The FNR $[4\text{Fe}:4\text{S}]^{2+}$ cluster is oxygen sensitive and is rapidly converted to $[2\text{Fe}:2\text{S}]^{2+}$ upon exposure to oxygen, which concomitantly results in loss of FNR site-specific DNA binding (Bates *et al.*, 2000). The regulatory mechanism of FNR prevents expression of anaerobic-specific genes such as the *frdABCD* operon during aerobic conditions in which oxygen serves as the preferred terminal electron acceptor.

The nucleotide sequences of *etrA* and *fnr* are only 69 % identical (Saffarini and Nealson, 1993) and in contrast to *fnr*, there is no FNR-binding site (Eiglmeier *et al.*, 1989; Saffarini and Nealson, 1993) upstream of the *etrA* sequence, suggesting that EtrA does not have an auto regulatory function under anaerobic conditions (Saffarini and Nealson, 1993). EtrA has four cysteine residues typical of oxygen-responsive regulatory proteins and contains a helix-turn-helix motif identical to that of FNR, suggesting that FNR and EtrA bind to similar DNA sequences and perhaps regulate the same terminal reductase operons (Saffarini and Nealson, 1993).

Indeed, the precise role of EtrA is linked to positive transcriptional regulation of the reductase genes required for fumarate and nitrate regulation (Maier and Myers, 2001; Beliaev *et al.*, 2002a), similar to the FNR analog of *E. coli* (Jones and Gunsalus, 1987). EtrA does not exert transcriptional regulation of reductase genes required for anaerobic growth on nitrite, thiosulfate, TMAO, DMSO, Fe(III) and sulfite (Maier and Myers, 2001), contrary to earlier misconceptions (Saffarini and Nealson, 1993). In addition to EtrA, a multitude of unidentified transcriptional regulators are predicted to control expression of redox proteins constituting the complex anaerobic respiratory chain (Maier and Myers, 2001; Saffarini and Nealson, 1993) and knowledge of the complete *S. oneidensis* MR-1 genome sequence (Heidelberg *et al.*, 2002; <http://www.tigr.org>) will facilitate identification of these proteins.

1.4 Unusual anaerobic-induced distribution of cytochromes

The complex anaerobic respiratory pathway of *S. oneidensis* MR-1 that is regulated at the transcriptional level comprises components of the electron transport chain localised to the outer membrane, which is extremely unusual compared to most other Gram-negative bacteria in which components of the electron transport chain are contained in the cytoplasmic membrane and periplasm (Nicholls and Ferguson, 2002; Jones, 1988). The utilisation of insoluble metal oxides as terminal oxidants during anaerobic respiration of *S. oneidensis* MR-1 is specifically linked to the anaerobic expression of multihaem *c*-type cytochromes to the outer membrane bilayer (Figure 1.4; Myers and Myers, 1992).

The anaerobic-induced distribution of cytochromes to the outer membrane is also common to manganese-reducing strains, *S. oneidensis* MR-4, *S. oneidensis* MR-8 (Myers and Myers, 1998), *S. frigidimarina* NCIMB 400 (Field *et al.*, 2000) and other metal-dissimilating bacteria of the genus *Geobacter* (Magnuson *et al.*, 2001).

S. oneidensis MR-1 is a motile bacterium that requires direct physical contact with insoluble Mn(IV) oxides in order to reduce and respire anaerobically with the insoluble substrates (Myers and Nealson, 1988). The switch in cytochrome expression from the cytoplasmic membrane to the outer membrane during anaerobiosis is proposed to facilitate direct contact and increase affinity between the bacterial cell and metal-containing substrates (Myers and Myers, 1992; Lower *et al.*, 2001) that are insoluble in the sedimentary environment sustained at pH 7.5-8.2 (Myers and Nealson, 1988). It was proposed that *S. oneidensis* MR-1 excretes quinones to the extracellular space to aid transfer of insoluble Fe(III) and Mn(IV) oxides to the site of electron transfer in the cytoplasmic membrane (Newman and Kolter, 2000). However, the outer membrane cytochromes are ideally situated to provide an electron transfer link between extracellular insoluble metal oxides and redox proteins of the electron transfer chain embedded in the cytoplasmic membrane (Myers and Myers, 1992). Four *c*-type respiratory cytochromes (150 kDa, 83 kDa, 65 kDa and 53 kDa; Figure 1.4) that are integral to the outer membrane of *S. oneidensis* MR-1 grown anaerobically with fumarate as terminal electron acceptor were identified to catalyse the formate-dependent *in vitro* reduction of Fe(III) and Mn(III).

These outer membrane cytochromes may serve as terminal metal oxide reductases or they may function as intermediary redox enzymes in the respiratory pathway towards reduction of metal oxides (Myers and Myers, 1997a). The outer membrane decahaem cytochrome, OmcB/MtrC (53 kDa; Beliaev *et al.*, 2001; Myers and Myers, 2001) is required for activity of the terminal Fe(III) reductase and may function as an essential component of a terminal reductase complex (Beliaev *et al.*, 2001).

The absence of the OmcA decahaem (83 kDa) in *S. oneidensis* MR-1 generates a mutant that is greatly impaired in its ability to respire anaerobically with MnO₂. This leads to the suggestion that OmcA is an essential component of the respiratory pathway toward reduction of insoluble Mn(IV) (Figure 1.4). Indeed, OmcA may function as the terminal Mn(IV) reductase whose function is replaced by secondary Mn(IV) reductases in the OmcA deletion mutant (Myers and Myers, 2001). Outer membrane and periplasmic proteins of *S. oneidensis* MR-1, designated MtrB and MtrA, respectively, are both required for Fe(III) and Mn(IV) reduction (Beliaev and Saffarini, 1998; Beliaev *et al.*, 2001; Figure 1.4). MtrA is a putative decahaem cytochrome, whereas MtrB contains one CxxC motif (Beliaev and Saffarini, 1998) and is postulated to facilitate proper incorporation of the OmcA and OmcB cytochromes into the outer membrane (Myers and Myers, 2002).

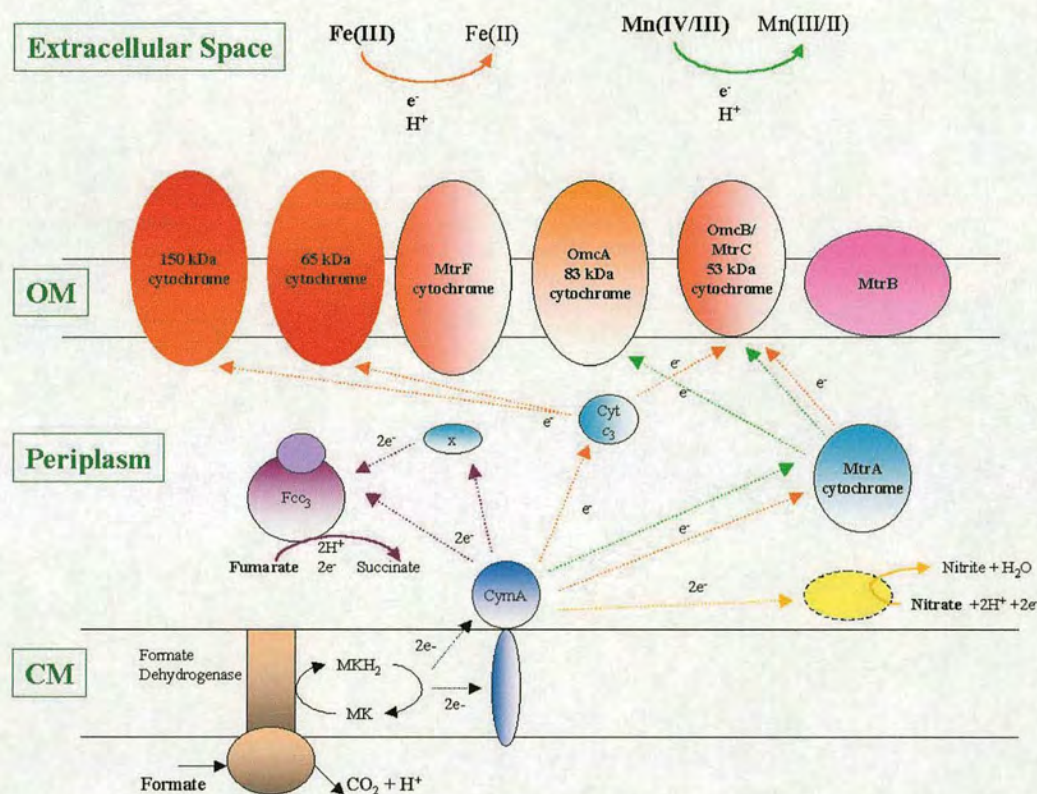


Figure 1.4: Anaerobic respiratory network of *S. oneidensis* MR-1

The diagram shows electron transfer pathways in *S. oneidensis* MR-1. Proton translocation and ATP synthesis is not shown. The electron transfer pathways are indicated by a dashed arrow and are classed as pathways toward Fe(III) reduction (orange), fumarate reduction (purple), nitrate reduction (yellow) and Mn(IV/III) reduction (green). The respiratory proteins that are shown include the soluble periplasmic cytochromes that may function as electron shuttles (cyan), the periplasmic fumarate reductase (purple), outer membrane cytochromes (orange), the putative periplasmic nitrate reductase (yellow), cytoplasmic membrane-bound CymA (dark blue), formate dehydrogenase (brown) and MtrB (pink). The membrane-bound electron carrier, menaquinone (MK) accepts electrons from the membrane-bound dehydrogenase to form menaquinol (MKH₂). This figure shows the electron transport pathways comprising proteins that are discussed in this chapter, and does not represent the complete picture of the respiratory proteins that have been characterised to date in *S. oneidensis* MR-1.

1.5 Anaerobic electron transfer pathways

An electron transfer pathway must be established in the periplasm to link the outer membrane cytochromes and the redox proteins of the cytoplasmic membrane during anaerobic respiration with insoluble metal oxides. A number of *c*-type cytochromes are localised to the periplasm of *Shewanella* species (Morris, 1987) and these may function to shuttle electrons between the outer membrane cytochromes and the electron transport redox proteins of the cytoplasmic membrane forming a continuous electron transfer chain (Myers and Myers, 1992). In support of this conjecture, a small (11.8 kDa) low-potential tetrahaem cytochrome *c*₃ isolated from the periplasm of *S. frigidimarina* NCIMB 400 is implicated in electron transfer to insoluble Fe(III) serving as the terminal electron acceptor (Gordon *et al.*, 2000; Figure 1.4). Similarly, metal-dissimilation of *G. sulfurreducens* is linked to periplasmic shuttle proteins, such as the small (9.6 kDa) periplasmic trihaem *c*-type cytochrome (PpcA) that is a putative intermediary electron carrier between acetate and outer membrane Fe(III) reductases and other enzymes involved in U(VI) and humic reduction (Lloyd *et al.*, 2003). A small, periplasmic low potential tetrahaem cytochrome *c* of *S. oneidensis* MR-1 (Tsapin *et al.*, 2001) may also be implicated in metal reducing respiratory pathways.

CymA is a cytoplasmic membrane-bound cytochrome *c* (21.4 kDa) that contains a globular tetrahaem domain putatively anchored to the outer face of the cytoplasmic membrane that is predicted to mediate electron transfer from the cytoplasmic membrane to acceptor proteins in the periplasm (Myers and Myers, 1997b; Figure 1.4). Therefore, CymA may serve to transfer electrons to periplasmic proteins for subsequent transfer to the outer membrane *c*-type cytochromes. The high sequence identity of CymA to TorC (Méjean *et al.*, 1994), NapC (Berks *et al.*, 1995) and NirT (Jüngst *et al.*, 1991) cytoplasmic membrane-bound *c*-type cytochromes involved in electron transfer to periplasmic proteins, lends further support that CymA will have a similar function (Myers and Myers, 1997b). These conjectures derived from sequence analysis correlate with findings that a soluble truncated form of CymA transfers electrons *in vitro* to the soluble periplasmic Fcc₃ fumarate reductase (Schwalb *et al.*, 2002). The haem reduction potentials (-175 and -261 mV) of CymA were identified to be more negative (Schwalb *et al.*, 2002) than the haem groups of Fcc₃ (-102, -146, -196 and -238 mV; Turner *et al.*, 1999), suggesting an *in vivo* electron transport pathway from CymA to the tetrahaem cytochrome domain of Fcc₃ may exist in *Shewanella* species (Figure 1.4). The cytoplasmic membrane-bound protein, CymA may therefore serve as the immediate electron donor to the periplasmic Fcc₃ fumarate reductase (Schwalb *et al.*, 2002). CymA also appears to function in formate-dependent anaerobic electron transport towards reduction of Fe(III), Mn(IV) and nitrate (Myers and Myers, 1997b; Figure 1.4).

The varied cellular distribution of these terminal oxidants common to electron transfer pathways involving CymA, leads to the proposal that CymA occurs at the divergence point of these anaerobic respiratory pathways (Myers and Myers, 1997b; Myers and Myers, 2000). The quinol pool entrapped in the cytoplasmic membrane provides a continuous source of electron carriers that shuttle electrons to terminal reductases of the electron transport chain embedded in the cytoplasmic membrane. CymA is proposed to mediate electron transfer between the membrane-bound quinol pool and terminal reductases located in the periplasm and outer membrane of *S. oneidensis* MR-1 (Figure 1.4). Mutant strains of *S. oneidensis* MR-1 that are deficient in CymA (MR1-CYMA; Myers and Myers, 2000) or menaquinone have a common phenotype characterised by an impaired ability of these strains to grow anaerobically on Fe(III) (Myers and Myers, 1993; Saffarini *et al.*, 2002), fumarate, Mn(IV) and nitrate (Myers and Myers, 1993), tentatively suggesting that menaquinone ($E'_o = -74$ mV; Myers and Myers, 1993) functions as the immediate reductant of CymA in the electron transport chain (Figure 1.4; Myers and Myers, 2000). Furthermore, the CymA homologue of *S. frigidimarina* NCIMB 400 is reduced *in vitro* by menaquinol (Field *et al.*, 2000), which may accept electrons via the membrane anchor for subsequent transfer to the soluble tetrahaem domain. Alternatively, the electrons released by menaquinol oxidation in the cytoplasmic membrane might be directly transferred to an exposed haem group of the CymA tetrahaem domain that lies in close proximity to the cytoplasmic membrane (Schwalb *et al.*, 2002; Figure 1.4).

The ability of *S. oneidensis* MR-1 to respire with many types of electron acceptor is evidently linked to a complex and branched anaerobic respiratory chain comprising a varied distribution of redox proteins. The mechanism of fumarate respiration has received considerable interest due to the widespread use of fumarate as terminal electron acceptor by non-fermentative facultative and strictly anaerobic bacteria. The recent X-ray crystal structures of bacterial fumarate reductases have provided a structural basis for understanding the complex electron transfer pathways and mechanism of chemiosmotic coupling.

1.6 Cytoplasmic membrane-bound fumarate reductases

Fumarate respiration has been most extensively studied in *Escherichia coli* and other Gram-negative facultative aerobes of the genus *Shewanella* and the obligate anaerobe *Wolinella succinogenes*. The terminal fumarate reductases (quinol: fumarate reductases, QFR) of *E. coli* (Iverson *et al.*, 1999; Figure 1.5) and *W. succinogenes* (Lancaster *et al.*, 1999; Figure 1.6) are multi-redox cytoplasmic membrane-bound enzyme complexes of the anaerobic electron transfer chain. X-ray crystal structures of the membrane-bound enzymes reveal a similar structural organisation of the multi-subunit fumarate reductases (Iverson *et al.*, 1999; Lancaster *et al.*, 1999). The *E. coli* fumarate reductase (FRD) that catalyses the terminal reduction of fumarate to succinate is composed of four associated subunits encoded by genes of the polycistronic *frdABCD* operon (Cole *et al.*, 1982; Grundström and Jaurin, 1982; Cole, 1982; Jones and Gunsalus, 1985). The genes constituting the *E. coli frdABCD* operon (Jones and Gunsalus, 1985) are widely conserved in *frd* operons of distantly related bacteria such as *Proteus vulgaris* (Cole, 1987).

Members of the fumarate reductase family exhibit striking similarities in primary structure and catalytic mechanism to members of the succinate dehydrogenase family. The *frdA* and *frdB* genes of *E. coli* (Cole *et al.*, 1982; Cole, 1982) show high sequence similarity, respectively, to *sdhA* and *sdhB*, encoding homologous subunits of the succinate dehydrogenase of *E. coli* (Wood *et al.*, 1984b; Darlison and Guest, 1984) and *B. subtilis* (Philips *et al.*, 1987). The overall structural fold determined for membrane-bound fumarate reductases is predicted to be similar to that of succinate dehydrogenase (succinate-ubiquinone oxidoreductase, Complex II) which catalyses the reverse reaction in the aerobic respiratory chain of bacteria and the citric acid cycle in the mitochondrial matrix of eukaryotic cells (Figure 1.1; Nicholls and Ferguson, 2002). The strong enzyme similarity is demonstrated in the ability of the *E. coli* succinate dehydrogenase to functionally replace the *E. coli* fumarate reductase and support anaerobic growth with fumarate as terminal electron acceptor (Maklashina *et al.*, 1998).

1.6.1 The flavoprotein catalytic subunit

The *E. coli* FrdA catalytic flavoprotein subunit (66 kDa; Iverson *et al.*, 1999) encoded by *frdA* (Cole, 1982) contains covalently bound FAD ($E^{\circ} = -48$ mV; Sucheta *et al.*, 1993; Weiner and Dickie, 1979; Figure 1.8) in close proximity to the catalytic active site of fumarate reduction and succinate oxidation (Iverson *et al.*, 1999). The structurally similar flavoprotein catalytic domains of the *E. coli* and *W. succinogenes* membrane-bound fumarate reductases share a Rossmann-type fold that provides the binding site for the FAD cofactor (Iverson *et al.*, 1999 and Lancaster *et al.*, 1999). The *W. succinogenes* fumarate reductase X-ray crystal structure forms, solved at 2.2 Å resolution [Protein data bank (PDB) entries; 1QLA and 1QLB] revealed the presence of a capping domain (106 amino acid residues) in the flavin subunit (73 kDa). The active site was identified at the hinge region between the capping and flavin domains (Lancaster *et al.*, 1999).

1.6.2 The iron-sulphur electron transfer subunit

The smaller FrdB subunit of *E. coli* (27 kDa) encoded by *frdB* (Cole *et al.*, 1982) is an iron-sulfur protein that contains three Fe-S redox centres that are trinuclear [3Fe:4S], tetranuclear [4Fe:4S] and binuclear [2Fe:2S] (Manodori *et al.*, 1992). FrdB is an electron-delivery subunit that associates with FrdA (Figures 1.5) to allow inter-subunit electron transfer via the Fe-S centres to the FAD cofactor. The *E. coli* FrdA and FrdB subunits associate to form a soluble catalytic complex that extends into the cytoplasm, the site of fumarate reduction (Iverson *et al.*, 1999). A structurally similar iron-sulfur protein subunit comprising two domains is present in the multi-subunit *W. succinogenes* fumarate reductase enzyme (Figure 1.6; Lancaster *et al.*, 1999).

1.6.3 The hydrophobic membrane anchor

The water-soluble catalytic domain of *E. coli* fumarate reductase (FrdA and FrdB) is anchored to the cytoplasmic membrane by two transmembrane hydrophobic subunits, FrdC (15 kDa) and FrdD (13 kDa; Figure 1.5 and 1.7; Iverson *et al.*, 1999). A single transmembrane subunit containing two *b*-type haem groups anchors the catalytic complex of the *W. succinogenes* fumarate reductase to the membrane (Figure 1.6 and 1.7; Körtner *et al.*, 1990). The membrane anchor of *E. coli* succinate dehydrogenase comprises two hydrophobic subunits (Wood *et al.*, 1984b), one of which binds a *b*-type haem group (Murakamia *et al.*, 1985). Therefore, the membrane-bound fumarate reductases and succinate dehydrogenases share structural similarities in the catalytic region and show major differences in the membrane anchor region. The distinct integral membrane component(s) of the multi-subunit protein complexes are suspected to share a common interaction with the enzyme reductant and provide a connection between the soluble catalytic domain and the respiratory electron transfer chain embedded in the cytoplasmic membrane (Iverson *et al.*, 1999).

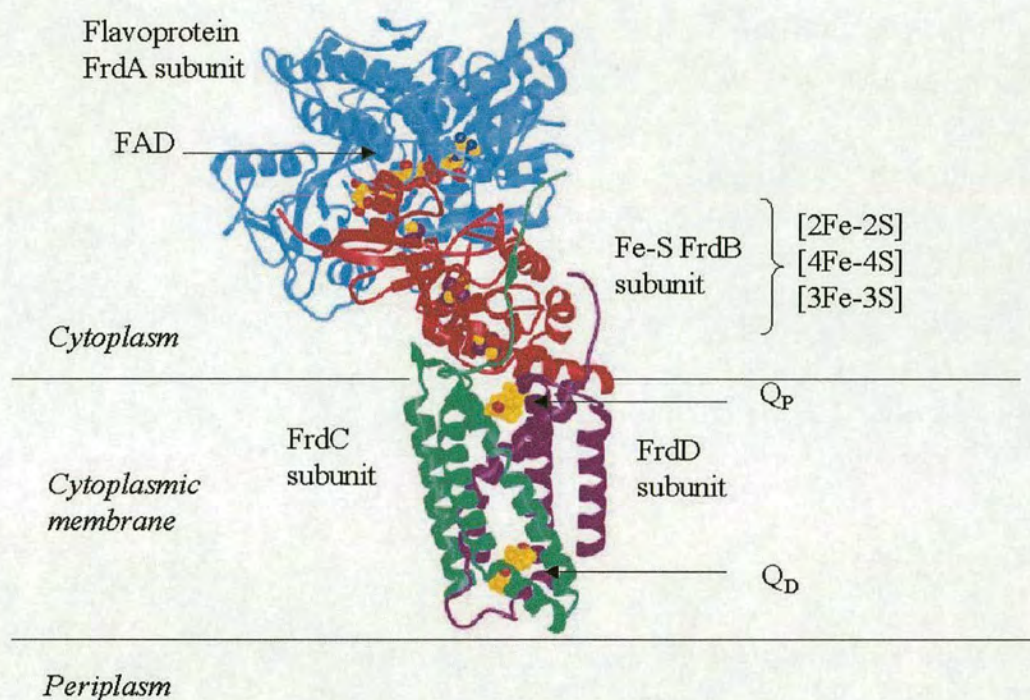


Figure 1.5: *E. coli* membrane-bound fumarate reductase

An *E. coli* membrane-bound fumarate reductase monomer (crystallised as a dimer) solved to 3.3 Å resolution (Iverson *et al.*, 1999) is shown. The FrdA flavoprotein subunit (blue) contains covalently bound FAD and the substrate-binding site. The FrdB iron-sulfur subunit (red) contains three iron-sulfur clusters and is connected to the flavin subunit to form a catalytic domain that protrudes into the cytoplasm. The catalytic domain is connected to the cytoplasmic membrane by two membrane anchor polypeptides, FrdC (green) and FrdD (purple) that contain two menaquinone binding sites located on either side of the membrane. The picture is adapted from Figure 1 of Iverson *et al.*, 1999.

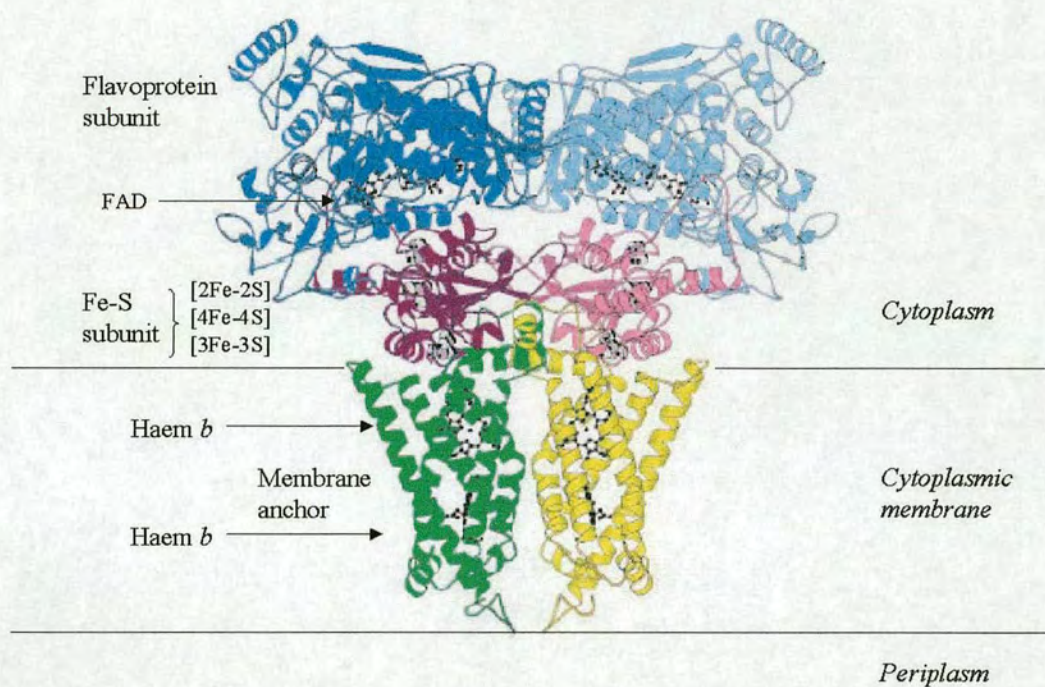


Figure 1.6: *W. succinogenes* membrane-bound fumarate reductase

The *W. succinogenes* membrane-bound fumarate reductase crystallised as a dimer and solved to 2.2 Å resolution (Lancaster *et al.*, 1999) is shown. The flavoprotein subunit (blue) containing covalently bound FAD and the substrate-binding site is connected to the iron-sulfur subunit (purple). The catalytic domain of the enzyme is connected to the cytoplasmic membrane by a single membrane anchor (green and yellow) containing two *b*-type haem groups. The figure is taken from Figure 1 of Lancaster and Simon, 2002.

1.6.4 Electron transfer in membrane-bound fumarate reductases

The fumarate respiratory pathway is dependent upon menaquinol, a membrane embedded electron carrier that shuttles freely between sequential membrane-bound oxidoreductase complexes. The terminal reduction of fumarate ($E^{\circ'} = 30 \text{ mV}$) to succinate catalysed by the membrane-bound fumarate reductases of *E. coli* and *W. succinogenes* is coupled to oxidation of menaquinol ($E^{\circ'} = -74 \text{ mV}$) to menaquinone (Jones, 1988). The two conjectural menaquinone binding sites in the membrane anchor of *E. coli* fumarate reductase (Westenberg *et al.*, 1990) were identified to reside on opposite sides of the membrane (separated by 27 \AA), positioned proximal (Q_P) and distal (Q_D) to the $[3\text{Fe}:4\text{S}]$ cluster (Iverson *et al.*, 1999; Figure 1.5). The location of solvent exposed menaquinone binding sites in close proximity to the $[3\text{Fe}:4\text{S}]$ cluster (Iverson *et al.*, 1999) lends further support that menaquinol functions to deliver electrons to the FrdB subunit as part of the electron transfer pathway to fumarate. The membrane spanning quinone distribution of *E. coli* fumarate reductase resembles that of cytochrome bc_1 (Complex III) of the aerobic respiratory chain (Zhang *et al.*, 1998) and succinate dehydrogenase of *Saccharomyces cerevisiae* (Figure 1.7; Oyedotun and Lemire, 2001). The $[2\text{Fe}:2\text{S}]$ is closest to the FAD cofactor of the FrdA subunit and is the most likely Fe-S candidate to transfer electrons directly to the flavin cofactor (Iverson *et al.*, 1999; Ohnishi *et al.*, 1981). The intra-molecular electron transfer conduit of menaquinol-fumarate oxidoreductases, as interpreted from the X-ray crystal structure of *E. coli* fumarate reductase (PDB, 1FUM; Figure 1.5) follows the sequence: Q_D - Q_P - $[3\text{Fe}:4\text{S}]$ - $[4\text{Fe}:4\text{S}]$ - $[2\text{Fe}:2\text{S}]$ -FAD-fumarate (Iverson *et al.*, 1999).

The redox cofactors of the *W. succinogenes* fumarate reductase are positioned in a similar arrangement relative to the *E. coli* fumarate reductase which suggests that a similar electron transfer conduit exists in the related enzymes (Lancaster *et al.*, 1999). However, the haem *b* groups in the transmembrane anchor of *W. succinogenes* fumarate reductase are arranged in close proximity to one another (shortest contact; 4.2 Å) and one of the haem groups lies near the cytoplasmic face of the membrane in close proximity to the [3Fe:4S] cluster (Figure 1.7; Lancaster *et al.*, 1999). This cofactor arrangement leads to the proposition that a transmembrane electron transfer pathway exists from menaquinol to the [3Fe:4S] cluster in the *W. succinogenes* fumarate reductase (Lancaster *et al.*, 1999). The menaquinone binding sites are predicted to be close to the dihaem binding sites of the *W. succinogenes* fumarate reductase (Lancaster *et al.*, 1999) to mediate efficient electron transfer upon menaquinol oxidation. Indeed, an essential residue (Glutamate 66) of the dihaem membrane anchor region required for forming the menaquinol oxidation site during fumarate respiration is located next to the haem group that is distal to the [3Fe:4S] cluster. The glutamate residue is postulated to accept protons from oxidised menaquinol during electron transfer to the distal haem group (Lancaster *et al.*, 2000). The close proximity of the essential glutamate residue to the periplasmic face of the membrane suggests that the protons will be expelled to the periplasm leading to the build up of positive charge. The subsequent abstraction of protons at the cytoplasmic face of the membrane for fumarate reduction leads to the conjecture that menaquinol oxidation by fumarate is coupled to the generation of an electrochemical proton potential across the membrane (Figure 1.7; Lancaster *et al.*, 2000).

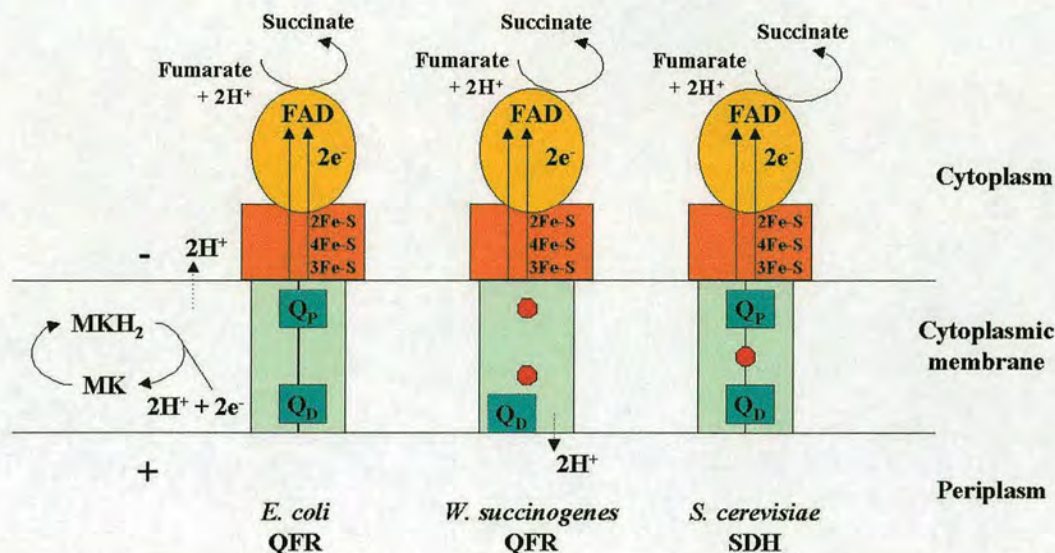


Figure 1.7: Electron transfer in fumarate reductases

The schematic diagram shows the overall structural arrangement of the *E. coli* and *W. succinogenes* fumarate reductases and succinate dehydrogenase of *S. cerevisiae*. The variation in the membrane anchor (light green) is shown. The *E. coli* fumarate reductase comprises two polypeptides and two menaquinone binding sites (Q_P and Q_D). The QFR of *W. succinogenes* contains a single polypeptide with two *b*-type haem groups (red circles). Succinate dehydrogenase of *S. cerevisiae* contains two polypeptides and one *b*-type haem group (red circle). The catalytic domain of the membrane-bound enzymes is similar, comprising a flavin subunit (yellow) and an iron-sulfur subunit (red). The quinone binding sites of the *W. succinogenes* QFR have yet to be determined (dashed box) but are thought to reside close to the haem *b* groups. The oxidation of menaquinol (MKH₂) to menaquinone (MK) yields two protons that may be released to the cytoplasmic face of the membrane to balance the number of protons required for fumarate reduction. Alternatively, the protons may be released to the periplasm by the *W. succinogenes* fumarate reductase generating an electrochemical proton potential across the membrane.

1.6.5 Bidirectional fumarate reductase activity

The flavinylated domain of the membrane-bound *E. coli* fumarate reductase and succinate dehydrogenase (Complex II) of bovine heart mitochondrion contains a highly conserved histidyl residue (Cole, 1982; Figure 1.8) that mediates covalent attachment to FAD. The N(3) imidazole ring moiety of this essential histidyl residue is covalently linked to the C8 α methyl group of FAD (Weiner and Dickie, 1979). A similar C8 α substituted flavin cofactor is also found in the *W. succinogenes* fumarate reductase (Kenney and Kröger, 1977).

The functionally important histidine side-chain lies within a strictly conserved nine-residue motif, representing a putative FAD binding site of succinate: quinone oxidoreductases (Cole, 1982; Figure 1.8). The covalent attachment of FAD to the membrane-bound *E. coli* fumarate reductase ($E^{\circ} = -48$ mV; Sucheta *et al.*, 1993) modulates the FAD redox activity of this enzyme and permits succinate oxidation at 25-30 % of the rate of fumarate reduction (Cecchini *et al.*, 1986).

```

Fcc GNAKLAAGG
EcF SHTVAAEGG
PvF SHTVAAEGG
ScS SHTVAAQGG
EcS SHTVSAQGG
WsF SHSAAAQGG
BsS SHSVCAQGG
      * *           * * *

```

Figure 1.8: The putative FAD binding site of fumarate reductases

The essential histidyl residue (red) required for covalent attachment of FAD in the family of fumarate reductases and succinate dehydrogenases, comprising: *E. coli* FrdA (EcF), *P. vulgaris* FrdA (PvF), *S. cerevisiae* SdhA (ScS), *E. coli* SdhA (EcS), *W. succinogenes* FrdA (WsF) and *Bacillus subtilis* SdhA (BsS), is shown. The histidyl residue is located in a conserved motif comprising nine amino acid residues (bold). The corresponding sequence of the soluble Fcc₃ fumarate reductase (Fcc) from *S. frigidimarina* NCIMB 400 is also shown. The sequence alignment is adapted from Figure 4 of Pealing *et al.*, 1992.

1.7 Soluble fumarate reductases related to Fcc₃

The fumarate reductase of *Shewanella* species is a soluble, periplasmic flavocytochrome *c*₃ (Fcc₃; Morris *et al.*, 1994) evolutionarily related to the more typically occurring membrane-bound fumarate reductases of *E. coli* and *W. succinogenes* (Pealing *et al.*, 1992). A putative membrane-bound fumarate reductase complex, comprising an FrdA flavoprotein subunit (ORF number; SO0398), FrdB iron-sulfur subunit (SO0399) and two FrdC cytochrome *b* subunits (SO0396 and SO0397) is apparently also expressed in *S. oneidensis* MR-1 (<http://www.tigr.org>) in addition to the soluble periplasmic Fcc₃ fumarate reductase. However, the soluble Fcc₃ fumarate reductase is the only respiratory fumarate reductase produced in *S. frigidimarina* NCIMB 400 (Gordon *et al.*, 1998). The specific expression of Fcc₃ is regulated at the transcriptional level (Gordon *et al.*, 1998) in response to anaerobic growth of *S. frigidimarina* NCIMB 400 with fumarate serving as terminal electron acceptor (Pealing *et al.*, 1992).

Another fumarate reductase of *S. frigidimarina* NCIMB 400 is specifically expressed during anaerobic respiration in the presence of ferric citrate or ferric pyrophosphate as the sole terminal electron acceptor (Dobbin *et al.*, 1999). This iron-induced fumarate reductase is a periplasmic *c*-type tetrahaem flavocytochrome *c*₃ (Ifc₃) that shares 43 % sequence identity to Fcc₃ (Dobbin *et al.*, 1999). The periplasmic location of the iron-induced enzyme suggests that this enzyme may function as an electron shuttle to deliver electrons to outer membrane cytochromes putatively linked to the terminal reduction of insoluble Fe(III) compounds (Dobbin *et al.*, 1999).

Alternatively, the novel Ifc₃ flavocytochrome may catalyse the terminal reduction of soluble Fe(III) compounds that cross the outer membrane impermeability barrier during anaerobic metabolism of *S. frigidimarina* NCIMB 400 (Dobbin *et al.*, 1999). The *c*-type haems and non-covalently bound FAD redox cofactor of Ifc₃ have low midpoint reduction potentials similar to Fcc₃ (Dobbin *et al.*, 1999). The structural homology (Bamford *et al.*, 1999) and shared redox properties of Ifc₃ and Fcc₃ (Dobbin *et al.*, 1999) are exemplified in the ability of the iron-induced isozyme to catalyse the *in vitro* unidirectional reduction of fumarate to succinate (Bamford *et al.*, 1999). However, the Ifc₃ enzyme is not induced anaerobically in the presence of fumarate (Dobbin *et al.*, 1999) and does not catalyse fumarate reduction *in vivo*, as shown by failure of Ifc₃ to catalyse fumarate reduction in the *S. frigidimarina* Fcc₃ deletion strain (EG301; Gordon *et al.*, 1998).

The folding topology of the flavin domain and a number of catalytic residues of Fcc₃ are also conserved in the L-aspartate oxidase (LASPO) flavoenzyme of *E. coli* which catalyses the oxidation of L-aspartate to iminoaspartate towards NAD⁺ biosynthesis (Mattevi *et al.*, 1999). This reaction is coupled to the reduction of molecular oxygen during aerobic respiration or fumarate during anaerobic respiration of *E. coli*. The LASPO redox reaction is mediated by the non-covalently bound FAD cofactor that has a dual function as an oxidant during the reductive half reaction and as a reductant during anaerobic electron transfer to fumarate (Tedeschi *et al.*, 1996). The LASPO enzyme catalyses the unidirectional reduction of fumarate, which is reflected in the low midpoint reduction potential (-216 mV) of FAD (Tedeschi *et al.*, 1997), that is also apparent in Ifc₃ (Dobbin *et al.*, 1999) and Fcc₃ (Turner *et al.*, 1999).

1.7.1 Flavocytochrome c_3 of *S. frigidimarina* NCIMB 400

Fcc₃ of *S. frigidimarina* NCIMB 400 is a single polypeptide enzyme that is encoded by *fccA* comprising an N-terminal sequence of 351 nucleotides encoding a cytochrome domain that is contiguous with a downstream 1362 nucleotide sequence encoding a flavin domain. The extreme N-terminal DNA sequence of *fccA* encodes a signal sequence for targeting the flavocytochrome to the periplasm via the Sec-dependent pathway (Pealing *et al.*, 1992; Figure 1.9). The region upstream of the *fccA* promoter does not appear to contain a motif matching the *E. coli* FNR-consensus sequence (Eiglmeier *et al.*, 1989). However, expression of *fccA* might be regulated by the EtrA transcriptional regulator, which perhaps binds to a DNA sequence distinct from the related FNR protein of *E. coli* (Gordon *et al.*, 1998). Indeed, the *fccA* fumarate reductase gene of *S. oneidensis* MR-1 was consistently repressed in an *etrA* knockout strain (ETRA1), indicating a role of EtrA in transcriptional activation of *fccA* under both fumarate and nitrate reducing conditions (Beliaev *et al.*, 2002a).

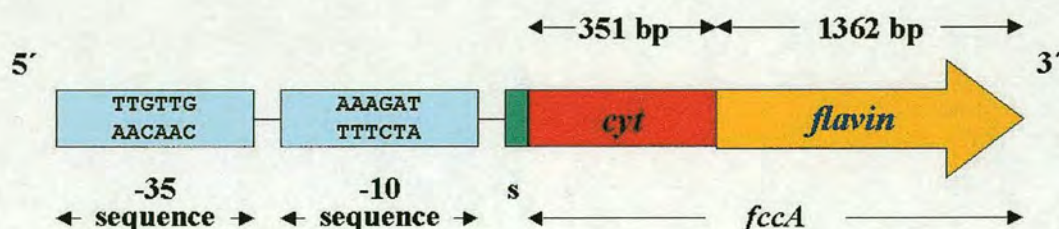


Figure 1.9: Map of the *fccA* gene

The *fccA* gene encoding Fcc₃ comprises sequence encoding a cytochrome (cyt) domain (red) and a flavin domain (yellow). The nucleotide lengths are indicated (bp). The possible -10 and -35 promoter sequences (Gordon *et al.*, 1998) are shown upstream (blue) in the 5' to 3' direction. The N-terminal sequence (green) encoding a putative Sec-dependent signal sequence (s) for cytoplasmic export of the flavocytochrome is shown. The diagram is not to scale.

The 571 amino acid polypeptide chain of Fcc₃ comprising a *c*-type tetrahaem cytochrome domain and a flavin domain (Pealing *et al.*, 1992) is structurally distinct compared to other bacterial flavocytochromes such as flavocytochrome *c* sulfide dehydrogenase of the purple phototrophic bacterium *Chromatium vinosum* (Chen *et al.*, 1994). The X-ray crystal structure of wild-type Fcc₃ (*S. frigidimarina* NCIMB 400) solved to 1.8 Å resolution (PDB, 1QJD; Taylor *et al.*, 1999; Figure 1.10) revealed that the 571 amino acid fumarate reductase contains a clamp domain (residues, His365-Gly502) in addition to the cytochrome domain (residues, Ala001-Arg100) and the flavin domain (residues, Asp111-Ala364 and residues, Val503-Asn571). The N-terminal *c*-type cytochrome domain contains four covalently bound haem groups that are solvent exposed and attached to a polypeptide chain that shows no sequence similarity to any other cytochrome of known structure (Taylor *et al.*, 1999). The C-terminal FAD-binding domain of Fcc₃ consists of a Rossmann fold and therefore shares structural and topological similarities to unrelated FAD-binding enzymes, including, lipoamide dehydrogenase (Mattevi *et al.*, 1993) and glutathione reductase (Mittl and Schulz, 1994). The most closely related flavoproteins to Fcc₃ that share structural and sequence similarity were identified as members of the fumarate reductase and succinate dehydrogenase families (Pealing *et al.*, 1992). High percentage sequence identity of residues constituting the Rossmann fold was observed for the Fcc₃ flavin domain aligned with the flavin subunits of L-aspartate oxidase (38 %; Mattevi *et al.*, 1999) and the membrane-bound *E. coli* fumarate reductase (45 %; Iverson *et al.*, 1999).

The third domain of Fcc₃, designated the 'clamp domain', comprises a unique structural fold consisting of seven short α -helices enfolding a four-stranded antiparallel β -pleated sheet (Taylor *et al.*, 1999; Figure 1.10). The Fcc₃ (*S. frigidimarina* NCIMB 400) X-ray crystal structure (Taylor *et al.*, 1999) is essentially structurally identical to the X-ray crystal structures for the related Fcc₃ soluble fumarate reductase of *S. oneidensis* MR-1 (Leys *et al.*, 1999).

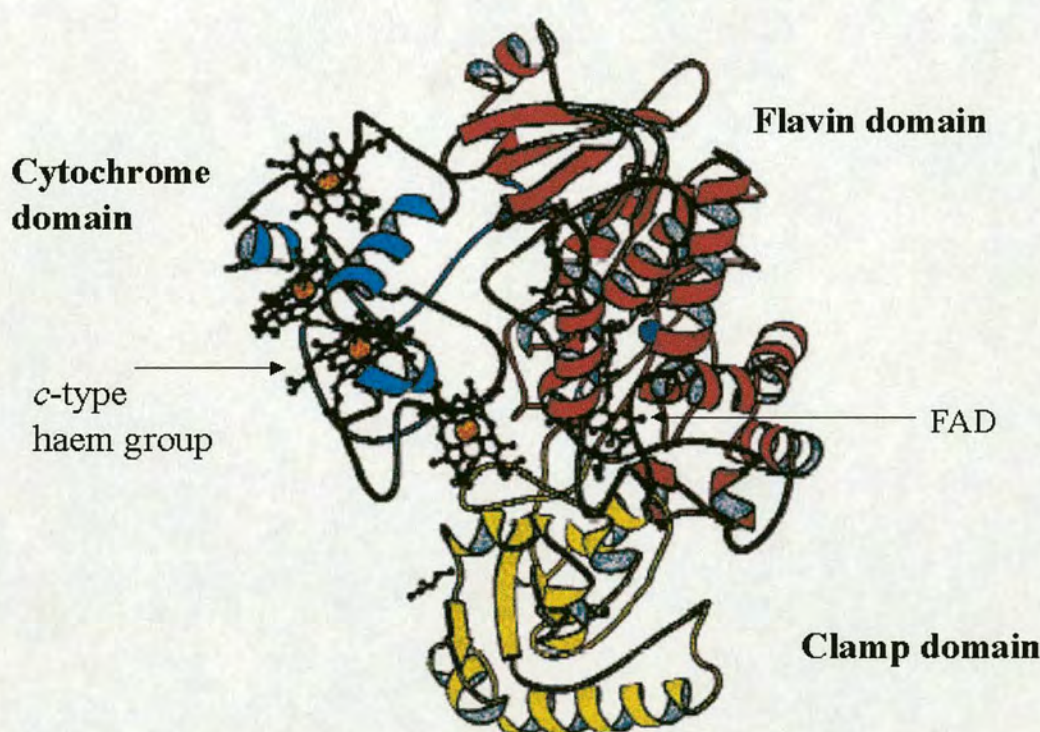


Figure 1.10: X-ray crystal structure of Fcc₃ solved to 1.8 Å resolution

The Fcc₃ fumarate reductase complexed with a malate-like substrate was solved to 1.8 Å resolution (Taylor *et al.*, 1999). The X-ray crystal structure revealed a novel mobile clamp domain (yellow) that controls access of substrate to the active site of the flavin domain (red). The N-terminal cytochrome domain (blue) is shown to contain 4 *c*-type haem groups that deliver electrons to non-covalently bound FAD (ball and stick) in the flavin-containing catalytic domain (red). The FAD cofactor lies in close proximity to the malate-like substrate bound in the enzyme active site of the flavin-containing domain. The picture is adapted from Figure 2a of Taylor *et al.*, 1999.

The flavin domain of Fcc₃ contains non-covalently bound FAD and accepts electrons from the electron transfer haem groups of the cytochrome domain for fumarate reduction. The X-ray crystal structure of Fcc₃ (*S. frigidimarina* NCIMB 400) reveals that three of the haem groups (I-III) are oriented in a similar spatial arrangement (Figure 1.10) to corresponding haem groups of the related tetrahaem cytochrome *c*₃ of *Shewanella* species (Pessanha *et al.*, 2001 and Leys *et al.*, 2002). A short peptide linker of Fcc₃ (residues, Asp101-Lys110) connects the N-terminal cytochrome domain to the flavin-binding domain, which results in positioning haem IV proximal to the FAD cofactor (edge-edge distance, 7.4 Å). This close haem-flavin distance is ideally suited to efficient inter-domain electron transfer for fumarate reduction in the active site of the Fcc₃ flavin domain (Taylor *et al.*, 1999). The low reduction potentials of the tetrahaem groups ($E^{\circ'} = -102, -146, -196$ and -238 mV) are suitable for forming an electron conduit to FAD, which has a greater tendency to accept electrons, due to a more positive reduction potential ($E^{\circ'} = -152$ mV; Turner *et al.*, 1999). The lower reduction potential (-229 mV) determined for haem IV of tetrahaem cytochrome *c*₃ (*S. frigidimarina* NCIMB 400) might be a conserved feature for haem IV in the cytochrome domain of Fcc₃, thereby mediating the thermodynamically favourable electron transfer from haem IV to FAD. The more negative reduction potentials determined for haems I and II compared to haem III for cytochrome *c*₃ leads to the proposition that electrons will also flow in the Fcc₃ molecular wire from haems I to IV to FAD (Pessanha *et al.*, 2003).

The substrate-bound enzyme active site of Fcc₃ is completely buried in the oxidised state of the flavocytochrome (Taylor *et al.*, 1999). Structural superposition of monomers obtained for the Fcc₃-fumarate complexed enzyme (*S. oneidensis* MR-1) revealed a 12 ° rotation of the clamp domain relative to the flavin domain. The flexibility in domain movement around an axis close to the active site suggests that the clamp domain mobility mediates substrate access to the buried enzyme active site (Leys *et al.*, 1999). The presence of a capping domain in the flavin subunit of the *W. succinogenes* fumarate reductase led to the suggestion that motion of the clamp domain will serve the same purpose in the related membrane-bound fumarate reductases (Lancaster *et al.*, 1999). Consistent with this conjecture, the capping domain and FAD-binding domain of the *W. succinogenes* fumarate reductase, are oriented by 14 ° in a new crystal form that was superimposed (Lancaster *et al.*, 2001) on the previous crystal forms of the enzyme (Lancaster *et al.*, 1999).

1.7.2 Fcc₃ is a unidirectional fumarate reductase

Fcc₃ was identified to contain 1 mol of non-covalently bound FAD per mol of protein (Morris *et al.*, 1994). This finding correlated with the initial sequence alignments of Fcc₃ and the membrane-bound fumarate reductases, which showed that the histidyl residue essential for covalent attachment of FAD (Weiner and Dickie, 1979; Cole, 1982) was absent in Fcc₃ (Pealing *et al.*, 1992; Figure 1.8). The non-covalently bound FAD of Fcc₃ is a cooperative two-electron redox centre with a low reduction potential of -152 mV (pH 7.0, 24 °C), which favours the terminal reduction of fumarate ($E^{\circ'} = 30 \text{ mV}$). This significantly low reduction potential of non-covalently bound FAD renders the Fcc₃ enzyme a unidirectional fumarate reductase since electron transfer from succinate to FAD is unfavourable (Turner *et al.*, 1999).

1.8 Novel flavocytochromes of *S. oneidensis* MR-1

1.8.1 Identification of novel *S. oneidensis* MR-1 genes

Sequencing of the *S. oneidensis* MR-1 genome (4,969,803 bp circular chromosome) (<http://www.tigr.org> and Heidelberg *et al.*, 2002) has led to the identification of a remarkable number of respiratory proteins including 14 *c*-type cytochromes containing four or more haem-binding sites (Heidelberg *et al.*, 2002). Further genome analysis has shown that each of the novel *fccB* structural genes (ORF numbers: SO1413, SO3300, SO3056 and SO3623; Table 1.1) encoding a new tetrahaem cytochrome (FccB54, FccB56, FccB63 and FccB342) is organised in a gene cluster with an *fccA* gene (ORF numbers: SO1414, SO3301, SO3058 and SO3624) encoding a putative flavoprotein (FccA54, FccA56, FccA63 and FccA342; Table 1.1, Figure 1.11). The predicted amino acid sequences of these putative flavin and cytochrome subunits share striking sequence identity to the flavin and cytochrome domains, respectively, of the Fcc₃ fumarate reductase of *S. frigidimarina* NCIMB 400 (Tables 1.2 and 1.3) and *S. oneidensis* MR-1. The predicted amino acid sequences of each novel flavin subunit (FccA54, FccA56, FccA63 and FccA342) of *S. oneidensis* MR-1 are also similar (38-44 % identity) to the putative FccA flavoprotein (52.4 kDa) of *W. succinogenes* (Simon *et al.*, 1998) which shares 33 % sequence identity to the flavin domain of Fcc₃ (Table 1.2). Each novel putative cytochrome subunit (FccB54, FccB56, FccB63 and FccB342) of *S. oneidensis* MR-1 shares significant sequence identity (29-34 %) to the putative FccB cytochrome subunit of *W. succinogenes* and the cytochrome domain of Fcc₃ (23-29 %; Table 1.3).

Furthermore, high amino acid sequence identity (35-42 %) was observed by pairwise sequence comparison of each novel flavin subunit. Lower sequence identity (30-37 %) was observed when comparing each of the novel cytochrome subunits against one another. The contiguous gene arrangement and observed sequence homology to Fcc₃ has led to the proposal that the separately encoded flavin subunits (FccA54, FccA56, FccA63 and FccA342) associate with the respective partner cytochrome subunits (FccB54, FccB56, FccB63 and FccB342) to form dimeric flavocytochromes.

The novel flavin and cytochrome proteins were given preliminary names according to the contig number that the genes were originally assigned during genome sequencing. The contig numbers were also used for naming the genes encoding each novel protein subunit. Throughout the thesis, the novel genes and encoded proteins are named according to the original contig number. The ORF numbers of the completed genome sequence which each of the genes corresponds to are shown in Table 1.1.

Protein name	Gene name	ORF number	Protein length (aa)		Molecular weight (Da)		pI
			Preprotein	Mature	Preprotein	Mature	
FccA54	<i>fccA54</i>	SO1414	506	477	54,927	52,178	8.34
FccB54	<i>fccB54</i>	SO1413	123	102	13,307	11,145	6.30
Chyp	<i>chyp</i>	SO1412	377	351	42,474	39,698	4.46
Hyp	<i>hyp</i>	SO1411	360	339	39,881	37,563	5.45
FccA56	<i>fccA56</i>	SO3301	499	480	53,763	51,786	8.28
FccB56	<i>fccB56</i>	SO3300	124	101	13,855	11,273	6.85
Hal56	<i>hal56</i>	SO3299	549	529	60,609	58,503	5.65
FccA63	<i>fccA63</i>	SO3058	517	482	55,237	51,737	8.38
Hal63	<i>hal63</i>	SO3057	550	524	59,513	56,824	6.13
FccB63	<i>fccB63</i>	SO3056	127	105	14,233	11,888	7.09
FccA342	<i>fccA342</i>	SO3624	494	473	53,540	51,130	8.08
FccB342	<i>fccB342</i>	SO3623	116	94	13,136	10,781	6.11
Cdmp	<i>cdmp</i>	SO3622	247	228	27,619	25,669	5.95
Chyp	<i>chyp</i>	SO3621	151	134	16,485	14,494	6.56

Table 1.1: Predicted properties of the novel flavoproteins related to Fcc₃

The open reading frame (ORF) numbers for each of the novel flavoproteins according to ‘The Institute for Genomic Research’ (<http://www.tigr.org>) are shown. The amino acid (aa) sequence lengths of the preprotein and mature protein are also shown. The preprotein lengths were calculated using SignalP (Nielsen *et al.*, 1997; <http://www.cbs.dtu.dk/services/SignalP/>). The estimated molecular weight of the apoproteins (preprotein and mature protein) and isoelectric point (pI) for each of the mature protein subunits (<http://www.expasy.org/tools/protparam.html>) is shown. The novel flavin (FccA54, FccA56, FccA63 and FccA342) and cytochrome (FccB54, FccB56, FccB63 and FccB342) subunits are preliminary named according to the contig number that the genes were originally assigned during genome sequencing. A conserved hypothetical protein (Chyp) and a hypothetical protein (Hyp) encoded by genes (ORF numbers: SO1412 and SO1411, respectively) that are associated with *fccA54* and *fccB54* are shown. A conserved domain protein (Cdmp) and a conserved hypothetical protein (Chyp) encoded by genes (SO3622 and SO3621, respectively) that are close to *fccA342* and *fccB342* are also shown.

Protein Name	AMINO ACID SEQUENCE IDENTITY (%)					
	SF FccA	FccA54	FccA56	FccA63	FccA342	WS FccA
SF FccA	-	-	-	-	-	-
FccA54	29	-	-	-	-	-
FccA56	31	35	-	-	-	-
FccA63	34	40	40	-	-	-
FccA342	32	38	38	42	-	-
WS FccA	33	38	42	44	42	-

Table 1.2: Flavoprotein amino acid sequence identities

The amino acid sequence identities of each novel flavoprotein subunit (FccA54, FccA56, FccA63 and FccA342) against the flavin domain of Fcc₃ (*S. frigidimarina* NCIMB 400; SF FccA) and the putative flavin subunit of *W. succinogenes* (WS FccA; Simon *et al.*, 1998) are shown. The mature protein sequences were aligned in pair-wise sequence alignments and the sequence identity calculated using Blast (<http://www.ncbi.nlm.nih.gov/blast/bl2seq/bl2.html>).

Protein Name	AMINO ACID SEQUENCE IDENTITY (%)					
	SF FccB	FccB54	FccB56	FccB63	FccB342	WS FccB
SF FccB	-	-	-	-	-	-
FccB54	29	-	-	-	-	-
FccB56	23	35	-	-	-	-
FccB63	29	30	31	-	-	-
FccB342	29	37	35	35	-	-
WS FccB	25	29	34	32	30	-

Table 1.3: Cytochrome protein amino acid sequence identities

The amino acid sequence identities of each novel cytochrome subunit (FccB54, FccB56, FccB63 and FccB342) against the cytochrome domain of Fcc₃ (*S. frigidimarina* NCIMB 400; SF FccB) and the putative cytochrome subunit of *W. succinogenes* (WS FccB; Simon *et al.*, 1998) are shown. The preprotein sequences were aligned in pair-wise sequence alignments and the sequence identity calculated using Blast (<http://www.ncbi.nlm.nih.gov/blast/bl2seq/bl2.html>).

1.8.2 Arrangement of the novel *S. oneidensis* MR-1 genes

The gene arrangement of the novel *S. oneidensis* MR-1 genes resembles that of the *W. succinogenes* *fccABC* operon containing *fccA* and *fccB*, which encode putative flavin (FccA) and cytochrome (FccB) subunits, respectively (Simon *et al.*, 1998; Figure 1.11). The *fccA* and *fccB* genes of *W. succinogenes* are co-transcribed with *fccC* (Figure 1.11) that encodes a putative membrane-bound tetrahaem cytochrome *c* similar in sequence to CymA (1.5). The encoded FccA and FccB subunits form a putative periplasmic oxidoreductase complex that is induced anaerobically in the presence of fumarate as terminal electron acceptor. However, the FccA catalytic subunit of *W. succinogenes* does not catalyse fumarate reduction (Simon *et al.*, 1998), which leads to the conjecture that the related putative flavocytochromes of *S. oneidensis* MR-1 will also catalyse reduction of an alternative substrate to fumarate. The N-terminal amino acid sequence of each novel *S. oneidensis* MR-1 flavoprotein (FccA54, FccA56, FccA63 and FccA342) is also remarkably similar to that of a periplasmic methacrylate reductase flavoprotein (50 kDa) of *Geobacter sulfurreducens* AM-1 (Mikoulinskaia *et al.*, 1999). This flavoenzyme couples the oxidation of benzyl viologen to the terminal reduction of methacrylate to produce isobutyrate. The activity of this methacrylate reductase was shown to be dependent on tight association of the catalytic flavoprotein with a periplasmic tetrahaem cytochrome *c* subunit (30 kDa). The putative dimeric structure of each novel *S. oneidensis* MR-1 flavocytochrome is therefore shared with the related periplasmic methacrylate reductase flavocytochrome of *G. sulfurreducens* AM-1.

The operon comprising *fccA54* and *fccB54* also contains genes (SO1412 and SO1411) encoding hypothetical proteins that may associate with the putative Fcc54 flavocytochrome in the periplasm. Likewise, genes (SO3622 and SO3621) downstream of *fccB342* encode hypothetical proteins that appear to contain N-terminal Sec-dependent signal sequences. These unknown proteins may associate to form a large complex with the putative FccB342 flavocytochrome in the periplasm. The hypothetical proteins may be involved in catalysis or electron transfer reactions preceding the reaction catalysed by the putative flavocytochromes.

The Fcc56 operon contains a histidine ammonia lyase-like gene (*hal*) downstream of *fccA56* and *fccB56*. A *hal* gene also occurs in the Fcc63 operon and maps between *fccA63* and *fccB63* (Figure 1.11). The presence of a gene encoding a histidase family protein in the same operon as genes encoding the putative flavin and cytochrome subunits has led to the suggested role of these flavocytochromes in the reduction of amino acids serving as terminal electron acceptor (Heidelberg *et al.*, 2002). Histidine ammonia-lyase is involved in the degradation of histidine and catalyses the elimination of the α -amino group to form α - β -unsaturated *trans*-urocanate. The double bond introduced in α - β -unsaturated *trans*-urocanate by deamination of histidine could subsequently be reduced by the associated flavocytochrome *c*₃ (Schwede *et al.*, 1999).

The reaction catalysed by histidine ammonia-lyase involves a reactive electrophile, 4-methylidene-imidazole-5-one, which abstracts a non-acidic proton from the substrate C_β atom. The α-ammonium group is subsequently eliminated and the urocanate product is released. The electrophile is formed autocatalytically by cyclisation and dehydration of histidase tripeptide residues Ala142-Ser143-Gly144 (histidase of *Pseudomonas putida* numbering). A similar reaction mechanism for the deamination of phenylalanine to cinnamic acid is proposed for the homologous plant enzyme, phenylalanine ammonia-lyase, which also contains the catalytic tripeptide (Ala-Ser-Gly). Sequence alignments of the *S. oneidensis* MR-1 putative histidase family proteins (Hal56 and Hal63, Table 1.1) against histidase of *P. putida* have shown that the essential catalytic tripeptide (Ala-Ser-Gly) is not conserved. This suggests that the novel histidase family proteins (Hal56 and Hal63, Table 1.1) associated with the novel flavocytochromes may catalyse the deamination of one or more amino acids via a different mechanism to produce the corresponding substituted acrylic acid. This product would then provide a suitable substrate for reduction by the associated flavocytochromes (FccA56: FccB56 and FccA63: FccB63).

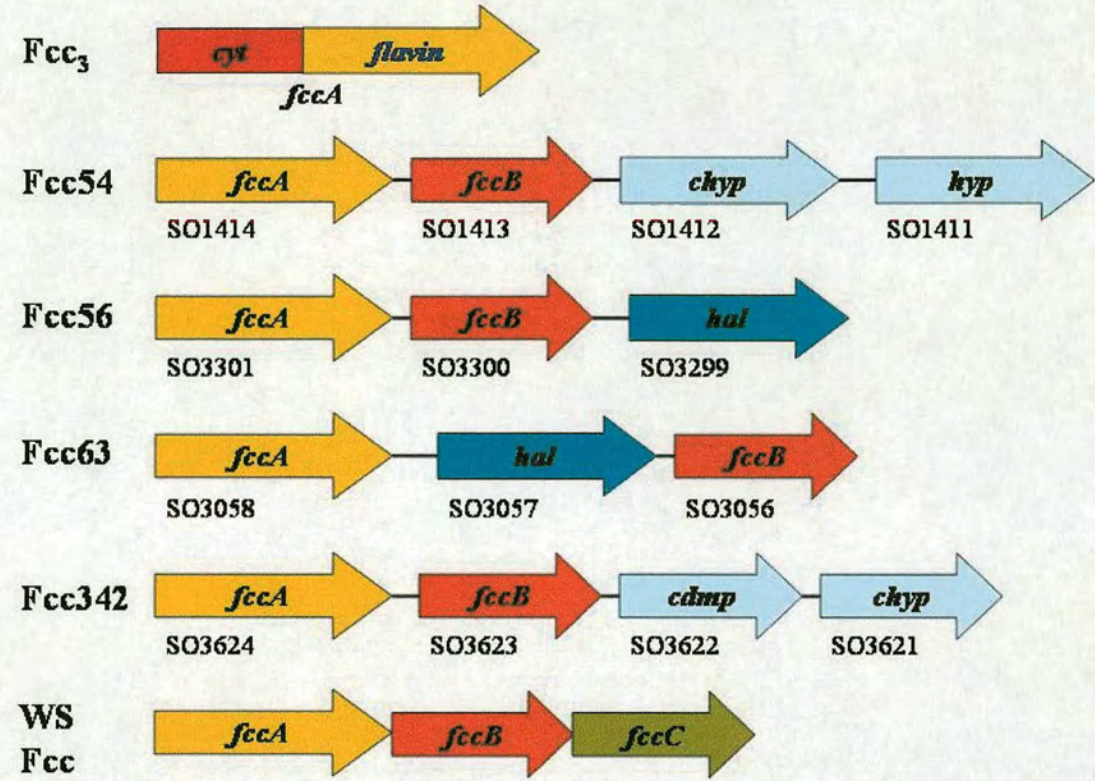


Figure 1.11: Gene arrangement of the novel *S. oneidensis* MR-1 genes

The arrangement of genes in each operon is shown for the novel *S. oneidensis* MR-1 flavoproteins (Fcc54, Fcc56, Fcc63 and Fcc342) compared to Fcc₃ (*S. frigidimarina* NCIMB 400) and the *fccABC* operon of *W. succinogenes* (WS Fcc; Simon *et al.*, 1998). The *fccA* gene encoding Fcc₃ comprises sequence encoding the cytochrome (cyt) domain (red) and the flavin domain (yellow). The open reading frame number is shown for each novel *S. oneidensis* MR-1 gene. The genes encoding flavoproteins (*fccA*), cytochrome subunits (*fccB* and *fccC*), histidase family protein (*hal*), conserved hypothetical protein (*chyp*), hypothetical protein (*hyp*) and conserved domain protein (*cdmp*), are shown. The diagram is not to scale.

1.8.3 Novel *S. oneidensis* MR-1 periplasmic flavocytochromes

The FccA flavoprotein of *W. succinogenes* and the methacrylate reductase of *G. sulfurreducens* AM-1 were both identified in the soluble periplasmic fraction of the cell (Mikoulinskaia *et al.*, 1999 and Simon *et al.*, 1998). There is substantial evidence to suggest that the related novel *S. oneidensis* MR-1 flavocytochromes (Table 1.1) are also targeted to the periplasm *in vivo*. The deduced N-terminal amino acid sequences of the FccA54, FccA56 and FccA63 preproteins reveal transfer peptides that contain residues of the “twin arginine” consensus sequence defined as (S/T)-R-R-x-F-L-K (Figure 1.12; Berks, 1996). The double-arginine signal peptides tend to be longer (26-58 amino acids; Berks, 1996) than standard bacterial Sec-dependent signal sequences (mean= 24-31 amino acids; von Heijne and Abrahmsén, 1989). The lengths of the transfer peptides were calculated for each of the novel flavoproteins using ‘SignalP’ (<http://www.cbs.dtu.dk/services/SignalP/>; Nielsen *et al.*, 1997). Indeed, the putative N-terminal signal peptides of FccA54 and FccA63 conform to the longer length of double-arginine signal sequences. However, the N-terminal transfer peptides of FccA56 and FccA342 are shorter compared to double-arginine signal peptides (Table 1.4) and resemble the length of Sec-dependent signal sequences (von Heijne and Abrahmsén, 1989).

Protein name	Transfer peptide length (aa)
FccA54	29
FccA56	19
FccA63	35
FccA342	21

Table 1.4: Tat transfer peptide lengths

The numbers of amino acids (aa) comprising the N-terminal Tat signal transfer peptides of each novel preprotein (FccA54, FccA56, FccA63 and FccA342) are shown. The signal peptide lengths were calculated using ‘SignalP’ (Nielsen *et al.*, 1997; <http://www.cbs.dtu.dk/services/SignalP/>).

The N-terminal transfer peptide containing the double arginine motif is found almost exclusively in bacterial redox preproteins targeted to the periplasm (Berks, 1996) via the Tat (*twin arginine translocation*) export system (Sargent *et al.*, 1998). This export system is restricted to proteins containing iron sulfur clusters, molybdopterin, tryptophan tryptophylquinone or FAD redox cofactors (Berks, 1996). The Tat system is a unique translocase that functions to target and export folded preproteins containing redox cofactors to the periplasm (Berks, 1996) and resembles the Δ pH-dependent protein import machinery of chloroplast thylakoid membranes (Mori *et al.*, 1999). The twin arginine residues of the Tat transfer peptide are required for efficient translocation of preproteins to the periplasm. The conservative site-directed mutagenesis of both arginine residues with lysine completely prevented export of the target SufI *E. coli* preprotein to the periplasm (Stanley *et al.*, 2000). The N-terminal transfer peptide of FccA342 does not contain the twin arginine residues (Figure 1.12) and is shorter than twin arginine signal sequences (Table 1.4).

The FccA342 transfer peptide therefore represents a unique Tat system signal peptide that perhaps operates differently to reported transfer peptides that appear to interact with the membrane translocase via electrostatic interactions (Stanley *et al.*, 2000).

FccA54	01	MH	DRRS	FLK	LGAG	13
FccA56	01	MA	GRRD	FLK	LATG	13
FccA63	08	NA	GRRQ	LLK	GGMV	20
FccA342	01	MI	----	YLK	IIRG	09
Consensus			SRRX	FLK		
			T			

Figure 1.12: N-terminal Tat signal peptide alignment of the novel flavoproteins

The novel *S. oneidensis* MR-1 flavoproteins contain an N-terminal Tat signal peptide sequence that is known to direct bacterial redox preproteins to the periplasm. The N-terminal sequences share the double arginine residues shown in the consensus motif. The N-terminal Tat signal peptide of FccA342 does not contain the twin arginine residues that are essential for translocation to the periplasm. Numbering of the preprotein sequences is shown. The sequence alignment was produced using 'ClustalW' (Thompson *et al.*, 1994).

The putative FccB54, FccB56, FccB63 and FccB342 cytochrome subunits comprise an N-terminal signal sequence typical of bacterial proteins targeted to the periplasm via the general secretory (Sec)-dependent pathway (von Heijne and Abrahmsén, 1989; Figure 1.14). This pathway is involved in the export of bacterial redox preproteins comprising *c*-type haem groups (Berks, 1996). The signal sequences (21-23 amino acid residues) all contain alanine at the -1 position relative to the peptidase cleavage site and contain positively charged residues at the extreme N-terminus followed by hydrophobic residues (Figure 1.14).

The novel *S. oneidensis* MR-1 flavin and cytochrome preproteins possess N-terminal signal sequences that target each subunit to the periplasm via distinct export pathways. The individual subunits are expected to associate in the periplasm to form a catalytic heterodimeric flavocytochrome. The predicted soluble nature of the novel flavoproteins is also shared with monomeric proteins such as Fcc₃ of *Shewanella* species (Morris *et al.*, 1994) and other soluble fumarate reductases located in the mitochondrial matrix of *Trypanosoma brucei* (Mracek *et al.*, 1991) and the cytoplasm of *S. cerevisiae* (Arikawa *et al.*, 1998).

1.8.4 FAD-dependent tetrahaem flavocytochromes

The N-terminal sequence of the novel flavoproteins shares particularly high sequence identity to Fcc₃ at the region containing the FAD adenine binding motif. Furthermore, replacement of the essential histidyl residue for covalent linkage of FAD (Weiner and Dickie, 1979; Cole, 1982) with an asparagine residue in Fcc₃ (Pealing *et al.*, 1992; Figure 1.8) is conserved in the related Fcc₃-like enzymes (Figure 1.13). This led to the suggestion that the novel Fcc₃-like flavoproteins are FAD dependent respiratory enzymes that also contain non-covalently bound FAD. This conjecture is supported by knowledge that the related methacrylate reductase contains non-covalently bound FAD (Mikoulinskaia *et al.*, 1999).

FccA54	WDETR	DIIVVGS	GFAGLSSAI	NAKRQ-GLGSILVLEKMQVIGGNSAINGGW	58
FccA56	WDKEF	DIIIIGS	GFAGLSAAY	SAHKA-GIKNIIVLEKMEAFGGNSAICGGL	63
FccA63	FDEIV	DVLVVGS	GFAGMSAAL	QARES-GVK-VMVIDKMPVFGNSTINGGA	57
FccA342	WDETY	EIVIVGS	GFAGLAAAI	EAGKL-GAKEVVLEKLG VYGGNSALNAGQ	56
SFFccA	PHDTV	DVVVGS	GGAGFSAAI	SATDS-GAK-VILIEKEPVIGGNAKLAAGG	54
FrdA	QTFQA	DLAIVG	AGGAGLRAAI	AAAQANPNAKIALISKVYPMRSHTVAAEGG	51
		::	::*: *	::: *	

Figure 1.13: Non-covalent attachment of FAD

The N-terminal amino acid sequences of each novel flavoprotein (FccA54, FccA56, FccA63 and FccA342) are aligned with that of Fcc₃ (*S. frigidimarina* NCIMB 400, SFFccA) and the FrdA subunit of the *E. coli* fumarate reductase (FrdA). The FAD adenine binding motif (cyan) of Fcc₃ and Frd are conserved in the related novel flavoproteins. The histidyl residue (red) of the *E. coli* fumarate reductase required for covalent linkage of FAD is absent in Fcc₃ and the novel flavoproteins which all contain asparagine at the equivalent position. The conserved nine-residue motif that is the putative FAD binding site of FrdA is shown in bold. The multiple sequence alignment was generated using ‘ClustalW’ (Thompson *et al.*, 1994). The numbering is according to the mature protein sequences.

Each of the novel *S. oneidensis* MR-1 cytochrome subunits contains four CxxCH motifs (Figure 1.14) that infer tetrahaem attachment to each protein (where x is any amino acid residue). The two cysteines are linked through thioether bonds to vinyl groups of protohaem IX and the histidine residue provides a ligand to the haem iron (Pealing *et al.*, 1992). Another histidine residue serving as the sixth ligand to form *c*₃-haems (Pealing *et al.*, 1995) appears to exist in each of the novel cytochrome proteins (Figure 1.14). However, this histidine residue is tentatively ascribed to serve this function because some of the histidines do not align with a sixth ligand histidine of Fcc₃ (*S. frigidimarina* NCIMB 400; Pealing *et al.*, 1995). Overall, the data interpreted from multiple sequence alignments of each novel flavoprotein against Fcc₃ suggests each novel enzyme of *S. oneidensis* MR-1 is also a tetrahaem flavocytochrome *c*₃.

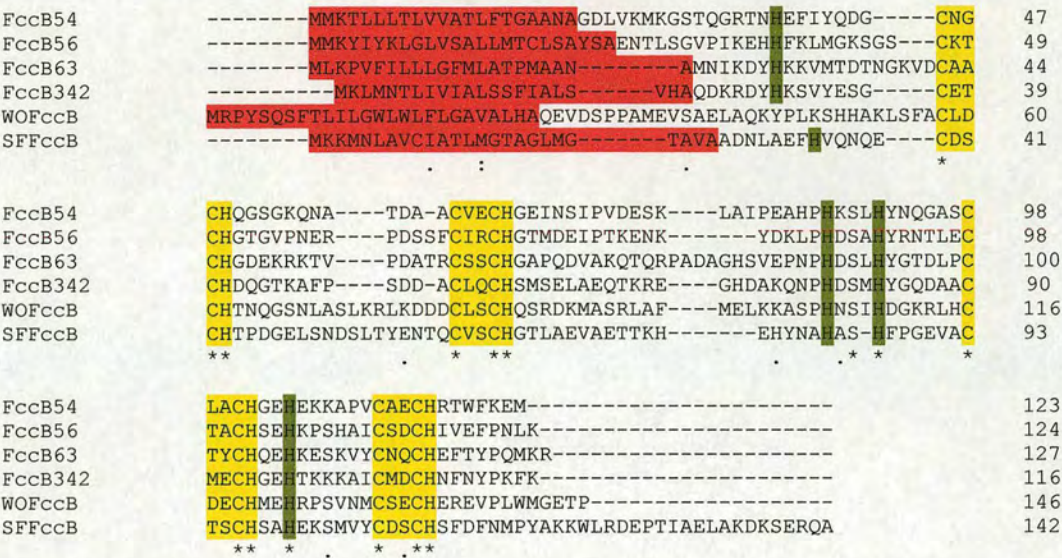


Figure 1.14: Tetrahaem c-type cytochrome proteins
The multiple sequence alignment of the cytochrome preproteins shows that FccB54, FccB56, FccB63 and FccB342 all contain four CxxCH motifs (yellow) characteristic of c-type cytochromes, as found for FccB of *W. succinogenes* (WOFccB) and the cytochrome domain of *S. frigidimarina* NCIMB 400 (SFFccB). Histidine residues that may provide the sixth ligand to the haems are shown (green). The N-terminal Sec-dependent signal sequences are also shown (red). The multiple sequence alignment was generated using 'ClustalW' (Thompson *et al.*, 1994).

1.8.5 Putative function of the novel periplasmic flavocytochromes

A gene deletion of *fccA* encoding Fcc₃ prevented the *S. frigidimarina* EG301 null mutant from respiring anaerobically with fumarate as terminal electron acceptor. This provided evidence that Fcc₃ is the sole respiratory fumarate reductase of *S. frigidimarina* NCIMB 400 (Gordon *et al.*, 1998). The inability of *S. frigidimarina* EG301 to respire anaerobically in the presence of fumarate suggests that the novel *S. oneidensis* MR-1 flavocytochromes related to Fcc₃ will catalyse the reduction of one or more substrates other than fumarate. Of particular interest, is the ability of these novel flavoproteins to catalyse the reduction of acrylate substrates, including methacrylate, crotonate, tiglate and ferulate (Figure 1.15) which are plant metabolites most probably found in sedimentary environments inhabited by *S. oneidensis* MR-1. The putative function of the novel *S. oneidensis* MR-1 flavoproteins correlates with the related methacrylate reductase of *G. sulfurreducens* that is able to catalyse reduction of other acrylate substrates such as crotonate and pentenoate (Mikoulinskaia *et al.*, 1999). The putative FccA flavoprotein located in the periplasm of *W. succinogenes* is also linked to methacrylate reduction via benzyl viologen oxidation (Gross *et al.*, 2001). The presence of a histidase family protein putatively associated with the novel flavocytochromes (FccA56: FccB56 and FccA63: FccB63) has led to the suggestion that these flavoproteins catalyse reduction of phenylacrylates such as cinnamate. Ferulate serves as an alternative terminal electron acceptor and sustains growth of the acetogenic bacterium *Peptostreptococcus productus* U-1 during CO₂-limited growth conditions (Misoph *et al.*, 1996).

This suggests that reduction of acrylate substrates by *S. oneidensis* MR-1 will conceivably generate sufficient energy during anaerobic electron transport to support growth of the bacterium.

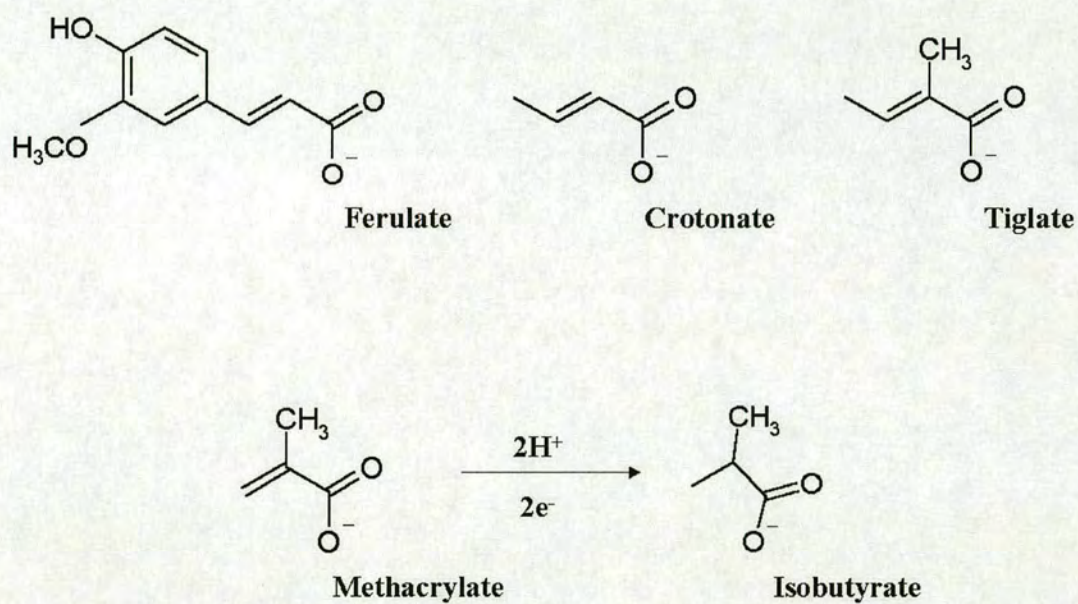


Figure 1.15: Potential acrylate substrates

Some acrylate substrates that are potential enzyme substrates of the novel flavoproteins are shown. The reduction of methacrylate to isobutyrate is shown as an example of the putative two-electron reduction catalysed by the novel flavoproteins.

1.9 Aims of project

The novel *S. oneidensis* MR-1 putative flavocytochromes that share high sequence identity to Fcc₃ are also related by sequence to methacrylate reductases of *W. succinogenes* (Gross *et al.*, 2001) and *G. sulfurreducens* (Mikoulinskaia *et al.*, 1999). Sequence analysis has led to the suggestion that these novel flavoenzymes may also catalyse the reduction of acrylates that are important plant metabolites (Wallace and Fry, 1994; Figure 1.15). The major aim was to characterise the novel flavoproteins and identify their biological function by using structural and genetic approaches. Experiments were designed for PCR amplification of the genes encoding the novel flavocytochromes from the *S. oneidensis* MR-1 genome. The intention was to clone the PCR fragments in plasmids suitable for overexpression of the flavoproteins and to purify the flavoproteins for crystallisation and structure determination. In parallel to the overexpression studies, molecular modelling of the novel flavoproteins based upon the known structure of Fcc₃ (Taylor *et al.*, 1999) aimed to provide insight into the architecture of each enzyme active site for elucidation of potential enzyme substrates. The enzymes FccA54, FccA56 and FccA342 were selected for molecular modelling studies. The construction of an *fccA54* and *fccB54* null mutant strain was designed to provide a means of identifying the biological function of the encoded Fcc54 putative flavocytochrome. The rationale for structure determination and functional analyses of these putative bacterial acrylate reductases is linked to biotechnological applications for the production of valuable acids with a chiral centre at the β -carbon. Furthermore, acrylate reduction may implicate *S. oneidensis* MR-1 in bioremediation of contaminated environments.

Chapter 2

Materials and Methods

2.1 Media and growth conditions

2.1.1 Luria-Bertani (LB) medium

Per litre:

Bacto-tryptone	10.0 g
Bacto-yeast extract	5.0 g
Sodium Chloride (NaCl)	10.0 g

For LB agar plates, 1.5 % (w/v) agar was added.

2.1.2 Small-scale aerobic growth of *Shewanella* species

Single colonies of *Shewanella oneidensis* MR-1 (Table 2.6) were selected from a LB plate containing a freshly plated -80°C dimethyl sulfoxide (DMSO) stock of the bacterium that was grown at 23°C for 2 days in a static incubator. $\frac{1}{2}$ oz bijou jars containing 5 ml of LB were inoculated with a single *S. oneidensis* MR-1 colony under aseptic conditions using a sterile toothpick. *S. oneidensis* MR-1 cultures were grown overnight in a shaking incubator (New Brunswick Scientific innova 4330) for approximately 20 hours at 23°C . Cultures of *S. oneidensis* MB5415 (Table 2.6) were grown as described above but with addition of kanamycin (Km; $50\text{ }\mu\text{g/ml}$) and rifampicin (Rm; $10\text{ }\mu\text{g/ml}$) to the LB media prior to inoculation. Cultures of *S. frigidimarina* EG301 (Gordon, 1996; Table 2.6) were prepared in LB supplemented with Km ($50\text{ }\mu\text{g/ml}$) and Rm ($10\text{ }\mu\text{g/ml}$) and the spontaneous rifampicin resistant strain of *S. oneidensis* MR-1 (Table 2.6) was selectively grown in LB containing Rm ($10\text{ }\mu\text{g/ml}$).

2.1.3 Small-scale aerobic growth of *E. coli*

Parent strains of *E. coli* TG1, *E. coli* DH5 α and *E. coli* SM10 (Table 2.6) were streaked from a -80 °C DMSO stock onto fresh LB plates and incubated overnight at 37 °C in a static incubator. A single colony was picked to inoculate 5 ml of LB in a ½ oz bijou jar and incubated at 37 °C for 16 hours, gentle shaking. Recombinant *E. coli* strains were grown on LB agar plates and in liquid culture, as described above but with an antibiotic selection to specifically select recombinant *E. coli* transformed with a plasmid carrying an antibiotic resistance gene. The appropriate antibiotic was added to the growth media at the following concentrations, unless otherwise stated: ampicillin (Ap; 50 µg/ml), Km (50 µg/ml) and streptomycin (Sm; 50 µg/ml).

2.1.4 Large-scale aerobic growth of *S. frigidimarina* EG301

Single colonies of *S. frigidimarina* EG301 containing pMB5 or pMB6 that were streaked from the prepared DMSO stock were picked to inoculate 1 x 100 ml of LB broth containing the appropriate antibiotics. The culture was grown with aeration (in a 250 ml conical flask) at 23 °C, with gentle shaking for approximately 18 hours to an OD₆₀₀ of 2.0. The overnight culture was extracted (20 ml) and subcultured in LB (1000 ml) supplemented with the appropriate antibiotics. The subculture was grown with aeration (in a 2.5 litre conical flask) at 23 °C for approximately 6-8 hours, with gentle shaking to an OD₆₀₀ of 0.5. The cells were induced with isopropylthiogalactoside (IPTG) to a final concentration of 1.0 mM and incubated overnight at 23 °C for 16 hours.

2.1.5 Large-scale aerobic growth of *E. coli*

Single colonies of recombinant *E. coli* containing plasmid pMB3 [*E. coli* (pMB3)] that were streaked from the prepared DMSO stock were picked to inoculate 1 x 100 ml of LB broth containing Ap (50 µg/ml). The culture was grown with aeration (in a 250 ml conical flask) at 37 °C, with gentle shaking for approximately 18 hours. The overnight culture was extracted (20 ml) and subcultured in 1000 ml of LB supplemented with Ap (25 µg/ml) to maintain the antibiotic selection. The subculture was grown with aeration (in a 2.5 litre conical flask) at 37 °C, with gentle shaking for approximately 2 hours 50 minutes to an OD₆₀₀ of 0.5. The cells were induced with IPTG (final concentration; 0.5 mM) and incubated overnight at 37 °C for 16 hours.

2.1.6 Preparation of *E. coli* cells for purification of FccA54

Cells that were pelleted from approximately 2.5 litres of *E. coli* TG1 (pMB3) were resuspended in 10 mM Tris buffer, pH 8.0 (200 ml). The resuspended cells were centrifuged (7,000 rpm, 20 minutes) and the supernatant was discarded. The pellet was completely resuspended in 60 ml 10 mM Tris buffer, pH 8.0 by using the stirrer block. The cells were incubated on ice and sonicated for 1 minute and left to stand for 1 minute over a duration of 10 minutes where the duty cycle was set to 50 % constant and the output control (micro tip limit) to 5.0 (Lucas Dawe Ultrasonics Soniprobe). Following sonication, the cells were then centrifuged (20,000 rpm, 20 minutes). The supernatant was extracted and more 10 mM Tris buffer, pH 8.0 was added to thin the sample for loading on the purification column. The sample was filter purified. Cell free extract (200 µl) was reserved for analysing on SDS-PAGE.

2.1.7 Preparation of *S. frigidimarina* EG301 cells for protein purification

A cell pellet of *S. frigidimarina* EG301 containing pMB5 obtained from 1000 ml of culture was washed in 10 mM Tris buffer pH 7.5 (100-200 ml) and centrifuged (9,000 rpm, 20 minutes). The supernatant was removed and the cell pellet was resuspended in 30 ml of Tris-HCl buffer, pH 8.4. The sample was sonicated, as before (2.1.6), then centrifuged (20,000 rpm, 30 minutes, 4 °C) and the supernatant was decanted and stored at -20 °C in 5 x 2 ml aliquots. The samples tended to precipitate when stored at -20 °C, therefore, prior to loading on the purification column, the samples were centrifuged (13,000 rpm, 5 minutes) and the required supernatant was transferred to a new tube.

2.1.8 Anaerobic growth of *Shewanella* species

S. frigidimarina NCIMB 400 minimal medium (Paul Dobbin, personal communication)

Per litre:

1.	(NH ₄) ₂ SO ₄	1.20 g
2.	K ₂ HPO ₄	1.00 g
3.	KH ₂ PO ₄	0.45 g
4.	NaHCO ₃	0.17 g
5.	MgSO ₄ ·7H ₂ O	0.25 g
6.	CaCl ₂ ·2H ₂ O	0.10 g
7.	Trace elements	50 ml
8.	Amino acids	0.1 ml

Components 1-6 were sequentially solubilised in sterilised distilled water in the order listed and the pH of the medium was adjusted to pH 7.4 using 5M NaOH (~100 µl). Prior to use as a growth medium, sterilised trace elements, amino acids and lactate were added. All solutions were made by solubilising the components in sterilised distilled water and filter sterilising using 0.2 µm filters.

Trace element solution*Per 2 litres:*

1.	Na ₂ EDTA	1.00 g
2.	H ₃ BO ₃	0.14 g
3.	NaCl	0.0234 g
4.	FeSO ₄ .7H ₂ O	0.06 g
5.	CoCl ₂ .6H ₂ O	0.05 g
6.	NiCl ₂ .6H ₂ O	0.05 g
7.	NaMoO ₄	0.04 g
8.	SeS ₂	0.01 g
9.	ZnSO ₄ .7H ₂ O	0.02 g
10.	CuSO ₄ .5H ₂ O	0.002 g
11.	MnSO ₄ .4H ₂ O	0.02 g

Amino acids*Per 100 ml:*

1.	L-Arginine	0.02 g
2.	L-Glutamate	0.02 g
3.	L-Serine	0.02 g

Carbon source

Lactate (1.5 M)

Final Concentration

15 mM

Electron Acceptor	Supplier	Type	Stock	Solution
Fumarate	Sigma	Disodium salt	0.5 M	dH ₂ O
Cinnamate	Aldrich	Free acid	0.3 M	dH ₂ O + Ethanol
Coumarate	Aldrich	Free acid	0.5 M	dH ₂ O + Ethanol
Caffeate	Aldrich	Free acid	0.3 M	dH ₂ O
Ferulate	Aldrich	Free acid	0.25 M	dH ₂ O
Acrylate	Aldrich	Free acid	0.5 M	dH ₂ O
Methacrylate	Sigma	Free acid	0.5 M	dH ₂ O
Mesaconate	Aldrich	Free acid	0.5 M	dH ₂ O
Tiglate	Sigma	Free acid	0.5 M	dH ₂ O + Ethanol
Crotonate	Sigma	Free acid	0.5 M	dH ₂ O
3-β-Indoleacrylate	n/a	Free acid	0.02 M	dH ₂ O + Ethanol
Senecioate	Aldrich	Free acid	0.3 M	dH ₂ O
Benzoate	Sigma	Free acid	0.5 M	dH ₂ O

The stock solutions of the electron acceptors were all adjusted to pH 7.0-8.1 using NaOH. The minimal media and all other solutions were stored at 4 °C. The minimal medium was preferably used within one week to avoid bacterial contamination. The supplemented minimal medium was dispensed into ½ oz bijou jars and the electron acceptor was added at a final concentration of 5 mM or 20 mM.

Single colonies of the *Shewanella* strain were picked to inoculate the jars. Alternatively, an overnight 5 ml culture of the *Shewanella* strain was centrifuged (5,000 rpm, 5 minutes) and the pellet resuspended in 5 ml minimal media (minus lactate). The resuspended cells (200 μ l) were used to inoculate the jars. The cultures were incubated at 23 °C for 4 weeks.

2.1.9 Colony counts of *Shewanella* strains

The *S. oneidensis* MR-1 or *S. oneidensis* MB5415 cultures (Table 2.6) grown in minimal media for four weeks were extracted (1.0 μ l) and diluted 1000-fold in sterilised distilled water (to 1 ml) in a 1.7 ml tube. The diluted solution was extracted (100 μ l) and plated on LB media using aseptic conditions. The plates were incubated at 23 °C for 2-3 days to allow the colonies to form. The number of bacterial cells per ml of culture was then calculated. To specifically select the mutant strain, aliquots of culture were plated on LB supplemented with Rm (10 μ g/ml) and Km (50 μ g/ml).

2.1.10 Single colonies of transformants

Transformant colonies of *E. coli* and *Shewanella* transconjugants were selected from the original plate using a sterile toothpick and under aseptic conditions were plated out for single colonies on fresh LB media containing the appropriate antibiotics. The single colonies were incubated overnight at 23 °C (*Shewanella* species) or 37 °C (*E. coli*). The single colonies were picked for growth in liquid culture as described in 2.1.2 and 2.1.3. DMSO stocks were made from these cultures prepared from single colonies (2.1.11).

2.1.11 Preparation of liquid culture –80 °C stocks

Freezer stocks were prepared for native and recombinant strains of *Shewanella* and *E. coli* for storage at – 80 °C. To a 1.7 ml tube, using aseptic conditions, 930 µl of dense overnight culture was mixed thoroughly with 70 µl of DMSO previously sterilised by autoclaving. The sample was stored at – 80 °C and was temporarily stored on ice to avoid defrosting when plating out for single colonies.

2.1.12 Optical density measurements

The optical density at a wavelength of 600 nm (OD₆₀₀) was measured by extracting 100 µl of cell culture and diluting 10 fold with 900 µl of LB in a plastic cuvette. The reference sample was 1 ml of LB. For cell cultures containing Rm (10 µg/ml), the reference also contained Rm (10 µg/ml).

2.2 Isolation and preparation of DNA

2.2.1 Preparation of plasmid DNA (QIAprep Spin Miniprep)

Plasmid DNA was isolated from *E. coli* and *Shewanella* strains using the QIAprep Spin Miniprep kit, following the protocol produced by the manufacturers (Qiagen). An overnight bacterial culture (5 ml) was used to produce 50 µl of high copy number plasmid DNA (~ 20 ng/µl). Low copy number plasmid DNA such as pMMB503EH was prepared from 10 ml of an overnight culture. All plasmid DNA preps were stored at -20 °C.

2.2.2 Preparation of plasmid DNA by alkaline lysis and PEG treatment

An overnight culture (5 ml) was centrifuged (5,000 rpm, 5 minutes) and the pellet was resuspended in triethylene glycol (TEG) buffer (200 µl). The sample was transferred to a 1.7 ml tube and mixed with freshly prepared alkaline lysis buffer (300 µl) and incubated on ice (5 minutes). The solution was neutralised with addition of 3M Sodium acetate, pH 5.2 (300 µl), mixed by inversion and incubated on ice (5 minutes). The cellular debris was removed by centrifuging (13,000 rpm, 15 minutes) and the supernatant was transferred to a 1.7 ml tube. The supernatant was extracted with Chloroform: isoamyl alcohol (24:1; 400 µl) and the upper aqueous phase (0.75 ml) was mixed with absolute isopropanol (0.75 ml) and incubated at 4 °C (30 minutes). The sample was centrifuged (13,000 rpm, 30 minutes), the isopropanol was completely removed and the DNA pellet was washed in 70 % ethanol (500 µl). The ethanol was removed and the DNA pellet was dried at room temperature (20 minutes).

The dried pellet was dissolved in 32 µl deionised water and mixed thoroughly with 4M NaCl (8.0 µl) and 13 % polyethylene glycol (PEG) 8000 (40.0 µl) then incubated on ice (20 minutes). The sample was centrifuged (13,000 rpm, 15 minutes, at 4 °C) and the DNA pellet was rinsed in 70 % ethanol (500 µl). The resulting purified DNA pellet was resuspended in deionised water (20 µl) and stored at -20 °C.

TEG buffer

25 mM Tris pH 8.0

10 mM EDTA pH 8.0

50 mM glucose

Alkaline lysis buffer

0.2 M NaOH

1 % SDS

2.2.3 Preparation and isolation of genomic DNA

A 1.5 ml aliquot of an overnight *S. oneidensis* MR-1 culture was centrifuged (13,000 rpm, 10 minutes) and the pellet was resuspended in 10 mM EDTA, pH 8.0 (400 µl). The cells were lysed using sodium dodecyl sulfate (SDS) to a final concentration of 1 %. The lysate was extracted with an equal volume of phenol (400 µl), phenol: chloroform: isoamyl alcohol (25:24:1) and chloroform: isoamyl alcohol (24:1). The DNA sample was ethanol precipitated by addition of 2.5 volumes of 100 % ethanol and 0.1 volumes of 3M sodium acetate, pH 5.2, followed by incubation (-80 °C, 1 hour). Following ethanol precipitation, the sample was centrifuged (13,000 rpm at 4°C, 10 minutes). The ethanol solution was carefully removed and the DNA pellet was washed in 70 % ethanol prior to being air-dried. The DNA pellet was re-suspended in 400 µl sterile water and further purified for future applications following the protocol of the Promega Wizard DNA Clean-Up System kit. The purified genomic DNA was eluted in 100 µl pre-warmed (80 °C) Tris-EDTA (TE) buffer, pH 8.0 and subsequently stored at -20 °C. Genomic DNA was prepared for potential *fccA54* and *fccB54* knockout strains using the same method.

2.2.4 Preparation of single-stranded DNA for automated sequencing

Recombinant cells containing a recombinant pGEM-T plasmid were grown overnight and subcultured to mid-log phase (OD_{600} of 0.5-0.7). The overnight culture (2 ml) was transferred to a ½ oz bijou jar and infected with 1.4 µl M13KO7 helper phage (Promega) and incubated (37 °C, 80 minutes). The infected cells (400 µl) were transferred to a 250 ml conical flask containing 10 ml LB supplemented with Ap (50 µg/ml) and Km (70 µg/ml) and incubated overnight (37 °C with gentle shaking). The overnight culture was divided into 6 x 1.5 ml aliquots in 1.7 ml tubes and centrifuged (13,000 rpm, 5 minutes). The supernatant from each tube (1.4 ml) was transferred to a clean tube and centrifuged (13,000 rpm, 5 minutes). The resulting supernatant from each tube was extracted, mixed with 2.0 M NaCl/20 % PEG 8000 (300 µl) and incubated (25 minutes, room temperature). The samples were centrifuged (13,000 rpm, 5 minutes) and the pellet in tube 1 was resuspended in TE buffer, pH 8.0 (200 µl). The solubilised pellet of tube 1 was transferred sequentially to the other tubes in order to combine the DNA samples. This procedure was repeated with TE buffer, pH 8.0 (100 µl), followed by phenol (400 µl) and Chloroform:isoamyl alcohol (24:1) (400 µl) extractions. The aqueous phase was mixed with 3M sodium acetate, pH 5.2 (40 µl) and absolute ethanol (1 ml) and incubated overnight at -20 °C. The precipitated DNA sample was centrifuged (13,000 rpm, 10 minutes, 4 °C) and the pellet was washed (75 % ethanol), air-dried (5-10 minutes) and resuspended in 50 µl TE buffer. The single-stranded DNA sample was stored at -20 °C.

TE buffer

10 mM Tris, pH 8.0

1 mM EDTA, pH 8.0

2.3 Restriction enzyme digests

Large-scale restriction digests of 2.5-7.5 kb plasmids were carried out in a total volume of 40-50 μ l in a 1.7 ml tube and incubated at 37 °C (28 °C for *Sma*I) for 3 hours. The reaction contained the appropriate restriction buffer (1 \times), acetylated bovine serum albumin (BSA; 0.1 mg/ml), plasmid DNA (0.10-0.25 μ g) and 30-50 units of each restriction enzyme (10-12 u/ μ l). For large-scale restriction digests of pMMB503EH (9.9 kb) and recombinant pMMB503EH, a greater quantity of plasmid (0.25-0.40 μ g) was used and required longer incubation at 37 °C (4 hours).

Pilot restriction digests of 2.5-7.5 kb plasmids were typically carried out in a total volume of 15.0 μ l in a 1.7 ml tube and incubated at 37 °C for 2-3 hours. The appropriate restriction enzyme buffer was added to a final concentration of 1 \times and the reaction was supplemented with BSA (0.1 mg/ml). Approximately 45-60 ng of plasmid DNA was incubated with 10-15 units of each restriction enzyme (10-12 u/ μ l) (Promega). Pilot restriction digests of large plasmids such as pMMB503EH (9.9 kb) were typically carried out in a total volume of 15-20 μ l in a 1.7 ml tube and incubated at 37 °C for 3-4 hours. Approximately 25-60 ng DNA was used.

2.4 Ligation reactions

The quantity of vector and insert DNA used in a ligation reaction depended upon the size of the fragment and plasmid vector. A range of vector: insert DNA molar ratios (1:1, 1:3 and 1:5) were typically used to increase the chance of successful ligation.

Ligation reactions (10-20 μ l) contained vector DNA of 2.5-7.5 kb (10-25 ng), insert DNA of 1-3 kb (10-50 ng), 1 \times ligase buffer, sterile water and T4 DNA ligase (1.5 units; Promega). Vector DNA such as pMMB503EH was added at 10-30 ng with 10-60 ng of insert DNA (1-3 kb in length). To enhance the ligation of blunt ends, hexaminecobalt chloride (HCC; 10 mM) was also added to the reaction tube at a final concentration of 1.0 mM. The reactions were gently mixed and incubated for a maximum of 16 hours at 16 °C. A 'vector only' control reaction was included in ligation experiments to obtain a background colony count for re-ligated vector.

2.5 Preparation of calcium competent cells

An overnight culture (200 μ l) of *E. coli* TG1, *E. coli* DH5 α , or *E. coli* SM10 (Table 2.6), was extracted and used to inoculate 5 ml of LB in a ½ oz bijou jar and was grown at 37 °C, gentle shaking for approximately 1.5 hours (*E. coli* TG1), 2.0 hours (*E. coli* SM10) or 2.5 hours (*E. coli* DH5 α) to an OD₆₀₀ of 0.4-0.6. The cells were centrifuged (5,000 rpm, 3 minutes) and the cell pellet was resuspended in 0.1 M pre-chilled (4 °C) CaCl₂ (2 ml) and stored on ice for 40 minutes. The chilled CaCl₂ treated cells were centrifuged (5,000 rpm, 3 minutes) and the cell pellet was resuspended in 0.1 M of pre-chilled (4 °C) CaCl₂ (1 ml) and the resuspended cells were stored on ice for a minimum duration of 40 minutes.

2.6 Transformation and selection of transformants

The CaCl₂ competent cells (200 µl) (2.5) were transferred to a 1.7 ml pre-chilled tube (4 °C) using pre-chilled pipette tips (4 °C). Half of the ligation mix was added directly to the cells with pre-chilled pipette tips (4 °C) and mixed gently. For plasmid DNA transfer from *E. coli* TG1 to *E. coli* SM10, plasmid DNA (10-30 ng) was added directly to the calcium competent *E. coli* SM10 cells. The transformation was carried out at 4 °C. The transformed cells were incubated on ice for 45 minutes and then heat shocked in a water bath (45 °C, 100 seconds). The cells were then immediately incubated on an ice-slurry (5 minutes). LB (800 µl) was added and the samples were incubated at 37 °C (1 hour). The cells were centrifuged (13,000 rpm, 3 minutes) and each cell pellet was resuspended in residual LB media (100 µl). The transformed cells (100 µl) were then plated on LB agar plates containing the appropriate antibiotic and incubated overnight at 37 °C in a static incubator. A ‘cells only’ control was included in all transformations to show that the antibiotic selection was effective. A ‘positive control’ to show transformation efficiency was achieved by transforming cells with recombinant plasmid (10 ng). Cells transformed with recombinant pGEM-T plasmid containing a disrupted *lacZ* gene were selected on LB supplemented with Ap (50 µg/ml) that contained a top layer of 5-bromo-4-chloro-3-indolyl- β -D-galactoside (Xgal) and IPTG. A solution comprising 40.0 µl of Xgal (40 mg/ml), 4.0 µl of IPTG (1 M) and sterile water (40.0 µl) was spread onto the surface of dried LB-Ap agar plates at least one hour prior to plating the transformants.

2.7 Conjugative transfer of DNA from *E. coli* to *Shewanella* species

E. coli SM10 (Table 2.6) was used as the donor strain for conjugative DNA transfer of recombinant pMMB503EH plasmids (Table 2.8) to *S. frigidimarina* EG301 Rm^R Km^R (Table 2.6). The *S. oneidensis* MR-1 Rm^R and *E. coli* S17 λ pir strains (Table 2.6) were used as the recipient and donor strains, respectively, for conjugative DNA transfer of plasmid pMBGK15 (Table 2.7) used for construction of the *fccA54* and *fccB54* gene knockout.

The *E. coli* and *Shewanella* strains were grown to an OD₆₀₀ of 0.8. An aliquot of each culture (1.5 ml) was centrifuged (13,000 rpm, 5 minutes) and the pellets were resuspended in LB (200 μ l). The *E. coli* culture (5.0 μ l) was mixed with the *Shewanella* culture (45 μ l) and the 50 μ l mixes were spotted onto 0.2 μ m sterile nitrocellulose filters (Whatman) and incubated on LB only medium overnight at 23 °C (static incubator). Samples (50 μ l) of '*E. coli* only' and '*Shewanella* only' were included as controls to show that the antibiotic resistant transconjugants were *Shewanella* strains containing recombinant plasmid. The filters were removed from the LB plates using sterile tweezers, transferred to 1.7 ml tubes containing LB (1 ml) and vortexed to suspend the bacteria in solution. The clean filters were removed, the samples centrifuged (13,000 rpm, 10 minutes) and the pellet resuspended in LB according to protocol 1 or 2 [overleaf].

1. Standard conjugation:

The pellets were resuspended in LB (1 ml) and 1.0 μ l was extracted and mixed with LB (49 μ l). The 50 μ l sample was mixed gently, plated on LB supplemented with the appropriate antibiotics for selection of the bacterial strain and plasmid and incubated at 23 °C in a static incubator for 2-3 days.

2. Conjugation for constructing an *fccA54* and *fccB54* gene knockout:

The pellets were resuspended in 100 μ l LB and the entire concentrated sample was plated on LB supplemented with Rm (10 μ g/ml) and Km (50 μ g/ml). The plates were incubated at 23 °C for 3 days in a static incubator for development of *S. oneidensis* MR-1 transconjugants.

2.8 The Polymerase Chain Reaction

2.8.1 PCR amplification using *PfuTurbo*

The homologous template DNA fusion PCR product used to construct the *fccA54* and *fccB54* gene knockout was amplified from the *S. oneidensis* MR-1 genome using the high fidelity thermostable DNA polymerase, *PfuTurbo* (Stratagene). The reactions for each of the three individual fusion PCR amplifications varied in the DNA template: primer ratio. Equivalent quantities of PCR product were used for the final fusion PCR. Ammonium chloride (NH₄Cl) was added to some reactions at varying concentrations to alter the enzyme activity and the PCR products were amplified using the programmed thermocycler conditions (Techne PHC-2 thermal cycler; Table 2.1). All PCR reactions detailed in the following section were thoroughly mixed and sealed with an overlay of mineral oil (50 μ l).

Reaction component	Quantity/concentration
DNA template:	
Genomic DNA	10-45 ng
PCR product	6.0-20.0 ng
Primers (Table 2.9)	25 pmol/μl
dNTPs (Roche) (10 mM)	0.4 mM
10 × Mg ²⁺ reaction buffer	5.0 μl
NH ₄ Cl (100 mM)	2-8 mM
<i>PfuTurbo</i> (2.5 u/μl)	2.5 u

Total reaction volume	50 μl

Program	Number of Cycles	Temperature (°C)	Duration
40	1	94	2 minutes
41	30	94	30 seconds
		a	30 seconds
		72	b
42	2	72	10 minutes
		4	24 hours

Table 2.1: PCR cycling parameters when using *PfuTurbo* DNA polymerase

The temperature and duration of thermocycles for PCR amplification using *PfuTurbo* DNA polymerase is shown. These are the optimised parameters to ensure efficient and accurate PCR amplification by *Pfuturbo*. The primer annealing temperature (^a) was set 5 °C below the lowest T_m (°C) in the primer pair. The extension time (^b) was programmed to allow 1 minute per 1 kb of amplified DNA sequence. The program numbers 40-42 refer to the programs set for PCR on the specified thermocycler.

2.8.2 PCR amplification using *Taq* DNA polymerase

The genes encoding the novel flavocytochromes, including IfcA-1, were amplified from the *S. oneidensis* MR-1 genome using *Taq* DNA polymerase (Promega), according to the thermocycler conditions (Table 2.2). The following conditions were used:

Reaction component	Quantity/concentration
Genomic template DNA	40.0 ng
Primers (Tables 2.10 and 2.11)	5.0 pmol/μl
dNTPs (Roche) (10 mM)	0.4 mM
10 × Mg ²⁺ reaction buffer	5.0 μl
<i>Taq</i> (5 u/μl)	1.25 u

Total reaction volume	50 μl

Program	Number of Cycles	Temperature (°C)	Duration
40	1	94	5 minutes
41	30	94	30 seconds
		42	30 seconds
		72	1 minute
42	2	72	5 minutes
		4	24 hours

Table 2.2: PCR cycling parameters when using *Taq* DNA polymerase
The temperature and duration of thermocycles for PCR amplification using *Taq* DNA polymerase is shown. The primer annealing temperature was set below the lowest T_m (°C) in the primer pair. The extension time was programmed to allow 1 minute per 1 kb of amplified DNA sequence. The program numbers 40-42 refer to the programs set for PCR on the specified thermocycler.

The PCR amplification product named 54FRB corresponding to the *fccA54* (including signal sequence) and *fccB54* genes was amplified using different conditions to those shown above. A total of six PCR reactions with varying concentrations of genomic DNA template were used to achieve PCR amplification of 54FRB. The thermocycler conditions used were specific for PCR amplification of the 54FRB fragment (Table 2.3).

Reaction component	Quantity/concentration
Genomic DNA	10-40 ng
54F and 54RB primers (Table 2.10)	30 pmol/μl
dNTPs (Roche) 10 mM	0.2 mM
10 × magnesium free buffer	5.0 μl
MgCl ₂ (25 mM)	1.5 mM
NH ₄ Cl (100 mM)	2.0-8.0 mM
<i>Taq</i> (5 u/μl)	5 u

Total reaction volume	50 μl

Program	Number of Cycles	Temperature (°C)	Duration
40	1	94	2.5 minutes
41	30	94	20 seconds
		50	30 seconds
		68	2 minutes
42	2	68	5 minutes
		4	24 hours

Table 2.3: PCR cycling parameters when using *Taq* DNA polymerase

The temperature and duration of thermocycles for PCR amplification of 54FRB using *Taq* DNA polymerase is shown. The primer annealing temperature was set 6 °C below the lowest T_m (°C) in the primer pair. The extension time was programmed to allow 1 minute per 1 kb of amplified DNA sequence. The temperature during extension was adjusted to 68 °C, which is the preferred temperature for optimal *Taq* PCR amplification. The program numbers 40-42 refer to the programs set for PCR on the specified thermocycler.

The FccA54 overexpression fragment was amplified from plasmid DNA using *Taq* DNA polymerase and equal quantities of PCR product (4.0-10.0 ng DNA) were used in the final fusion PCR. The thermocycler conditions are shown (Table 2.4).

Reaction component	Quantity/concentration
Plasmid DNA	1.5-15.0 ng
Primers (Table 2.10)	5 pmol/μl
dNTPs (Roche) (10 mM)	0.2 mM
10 × Magnesium free buffer	5.0 μl
MgCl ₂ (25 mM)	1.5 mM
NH ₄ Cl (100 mM)	2.0- 4.0 mM
<i>Taq</i> (5 u/μl)	2.5 u

Total reaction volume	50 μl

Program	Number of Cycles	Temperature (°C)	Duration
40	1	94	3.0 minutes
41	30	94	30 seconds
		^a	25 seconds
		68	^b
42	2	68	10 minutes
		4	24 hours

Table 2.4: PCR cycling parameters when using *Taq* DNA polymerase
The temperature and duration of thermocycles for fusion PCR amplification of the FccA54 overexpression fragment using *Taq* DNA polymerase is shown. The primer annealing temperature (^a) was set 5 °C below the lowest T_m (°C) in the primer pair. The extension time (^b) was programmed to allow 1 minute per 1 kb of amplified DNA sequence. The temperature during extension was adjusted to 68 °C, which is the preferred temperature for optimal *Taq* PCR amplification. The program numbers 40-42 refer to the programs set for PCR on the specified thermocycler.

The PCR product cloned in pMBGK41 that was amplified using primers 54gk9 and 54gk10 to confirm that *S. oneidensis* MB5415 was a deletion strain was PCR amplified using *Taq* DNA polymerase. Five reactions differing in concentrations of genomic DNA template DNA were used to achieve PCR amplification of the segment containing the kanamycin cassette. The thermocycler conditions specified for PCR amplification of the *S. oneidensis* MB5415 fragment are shown (Table 2.5).

Reaction component	Quantity/concentration
Genomic DNA	10-40 ng
Primers (Table 2.9)	20 pmol/μl
dNTPs (Roche) 10 mM	0.2 mM
10 × MgCl ₂ free buffer	5.0 μl
MgCl ₂ (25 mM)	1.5 mM
<i>Taq</i> (5 u/μl)	2.5 u

Total reaction volume	50 μl

Program	Number of Cycles	Temperature (°C)	Duration
40	1	94	3 minutes
41	30	94	30 seconds
		54	30 seconds
		68	3 minutes
42	2	68	10 minutes
		4	24 hours

Table 2.5: PCR cycling parameters when using *Taq* DNA polymerase
The temperature and duration of thermocycles for PCR amplification of the *S. oneidensis* MB5415 fragment containing the kanamycin cassette using *Taq* DNA polymerase is shown. The primer annealing temperature was set 5 °C below the lowest T_m (°C) in the primer pair. The extension time was programmed to allow 1 minute per 1 kb of amplified DNA sequence. The temperature during extension was adjusted to 68 °C, which is the preferred temperature for optimal *Taq* PCR amplification. The program numbers 40-42 refer to the programs set for PCR on the specified thermocycler.

2.9 Preparation of samples for automated sequencing

Automated cycle sequencing was used to sequence single-stranded and double-stranded DNA templates. The samples were mixed in 0.6 ml tubes suitable for use in the thermocycler (Techne PHC-2 thermal cycler) and were prepared as follows:

Reaction components	Quantity
DNA template:	
Single-stranded	50-100 ng
Double-stranded	250-500 ng
Primer	3.2 pmol
Terminator ready reaction mix	8.0 μ l

Total reaction volume	20 μ l

The terminator ready reaction mix ('ABI PRISM' dRhodamine terminator cycle sequencing kit) comprises dye-labelled terminators; dATP, dCTP, dTTP, dITP; Tris HCl, pH 9.0; MgCl₂, thermal stable pyrophosphatase and AmpliTaq DNA polymerase FS). The samples were mixed and overlayed with mineral oil (40 μ l).

The thermocycler conditions comprising 25 cycles were as follows: denaturation (96 °C, 30 seconds), annealing (50 °C, 15 seconds) and extension (60 °C, 4 minutes).

The samples were removed from beneath the mineral oil, transferred to a clean tube and ethanol precipitated overnight at -20 °C (40 μ l of 100 % ethanol, and 2.0 μ l of 3M sodium acetate, pH 5.2). The samples were centrifuged (13,000 rpm, 20 minutes), washed in 50 μ l ethanol (70 %) and air-dried for 20 minutes. The samples were processed by the Institute of Cell and Molecular Biology Automated Sequencing service using the ABI 3100 genetic analyser.

2.10 Purification of PCR products and restriction fragments

Purification of a specific PCR product in a reaction sample and purification of DNA in a restriction digest were achieved using agarose gel electrophoresis. The sample (50 µl) was mixed with 10.0 µl gel loading buffer (10 ×) and loaded in three fused wells of a 0.7 % preparative agarose gel (Appligene). Following gel electrophoresis, the desired DNA band was excised from the gel and purified using the QIAEX II Gel Extraction kit (Qiagen) or the QIAquick gel extraction kit (Qiagen) according to the manufacturer's protocol. Confirmation that the correct DNA fragment was purified was achieved by loading a sample of the purified product on a standard 0.7 % agarose gel (Bioline). Ethanol precipitation was used to purify linear DNA generated from single restriction enzyme digests. A 50 µl digest was combined with 3M Sodium acetate pH 5.2 (5.0 µl) and 100 % ethanol (125 µl) and incubated overnight at -20 °C. The sample was then centrifuged (13,000 rpm, 10 minutes, 4 °C), washed in 70 % ethanol and air-dried.

2.11 Detection and analysis of DNA samples

DNA samples from genomic DNA preps, plasmid DNA preps and PCR were analysed using agarose gel electrophoresis. A 0.7 % agarose gel was typically made unless otherwise stated by using standard agarose (Bioline) and heating with 1 × Tris-acetate-EDTA (TAE) buffer to a final volume of 25 ml for small gels and 70 ml for long gels. Ethidium bromide (10 mg/ml) was added to the solution upon cooling to a final concentration of 1.0 µg/ml.

The DNA bands were detected upon ultraviolet irradiation. 1 kb DNA ladder (GibcoBRL; 4.5 μ l) was used as a marker to detect the molecular weight of the sample DNA bands apparent on the agarose gel. Samples (2.0-3.0 μ l) for loading on the agarose gels were mixed with loading buffer (4.0 μ l).

50 \times TAE buffer

Tris-acetate	2.0 M
EDTA, pH 8.0	50 mM

2.12 IPTG induction experiments

Small-scale induction experiments were used to identify the optimal duration of IPTG induction. A control culture corresponding to the parent strain was included in the experiment to show the level of overexpressed protein produced in the recombinant strain. *E. coli* TG1 (1 \times 5 ml) and *E. coli* (pMB3) cultures (2 \times 5 ml) were grown to an OD₆₀₀ of 0.4. The *E. coli* TG1 culture was divided into 5 \times 1 ml aliquots each added to a clean ½ oz bijou jar. Recombinant *E. coli* TG1 (pMB3) cultures were divided as 10 \times 1 ml aliquots into clean ½ oz bijoux jars. To five of the 1 ml *E. coli* TG1 (pMB3) cultures, 1 mM IPTG (1 M stock) was added. Ampicillin (25 μ g/ml) was added to the appropriate cultures to maintain antibiotic selection. Each of the 5 \times 1 ml cultures of *E. coli* TG1 were grown in parallel with 5 \times 1 ml IPTG-induced and 5 \times 1 ml uninduced cultures of *E. coli* (pMB3) for 1 hour, 2 hours, 4 hours and 16 hours, post IPTG induction. Growth of the cultures was arrested at these times and the OD₆₀₀ was measured. Cultures were also extracted immediately after IPTG induction (0 hour control). The 1 ml culture was transferred to a 1.7 ml tube and centrifuged (13,000 rpm, 10 minutes).

The supernatant was discarded and the pellet was resuspended in $3 \times$ SDS-loading buffer (New England Biolabs), as follows: $OD_{600} = 0.50$, resuspend in $0.50 \mu\text{l}$ SDS loading buffer. Small-scale IPTG induction experiments for cultures of *Shewanella* strains were prepared as described above, except that the initial overnight cultures of parent and recombinant *S. frigidimarina* EG301 (pMB5 or pMB6) were grown to an OD_{600} of 0.5-0.6. The antibiotics, comprising, Rm ($5 \mu\text{g/ml}$), Km ($25 \mu\text{g/ml}$) and Sm ($25 \mu\text{g/ml}$) were added to the appropriate cultures prior to IPTG induction to maintain the antibiotic selection.

2.13 Tris-glycine SDS polyacrylamide gel electrophoresis

The protein samples (2.12) resuspended in $3 \times$ SDS-loading buffer (New England Biolabs) were boiled for 3-5 minutes prior to loading $10\text{-}20 \mu\text{l}$ of each sample on the SDS-PAGE mini gel. Prestained broad range protein marker ($13 \mu\text{l}$; New England Biolabs) was mixed with $5.0 \mu\text{l}$ $3 \times$ SDS-loading buffer and incubated in a hot water bath prior to loading on the SDS-PAGE gel.

A 10 % (w/v) acrylamide resolving gel (10 ml) (A) and a 5 % (w/v) acrylamide stacking gel (4 ml) (B) were prepared to pour 2 mini SDS-PAGE gels. The components were mixed in the order listed overleaf. The 10 % (w/v) ammonium persulfate (APS) solution was freshly prepared immediately prior to making the SDS-PAGE gel. Tris-glycine electrophoresis buffer, pH 8.3 ($1 \times$) was used in the reservoirs of the gel system to provide a discontinuous system.

The SDS-PAGE gels were run at 200 V for approximately 1 hour to achieve good separation of the proteins. The mini-Protean gel electrophoresis SDS-PAGE system was used (Biorad).

A long (20.0 cm) 10 % (w/v) acrylamide gel was prepared by making a 35 ml acrylamide resolving gel (A) and a 5 % (w/v) acrylamide stacking gel (15 ml; B). The volumes of the components listed were scaled up accordingly. The protein samples (2.12) and protein marker were prepared as described above. 20 μ l of sample and 30 μ l of protein marker were loaded on the long SDS-PAGE gel. The duration of electrophoresis for the long gel was approximately 6 hours at 200 V.

Components of A	(ml)	Components of B	(ml)
H ₂ O	4.0	H ₂ O	2.7
30 % acrylamide mix	3.3	30 % acrylamide mix	0.67
1.5 M Tris (pH 8.8)	2.5	1.0 M Tris (pH 6.8)	0.5
10 % SDS	0.1	10 % SDS	0.04
10 % ammonium persulfate	0.1	10 % ammonium persulfate	0.04
TEMED	0.004	TEMED	0.004

A 5 \times stock solution of Tris-glycine buffer, pH 8.3, was made by dissolving 15.1 g of Tris base and 94.0 g of glycine in 900 ml of deionised H₂O. 10 % SDS (50 ml) was then added and the volume was adjusted to 1000 ml with dH₂O. The pH of the solution was checked.

1 \times Tris-glycine buffer, pH 8.3

25 mM Tris, pH 8.3
250 mM glycine (electrophoresis grade)
0.1 % SDS

The NuPAGE electrophoresis system (Invitrogen) that operates at neutral pH was used to achieve accurate migration of FccA54. The Bis-Tris pre-cast gels with a 4-12 % acrylamide concentration were used according to the manufacturers instructions. Protein samples (10 μ l) eluted from a purification column were resuspended in 4 \times NuPAGE lithium dodecyl sulfate (LDS) sample buffer (10 μ l) in a final volume of 40 μ l and boiled for 5 minutes prior to loading on the acrylamide gel. NuPAGE 2-(N-morpholino)ethane sulfonic acid (MES) SDS running buffer (1 \times) was used in the reservoir chambers of the electrophoresis system. For periplasmic samples, a range of protein concentrations were tested, the volume of protein loaded on the gel ranged from 5-20 μ l.

2.14 Staining of SDS-PAGE gels

2.14.1 Coomassie Blue staining of SDS-PAGE gels

Coomassie Blue was used to stain the SDS-PAGE gels for approximately 1-2 hours, with gentle shaking, to detect all the proteins in each sample loaded on the SDS-PAGE gel. The gel was subsequently incubated in destaining solution to reveal the proteins.

Coomassie Brilliant Blue stain

0.25 % (w/v) Coomassie Brilliant Blue R250
in destaining solution

Destaining solution

45 % methanol
45 % dH₂O
10 % glacial acetic acid

2.14.2 Silver staining of SDS-PAGE gels

The SDS-PAGE gels were fixed for 4-12 hours in a 100 ml solution comprising ethanol: glacial acetic acid: water (30: 10: 60). The fixing solution was discarded and the gel was incubated twice in 5 gel volumes of 30 % ethanol for 30 minutes. The gel was washed three times in 10 gel volumes of water for 10 minutes. The gel was incubated in 5 gel volumes of 0.1 % silver nitrate for 30 minutes. The silver nitrate was discarded and the gel was washed in water. 5 volumes of 2.5 % sodium carbonate and 0.2 % formaldehyde were added. The reaction was quenched by addition of 1.0 % acetic acid for 3 minutes followed by washes with water.

2.14.3 Cytochrome haem staining

The SDS-PAGE gel was washed in 100 ml of haem staining solution A and incubated (gentle shaking, 5-10 minutes). The components of solution A were added in the order listed. Solution A was discarded and replaced with 100 ml haem staining solution B, mixed gently and immediately incubated in the dark for 15 minutes. The gel was removed from the dark and 1 ml of hydrogen peroxide was added, the gel was incubated for several minutes, gentle shaking until the bands were visible. The reaction was stopped with addition of dH₂O.

Haem staining solution A

- (1) 30 ml methanol
- (2) 60 ml dH₂O
- (3) 10 ml 2.5 M Sodium acetate pH 5.2

Haem staining solution B

Haem staining solution A containing
40 µg 3,3',5,5'-Tetramethylbenzidine
Dihydrochloride solubilised in (1)

2.15 Periplasmic extraction

The periplasm was prepared from a 500 ml culture of recombinant *S. frigidimarina* EG301 (2.1.4). The large scale overnight culture was centrifuged (9,000 rpm, 20 minutes) and the cell pellet was resuspended in 10 mM Tris HCl, pH 7.0, containing 0.1 M NaCl (200 ml). The washed cells were centrifuged (9,000 rpm, 20 minutes) and the pellet was resuspended in 0.1 M Tris-HCl, pH 8.0 containing 0.5 M sucrose (50 ml) and transferred to a small centrifuge pot. When the cells were completely resuspended, 200 mM EDTA, pH 9.0 was added to a final concentration of 1 mM and the cells were incubated at room temperature for 20 minutes. The cells were then centrifuged (13,000 rpm, 20 minutes). The light orange supernatant was decanted and the orange/red pellets were resuspended in 50 ml dH₂O. The cells were incubated at room temperature for 5-10 minutes until they became dense. At this stage, 2.5 M Magnesium Chloride (MgCl₂) was added to a final concentration of 1 mM to stop the reaction. The cells were centrifuged (13,000 rpm, 20 minutes) and the soluble periplasmic fraction was decanted. The periplasm was stored in 25 ml volumes at -20 °C.

2.16 Purification of FccA54 from *E. coli* TG1 (pMB3)

The FccA54 protein was purified using a HiLoad 26/10 Q-Sepharose HP (Amersham Pharmacia Biotech) anion exchanger column (53 ml; packed length of 10 cm) with the fast performance liquid chromatography (FPLC) AKTA system (Amersham Pharmacia Biotech). The column was equilibrated with 10 mM Tris buffer pH 8.0 (buffer A) and the sample (pH 8.0) containing 1.2 g of total protein was loaded onto the column. The flow rate was set to 1 ml per minute.

A salt gradient of 0-100 % 10 mM Tris buffer, pH 8.0, containing 1 M NaCl (buffer B) in 11 column volumes was used to elute proteins adsorbed to the positively charged matrix. The chromatography system was set to measure the ultraviolet (UV) spectra of the protein fractions collected. The absorbance spectra (280-680 nm) were measured for the fractions that were yellow or that showed traces of yellow. The spectrophotometer was blanked with 10 mM Tris buffer, pH 8.0.

2.17 Protein concentration

A centrifugal protein-concentrating filter (Vivaspin 20; 10 kDa) was used to concentrate the protein fractions containing the highest concentration of FccA54. The filters were rinsed with dH₂O and centrifuged (20 minutes, 7,000 rpm) prior to concentration of the protein.

2.18 Co-purification of FccA54 and FccB54

The Biocad purification system was used to assess the best conditions for co-purification of the FccA54 and FccB54 subunits. A Poros 20 HS 1.66 ml cation exchanger column (4.6 mm in diameter and 100 mm in length) was used on the automated protein purification system. The flow rate was set to 5.00 ml per minute. The column was equilibrated with 10 mM Tris HCl, pH 7.0. Any protein bound to the negatively charged column was eluted during a salt gradient of 0-100 % 10 mM Tris HCl, pH 7.0 containing 2.0 M NaCl in 37 column volumes. The sample (2.1.7) (2 ml) was loaded on the column by injection into the loop. The fractions were collected in 1.40 ml volumes. The UV absorption spectra were measured at 254 nm and 280 nm.

2.19 Fumarate reduction assay

A purified sample of FccA54 was tested for fumarate reductase activity using a spectrophotometer (Shimadzu UV-PC-1201) enclosed in an anaerobic chamber at 25 °C and less than 6 parts per million (ppm) of oxygen. The fumarate-dependent reoxidation of reduced methyl viologen was monitored at 600 nm. The standard fumarate reductase assay buffer (1 ml) was adjusted to the correct pH using Trizma base (pH 7.0). Methyl viologen was reduced with addition of sodium dithionite until an absorbance reading of approximately 1.0 was obtained at A_{660} nm. Fumarate adjusted to pH 7.0 (500 μ M) was added and the reaction initiated by the addition of purified FccA54 protein in 10 mM Tris buffer, pH 7.2 (5.0 μ M).

Fumarate reductase assay buffer

Component	Amount per litre
(1M) Hydrochloric acid	50 ml
NaCl	26.3 g
Methyl viologen	5.5 g

2.20 Succinate oxidation assay

The ability of FccA54 to catalyse succinate oxidation was determined spectrophotometrically (Shimadzu UV-PC-1201) under aerobic conditions. The assay buffer (1) was added to a cuvette with ferricyanide (FeCN) as the electron acceptor (2) and succinate as the electron donor (3). The rate of succinate oxidation was monitored upon addition of 5.0 μ M FccA54 (4) at a wavelength of 420 nm, over a period of 10 minutes.

1. 1.5 M Cyclo-hexylaminoethanesulfonic acid (CHES) buffer pH 9.0 (1 ml)
2. 1.0 M FeCN (5.0 μ l)
3. 1.0 M succinate (100 μ l)
4. FccA54 protein sample

2.21 Preparation of samples for N-terminal Sequencing

The protein samples to be sequenced were provided on a Western blot that was obtained using the NOVEX Xcell II blotting apparatus (Invitrogen). The protein samples were run on a pre-cast gel (2.13) and then transferred onto a pre-cut polyvinylidene fluoride (PVDF) blotting membrane. The Western blotting protocol was followed according to the manufacturer's instructions (Invitrogen). The Western blot was Coomassie stained and the desired bands were cut as a single strip and transferred to a 1.7 ml tube that was stored at -20°C until use. For sequencing of cytochrome proteins, the Western blot was divided in two and stained with Coomassie blue and haem staining solution, respectively. Alignment of the blots was subsequently used to estimate the position of the cytochromes on the Coomassie stained Western blot. The desired 'bands' were cut from the Coomassie stained Western blot and provided as a sample for N-terminal Edman sequencing, carried out on an Applied Biosystems Procise 4HT microsequencer.

2.22 Preparation of samples for mass spectrometry

The sample of FccA54 for mass spectrometry was taken from a culture of *E. coli* TG1 (pMB3) that was induced with 1 mM IPTG for overexpression of FccA54 (2.1.5). The overnight cultures were centrifuged (13,000 rpm, 30 minutes), the supernatant removed and the pellet resuspended in 10 mM Tris buffer, pH 7.5 (3.6 ml). The cells were sonicated and centrifuged (13,000 rpm, 30 minutes). The supernatant was extracted and was used for obtaining a mass spectrometry result.

A liquid chromatography-mass spectrometry (LS-MS) instrument comprising a C5 reverse phase column (Waters 2790 HPLC) was used to desalt the protein sample. The sample was analysed using positive electrospray ionisation on a Micromass platform mass spectrometer.

The sample obtained for mass spectrometry of FccB54 was obtained from a culture of *S. frigidimarina* EG301 (pMB5) (2.1.4) that was induced with IPTG (1 mM) for 16 hours. The OD₆₀₀ was measured for the overnight culture; 1 ml of culture was extracted and added to a clean 1.7 ml tube. The culture was centrifuged (13,000 rpm, 10 minutes) and the cell pellet was resuspended in loading buffer minus SDS according to the formula, where the OD₆₀₀ is 0.5, the cell pellet is resuspended in solution to a volume of 50 µl. The sample was stored at -20 °C. The mass spectrometry analyses were carried out on an Applied Biosystems Voyager DE-STR matrix-assisted laser/desorption ionisation, time of flight (MALDI-TOF) instrument.

2.23 Homology modelling

A sequence and secondary structures prediction tool was used to generate optimised pairwise sequence alignments including secondary structure prediction for each flavoprotein (FccA54, FccA56 and FccA342) against Fcc₃ (*S. frigidimarina* NCIMB400) (http://www.icmb.ed.ac.uk/sss_align/sss_align.html). These sequence alignments were subsequently used to construct homology models of each flavoprotein catalytic domain using SYBYL Composer (Blundell *et al.*, 1988). The active site of the Fcc₃ enzyme was used as a molecular framework to structurally align each flavoenzyme as predicted from the sequence alignments.

The initial seed alignments of each flavin domain against Fcc₃ that were produced by SYBYL Composer were modified to achieve the best structural alignments. The exact length of each signal sequence is unknown for the novel flavoproteins and double-arginine signal sequences tend to be longer than standard Sec peptides. Therefore, to ensure only mature protein was modelled, the amino acid sequences of FccA54, FccA56 and FccA342 used for molecular modelling began three residues upstream of the highly conserved FAD-adenine ring-binding site. A molecular mechanics algorithm incorporated in the program suite CNS was used to refine the holoenzyme models produced by SYBYL Composer. Minimisation functions were used to optimise the side chain orientations in the flavoenzymes and to minimise any strain in the models. Backbone atoms shifts were restrained to prevent any large alterations in the polypeptide backbone.

2.24 Plasmids, bacterial strains and primers

Bacterial Strain	Genotype/ Description	Source/ Reference
<i>E. coli</i> DH5 α	<i>supE44 ΔlacU169 (φ80 lacZ ΔM15) hsdR17 recA1 endA1 gyrA96 thi-1 relA1</i>	Lab stock
<i>E. coli</i> TG1	<i>supE hsdΔ5 thi (Δlac-proAB) F' [traD36 proAB⁺ lacI^q lacZΔM15]</i>	Lab stock
<i>E. coli</i> S17 λ pir	Tp ^R Sm ^R <i>recA</i> , <i>thi</i> , <i>pro</i> , <i>hsdR</i> M ⁺ RP4: 2-Tc:Mu: Km Tn7 λ pir	Lab stock
<i>E. coli</i> SM10	<i>thi-1 thr leu tonA lacY supE recA::RP4-2-Tc::Mu (Km^R)</i>	Lab stock
<i>S. oneidensis</i> MR-1	Wild type manganese reducing strain, isolated from sediments of Lake Oneida, New York	Lab stock
<i>S. oneidensis</i> MR-1Rm ^R	Spontaneous rifampicin resistant strain	Lab stock
<i>S. frigidimarina</i> EG301	<i>S. frigidimarina</i> NCIMB 400 Rm ^R , $\Delta fcc_3::ahp$ Km ^R	Gordon, 1996
<i>S. oneidensis</i> MB5415	<i>S. oneidensis</i> MR-1 Rm ^R , $\Delta fccAB54::ahp$ Km ^R ; Cm ^S	This work
<i>S. oneidensis</i> MB5413	<i>S. oneidensis</i> MR-1 Rm ^R , Km ^R , Cm ^S	This work
<i>S. oneidensis</i> MB541	<i>S. oneidensis</i> MR-1 Rm ^R , Km ^R , Cm ^R	This work

Table 2.6: Bacterial strains used and constructed

The bacterial strains that were used for transformation and conjugation of plasmid constructs for protein overexpression are shown. Details of the *S. oneidensis* MB5415 and *S. oneidensis* MB5413 strains that were constructed in this work are also shown.

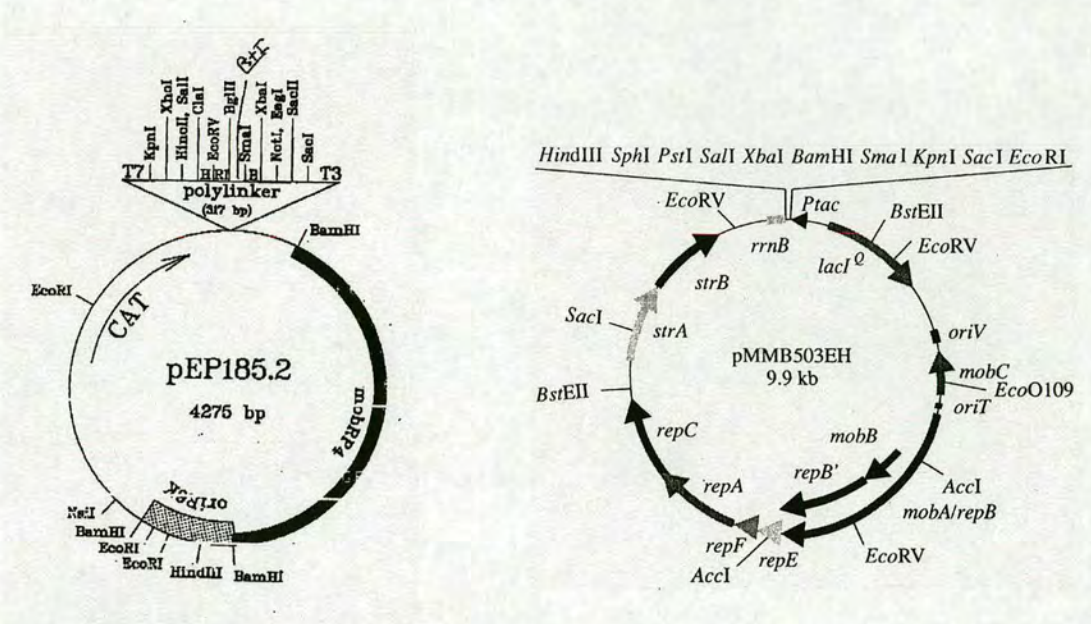


Figure 2.1 Selected plasmid maps
The pEP185.2 suicide plasmid (Pepe and Miller, 1993) was used to construct a deletion mutant of *S. oneidensis* MR-1 Rm^R. The pMMB503EH overexpression plasmid (Overbye Michel *et al.*, 1995) was used for protein overexpression in *Shewanella* species.

Plasmid	Host	Properties	Source/Reference
pUC19	<i>E. coli</i> DH5α	Cloning plasmid, 2686 bp; Ap ^R	Yanisch-Perron <i>et al.</i> , 1985
pEP185.2	<i>E. coli</i> VM229 Sy327λpir	Suicide plasmid, 4275 bp; oriR6K, mobRP4, Cm ^R	Pepe and Miller, 1993
pGEM-T/Km Tn5	<i>E. coli</i> TG1	pGEM-T cloning plasmid containing kanamycin cassette; 3945 bp, Ap ^R , Km ^R	Lab stock
pMBGK9	<i>E. coli</i> DH5α	pUC19 and <i>fccA54/fccB54</i> homologous template DNA, 3626 bp; Ap ^R	This work
pMBGK2	<i>E. coli</i> DH5α	pUC19 and gene replacement fragment, 4565 bp; Ap ^R , Km ^R	This work
pMBGK15	<i>E. coli</i> S17λpir	pEP185.2 and gene replacement fragment, 6163 bp; Cm ^R , Km ^R	This work
pMBGK41	<i>E. coli</i> TG1	pGEM-T containing the 54gk9/54gk10 2091 bp PCR product; 5091 bp; Ap ^R , Km ^R	This work

Table 2.7: Plasmids for construction of the *fccA54* and *fccB54* gene knockout
Details of the plasmids used for construction of the *fccA54* and *fccB54* gene knockout, including, transformed host, plasmid length, antibiotic resistance properties and the source/reference of the plasmid are shown.

Plasmid	Host	Properties	Source/ Reference
pGEM-T	-	Cloning plasmid, 3000 bp; Ap ^R	Promega
pMB1-2	<i>E. coli</i> TG1	pGEM-T containing <i>fccA54</i> 54FRA PCR product; 4539 bp; Ap ^R	This work
pMB2-1	<i>E. coli</i> TG1	pGEM-T containing mutated <i>fccAB54</i> 54FRB <i>Bam</i> HI/ <i>Pst</i> I fragment; 4914 bp; Ap ^R	This work
pMB2-1-4	<i>E. coli</i> TG1	pGEM-T containing <i>fccAB54</i> 54FRB <i>Bam</i> HI/ <i>Pst</i> I fragment; 4914 bp; Ap ^R	This work
pMB3-4	<i>E. coli</i> TG1	pGEM-T containing <i>fccA54</i> 54FMRA PCR product; 4455 bp; Ap ^R	This work
pMB4-11	<i>E. coli</i> TG1	pGEM-T containing <i>fccAB54</i> 54FMRB <i>Bam</i> HI/ <i>Pst</i> I fragment; 4830 bp; Ap ^R	This work
pMB5-4	<i>E. coli</i> TG1	pGEM-T containing <i>fccA342</i> 342FRA <i>Bam</i> HI/ <i>Pst</i> I fragment; 4503 bp; Ap ^R	This work
pMB6-14	<i>E. coli</i> TG1	pGEM-T containing <i>fccAB342</i> 342FRB <i>Bam</i> HI/ <i>Pst</i> I fragment; 4864 bp; Ap ^R	This work
pMB7A-1	<i>E. coli</i> TG1	pGEM-T containing <i>fccA342</i> 342FMRA <i>Bam</i> HI/ <i>Pst</i> I fragment; 4443 bp; Ap ^R	This work
pMB8-3	<i>E. coli</i> TG1	pGEM-T containing <i>fccAB342</i> 342FMRB <i>Bam</i> HI/ <i>Pst</i> I fragment; 4804 bp; Ap ^R	This work
pMB9-5	<i>E. coli</i> TG1	pGEM-T containing <i>IfcA-1</i> <i>Bam</i> HI/ <i>Pst</i> I fragment; 4788 bp; Ap ^R	This work
pMMB503EH	<i>E. coli</i> DH5α	Broad host range expression plasmid; 9.9 kb; Sm ^R ; <i>Ptac</i>	Overbye Michel <i>et al.</i> , 1995
pEX129	<i>E. coli</i> DH5α	pMMB503EH containing gene <i>l29</i> <i>Bam</i> HI/ <i>Pst</i> I PCR product; 12.2 kb; Sm ^R ; <i>Ptac</i>	Atanasiu, 2001
pMB3-4-2	<i>E. coli</i> DH5α <i>E. coli</i> SM10	pEX129 containing <i>fccA54</i> 54FMRA <i>Bam</i> HI/ <i>Pst</i> I PCR product; 11.4 kb; Sm ^R ; <i>Ptac</i>	This work
pMB5	<i>E. coli</i> DH5α <i>E. coli</i> SM10 <i>S. f.</i> EG301	pMMB503EH containing <i>fccAB54</i> 54FRB pMB4 <i>Mlu</i> I/ <i>Pst</i> I fragment; 11.8 kb; Sm ^R ; <i>Ptac</i>	This work
pMB6	<i>E. coli</i> DH5α <i>E. coli</i> SM10 <i>S. f.</i> EG301	pMB5 containing <i>fccAB342</i> 342FRB <i>Bam</i> HI/ <i>Pst</i> I fragment; 11.7 kb; Sm ^R ; <i>Ptac</i>	This work
pJF118	<i>E. coli</i> TG1	Broad host range expression plasmid; 5267 bp; Ap ^R ; <i>Ptac</i>	Fürste <i>et al.</i> , 1986
pGEM-T + <i>fccA54</i> fragment	<i>E. coli</i> TG1	pGEM-T containing the <i>fccA54</i> overexpression fragment; 4396 bp; Ap ^R	This work
pMB1	<i>E. coli</i> TG1	pJF118 containing <i>fccA54</i> 54FMRA <i>Eco</i> RI/ <i>Pst</i> I PCR product; 6743 bp; Ap ^R ; <i>Ptac</i>	This work
pMB2	<i>E. coli</i> TG1	Modified pJF118 containing <i>fccA54</i> 54FMRA <i>Mlu</i> I/ <i>Bgl</i> II fragment; 6722 bp; Ap ^R ; <i>Ptac</i>	This work
pMB3	<i>E. coli</i> TG1	Modified pJF118 containing <i>fccA54</i> 54FMRA <i>Bam</i> HI/ <i>Pst</i> I fragment; 6722 bp; Ap ^R ; <i>Ptac</i>	This work
pMB4	<i>E. coli</i> TG1	pMB3 containing <i>fccAB54</i> 54FRB <i>Bam</i> HI/ <i>Pst</i> I fragment; 7157 bp; Ap ^R	This work

Table 2.8: Plasmids used for overexpression of FccA54, FccB54, FccA342, FccB342 and IfcA-1
 Details of the plasmids used for cloning and overexpression of the related Fcc₃ flavoenzymes, including transformed host, plasmid length, antibiotic resistance and the plasmid source/reference, are shown. *S. frigidimarina* is denoted *S. f.*

PRIMER NAME	OLIGONUCLEOTIDE PRIMER SEQUENCE (5'-3')	T _m (°C)	FUNCTION/ DESCRIPTION
54gk1	TAGAG <u>GATATC</u> CACCGTACTTGGTTCA	58.1	PCR amplification
54gk2	CGGTG <u>GATATC</u> CCTCTATGTCAGTTACAAGC	61.5	PCR amplification
54gk3	GCCGATGTCATGGTCATC	50.2	PCR amplification PCR screening
54gk4	CACCTCATGCGCAAGC	48.3	PCR amplification PCR screening
54gk5	GGATGTGCTGCAAGGC	54.3	Sequencing
54gk6	GGAATTGTGAGCGGATA	50.4	Sequencing
54gk7	AGACGCGGTTTCATAAC	49.2	PCR screening <i>Forward primer</i> <i>Anneals to fccA54</i>
54gk8	GTTGCCACCATGGAC	50.6	PCR screening <i>Reverse primer</i> <i>Anneals to fccB54</i>
54gk9	CGGTAAGTGATTTGAGGTTGCG	60.3	PCR screening
54gk10	GGTGCCGGTATACAAGTCAG	59.4	PCR screening
54gkC1	GCCACTCATCGCAGTAC	55.2	PCR screening <i>Forward primer</i> <i>Anneals to cat gene of pEP185.2</i>
54gkC2	CCAGACCGTTCAGCTG	54.3	PCR screening <i>Reverse primer</i> <i>Anneals to cat gene of pEP185.2</i>

Table 2.9: Primers used in construction of the *fccA54* and *fccB54* gene-knockout

The sequences of oligonucleotide primers that were used in construction of the *fccA54* and *fccB54* gene knockout are shown in the 5'-3' direction. The function of the primers and the primer melting temperatures (T_m, °C) are also shown. The supplied primer DNA pellets (MWG-Biotech AG) were solubilised in 1 ml sterile water and stored at -20 °C. The other primers supplied (Oswel DNA services) were obtained as 1 ml aliquots. The *Eco*RI restriction sites at the 5'ends of 54gk1 and 54gk2 are shown in bold underlined.

PRIMER NAME	OLIGONUCLEOTIDE SEQUENCE (5'-3')	T _m (°C)	FUNCTION/ DESCRIPTION
54FM	TCAG <u>GGATCC</u> ATGACTGAATGCGCCTCAAAC	62.8	PCR amplification
54F	TCAG <u>GGATCC</u> ATGCATGATAGAAGAAG	56.2	PCR amplification
54RA	GAT <u>CTGCAG</u> TTAGGCCTGCATGTCA	59.2	PCR amplification
54RB	GAT <u>CTGCAG</u> TTACATTTCTTTGAACCAAG	57.1	PCR amplification
54P1	GAAGGCTTTAACCAACAAG	46.6	Sequencing
54P2	TGTGTTAGACGGTAAGCG	47.8	Sequencing
54P3	GAGTGCTGCATAGCCAG	49.3	Sequencing
54P4	GGTTGATGAGTCCAAGCT	47.8	Sequencing
54P5	TAGGTGCAACCGGTGAAG	50.1	Sequencing
54RP1	TGGCTATGCAGCACTCTT	47.8	Sequencing
54RP2	CCGTCTAACACATTGACTG	48.7	Sequencing
54RP3	ACGGTATTCAACGCCTTC	47.8	Sequencing
54RP4	TCGAGCCTAGACCTTGAC	50.1	Sequencing
54JF1	GGAAACAGGATCCATGACTGAATG	55.6	Fusion PCR amplification
54JF2	CATGGATCCTGTTTCCTGTGTGAA	55.6	Fusion PCR amplification
54JF3	TGGCTTTGATGTAGATCGT	46.6	Fusion PCR amplification
54JF4	CAGCAATGGCATCCTGG	49.3	Fusion PCR amplification
54JF5	GATGTCGCAGAGTATGC	46.9	Sequencing
54JF6	ACGACCTGCACAGCCAT	49.3	Sequencing

Table 2.10: Primers used for PCR amplification and sequencing of *fccA54* and *fccB54*

The sequences of oligonucleotide primers that were used for initiating PCR amplification of *fccA54* and *fccB54* are shown in the 5'-3' orientation. The primers 54JF1-54JF4 that were used for fusion PCR amplification of the *FccA54* overexpression fragment are shown. The function of the primers and the primer melting temperatures (T_m, °C) are also shown. The DNA pellets supplied for each primer (MWG) were solubilised in 1 ml sterile water and stored at -20 °C. The other primers (Perkin-Elmer Applied Biosystems and Oswel DNA service) were supplied as 1 ml aliquots. The *Bam*HI (primers 54F and 54FM) and *Pst*I (primers 54RA and 54RB) restriction sites are shown in bold underlined.

PRIMER NAME	OLIGONUCLEOTIDE PRIMER SEQUENCE (5'-3')	T _m (°C)	FUNCTION/ DESCRIPTION
342FM	TCAG <u>GGATCC</u> ATGAATACAGCAGGAGTTAAATGG	61.8	PCR amplification
342F	TCAG <u>GGATCC</u> ATGATTTATCTGAAAATCATC	56.0	PCR amplification
342RA	GAT <u>CTGCAG</u> CTATGCTTTCATCATCGAAC	60.0	PCR amplification
342RB	GAT <u>CTGCAG</u> TTATTTAAACTTAGGGTAG	55.4	PCR amplification
342P1	TGATGATGGCACAGTGCT	47.8	Sequencing
342P2	GCACTGTTAATTGCGCCT	47.8	Sequencing
342P3	CTGCTCGTTCGATGATGA	47.8	Sequencing
342P4	CTAGTGCTAACCGTAGTC	47.9	Sequencing
342P5	GGTGCACTATTGCCAAG	52.8	Sequencing
342RP1	CGGCATACAGCTTAGGAA	47.8	Sequencing
342RP2	AGGCGCAATTAACAGTGC	47.8	Sequencing
342RP3	AGCACTGTGCCATCATCA	47.8	Sequencing
342RP4	ACAAGCTTGACCTGCGTT	47.8	Sequencing
IFC3F	TCAG <u>GGATCC</u> ATGTTGAATACCAAATTATTACC	57.8	PCR amplification
IFC3R	GAT <u>CTGCAG</u> TTATTTAATAGAATTAGCTACTTG	56.8	PCR amplification
M13 (-20)	GTAAAACGACGGCCAGT	52.0	Sequencing
M13 (-40)	GTTTTCCCAGTCACGAC	50.0	Sequencing

Table 2.11: Primers used for PCR amplification and sequencing of *fccA342*, *fccB342* and *IfcA-1*

The sequences of oligonucleotide primers that were used for initiating PCR amplification and sequencing of *fccA342*, *fccAB342* and *IfcA-1* are shown in the 5'-3' orientation. The function of the primers and the primer melting temperatures (T_m, °C) are also shown. The 342P5 primer DNA pellet (MWG-Biotech AG) was solubilised in 1 ml sterile water and stored at -20 °C. The other primers (Perkin-Elmer Applied Biosystems and Oswel DNA service) were supplied as 1 ml aliquots. The M13 primers are complementary to pGEM-T and are available from Promega. The *Bam*HI (primers 342F, 342FM and IFC3F) and *Pst*I (primers 342RA, 342RB and IFC3R) restriction sites are shown in bold underlined.

2.25 Preparation of antibiotics

Antibiotic Name	Solution	Filter Sterilised (0.2 µm filter)	Concentration	
			Stock	Final
Ampicillin	Sterile dH ₂ O	✓	50 mg/ml	50 µg/ml
Chloramphenicol	Ethanol	✗	34 mg/ml	25 µg/ml
Kanamycin	Sterile dH ₂ O	✓	50 mg/ml	50 µg/ml
Rifampicin	Methanol	✗	10 mg/ml	10 µg/ml
Streptomycin	Sterile dH ₂ O	✓	50 mg/ml	50 µg/ml

Table 2.12: Antibiotic preparation
The details of antibiotic preparation are shown. All antibiotics were dispensed into 1.7 ml tubes and stored at -20 °C.

2.26 Sterilisation

All tubes (0.6 ml and 1.7 ml) and pipette tips that were used for molecular biology were sterilised prior to use by autoclaving. All solutions used for molecular biology such as CaCl₂ were sterilised by autoclaving or filtration (0.2 µm filters). Buffers that were used during protein purification were filter sterilised prior to use.

2.27 Restriction enzymes

Name	Source	Restriction cleavage site
<i>Ava</i> I	Promega	5' C [↓] (T/C)CG(A/G) G 3' 3' G (A/G)GC(T/C) C 5'
<i>Bam</i> HI	Promega	5' G [↓] GATC C 3' 3' C CTAG G 5'
<i>Bgl</i> II	Promega	5' A [↓] GATC T 3' 3' T CTAG A 5'
<i>Bsu</i> 36I	New England Biolabs	5' CC [↓] TNAGG 3' 3' GGANT CC 5'
<i>Eco</i> RI	Promega	5' G [↓] AATT C 3' 3' C TTAA G 5'
<i>Eco</i> RV	Promega	5' GAT [↓] ATC 3' 3' CTA [↓] TAG 5'
<i>Kpn</i> I	Promega	5' G GTAC [↓] C 3' 3' C CATG [↓] G 5'
<i>Mlu</i> I	Promega	5' A [↓] CGCG T 3' 3' T GCGC [↓] A 5'
<i>Pst</i> I	Promega	5' C TGCA [↓] G 3' 3' G ACGT [↓] C 5'
<i>Sma</i> I	Boehringer Mannheim	5' CCC [↓] GGG 3' 3' GGG [↓] CCC 5'
<i>Xba</i> I	Promega	5' T [↓] CTAG A 3' 3' A GATC [↓] T 5'

Table 2.13: Restriction enzymes

The restriction enzymes that were used are listed. The restriction site and the source of each enzyme are given, where N is any nucleotide.

Chapter 3

Molecular modelling of *Shewanella oneidensis* MR-1 flavoproteins

3.1 INTRODUCTION

The Fcc₃ X-ray crystal structure solved to 1.8 Å resolution (Taylor *et al.*, 1999; PDB, 1QJD) provided the first detailed insight into the architecture of a fumarate reductase enzyme active site and the catalytic mechanism of fumarate reduction. Structural modelling and close contact measurements were initially used to analyse the precise structural and functional role of Fcc₃ active site residues: His365, Thr377, Arg402, His504 and Arg544 that are conserved in the family of fumarate reductases. Site-directed mutagenesis of some active site residues was subsequently used to ascertain their role in fumarate reduction.

3.1.1 The catalytic mechanism of Fcc₃

The close-fitting enzyme active site of Fcc₃ was identified to contain a malate-like substrate molecule that lies close to the FAD cofactor and is held in position via hydrogen bonds to key substrate-binding residues (Figure 3.1). Modelling studies showed that closure of the clamp domain induces a twist in the C1 carboxylate group of the malate-like substrate that concomitantly acts to alleviate steric constraints imposed on the planar molecule by Met236 and Met375 (Figure 3.1). The short substrate contacts made to these methionine residues in the close-fitting active site induces a change in the planar conformation that weakens the conjugation throughout the dicarboxylate substrate (Taylor *et al.*, 1999). The twisted C1 carboxylate group of the substrate establishes close contacts with His365 and Thr377 (Figure 3.1) that are key substrate-binding residues located in the clamp domain of Fcc₃ (Taylor *et al.*, 1999).

The C4 carboxylate group of the intermediate malate-like substrate extends into the flavin domain and forms hydrogen bonds with His504 and Arg544 (Figure 3.1). These substrate-binding contacts create a highly polar hydrogen-bonding environment that acts to polarise the C2-C3 bond of the substrate. The combined steric and electrostatic effects that are initiated upon substrate binding lead to the generation of positive charge at C2 of the substrate making it amenable to nucleophilic attack (Taylor *et al.*, 1999).

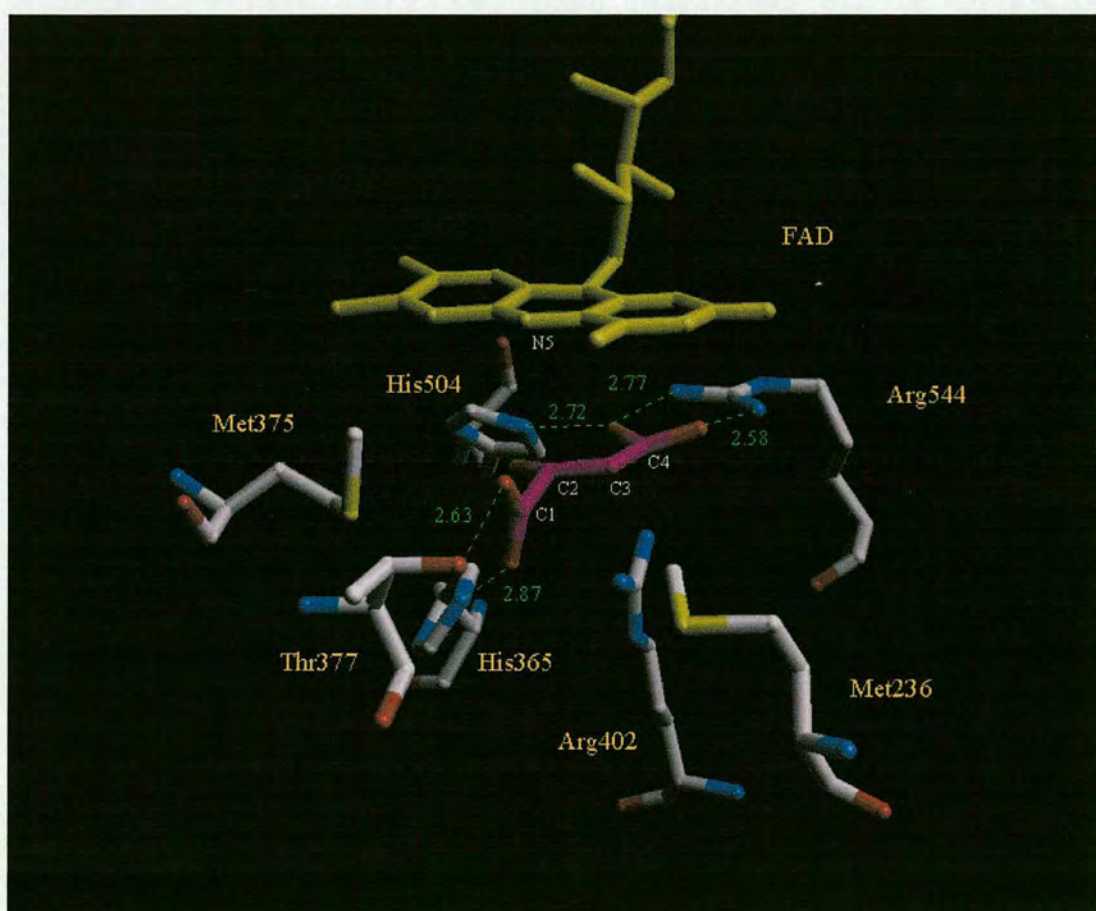


Figure 3.1: The active site of Fcc₃ solved to 1.8 Å resolution

The active site of the Fcc₃ fumarate reductase solved to 1.8 Å resolution is shown (Taylor *et al.*, 1999). The FAD cofactor (yellow) and the key active site residues of Fcc₃ (atom type) are shown. The malate-like intermediate substrate molecule (magenta) is shown in the Fcc₃ active site, where the oxygen atoms are in red. The close substrate contacts (Å; green) between the substrate carboxylate groups and protein atoms are indicated. The four carbon atoms of the malate-like substrate and N5 of FAD are labelled in white. The picture was produced using the molecular modelling graphics program WITNOTP (Widmer, 1999).

The close proximity of FAD to the substrate molecule facilitates hydride transfer from N5 of reduced flavin to C2 of the twisted and polarised substrate (Figure 3.2a). The exceptionally close contact (3.00 Å) of Arg402 (NH₂) from C3 of the substrate (Figure 3.2b) makes this residue suitable for subsequent proton transfer in the stepwise reduction mechanism towards production of succinate (Figure 3.2a; Taylor *et al.*, 1999).

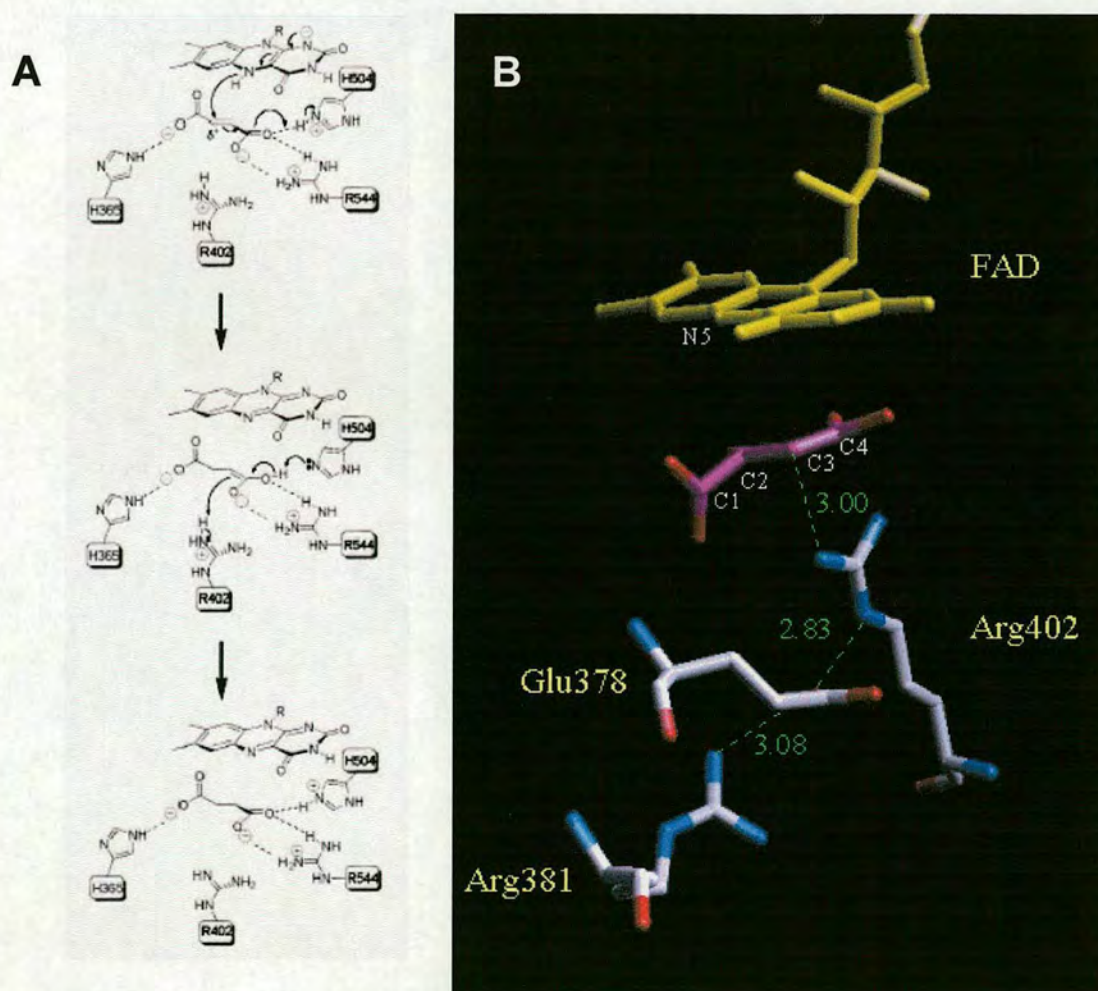


Figure 3.2: Fcc₃ catalytic mechanism involves a proton delivery pathway for fumarate reduction (A) The schematic diagram from Figure 4a of Taylor *et al.*, 1999 shows the stepwise catalytic mechanism of Fcc₃. (B) The X-ray crystal structure of Fcc₃ (Taylor *et al.*, 1999) revealed the position of residues involved in the proton delivery pathway (Å; green): Glu378, Arg381 and Arg402 (atom-type). FAD (yellow) and the substrate molecule (magenta), where the oxygen atoms are highlighted in red, are shown. The NH₂ group of Arg402, the active site acid of Fcc₃ is ideally positioned at 3.00 Å from C3 of the substrate molecule for proton transfer leading to production of succinate. The four carbon atoms of the malate-like substrate and N5 of FAD are labelled in white. The picture was produced using the molecular modelling graphics program WITNOTP (Widmer, 1999).

The X-ray crystal structures of Fcc₃ showed that Arg402 (numbering of *S. frigidimarina* NCIMB 400 enzyme) was the only key active site residue suitably positioned to function as the active site acid for fumarate reduction (Taylor *et al.*, 1999 and Leys *et al.*, 1999). Site-directed mutagenesis of Arg402 and the other candidate active site acid residues, His365 (Schröder *et al.*, 1991) and His504 (Bamford *et al.*, 1999) to alanine, showed that only the Arg402→Ala402 mutant enzyme had no detectable fumarate reductase activity (Doherty *et al.*, 2000). This provided substantial evidence that Arg402 is indeed the essential proton donor required for fumarate reduction in Fcc₃ (Doherty *et al.*, 2000). The guanidinium group of the arginine side chain allows simultaneous occupation of key sites close to C3 and C4 of the substrate molecule required for fumarate reduction. Substituted amino acid residues of Arg402 such as lysine, tyrosine and alanine only occupy the site close to C3 of the substrate molecule (Figure 3.3). Interaction of an Arg402 guanidinium NH₂ group with the C4 position of the substrate enables Arg402 to function as a Lewis acid to stabilise the negative charge across C3-C4 of the substrate that is generated by hydride transfer. The concurrent interaction of the second NH₂ guanidinium moiety with C3 of the substrate fulfils the role of Arg402 as a Brønsted-Lowry acid involved in direct proton transfer to C3 of the substrate molecule (Mowat *et al.*, 2001).

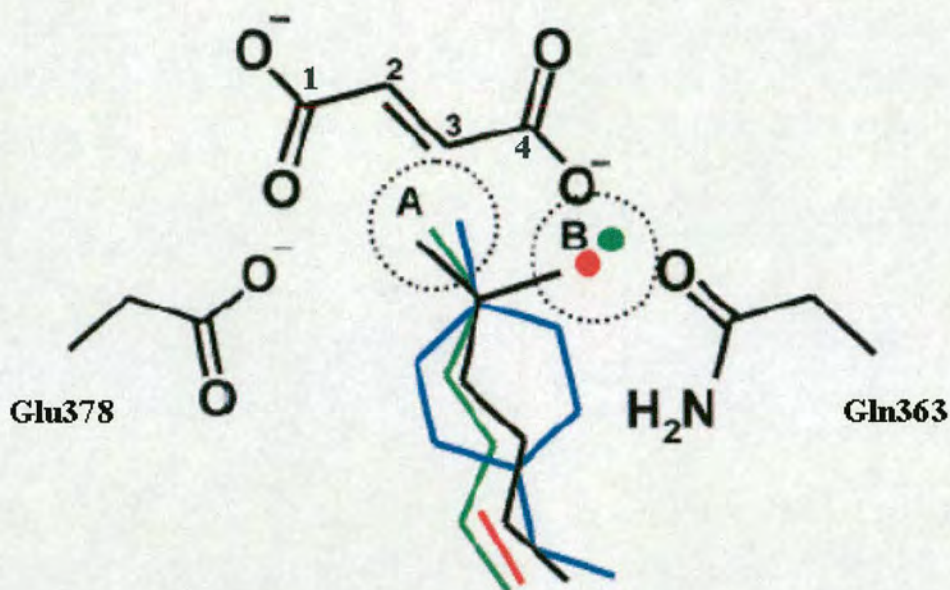


Figure 3.3: Position of the Arg402 side chain

Arg402 of Fcc₃ is the active site acid for fumarate reduction. The guanidinium group of Arg402 occupies positions A and B that lie close to C3 and C4 of fumarate, respectively. Occupation of both sites is essential for fumarate reduction. Other residues substituted in position of Arg402; Ala (red), Lys (green) and Tyr (blue) occupy position A but not position B. Water molecules (red and green circles) occupy position B in the Ala and Lys substituted mutant Fcc₃ enzymes, respectively. Glu378 and Gln363 are also shown, to the left and right, respectively of Arg402 and the substituted residues. The schematic diagram is adapted from Figure 4 of Mowat *et al.*, 2001.

A proton delivery pathway of Fcc₃ involving Glu378 and Arg381 is proposed to facilitate rapid delivery of protons to the Arg402 guanidine to reprotonate the group for enzyme catalysis (Figure 3.2b; Doherty *et al.*, 2000). Arginine residues equivalent to Arg402 are conserved in the family of fumarate reductases suggesting that a similar proton pathway will operate in the *Escherichia coli* and *Wolinella succinogenes* fumarate reductases (Lancaster *et al.*, 2001) and will not involve a histidine residue (His365; Fcc₃ of *S. frigidimarina* NCIMB 400) (Schröder *et al.*, 1991) or a water molecule (Lancaster *et al.*, 1999), as previously suggested. Indeed, the catalytic mechanism for fumarate reduction in L-aspartate oxidase is also similar to that of the soluble Fcc₃ fumarate reductase (Tedeschi *et al.*, 2001).

3.2 RESULTS AND DISCUSSION

3.2.1 Sequence analyses of *S. oneidensis* MR-1 flavoproteins

The novel FccA54, FccA56 and FccA342 flavin subunits share high sequence identity to the flavin-containing catalytic domain of Fcc₃ isolated from *Shewanella* species. A 'ClustalW' (Thompson *et al.*, 1994) multiple sequence alignment of the novel flavoproteins against the flavoprotein domain of Fcc₃ (*S. frigidimarina* NCIMB 400) showed strict conservation of key catalytic residues (Figure 3.4). The X-ray crystal structure of the Fcc₃-substrate complex (Taylor *et al.*, 1999) showed that the substrate-binding residues of the flavin domain, His504 and Arg544 form hydrogen bonds to the C4 carboxylate group of fumarate (Figures 3.1). Interpretation of the 'ClustalW' multiple sequence alignment revealed that basic residues equivalent to His504 and Arg544 of Fcc₃ are strictly conserved in flavin-containing catalytic subunits of FccA54, FccA56 and FccA342 (Figure 3.4). These related flavoproteins were also shown to contain an arginine residue that aligned with Arg402, the active site acid of Fcc₃ (Figure 3.4). This observation leads us to the theory that a proton transfer mechanism similar to that of Fcc₃ operates in these related enzymes. The absence of charged residues equivalent to Glu378 and Arg381 (Figure 3.4) of the Fcc₃ proton delivery pathway (Doherty *et al.*, 2000) leads to the supposition that an alternative pathway exists in these related enzymes. The Fcc₃ substrate-binding residues of the clamp domain, His365 and Thr377 form hydrogen bonds to the C1 carboxylate group of fumarate (Figure 3.1; Taylor *et al.*, 1999). Analysis of the 'ClustalW' multiple sequence alignment showed that His365 of Fcc₃ is substituted with glycine in each of the three related flavoprotein subunits and that Thr377 is not conserved amongst the related flavoproteins (Figure 3.4).

Fcc	KSERQAALASAPHD	TVDVVVVGSGGAGFSA	AI	SATDSGAK-VILIEKEPVIGGNAKLAAG	170
FccA54	ASATECASNIKWDETRD	IIIVVGS	GFAGLSSALNAKRQGLGSILVLEKMQVIGGNSAINGG		60
FccA56	IKASNDNYGR	TWDEFDIIIIIGSG	GFAGLSAAYS	SAHKAGIKNIIVLEKMEAFGGNSAICGG	60
FccA342	FSANANTAGVKWDETYE	IVIVVGS	GFAGLAAAIEAGKLGAKEVVLEKLG	GVYGGNSALNAG	58
		..	:::::*** **:::*	.. * :::::*** . ***: : *	
Fcc	GMNAAWTDQQAKKITD	-SPELMFEDTMKGGQ	NINDPALVKVLSSHSKDSVDWMTAMGAD		229
FccA54	WLAI PKNPIQLAQGIQDD	SPPEELVKDQIIISGRGMQNTDMLRQMANRALDAYQLCIDAGVK			120
FccA56	LMCMPLTPMQKKLGIED	-SAELMIKMDLKAGRGFNHPELCRTLATEAHKAYDMLMECGVK			119
FccA342	QACFAGTDIQKKHGIED	-SPDLMVKDQLISGRGYAHEDLLRHS	AELGAYIYQMTKDCGC		117
		. . *	* * * . : : * : . * . : : : . : *		
		236			
Fcc	LTD--VGM	GGASVNR	AHRPTGGAGVGAHVQVLYDNAVKRNIDLRMNTRGIEVLKDDKG		287
FccA54	FREGFNQQV	GGHNKARAI	RTHQGV--GGDITTKLYEVGKKEGVEYRLQHYVEDFIMDQV		177
FccA56	FQD-KVIR	LGGHSAPRAHLPESAS--GGGIVVPMHNYLRKAGIIFQNR	TNVEEIRGDS-		175
FccA342	YRD-HIINT	GGTSANRSHQVVERS--GAGFIRPMLKTARSYGVKTKRHKFEHLITADDG			174
		:	** . * :	* . . : . . : : . . : : . .	
Fcc	TVKGILVKGMYKG-----	YYVWKADAVILATGGFAKNN	ERVAKLDP	SLKGFIS-TNQ	338
FccA54	QIVGLKVRQNYRFPDLKTGKTI	YIKANKAVILAHGGF	SRNLVRELVD	PALDKTLDCTNA	237
FccA56	GVTGIVVSEKYDFKSGSNRQGFAY	KAKKGVIVASGGWGQDHQFIKT	MPAY-QKLESTAQ		234
FccA342	TVLGIQVRKDYHFGHEDSGK	LINIKAEKGVLIATGGFAAN	VAFRQALDPTLGSEV	GCTNA	234
		: * : *	..:::*** **.. :	* : : *	
		365 367	375 377 381		
		*	378		
Fcc	PGAVGDGLDVAENAGGALKDMQYIQ	HP	TL	SVKGG-----VMT	EA
FccA54	LGATGEVTLTAMAHGAF	PVHMSFIQTGH	WGS	PDEGGFGWSN	ALLS
FccA56	PGATATMIKSLLSIRALP	VMLDMYQLG	PWATPDEK	GAGPAS	FFAD
FccA342	RGATGDGLIAMLAEGAMP	VGLSFIQSG	PWAS	PDEGGFGYGS	GFSL
		**.. . :. *	: : . : *		
		402			
Fcc	RFVNEIT	TRDKASAA	ILAQ	TGK-----SAYLIFDDSVRKSLSKIDKYIGLGVAPTADS	446
FccA54	RFMNERAD	RTCSDAIMKNRNP--DGSPAYPVVFFNHDDHVGAE	EVTRA	VRDQIAWKVDS	355
FccA56	RFMNELAD	RTTRADAQLAVLASGTKEKPNMPFVFCGEATANHAEGFKAAYR	DAIKKSET		354
FccA342	RFMNETAD	RTTRADLEIQRRDK--EGKPNPALLIAPKHEAQKDP	SMENVLKYNVAWEFDS		352
		:: : * . : :	. : :	::	
					504
Fcc	LVKLGKMEGIDGKALTET	VARYNSLVSSGKDTDFERP	NLPR--ALNEGNY	YAEVTPGV	H
FccA54	LEQLAKQFNIP	LAQLKQTVAEY	NKQVPQRIDPLFGR	MMDTA--VELKAPFIVSRIWPKV	H
FccA56	LEELAKRYD	VDINALQNSIN	EWNEIVQGKAKDPFNKPLDEK--TILKPPYYSIRLSPKL	H	412
FccA342	VEAIAKHFNLP	PEEAFKKQVSDWNE	YVKTGVDPQFGK	RMVMKDIYLT	PPFIVQRLWPKV
		: :.* :. : : : :.* *	. * :	: : . : * : *	
			534	544	
Fcc	HTMGGMIDTKAEVMNAK	-QVIPGLYGAGE	VTGGVHG	ANRLGGNAISDIITFGR	LAGEE
FccA54	YCMGGLKTDLGARVLHSQ	TLAPMKNLYAVGE	ATGGTHGGT	RLSSTACLECLTMGI	IVAET
FccA56	YCMGGVAITPNAEVIDS	NTCEPISGLFAAGE	VTGGTHGMD	RLGGCSSIDGLVFG	QIAGN-
FccA342	YCQGGIQINTKA	EVIAAKNGKPIPKLYAAGE	VTGGVHGVS	RLGGCSTPECM	AFGVTAAR-
		: ** : * . : : . : * : ** * * . : : : * . .			
Fcc	AAKYSKKN	571			
FccA54	IKSDMQA-	480			
FccA56	-QAIRKV	478			
FccA342	--SMMKA-	476			
		:			

Figure 3.4: ‘ClustalW’ multiple sequence alignment of Fcc₃ and the novel flavoenzymes

The sequences of FccA54, FccA56 and FccA342 were aligned with the Fcc₃ flavin domain of *S. frigidimarina* NCIMB 400 (Fcc) using ‘ClustalW’ (Thompson *et al.*, 1994). The related flavoproteins are numbered according to the preprotein sequence. The sequence that is shown begins directly upstream of the FAD-binding site of Fcc₃ and the corresponding region of the related proteins (bold). The highlighted residues are numbered according to the Fcc₃ protein sequence. The active site residues of Fcc₃ (magenta) that are strictly conserved in the related enzymes (magenta) and the Fcc₃ residues that are not conserved (orange) are shown. The corresponding substituting residues of the related flavoproteins that are conserved in all three enzymes (green) and those which are variable (cyan) are shown. The conserved proline residue of the fumarate reductase family is shown (*).

With regard to the view that the related flavoproteins and Fcc₃ have a common catalytic mechanism, the substitution of His365 by glycine in all three flavoproteins lends further support against His365 being the active site acid of Fcc₃. The 'ClustalW' multiple sequence alignment showed that the active site proline residue (Pro366; Fcc₃ of *S. frigidimarina* NCIMB 400), conserved in the subfamily of respiratory flavoenzymes (Pealing *et al.*, 1992) was substituted with histidine in FccA54 (Figure 3.4). Sequencing of the *fccA54* gene PCR amplified from the *S. oneidensis* MR-1 genome subsequently provided evidence that a histidine residue does indeed occur at an equivalent position to Pro366 of Fcc₃ (5.2.3). Perhaps, this histidyl residue is positioned in the FccA54 active site to provide substrate-binding interactions, as found for His365 in Fcc₃ (Taylor *et al.*, 1999). An invariant tryptophan residue of each flavoenzyme that maps to a position equivalent to Thr367 of Fcc₃ (Figure 3.4) may have a structural role to compensate for the existence of glycine at the active site. Alternatively, the conserved tryptophan residue may have an important role in substrate binding or catalysis. Analysis of the 'ClustalW' multiple sequence alignment also revealed that Glu534 of Fcc₃ implicated in sodium ion association is strictly conserved in the related flavoenzymes (Figure 3.4).

It was observed from the 'ClustalW' multiple sequence alignment (Figure 3.4) that important active site residues of the Fcc₃ flavin domain involved in substrate binding and catalysis are strictly conserved in the related *S. oneidensis* MR-1 flavoproteins (Figure 3.5). Conversely, key substrate-binding residues located in the Fcc₃ clamp domain are poorly conserved in the related flavoenzymes (Figures 3.4 and 3.5). The absence of carboxylate substrate-binding residues in the clamp domain of FccA54, FccA56 and FccA342 (Figure 3.5) leads us to suggest that these related enzymes bind to acrylates comprising a single carboxylate group. Furthermore, the active sites of these related flavoproteins might accommodate substrates with larger functional groups due to the amino acid substitution of His365 with glycine.

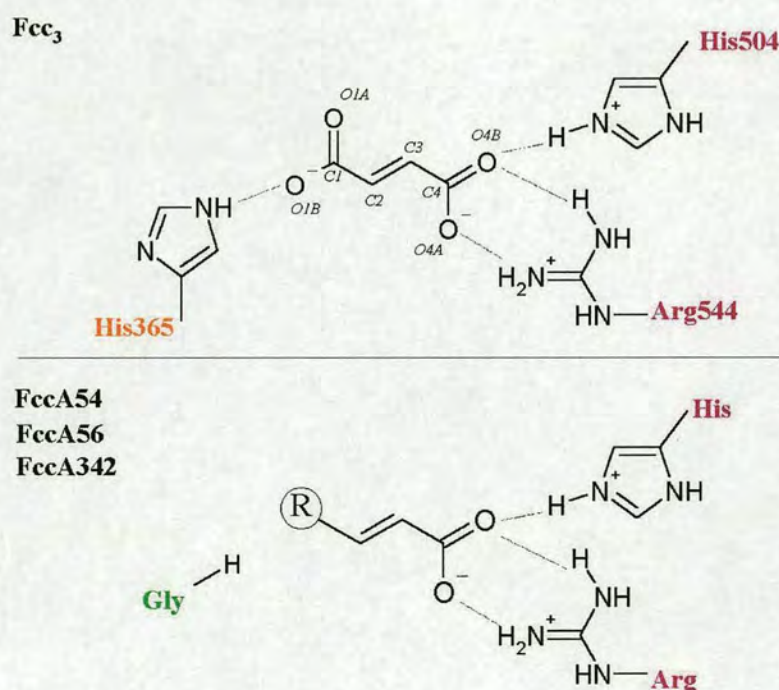
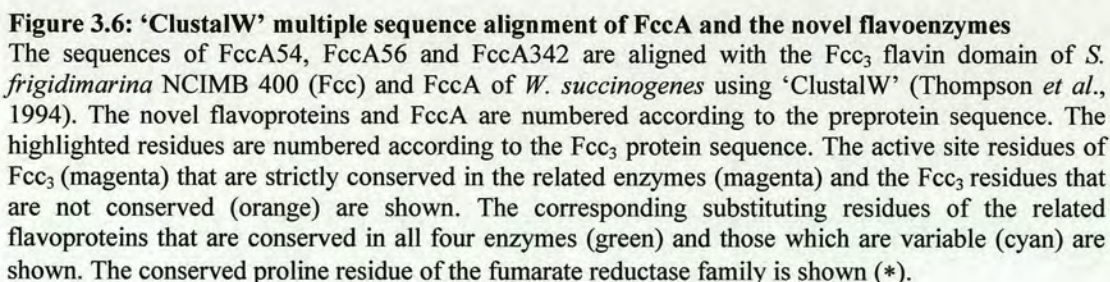


Figure 3.5: Schematic diagram of the novel flavoprotein active sites compared to Fcc₃

The flavoproteins related to Fcc₃ contain basic residues of the flavin subunit equivalent to His504 and Arg544 involved in binding the C4 carboxylate group of fumarate. His365 of Fcc₃ that is a substrate-binding residue located in the clamp domain is not conserved and is replaced by glycine in FccA54, FccA56 and FccA342. Thr377 of Fcc₃ is not conserved and is replaced by a residue that is variable amongst the flavoproteins. For simplicity, Thr377 and the equivalent residues are not shown. The absence of C1 carboxylate substrate-binding residues equivalent to His365 and Thr377 of Fcc₃ leads us to suggest that the related flavoproteins catalyse reduction of acrylates rather than dicarboxylates such as fumarate.

A 'ClustalW' multiple sequence alignment of the novel flavoenzymes against the FccA flavin subunit of *W. succinogenes* revealed striking sequence similarity of active site residues (Figure 3.6). The key active site residues of Fcc₃, Arg402, His504 and Arg544 that are conserved in the related *S. oneidensis* MR-1 flavoenzymes are also conserved in FccA of *W. succinogenes* (Figure 3.6). The Fcc₃ His365 substitution with glycine in the clamp domain of the novel respiratory *S. oneidensis* MR-1 flavoenzymes also occurs in the FccA flavoenzyme subunit. The other dicarboxylate substrate-binding and catalytic residues of the Fcc₃ active site that map to the clamp domain; Met375, Thr377 and Arg381 are not conserved in the FccA flavin subunit of *W. succinogenes*. The specific function of the FccA flavin subunit from *W. succinogenes* is unknown but is recognised not to catalyse fumarate reduction (Simon *et al.*, 1998). The high sequence identity observed between the FccA active site residues and FccA54, FccA56 and FccA342 provides further support that these enzymes will similarly not catalyse reduction of dicarboxylate containing substrates.



The 'ClustalW' multiple sequence alignments provided information on conserved residues between Fcc₃ and the related flavoenzymes based upon the primary structure of the proteins. A 'Sequence and Secondary Structures' alignment tool (http://www.icmb.ed.ac.uk/sss_align/sss_align.html) was used to obtain sequence alignments of the related flavoproteins against Fcc₃ based upon both primary and secondary structure. Various parameters were adjusted to optimise the pair-wise sequence alignments. The sequence alignments that included secondary structure prediction for FccA54 (Figure 3.7), FccA56 (Figure 3.8) and FccA342 (Figure 3.9) revealed structural similarity to the flavin domain of Fcc₃. In contrast, the clamp domain was structurally less well conserved due to the insertion of a loop in FccA54, FccA56 and FccA342. The 'clamp domain loop' was introduced at a different position in the sequence alignment generated using the 'Sequence and Secondary Structures' alignment tool compared to the 'ClustalW' sequence alignment (Figure 3.4). This caused a variation in aligned residues corresponding to Met375, Thr377, Glu378, Arg381 and Arg402 of Fcc₃. The optimised sequence alignments (Figures 3.7-3.9) that contained secondary structure information were used to construct molecular models of FccA54, FccA56 and FccA342.



Figure 3.7: Pair-wise sequence alignment of Fcc₃ and FccA54

The sequence alignment generated using a 'Sequence and Secondary Structures' alignment tool (http://www.icmb.ed.ac.uk/sss_align/sss_align.html) incorporated the secondary structure prediction for FccA54 aligned with the known structure of Fcc₃ (*S. frigidimarina* NCIMB 400; Fcc). 'H' denotes alpha helices and 'E' indicates beta-sheets, where lower case (not conserved) and upper case (conserved) are used to clearly show the regions of conserved secondary structure between the aligned proteins. The FAD binding motif of Fcc₃ and the corresponding sequence of FccA54 are shown (bold). The numbering of FccA54 corresponds to that of the preprotein sequence and does not correspond to residue numbers in the FccA54 molecular model. The boxed area indicates the sequence of key active site residues that are aligned differently compared to the 'ClustalW' (Thompson *et al.*, 1994) multiple sequence alignment (Figure 3.4). The active site residues of Fcc₃ (magenta) that are strictly conserved in FccA54 (magenta) and the Fcc₃ residues that are not conserved (orange) are shown. The corresponding substituting residues of FccA54 that are conserved (green) and those that are variable (cyan) are shown.

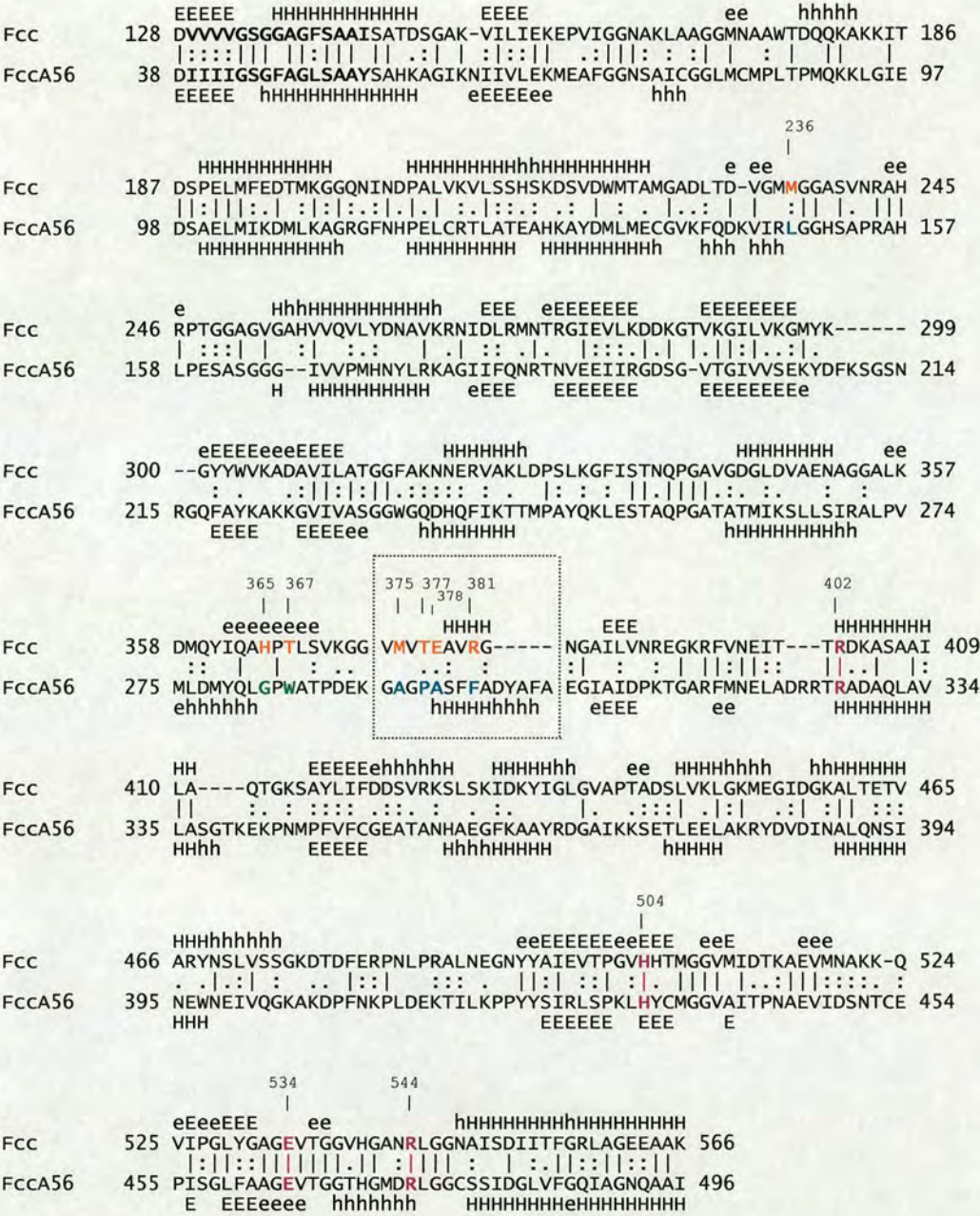


Figure 3.8: Pair-wise sequence alignment of Fcc₃ and FccA56
The sequence alignment generated using a ‘Sequence and Secondary Structures’ alignment tool (http://www.icmb.ed.ac.uk/sss_align/sss_align.html) incorporated the secondary structure prediction for FccA56 aligned with the known structure of Fcc₃ (*S. frigidimarina* NCIMB 400) (Fcc). ‘H’ denotes alpha helices and ‘E’ indicates beta-sheets, where lower case (not conserved) and upper case (conserved) are used to clearly show the regions of conserved secondary structure between the aligned proteins. The FAD binding motif of Fcc₃ and the corresponding sequence of FccA56 are highlighted in bold. The numbering of FccA56 corresponds to that of the preprotein sequence and does not correspond to the numbering of residues in the FccA56 molecular model. The boxed area indicates the sequence of key active site residues that are aligned differently compared to the ‘ClustalW’ (Thompson *et al.*, 1994) multiple sequence alignment (Figure 3.4). The active site residues of Fcc₃ (magenta) that are strictly conserved in FccA56 (magenta) and the Fcc₃ residues that are not conserved (orange) are shown. The corresponding substituting residues of FccA56 that are conserved (green) and those that are variable (cyan) are shown.



Figure 3.9: Pair-wise sequence alignment of Fcc₃ and FccA342

The sequence alignment generated using a 'Sequence and Secondary Structures' alignment tool (http://www.icmb.ed.ac.uk/sss_align/sss_align.html) incorporated the secondary structure prediction for FccA342 aligned with the known structure of Fcc₃ (*S. frigidimarina* NCIMB 400; Fcc). 'H' denotes alpha helices and 'E' indicates beta-sheets, where lower case (not conserved) and upper case (conserved) are used to clearly show the regions of conserved secondary structure between the aligned proteins. The FAD binding motif of Fcc₃ and the corresponding sequence of FccA342 are highlighted in bold. The numbering of FccA342 corresponds to that of the preprotein sequence and does not correspond to the numbering of residues in the FccA342 molecular model. The boxed area indicates the sequence of key active site residues that are aligned differently compared to the 'ClustalW' (Thompson *et al.*, 1994) multiple sequence alignment (Figure 3.4). The active site residues of Fcc₃ (magenta) that are strictly conserved in FccA342 (magenta) and the Fcc₃ residues that are not conserved (orange) are shown. The corresponding substituting residues of FccA342 that are conserved (green) and those that are variable (cyan) are shown.

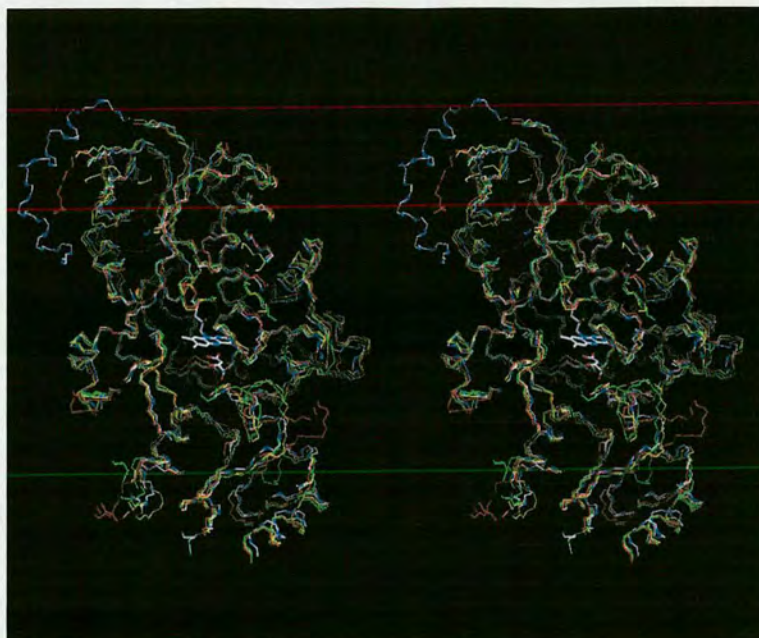
3.2.2 Molecular models of the novel *S. oneidensis* MR-1 flavoproteins

The sequence alignments (3.2.1) provided some insight into the biological function of the related Fcc₃ flavoproteins and led us to the suggestion that these enzymes catalyse the reduction of acrylates (Figure 3.5). The information obtained from sequence alignments that included secondary structure prediction (Figures 3.7-3.9; http://www.icmb.ed.ac.uk/sss_align/sss_align.html) was used to construct molecular models of the flavoprotein active sites. Comparative modelling was used to provide a three-dimensional insight of each enzyme active site to investigate which acrylates were possible enzyme substrates. The molecular modelling program, 'SYBYL Composer' (Blundell *et al.*, 1988) provided a systematic approach for constructing molecular models of FccA54, FccA56 and FccA342. 'SYBYL Composer' uses a knowledge-based approach to predict the structure of a protein based upon the known X-ray crystal structure of a homologous protein. The program is designed to structurally align the conserved regions on the basis of sequence homology, select these regions and align them with the known structural framework. Loops are subsequently inserted in the model based upon homology to the known structure (Blundell *et al.*, 1988). Molecular models of FccA54, FccA56 and FccA342 were constructed using the known Fcc₃ (*S. frigidimarina* NCIMB 400) X-ray crystal structure solved to 1.8 Å resolution (Taylor *et al.*, 1999; Figure 3.1). The homologous Fcc₃ flavin domain sequence (Figures 3.7-3.9) was selected to generate a structural framework for alignment of the FccA54, FccA56 and FccA342 flavin subunits.

3.2.2.1 Structural details of the molecular models

Molecular models of FccA54, FccA56 and FccA342 revealed that the fold of the flavin domain is structurally and topologically similar to the flavin domain of Fcc₃ (Figure 3.10a). This finding correlates with high structural similarity found in the family of FAD-binding flavoproteins. The folding topology of the Fcc₃ clamp domain is less well conserved in FccA54 (Figure 3.10b), FccA56 and FccA342 consistent with the view that the clamp domain of Fcc₃ is composed of a novel structural fold (Taylor *et al.*, 1999). Low structural similarity localised to the clamp domain was attributed to a loop in the related flavoproteins that was orientated towards the active site in the molecular models constructed with 'SYBYL Composer' (Figure 3.10a). However, extension of the loop from the surface of each protein is likely to represent a more realistic orientation. Therefore, orientation of the loop was amended prior to minimisation for the molecular model of FccA54. However, modification of the loop did not improve the structural alignment in the FccA54 clamp domain (Figure 3.10b). Poor structural alignment with Fcc₃ was also localised to helical breaks that mapped to residues out with the enzyme active site. Minimisation subsequently improved the structural superposition resulting in low root mean square deviation (r.m.s.d) values of main chain atoms (Table 3.1).

A



B

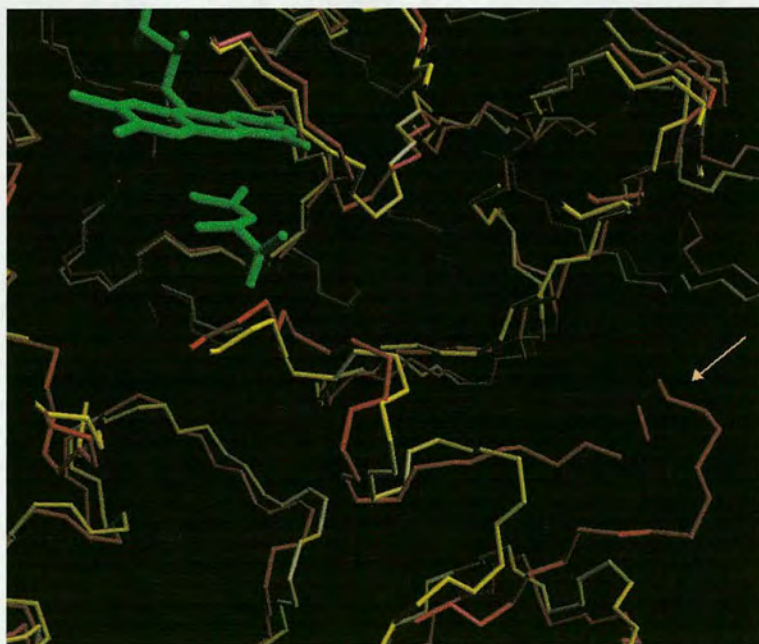


Figure 3.10: Overlay of the molecular models with Fcc₃

(A) The structural topology and fold of the Fcc₃ (atom-type) flavin domain is conserved in each of the novel flavoproteins, FccA54 (red), FccA56 (yellow) and FccA342 (green), as shown by structural superposition of residues 1-465 of FccA54, FccA56 and FccA342 with residues 125-567 of Fcc₃ (r.m.s.d = 0.641, 0.622 and 0.610 Å, respectively). The fold of the clamp domain is less well conserved due to insertion of a loop in each of the novel flavoproteins. The C-alpha trace of the structural alignment is shown in crossed stereo view. The FAD cofactor and substrate of Fcc₃ are shown (atom-type). (B) The 'clamp domain loop' (indicated by arrow) that contributes to the poorer structural alignment in the clamp domain of the novel flavoproteins aligned with Fcc₃ is shown. The C-alpha trace of the structural alignment shows FccA54 (red) aligned with Fcc₃ (yellow) to clearly show the position of this loop. The FAD cofactor and malate-like substrate of Fcc₃ are shown (green). The pictures were produced using the molecular modelling graphics program WITNOTP (Widmer, 1999).

Table 3.1 Structural data of molecular models					
Helical Breaks			Clamp domain loop		
	Position	Distance (Å)		Position	Orientation
FccA54	Q24/C-G25/N	2.014[*]	FccA54	S269-H273	+[-]
FccA56	A24/C-G25/N	2.017 [*]	FccA56	D266-A270	+ [+]
	G130/C-G131/N	2.819 [3.356]	FccA342	L268-F271	+ [+]
FccA342	G130/C-A131/N	2.826 [4.353]			
	I134/C-R135/N	2.123 [*]			
Root mean square deviations					
	Backbone main chain atoms (Å)				
FccA54	0.596	[0.850]			
FccA56	0.612	[0.820]			
FccA342	0.676	[0.867]			
[] values after minimisation * break amended + Orientation toward active site - Orientation away from active site					

Table 3.1: Structural data of molecular models

The amino acid positions of the helical breaks that occurred in the molecular models of FccA54, FccA56 and FccA342 are shown. Most of these helical breaks were amended following minimisation. The 'clamp domain loop' comprising 4-5 amino acid residues occurred in the clamp domain of the FccA54, FccA56 and FccA342 molecular models and caused poor structural alignment with the Fcc₃ active site. The loop was positioned facing into the active site of each flavoenzyme molecular model. Prior to minimisation, the orientation of the 'clamp domain loop' was changed to project away from the active site in the FccA54 molecular model. However, this rearrangement had no effect on improving the structural alignment in the clamp domain of FccA54. The root mean square deviation of the backbone main chain atoms of each flavoenzyme molecular model with the active site of Fcc₃ showed that overall a high structural alignment was obtained between the homologous enzymes.

The molecular models were generated for the entire flavin subunit of each novel flavoenzyme; however, of particular interest were the structural alignment of putative active site residues with the known active site of Fcc₃. The structural similarity observed in the flavin domain of each molecular model with Fcc₃ was further improved by manually altering the orientation of key active site residues. The conserved substrate-binding residues located in the flavin domain of each molecular model were precisely aligned with the corresponding substrate-binding residues of Fcc₃ (His504 and Arg544). The conserved arginine residue in each molecular model was manually aligned with the equivalent Arg402 residue of Fcc₃.

Superposition of the conserved basic residues established some close contacts (within a distance of 3.7 Å) to the twisted malate-like substrate molecule of Fcc₃ (Table 3.2). The close contacts present in the Fcc₃ flavin domain between His504 and Arg544 to O4B and O4A atoms, respectively, of the malate-like substrate (Figure 3.1) are well conserved in the molecular models of the related flavoproteins (Table 3.2). The close contact between Arg402 and C3 of the substrate molecule in Fcc₃ (Figure 3.2b) is also well conserved in the related flavoenzymes (Table 3.2). Other close contacts are less well conserved in the clamp domain of the three molecular models compared to the active site of Fcc₃ (Table 3.2). Substitution of His365 (Fcc₃) with glycine in each of the molecular models creates space at this region of each enzyme active site (Figures 3.11, 3.13 and 3.15), as was evident from absence of close contacts made between His365 and O1B and O2 atoms of the malate-like substrate of Fcc₃ (Table 3.2).

Substrate Atom	Close contacts between substrate and protein atoms (Å)							
	Fcc ₃		FccA54		FccA56		FccA342	
	Residue/atom	(Å)	Residue/atom	(Å)	Residue/atom	(Å)	Residue/atom	(Å)
C1 Mal_806	R402/NH2	3.698			R293/NH2	3.450		
	T377/OG1	3.239	W263/C	3.662	P260/O	3.080	Y262/C	2.767
			F261/CE1	3.648			F260/CE2	2.918
C2 Mal_806	R402/NH2	3.252			R293/NH2	3.090		
			F261/CE1	3.374			F260/CE2	2.692
O1A Mal_806	T377/OG1	2.628	W263/C	3.618	P260/O	2.478	Y262/CA	2.954
							F260/CE2	3.637
O1B Mal_806	H365/NE2	2.871						
	T377/OG1	3.359	W263/C	3.125	P260/O	3.191	Y262/C	2.070
	R402/NH2	3.242			R293/NH2	2.832		
			F261/CE1	3.455			F260/CEZ	2.745
C3 Mal_806	R402/NH2	2.995	R293/NH2	3.539	R293/NH2	3.187		
O2 Mal_806	H365/CD2	3.187						
	R402/NH2	3.526			R293/NH2	3.144		
	H504/NE2	2.997	H400/NE2	3.292	H399/NE2	2.884	H401/NE2	3.625
			F261/CE1	2.298			F260/CE2	1.748
C4 Mal_806	R402/NH2	3.132	R293/NH2	3.319	R293/NH2	3.460	R292/NH2	3.321
	R544/NH2	3.570	R441/NH2	3.405	R440/NH2	2.972	R442/NH2	3.013
O4A Mal_806	R402/NH1	3.597						
	R544/NH2	2.584	R441/NH2	2.676	R440/NH2	2.289	R442/NH2	2.317
O4B Mal_806	R402/NH1	2.837	R293/NH1	3.250	R293/NH1	3.305	R292/NH1	2.742
	H504/NE2	2.723	H400/NE2	3.575	H399/NE2	2.508	H401/NE2	3.424
	R544/NH2	2.768	R441/NH2	2.76	R440/NH2	2.781	R442/NH2	2.649

Table 3.2: Close contacts between the Fcc₃ substrate and protein atoms

The close contacts made between the malate-like substrate of Fcc₃ and protein atoms of Fcc₃ and the molecular models of FccA54, FccA56 and FccA342 were calculated. The conserved substrate-binding and catalytic residues of each molecular model were precisely aligned with the corresponding substrate-binding and catalytic residues of Fcc₃ (Arg402, His504 and Arg544). The table shows that close contacts present in the Fcc₃ structure between Arg402, His504 and Arg544 and the malate-like substrate are well conserved in the molecular models of the related flavoproteins. Conversely, close contacts are less well conserved in the clamp domain of the three molecular models compared to the active site of Fcc₃. The large aromatic residues of the molecular models that substitute Thr377 maintain close contacts to the malate-like substrate of Fcc₃. However, the close contacts made between His365 and the malate-like substrate of Fcc₃ are absent in the molecular models of FccA54, FccA56 and FccA342 due to the presence of glycine. These close contacts are calculated for residues that were manually twisted to align with residues of Fcc₃, therefore, there may be some variation in these distances mentioned elsewhere in the chapter, as the manual alignment was repeated each time the models were analysed.

3.2.2.2 Molecular model of the FccA54 enzyme active site

The molecular model of the FccA54 active site superimposed on the known structure of Fcc₃ showed the putative position of key active site residues relative to Fcc₃ (Figure 3.11). The FccA54 basic residues equivalent to His504 and Arg544 of Fcc₃ maintain close contact to the substrate C4 carboxylate group (Table 3.2; Figure 3.11). The close interaction observed between NH₂ of the FccA54 arginine residue (Fcc₃; Arg544) and O4B of the substrate molecule (2.76 Å; Figure 3.11), is particularly similar to the close contact observed between equivalent atoms in Fcc₃ (2.77 Å; Figure 3.1).

Substrate-binding interactions and close contacts observed for the FccA54 molecular model in the clamp domain region of the active site are less well conserved compared to those of Fcc₃. A tryptophan residue of FccA54 (Fcc₃; Thr367; Figure 3.4) is directed toward the active site and the aromatic ring is arranged parallel to the second tryptophan residue (Fcc₃; Thr377; not shown). The large hydrophobic side chains are oriented in the active site to flank the substrate molecule (not shown). This gave rise to a highly hydrophobic small close-fitting active site for FccA54. Furthermore, the tryptophan side chains caused His252 of FccA54 (Pro366; Fcc₃) to extend away from the active site (not shown), which prevented His252 from forming close contacts to the substrate, as originally predicted from sequence alignments (3.2.1).

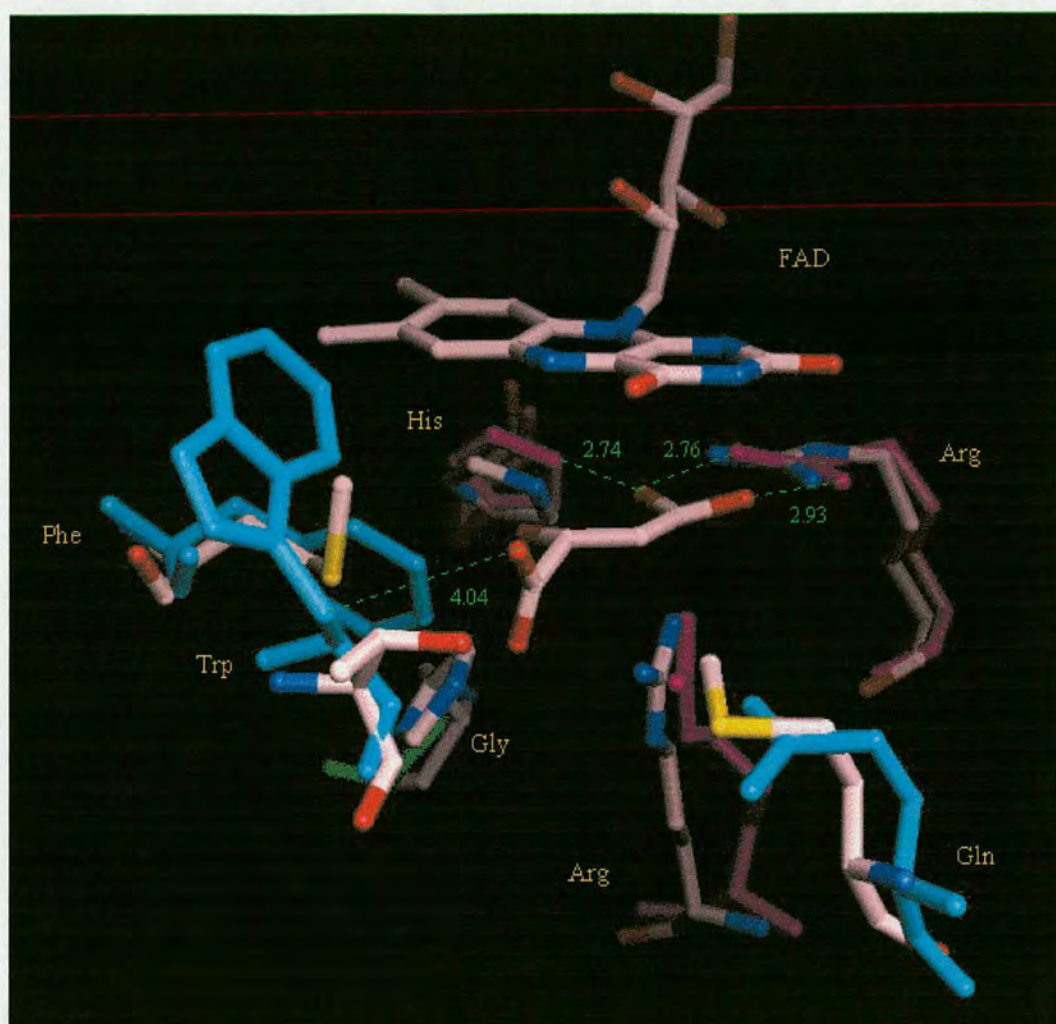


Figure 3.11: An overlay of the FccA54 molecular model with the Fcc₃ active site

The molecular model of FccA54 generated using 'SYBYL Composer' (Blundell *et al.*, 1988) is shown superimposed on the known active site of Fcc₃. The FAD cofactor, malate-like substrate of Fcc₃ (atom type) and the key active site residues are shown. The active site residues of Fcc₃ are all shown in atom type and those of FccA54 are in magenta, cyan and green. For simplicity, only the FAD cofactor of Fcc₃ is shown. The residues highlighted in magenta are substrate binding and catalytic residues of FccA54 that are strictly conserved in Fcc₃ and other members of the fumarate reductase family. Residues of Fcc₃ involved in catalysis and substrate binding, (Met236, Met375 and Thr377), which are not conserved in FccA54 and are variable in the novel flavoenzymes are shown in cyan. His365 of Fcc₃ is not conserved in FccA54 and is replaced by Gly (green) which is a conserved substitution found in all three related novel enzymes. For simplification, only the close contacts between the substrate-binding residues and the substrate are shown for FccA54. The picture was produced using the molecular modelling graphics program WITNOTP (Widmer, 1999).

The alternative orientation of the tryptophan residue (Fcc₃; Thr367) projecting away from the active site was also sterically possible for FccA54. Each of the novel flavoproteins (FccA54, FccA56 and FccA342) contain a tryptophan residue equivalent to Thr367 of Fcc₃ (Figure 3.4), which extends away from the interior of the FccA56 and FccA342 molecular models (not shown). The orientation of the large aromatic side chain in the molecular models dictated the size and hydrophobicity of each active site and was critical in determining possible enzyme substrates. The tryptophan residue (Fcc₃; Thr377) of FccA54 is predicted to constitute one of the key substrate-binding residues in the clamp domain and was shown to make contact to O1A of the substrate (4.04 Å) (Figure 3.11). This is considerably longer than the shortest contact (2.63 Å) made between O1A of the twisted substrate and Thr377 of Fcc₃ (Figure 3.1). One of the major differences of the FccA54 molecular model compared to the active site of Fcc₃ is substitution of His365 (Fcc₃) with Gly and the absence of close substrate contacts to the twisted malate-like substrate molecule (Figures 3.1 and 3.11).

In addition to the two aromatic tryptophan residues present in the active site of the FccA54 molecular model, a phenylalanine residue (Fcc₃; Met375) contributes to a highly hydrophobic tight binding pocket for FccA54 (Figure 3.11). This phenylalanine residue (Phe261) maintains close contact to the C1, C2, O1B and O2 atoms of the twisted substrate molecule (Table 3.2). This indicated the close proximity of the hydrophobic side chain to the twisted conformation of the substrate, which is not found in Fcc₃ with loss of Met375 contacts to the non-planar substrate configuration (Figure 3.1; Table 3.2).

The absence of close substrate contacts with residues in the clamp domain of the FccA54 molecular model, partially due to replacement of His365 (Fcc₃) with glycine (Figure 3.11) initially led us to suggest that FccA54 would accommodate an acrylate substrate with a larger functional group. However, molecular modelling of the FccA54 flavoenzyme has shown that the glycine substitution is counteracted with the presence of large hydrophobic side chains in the active site. These aromatic groups of FccA54 are arranged in the clamp domain to form a tightly enclosed and highly hydrophobic active site (Figure 3.11). The small interior of the FccA54 active site, as observed from the molecular model, led to the conjecture that FccA54 will accommodate small acrylates such as methacrylate and crotonate (Figure 3.17).

An arginine residue equivalent to Arg402 (Fcc₃) exists in FccA54 and molecular modelling of the novel flavoenzyme showed that this arginine side chain maintains close contact to the substrate (Figure 3.12). An NH₂ moiety of the FccA54 arginine guanidinium group is positioned in close proximity to C3 of the substrate (3.64 Å), resembling the close interaction for Arg402 (3.00 Å; Figure 3.12). This FccA54 arginine residue (Arg402; Fcc₃) is therefore also located in an ideal position to protonate the substrate at C3 (or equivalent carbon) leading to formation of the product. The proton delivery pathway of Fcc₃ comprising Glu378 and Arg381 that functions to deliver protons to Arg402 (Doherty *et al.*, 2000) appears to operate differently in FccA54. The proton transfer residues of Fcc₃, Glu378 and Arg381, are not conserved in FccA54 and are replaced with Ser and Leu, respectively (Figure 3.12).

The molecular model of FccA54 showed that the conserved arginine residue (Arg402; Fcc₃) is in a suitable position to function as the active site acid, which accepts protons via a different route compared to the proton delivery pathway of Fcc₃ (Figure 3.12).

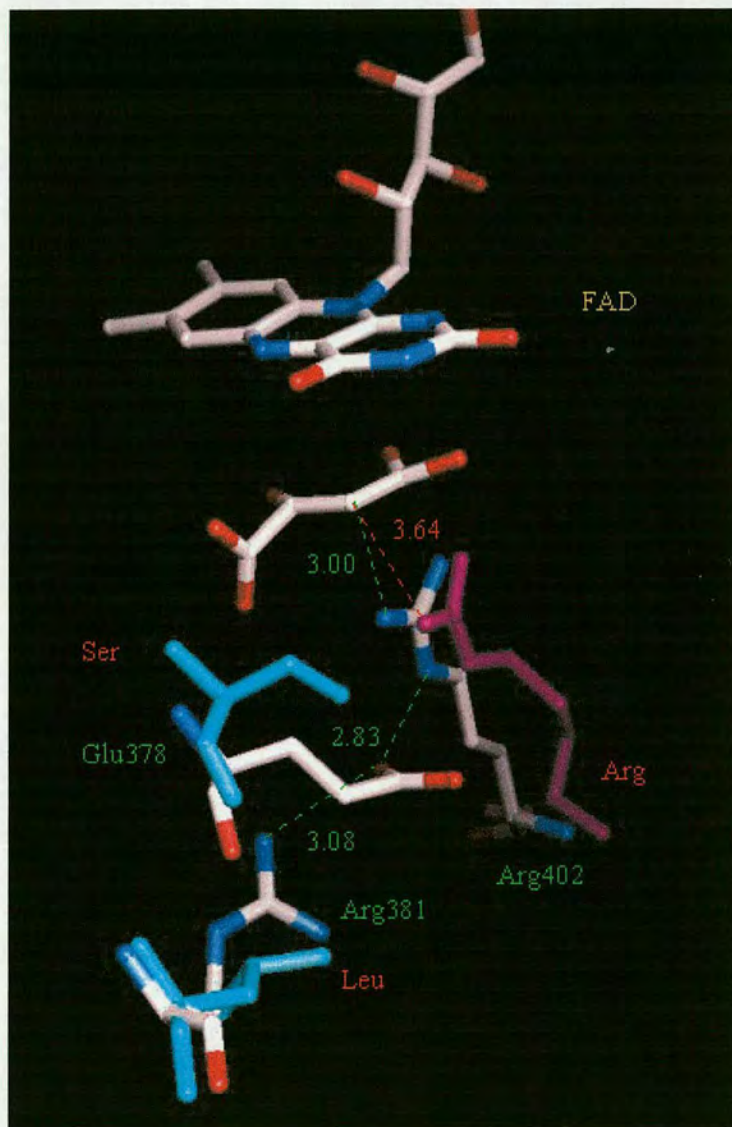


Figure 3.12: An alternative proton delivery pathway for FccA54

The proton delivery residues of Fcc₃: Arg381, Glu378 and Arg402 (atom type) are shown with the route of proton transfer (green; Å). Arg402 of Fcc₃ is conserved in FccA54 (magenta) and an NH₂ group of the FccA54 arginine residue is within close contact (3.64 Å, red) to C3 of the malate-like substrate (atom type) for proton delivery. However, Arg381 and Glu378 of Fcc₃ are replaced in FccA54 with Leu and Ser (cyan), respectively. This suggests that an alternative proton delivery pathway towards the conserved arginine residue exists in FccA54. The residues of Fcc₃ are labelled in green and the residues of FccA54 are labelled in red. FAD of Fcc₃ is also shown (atom type). The picture was produced using the molecular modelling graphics program WITNOTP (Widmer, 1999).

3.2.2.3 Molecular model of the FccA56 enzyme active site

The molecular model of FccA56 superimposed with the known active site of Fcc₃ (Figure 3.13) revealed that the conserved substrate-binding residues of the flavin domain corresponding to His504 and Arg544 of Fcc₃ maintain close contact to the C4 carboxylate group of the substrate. In particular, the close contact observed between the imidazole ring of His399 of FccA56 (Fcc₃; His504) and O4B of the substrate molecule (2.70 Å; Figure 3.13) is similar to the close contact observed between equivalent atoms in Fcc₃ (2.72 Å; Figure 3.1).

The molecular model of FccA56 (Figure 3.13) revealed that the active site lacks large hydrophobic groups characteristic of the FccA54 clamp domain (Figure 3.11). A proline residue (Pro260) of FccA56 is located in place of Thr377 (Fcc₃) and causes the backbone to shift away from the active site providing an enlarged cavity for substrate-binding (Figure 3.13). The shortest contact made between the side chain of proline extending away from the active site and the substrate molecule (O1A) is 4.46 Å. The absence of close substrate contacts with residues in the clamp domain of FccA56 is also attributed to the presence of glycine that substitutes His365 (Fcc₃; Figure 3.13). The conserved tryptophan side chain (Thr367; Fcc₃) is oriented away from the active site in the molecular model of FccA56 and was shown to interact with neighbouring aromatic residues that are absent in FccA54 (not shown). The external orientation of the tryptophan residue (Thr367; Fcc₃) is perhaps determined by constraints imposed by the adjacent proline residue (Pro366; Fcc₃) that is conserved in the family of fumarate reductases, except FccA54.

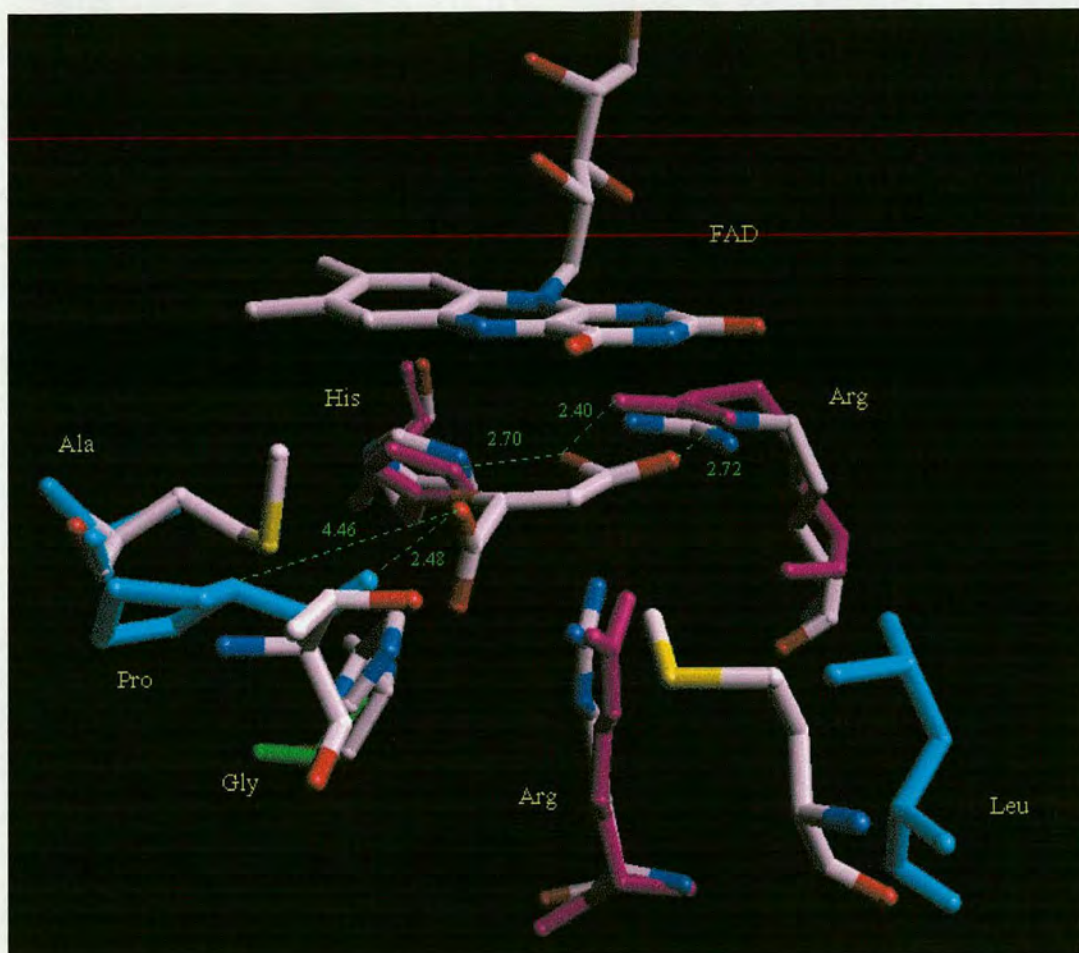


Figure 3.13: An overlay of the FccA56 molecular model with the Fcc₃ active site

The molecular model of FccA56 generated using 'SYBYL Composer' (Blundell *et al.*, 1988) is shown superimposed on the known active site of Fcc₃. The FAD cofactor, malate-like substrate of Fcc₃ (atom type) and the key active site residues are shown. The active site residues of Fcc₃ are all shown in atom type and those of FccA56 are in magenta, cyan and green. For simplicity, only the FAD cofactor of Fcc₃ is shown. The residues highlighted in magenta are substrate binding and catalytic residues of FccA56 that are strictly conserved in Fcc₃ and other members of the fumarate reductases family. Residues of Fcc₃ involved in substrate binding and catalysis, (Met236, Met375 and Thr377), which are variant in FccA56 and the other novel flavoenzymes are shown in cyan. His365 of Fcc₃ is not conserved in FccA56 and is replaced by Gly (green) which is a conserved substitution found in all three related novel enzymes. For simplification, only the close contacts between the substrate-binding residues and the substrate are shown for FccA56. The picture was produced using the molecular modelling graphics program WITNOTP (Widmer, 1999).

The structural deviation observed in the FccA56 polypeptide backbone due to proline (Thr377, Fcc₃) and absence of close contacts that are established by His365 in Fcc₃ results in the formation of an enlarged active site. The FccA56 binding site (Figure 3.13) has a greater capacity compared to the active site of FccA54 (Figure 3.11) and could potentially accommodate substrates such as phenylacrylates. Indeed, the *fccA56* gene is associated with a gene encoding a histidase family protein (1.8.2) which has led to the suggestion that FccA56 catalyses the reduction of phenylacrylates such as cinnamate (Figure 3.17).

The active site acid of Fcc₃ (Arg402) is conserved in FccA56 (Figure 3.4) and the molecular model of FccA56 superimposed on the known structure of Fcc₃ showed that the position of the arginine residue is conserved (Figure 3.14). The close contact (3.00 Å) observed in the Fcc₃ enzyme between an NH₂ moiety of the guanidinium group of Arg402 and C3 of the substrate is also observed in the molecular model of FccA56 (2.90 Å; Figure 3.14). This result indicates that the conserved arginine residue in FccA56 also functions as an active site acid to protonate C3 (or equivalent carbon) of the putative acrylate substrate. The residues of the Fcc₃ proton delivery pathway (Glu378 and Arg381; Doherty *et al.*, 2000) are not conserved in FccA56 and are replaced with Ala and Phe, respectively (Figure 3.14). This suggests that the conserved arginine in FccA56 (Arg402; Fcc₃) will function as the active site acid and obtain protons from a pathway that is structurally dissimilar to that of Fcc₃.

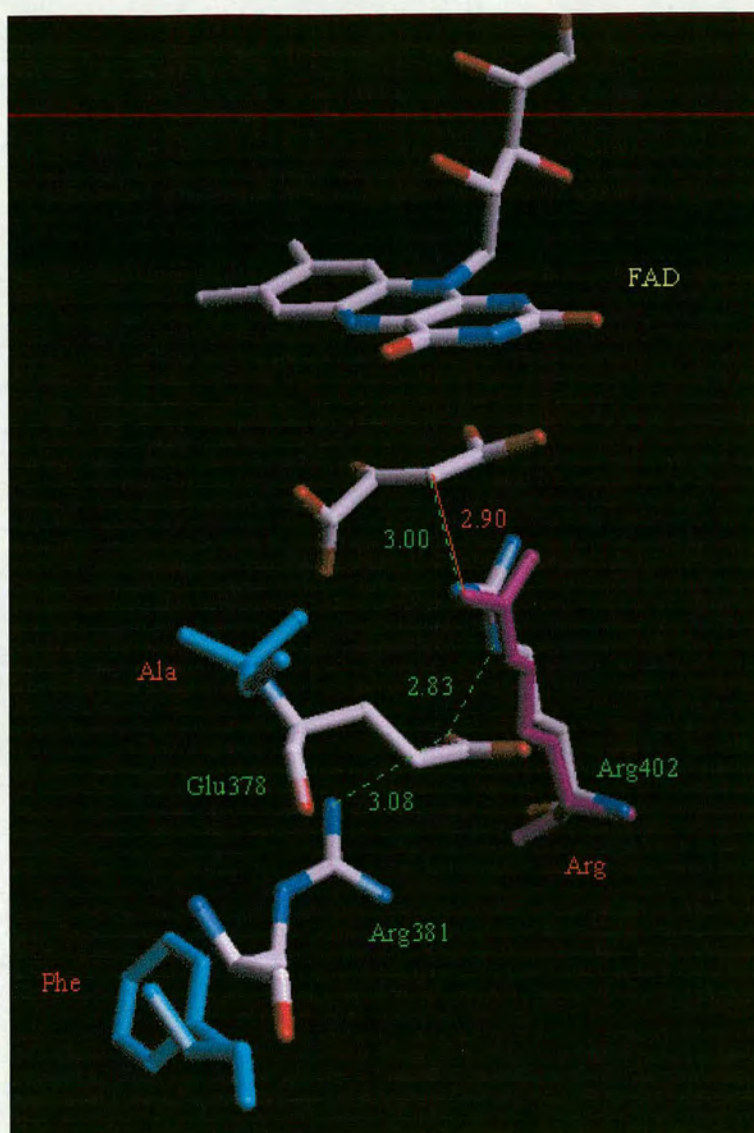


Figure 3.14: An alternative proton delivery pathway for FccA56

The proton delivery residues of Fcc₃: Arg381, Glu378 and Arg402 (atom type) are shown with the route of proton transfer (green; Å). Arg402 of Fcc₃ is conserved in FccA56 (magenta) and an NH₂ group of the FccA56 arginine residue is within close contact (2.90 Å, red) to C3 of the substrate for proton delivery. However, Arg381 and Glu378 of Fcc₃ are replaced in FccA56 with Phe and Ala (cyan), respectively. This suggests that an alternative proton delivery pathway towards the conserved Arg residue exists in FccA56. The residues of Fcc₃ are labelled in green and the residues of FccA56 are labelled in red. FAD of Fcc₃ is shown (atom type). The picture was produced using the molecular modelling graphics program WITNOTP (Widmer, 1999).

3.2.2.4 Molecular model of the FccA342 enzyme active site

The structural model of FccA342 superimposed on the known structure of Fcc₃ (Figure 3.15) clearly showed the structural identity with Fcc₃ concerning active site residues that map to the flavin domain. The histidine and arginine substrate-binding residues of FccA342 were slightly misaligned with respect to the corresponding residues in Fcc₃ (His504 and Arg544, respectively). However, these conserved basic substrate-binding residues in FccA342 maintain significantly close contact with the C4 carboxylate group of the malate-like substrate. The close interaction observed between the guanidinium group of the FccA342 arginine residue (Fcc₃; Arg544) with O4A and O4B of the substrate molecule (3.07 and 2.68 Å, respectively) (Figure 3.15), is similar to the close contacts observed between equivalent atoms in Fcc₃ (2.58 and 2.77 Å, respectively; Figure 3.1). The FccA342 histidine side chain equivalent to His504 (Fcc₃) forms close contact (3.31 Å) to O4B of the malate-like substrate (Figure 3.15), an interaction also conserved in Fcc₃ (2.72 Å; Figure 3.1).

The active site region of FccA342 formed by residues of the clamp domain is less well conserved compared to Fcc₃. A tyrosine side chain (Thr377; Fcc₃) projects into the active site and the C β atom forms the shortest contact (3.37 Å) to O1A of the malate-like Fcc₃ substrate (Figure 3.15). The tyrosine residue also forms close contact to O1A, O1B and C1 atoms of the substrate molecule (Table 3.2). The key substrate-binding contacts observed in Fcc₃ between His365 and the substrate C1 carboxylate group (Figure 3.1) are absent in FccA342 due to the presence of glycine instead of His365 (Figure 3.15).

The tryptophan residue that is conserved in each of the novel flavoenzymes (Thr367, Fcc₃) is oriented away from the active site interior of FccA342 and interacts with other hydrophobic residues (not shown). As postulated for the molecular model of FccA56, the conserved proline residue of FccA342 (Pro366; Fcc₃) may affect the orientation of the neighbouring tryptophan side chain (Thr367; Fcc₃; not shown). In addition to the tyrosine residue (Thr377; Fcc₃) that extends into the active site pocket of FccA342, a phenylalanine side chain (Met375; Fcc₃) is present (Figure 3.15) that forms close contacts to C1, C2, O1A, O1B and O2 of the twisted substrate molecule (Table 3.2).

The size and hydrophobicity of the FccA342 active site is intermediate in comparison to the molecular models of FccA54 (Figure 3.11) and FccA56 (Figure 3.13). The loss of substrate contacts in FccA342 due to the presence of glycine (His365; Fcc₃) and the generation of a potentially larger active site was precluded by the presence of tyrosine and phenylalanine hydrophobic groups (Thr377 and Met375, respectively; Fcc₃). These aromatic groups project into the active site of FccA342 and contribute to formation of a small hydrophobic binding pocket (Figure 3.15), which is most likely to bind smaller acrylate substrates, as predicted for FccA54.

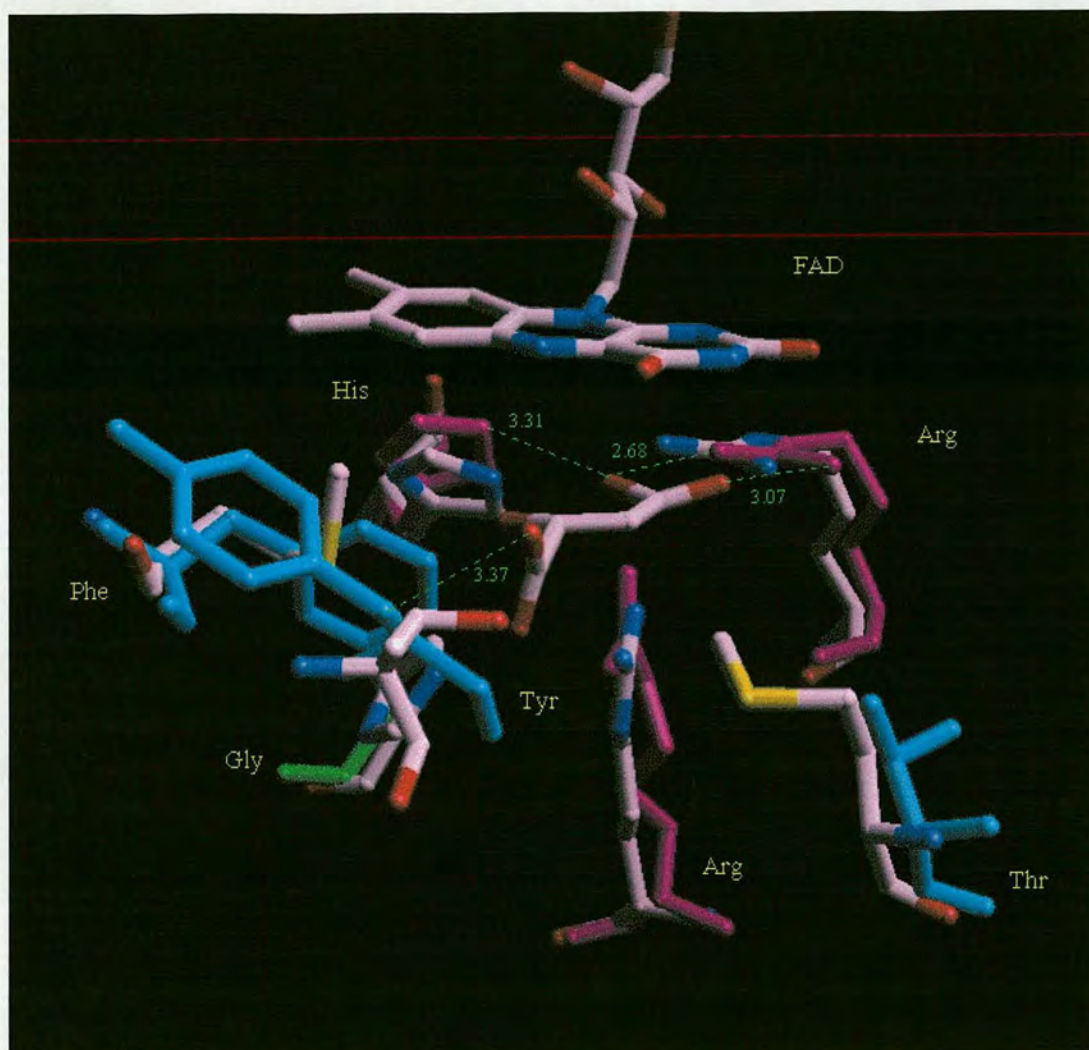


Figure 3.15: An overlay of the FccA342 molecular model with the Fcc₃ active site

The molecular model of FccA342 generated using 'SYBYL Composer' (Blundell *et al.*, 1988) is shown superimposed on the known active site of Fcc₃. The FAD cofactor, malate-like substrate of Fcc₃ (atom type) and the key active site residues are shown. The active site residues of Fcc₃ are all shown in atom type and those of FccA342 are in magenta, cyan and green. For simplicity, only the FAD cofactor of Fcc₃ is shown. The residues highlighted in magenta are substrate binding and catalytic residues of FccA342 that are strictly conserved in Fcc₃ and other members of the fumarate reductases family. Residues of Fcc₃ involved in substrate binding and catalysis, (Met236, Met375 and Thr377), which are variant in FccA342 and the other novel flavoenzymes are shown in cyan. His365 of Fcc₃ is not conserved in FccA342 and is replaced by Gly (green) which is a conserved substitution found in all three related novel enzymes. For simplification, only the close contacts between the substrate-binding residues and the substrate are shown for FccA342. The picture was produced using the molecular modelling graphics program WITNOTP (Widmer, 1999).

The arginine residue of FccA342 that is equivalent to the active site acid of Fcc₃ (Arg402) is positioned in a similar orientation to Arg402, as shown by superimposition of the FccA342 molecular model with Fcc₃ (Figure 3.16). The exceptionally close contact of the Arg402 NH₂ moiety (Fcc₃) with C3 of the substrate molecule (3.00 Å) is conserved in FccA342 (3.87 Å; Figure 3.16). This result leads us to suggest that the conserved arginine residue in FccA342 (Arg402; Fcc₃) will also act to protonate the substrate required for formation of the product. The proton delivery residues of Fcc₃ (Glu378 and Arg381) that constitute a pathway towards Arg402 (Doherty *et al.*, 2000) are not conserved in FccA342. The Glu378 and Arg381 residues of Fcc₃ are substituted with Gly and Phe, respectively (Figure 3.16). This suggests that an alternative proton pathway towards the conserved arginine residue in FccA342 will function to reprotonate the arginine side chain.

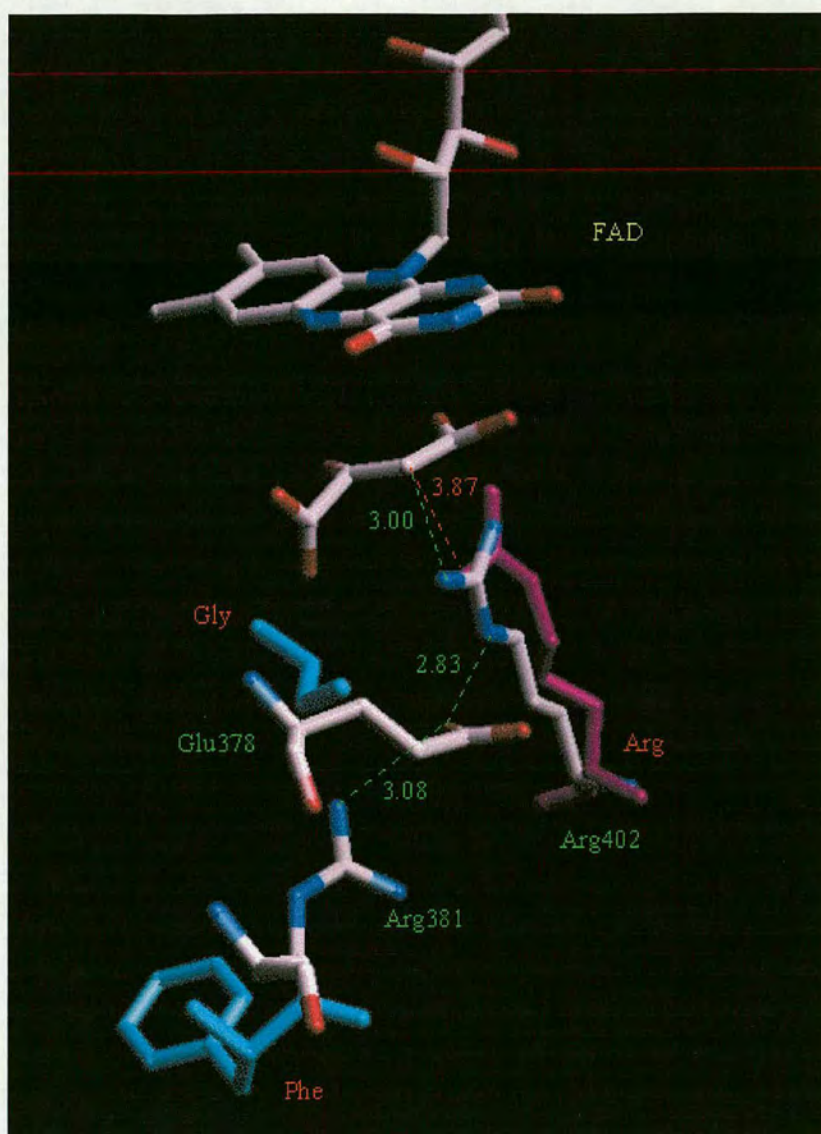


Figure 3.16: An alternative proton delivery pathway for FccA342

The proton delivery residues of Fcc₃: Arg381, Glu378 and Arg402 (atom type) are shown with the route of proton transfer (green; Å). Arg402 of Fcc₃ is conserved in FccA342 (magenta) and an NH₂ group of the FccA342 Arg residue is within close contact (Å, red) to C3 of the substrate for proton delivery. However, Arg381 and Glu378 of Fcc₃ are replaced in FccA342 with Phe and Gly (cyan), respectively. This suggests that an alternative proton delivery pathway towards the conserved Arg residue exists in FccA342. The residues of Fcc₃ are labelled in green and the residues of FccA342 are labelled in red. FAD of Fcc₃ is shown (atom-type). The picture was produced using the molecular modelling graphics program WITNOTP (Widmer, 1999).

3.2.3 Acrylate substrates modelled in the enzyme active sites

A range of biologically relevant plant metabolites that may be frequently encountered in the natural habitat of *S. oneidensis* MR-1 were selected as potential substrates of the flavoproteins. The various plant metabolites consisted of C₆-C₃ phenylacrylates and smaller C₃ or C₄ acrylates that contain a single carboxylate group (Figure 3.17). A range of C₆-C₃ phenylacrylates incorporated into lignin are synthesised from the deamination of phenylalanine to *trans*-cinnamic acid, catalysed by phenylalanine ammonia-lyase. For incorporation into lignin, cinnamate is converted to hydroxycinnamyl alcohols; *p*-coumaryl alcohol, coniferyl alcohol and syringyl alcohol that form lignan dimers via oxidative coupling that further polymerise to form lignin (Wallace and Fry, 1994). Lignin is a structural component of both primary and secondary cell walls of tracheids and vessel elements of xylem tissue. It is highly probable that the anaerobic freshwater lake sediments inhabited by *S. oneidensis* MR-1 are a rich source of lignin deposits. The specific content of lignin varies with taxa, tissues and changing physiological conditions, which would affect the type and abundance of specific acrylates in the anaerobic sedimentary environment. Some of the lignin within the plant cell wall is covalently bound to structural polysaccharides that may affect degradation and release of phenylacrylates (Wallace and Fry, 1994). Ferulate and coumarate are phenylacrylates found predominantly in their *trans* form and are identified to exist as covalently bound cell wall components. However, caffeate is incorporated into chlorogenic acid that is located in soluble parts of plants.

The phenylacrylates may be readily released into the environment in an uncombined free form to serve as terminal electron acceptors (Wallace and Fry, 1994). Indeed, some microorganisms such as the bacterial acetogens are reported to utilise lignin derivatives as terminal oxidants to conserve energy for growth (Misoph *et al.*, 1996).

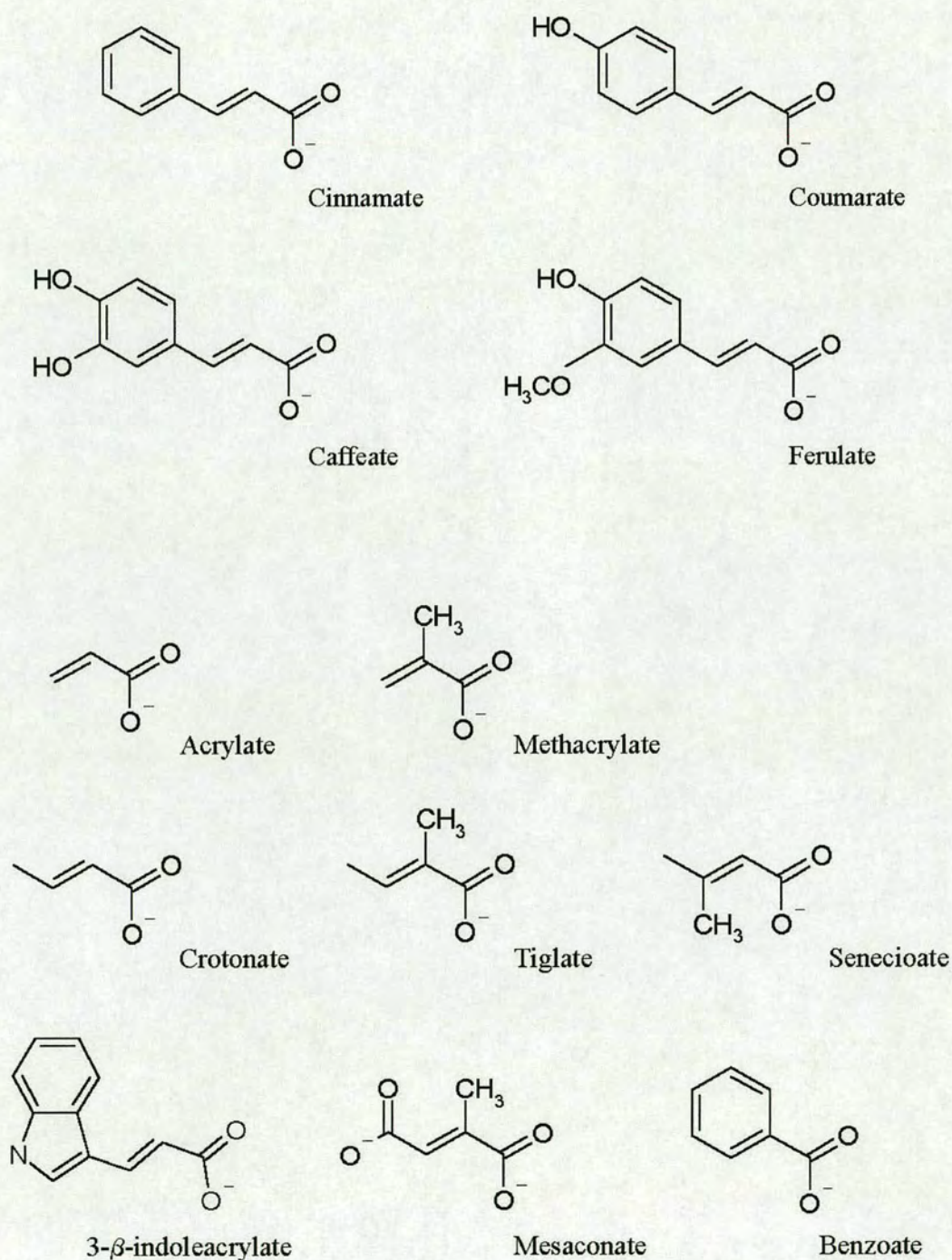


Figure 3.17: Acrylate substrates of the novel flavoproteins

The chemical structures of the acrylates selected as potential enzyme substrates of FccA54, FccA56 and FccA342 are shown.

3.2.3.1 Molecular modelling of the acrylate substrates

The acrylates (Figure 3.17) were incorporated in the molecular models of FccA54, FccA56 and FccA342 by superimposition of the carboxylate group with the C₄ carboxylate group of the malate-like substrate of Fcc₃. Phenylacrylates were modelled in the enlarged active site of the FccA56 molecular model (Figure 3.13) that appeared suitable for accommodating large functional groups. However, steric constraints were observed between the aromatic ring of cinnamate and the polypeptide backbone of the clamp domain (Figure 3.18). This raises the possibility that phenylacrylates are not suitable substrates for the novel flavoenzymes. The close-fitting active site model of FccA54 (Figure 3.11) showed that this enzyme perhaps binds to smaller C₃ acrylate substrates (e.g. methacrylate) and C₄ acrylate substrates, (e.g. crotonate), rather than C₆-C₃ phenylacrylates (e.g. ferulate). A wide range of smaller acrylates (Figure 3.17), including crotonate and methacrylate were modelled in the active site of FccA54. Crotonate was easily accommodated in the active site of FccA54 and was shown to establish close contacts to the key substrate-binding residues (Figure 3.19). The smaller C₃ substrates such as methacrylate also formed close contacts to the FccA54 substrate-binding residues (not shown). The molecular model of FccA54 (Figure 3.11) leads us to the prediction that FccA54 is unlikely to bind large aromatic phenylacrylates but may function to catalyse the reduction of smaller acrylates such as methacrylate and crotonate. The catalytic function of FccA54 may resemble that of the related methacrylate reductase flavoprotein from *Geobacter sulfurreducens* AM-1 (Mikoulinskaia *et al.*, 1999).

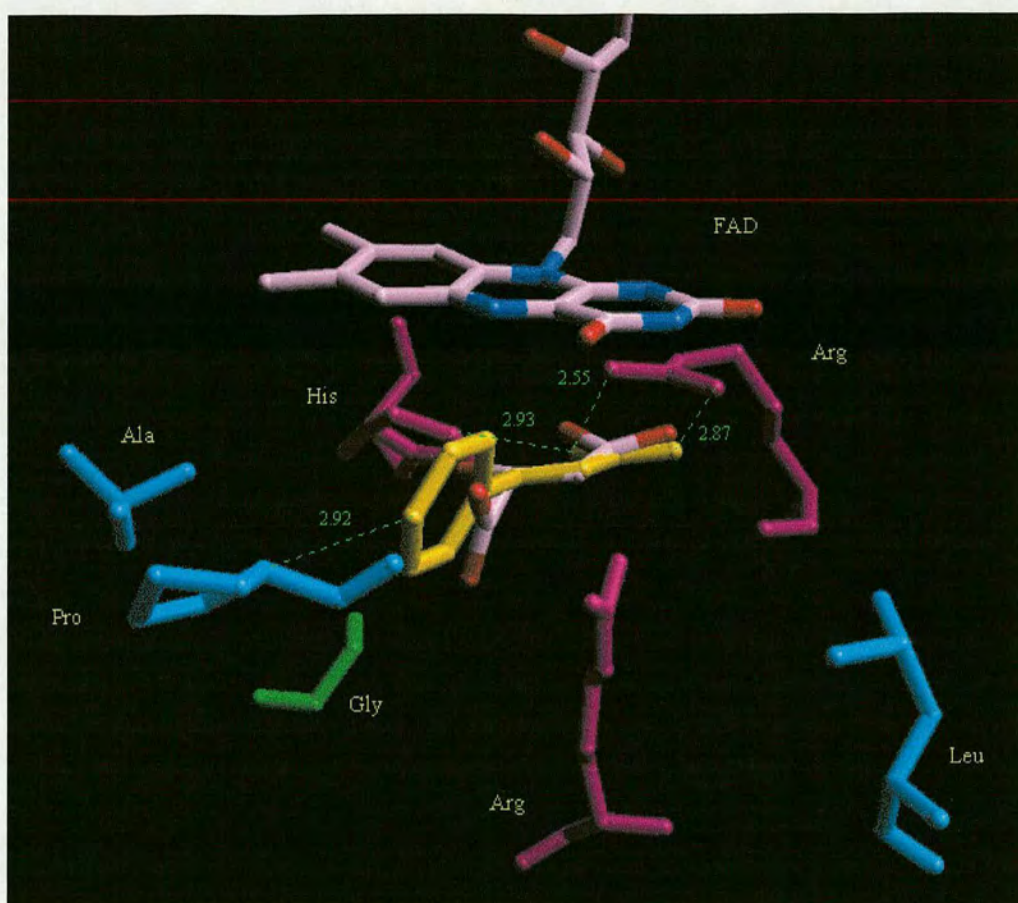


Figure 3.18: FccA56 complexed with cinnamate

The molecular model of FccA56 generated using 'SYBYL Composer' (Blundell *et al.*, 1988) is shown to contain cinnamate (yellow) bound in the active site. The substrate carboxylate group was aligned with the C₄ carboxylate group of the malate-like substrate of Fcc₃ (atom-type). The FAD cofactor is shown in atom type and the key active site residues of FccA56 are shown in magenta, cyan and green, consistent with Figure 3.13. The residues in magenta are active site residues strictly conserved in the fumarate reductase family; the residues in cyan are not conserved and are completely variable, whereas glycine (green) is a conserved substitution in the novel flavoenzymes. The close contacts between cinnamate and the key substrate-binding residues are shown (green, Å). The picture was produced using the molecular modelling graphics program WITNOTP (Widmer, 1999).

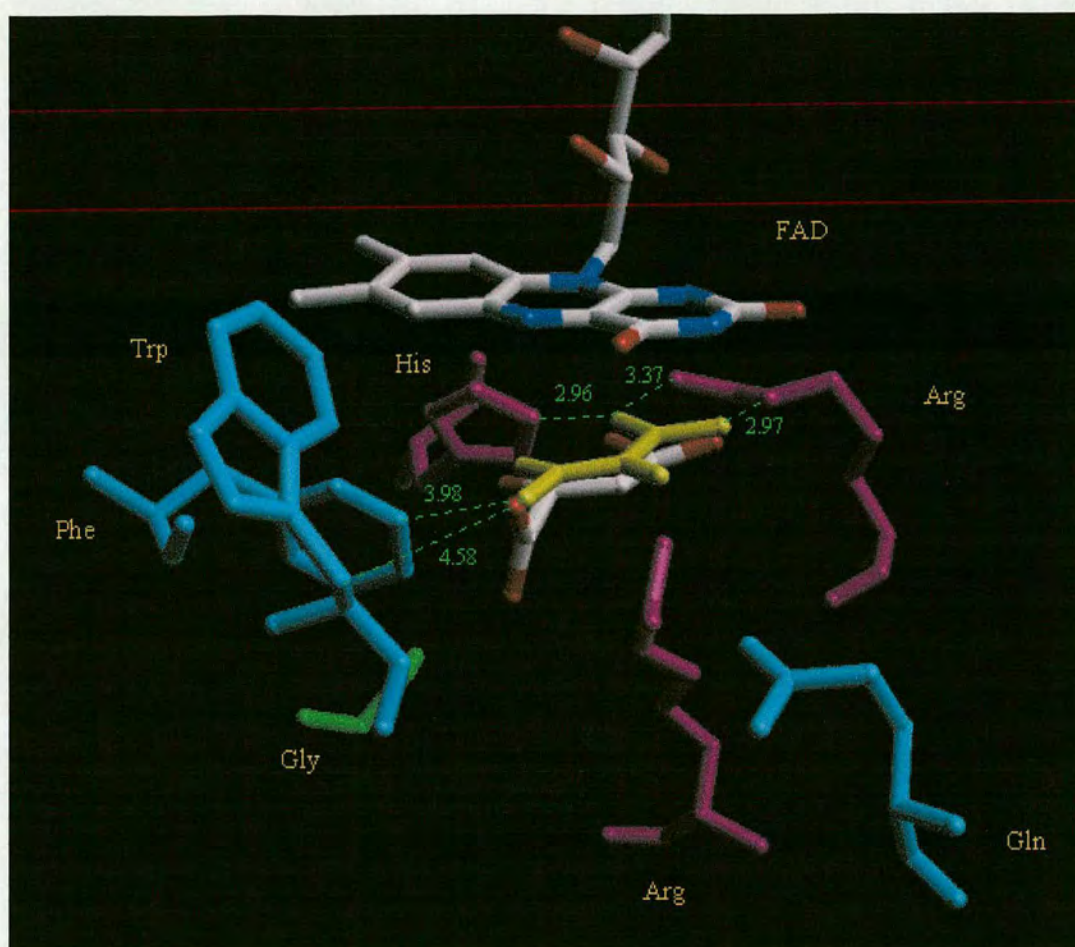


Figure 3.19: FccA54 complexed with crotonate

The molecular model of FccA54 generated using 'SYBYL Composer' (Blundell *et al.*, 1988) is shown to contain crotonate (yellow) bound in the active site. The substrate carboxylate group was aligned with the C₄ carboxylate group of the malate-like substrate of Fcc₃ (atom-type). The hydrogen atoms are shown for the modelled substrate. The FAD cofactor is shown in atom type and the key active site residues of FccA54 are shown in magenta, cyan and green, consistent with Figure 3.11. The residues in magenta are active site residues strictly conserved in the fumarate reductase family; the residues in cyan are not conserved and are completely variable, whereas glycine (green) is a conserved substitution in the novel flavoenzymes. The close contacts between crotonate and the substrate-binding residues are shown (green, Å). The picture was produced using the molecular modelling graphics program WITNOTP (Widmer, 1999).

3.3 Conclusions derived from molecular modelling

The multiple sequence alignments of the novel flavoproteins against Fcc₃ that were generated using 'ClustalW' (Figure 3.4) and the 'Sequence and Secondary Structures' alignment tool (Figures 3.7-3.9) showed differences in alignment of residues located to the clamp domain. The sequence alignments that incorporated secondary structure information were used to generate molecular models of FccA54 (Figure 3.11), FccA56 (Figure 3.13) and FccA342 (Figure 3.15), based upon the known structure of the homologous Fcc₃ enzyme (Figure 3.1; Taylor *et al.*, 1999). The molecular models showed good structural alignment with Fcc₃, as exemplified in the low r.m.s.d values (0.82-0.87 Å) obtained for the polypeptide backbone main chain atoms (Table 3.1). Despite the overall structural alignment of the homologous enzymes, a loop was inserted in the clamp domain of the molecular models that was absent in Fcc₃ (Figure 3.10a and b). This loop comprising 4-5 amino acid residues caused ambiguity in structural alignment of residues located to the clamp domain of each molecular model.

The molecular models revealed that the structural topology and key catalytic residues of Fcc₃ are highly conserved in the flavin domains of FccA54, FccA56 and FccA342. The analyses of the close contacts (Table 3.2) clearly showed the structural differences in the substrate-binding sites of the FccA54, FccA56 and FccA342 molecular models compared to the active site of Fcc₃. In particular, the molecular models clearly showed differences in substrate-binding residues located to the clamp domain of the novel flavoproteins and lend further support that the substrate comprises an alternative functional group to the carboxylate group of fumarate.

The three-dimensional molecular models of the novel flavoproteins provided structural templates for modelling a wide range of possible acrylate substrates (Figure 3.17) that may support anaerobic metabolism of *S. oneidensis* MR-1. Comparative modelling using the known structure of Fcc₃ (Taylor *et al.*, 1999) was successfully used to reinforce sequence analysis predictions that the native substrate of FccA54, FccA56 and FccA342 is an acrylate substrate comprising a single carboxylate group.

Chapter 4

Gene replacement of *fccA54* and *fccB54* in *Shewanella oneidensis* MR-1 and phenotypic analysis of the deletion strain

4.1 INTRODUCTION

4.1.1 Mechanisms of genetic change

Spontaneous mutations that cause genetic change are naturally occurring in all cells. They may arise from errors in DNA replication resulting from tautomeric shifts that lead to mispairing of bases in duplex DNA. DNA replication errors can also lead to frameshift mutations that commonly occur at hot spot regions of repeated DNA sequence. In addition to DNA replication errors, spontaneous mutations can arise from naturally occurring DNA damage. Hydrogen peroxide generated as a by-product of aerobic respiration can cause oxidative damage to DNA that leads to base mispairing. Spontaneous mutations also arise from the ability of transposable genetic elements such as transposons to move from one plasmid to another plasmid or from a plasmid to a bacterial chromosome. The genetic change can be a result of conservative or replicative transposition that gives rise to one or two copies of the transposable element, respectively. The target DNA is further modified to contain a short repeated sequence of the target gene upon integration of the transposable genetic element. Transposon mutagenesis led to the generation of a *Shewanella oneidensis* MR-1 mutant that was unable to respire anaerobically with fumarate as the terminal electron acceptor. This mutant phenotype was consistent with the absence of a 65 kDa cytochrome protein corresponding to the size of the fumarate reductase enzyme (Myers and Myers, 1997c). An *S. oneidensis* MR-1 transposon mutant, CMTn-1, that was deficient in Fe(III), Mn(IV), fumarate and nitrate reduction (Myers and Myers, 1993) was identified to contain the *TnphoA* transposon in the *cymA* gene (Myers and Myers, 1997b).

The ability of *cymA* to complement the mutant phenotype led to the suggestion that CymA is a common electron transport protein of a branched anaerobic electron transfer pathway (1.5; Myers and Myers, 1997b).

In addition to the occurrence of spontaneous mutations, the sequence of a target gene can be modified using mutagenic agents that induce specific mutations. Alkylating agents such as ethyl methanesulfonate (EMS) and nitrosoguanidine (NG) favour addition of an alkyl group to guanine causing GC \rightarrow AT transitions. The EMS chemical mutagen was used to generate an array of *S. oneidensis* MR-1 mutant strains that were deficient in Fe(III) reduction (Dichristina and Delong, 1994) and Mn(IV) reduction (Burnes *et al.*, 1998). Other types of mutagens are capable of inducing mutations by mimicking a normal base of DNA. For example, 5-bromouracil is a base analogue of thymine that can exist in an ionised form that mispairs with guanine forming AT \rightarrow GC transitions. Another common method of specifically mutating target chromosomal genes involves gene disruption in which a portion of the gene sequence is precisely deleted. This is a useful method for determining the function of the protein encoded by the deleted gene.

4.1.2 The generation of gene disruptions in *S. oneidensis* MR-1

Variations of a gene disruption method were used to construct a number of anaerobic respiratory mutants of *S. oneidensis* MR-1. The method is based upon constructing a recombinant suicide plasmid that contains the target gene sequence disrupted by a selectable marker. Subsequent transfer of the suicide plasmid into *S. oneidensis* MR-1 promotes recombination between the cloned gene sequence and the homologous chromosomal gene. This leads to insertion of the selectable marker within the endogenous target gene. The proposed function of electron transport regulator A (EtrA) in regulating gene expression for anaerobic electron transport was investigated by constructing an *etrA* knockout strain (ETRA-153). The *etrA* gene disruption strategy involved inverse PCR with the cloned *etrA* sequence that led to a deletion of 246 bp of internal *etrA* sequence. A kanamycin resistance gene was inserted in place of the deleted *etrA* sequence and the gene disruption fragment was transferred into the pEP185.2 suicide plasmid for homologous recombination in *S. oneidensis* MR-1 (Maier and Myers, 2001). A similar gene disruption strategy that used a recombinant pKNOCK-Km^R suicide plasmid integrated into the endogenous target gene was used to generate an *etrA* mutant (Beliaev *et al.*, 2002a) and a mutant of the *fur* gene encoding a ferric uptake regulator protein (Thompson *et al.*, 2002).

4.1.3 Constructing an *fccA54* and *fccB54* gene replacement

The major aims of this project were to delete the *fccA54* and *fccB54* target genes from the *S. oneidensis* MR-1 genome and determine the effect on anaerobic growth of the null mutant. The *S. oneidensis* MR-1 knockout strains (4.1.2) were all constructed using a similar gene disruption strategy that led to the deletion of internal gene sequence. It is possible that truncated polypeptide encoded by the remainder of the target gene was synthesised in the mutant strains. Therefore, it is possible that phenotypic analysis of these insertional mutant strains (Maier and Myers, 2001 and Beliaev *et al.*, 2002a) was hampered by synthesis of target polypeptide. In order to avoid such complications when identifying the *fccA54* and *fccB54* null mutant phenotype, a 'gene replacement' strategy was devised to knockout the entire *fccA54* and *fccB54* gene coding sequences. This involved deleting both the *fccA54* and *fccB54* genes together since the encoded proteins are expected to associate and form a functional heterodimer.

The gene replacement construction and phenotypic characterisation were designed to further the molecular modelling findings. Molecular modelling of the flavoprotein active sites led to the identification of various acrylates as potential enzyme substrates (3.2.3). The aim was to test whether these acrylates served as terminal electron acceptors during anaerobic growth of the *fccA54* and *fccB54* null mutant.

4.1.4 A novel gene replacement strategy

An effective method for gene replacement is the synthesis of a gene replacement fragment using fusion PCR (Wang *et al.*, 2002). A novel fusion PCR method was devised to amplify homologous template DNA comprising the *fccA54* and *fccB54* gene-flanking DNA synthesised as a contiguous sequence. This sequence was designed to contain an *EcoRV* cleavage site (5'-GATATC-3') for insertion of a kanamycin cassette to form a gene replacement fragment. The strategy involved insertion of the gene replacement fragment in a mobilisable plasmid for conjugative transfer to *S. oneidensis* MR-1. The strategy was based upon the ability to screen transconjugants for the null mutant using antibiotic selection and PCR screening.

4.2 RESULTS AND DISCUSSION

4.2.1 Fusion PCR amplification and primer design

The fusion PCR amplification was designed to precisely delete the putatively co-expressed *fccA54* and *fccB54* genes and to replace the coding sequences with a selectable marker gene. The DNA sequence that flanks *fccA54* and *fccB54* in the wild-type *S. oneidensis* MR-1 genome was amplified and modified to become a contiguous sequence using fusion PCR. This PCR amplified homologous template DNA was designed to contain an *EcoRV* cleavage site at the fusion junction for insertion of a kanamycin cassette (Figure 4.1). Oligonucleotide primers, 54gk3 and 54gk4 that were distal to the point of kanamycin cassette insertion were designed to initiate amplification of the homologous template DNA fragment (Figure 4.1). The 5'-end of the forward oligonucleotide primer, 54gk4 was designed to complement genomic DNA 457 bp upstream of the *fccA54* ATG start codon.

The 5'-end of the 54gk3 reverse oligonucleotide primer sequence was complementary to genomic DNA 463 bp downstream of the *fccB54* TAA stop codon (Figure 4.1). The sequences of 54gk3 and 54gk4 were designed to initiate amplification of a 940 bp fusion PCR product that was a suitable length to promote specific homologous recombination.

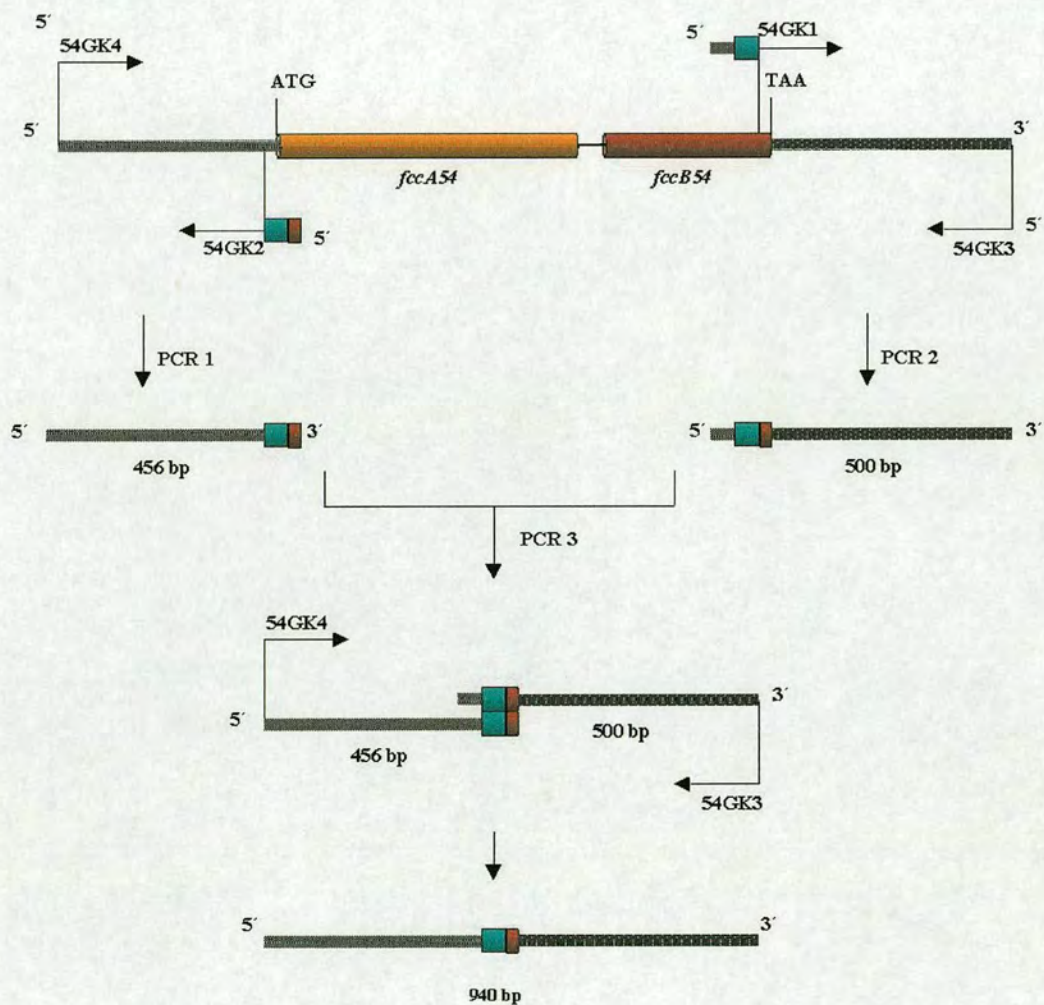


Figure 4.1: A schematic diagram of the fusion PCR procedure

The steps of fusion PCR are shown for synthesis of homologous template DNA required for *fccA54* and *fccB54* gene replacement. Arrows indicate the primer positions and direction of synthesis. Grey and black lines, respectively, represent the upstream and downstream *S. oneidensis* MR-1 genomic DNA sequences that constitute the fusion PCR product. The *EcoRV* site (cyan box) was inserted in 5'-overhang sequences of the proximal primers, 54gk1 and 54gk2, for incorporation into the 940 bp fusion PCR product. The diagram is not to scale.

The primers proximal to the point of kanamycin cassette insertion, 54gk1 and 54gk2, were intended to complement the *fccA54* and *fccB54* gene-flanking DNA sequences. However, the 5'-end of the 54gk1 forward primer sequence was complementary to *fccB54* and specifically mapped 24 nucleotides upstream of the *fccB54* TAA stop codon (Figure 4.1). The localisation of primer 54gk1 to the C-terminal sequence of *fccB54* was unavoidable due to poly-T and poly-A sequence immediately downstream of the *fccB54* TAA stop codon. The 5'-end of the 54gk2 reverse primer sequence was ideally positioned 12 nucleotides upstream of the *fccA54* ATG start codon (Figure 4.1).

The proximal primers were engineered to contain a 5' *EcoRV* cleavage site to facilitate insertion of the kanamycin cassette into the homologous template DNA fragment (Figure 4.1). *EcoRV* was selected as a suitable restriction enzyme to generate blunt ends because it does not cut in the kanamycin cassette or in the gene-flanking DNA sequences. The sequences of the proximal primers were designed to be complementary and form duplex DNA over a region of 16 nucleotides (Figure 4.2). This aimed to provide a stable interaction between the primary PCR products to promote the final fusion PCR amplification. The *EcoRV* cleavage site maps within the overlapping region of the two proximal primers (Figure 4.2).



Figure 4.2: Engineering of the proximal primers to optimise fusion PCR
The 16-nucleotide overlap of the proximal primer pair is shown. The *EcoRV* cleavage site is indicated in cyan and arrows indicate the position of enzyme cutting that generates blunt ends. The primer sequence complementary to the C-terminal coding region of *fccB54* (red) and the upstream gene-flanking DNA sequence (black) is shown.

4.2.2 Synthesis of the homologous template DNA by fusion PCR

In the first step of fusion PCR, primers 54gk2 and 54gk4 initiated amplification of a 456 bp genomic DNA fragment upstream of the *fccA54* gene (Figure 4.1). A high yield of PCR product (approximately 0.03 µg DNA) was successfully amplified for each PCR sample (Figure 4.3). The samples differed in the DNA: primer ratio and samples 2, 4 and 6 contained varying quantities of NH₄Cl. There was no yield enhancement when NH₄Cl was added to the PCR sample (Figure 4.3). However, the fidelity of the DNA polymerase may have been affected which could only be detected by sequencing all of the PCR products.

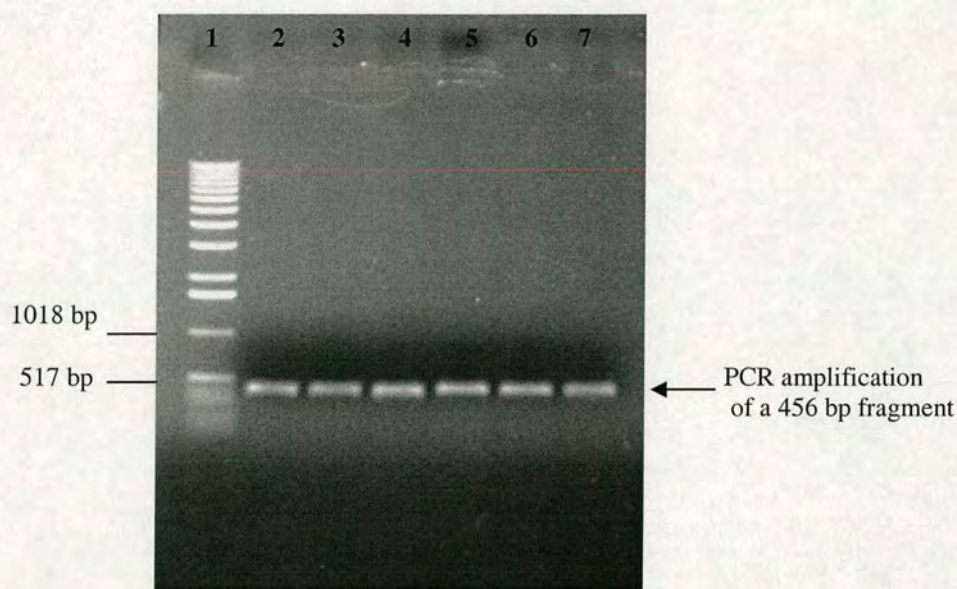


Figure 4.3: PCR amplification of genomic DNA upstream of *fccA54*

Primers 54gk2 and 54gk4 successfully initiated PCR amplification of *S. oneidensis* MR-1 genomic DNA upstream of *fccA54*. The results of PCR were analysed using agarose gel electrophoresis that revealed specific amplification of a product corresponding to the expected 456 bp fragment. The PCR samples 1-6 (lanes 2-7, respectively) that contained different DNA: primer ratios showed similar PCR product yields. The addition of NH_4Cl to reactions 2, 4 and 6 (lanes 3, 5 and 7) did not improve the yield of the PCR product. 1 kb DNA ladder (lane 1) was used to indicate the size of the PCR amplification products.

In the second amplification of fusion PCR, a 500 bp fragment corresponding to the *fccB54* gene-flanking DNA sequence was successfully amplified using primers 54gk1 and 54gk3 (Figure 4.1). A high yield of PCR product (approximately 0.03 μg DNA) was amplified for each PCR sample (Figure 4.4). The PCR samples 1-6 varied in the DNA: primer ratio and NH_4Cl was added to samples 2, 4 and 6. The variation in each reaction did not affect the desired PCR product yield (Figure 4.4). For each sample, a low molecular weight secondary PCR product was amplified that probably corresponded to primer-dimers (Figure 4.4). To eliminate amplification of erroneous products during the final fusion PCR step, the desired 500 bp PCR product was excised from a preparative agarose gel and purified. A high yield of the 500 bp PCR product was recovered to provide a suitable template for fusion PCR.

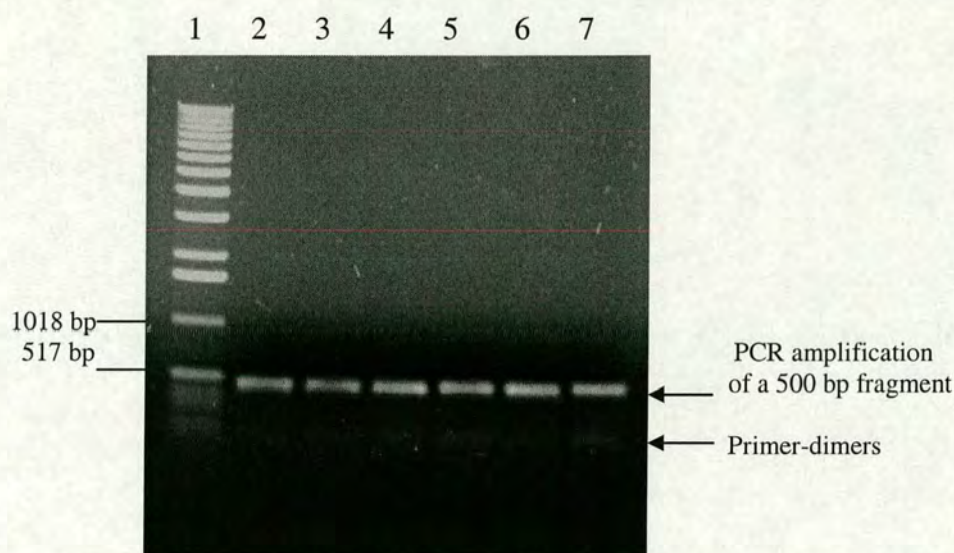


Figure 4.4: PCR amplification of genomic DNA downstream of *fccB54*

Primers 54gk1 and 54gk3 successfully initiated PCR amplification of an *S. oneidensis* MR-1 genomic DNA fragment downstream of *fccB54*. The PCR samples 1-6 that differed in the DNA: primer ratio were analysed using agarose gel electrophoresis (lanes 2-7, respectively). A PCR product corresponding to the size of the 500 bp downstream gene-flanking DNA fragment was amplified in all reactions. The product yield was similar for all six reactions and was not improved with addition of NH_4Cl to reactions 2, 4 and 6 (lanes 3, 5 and 7, respectively). A second non-specific PCR product was amplified in all reactions and was likely to correspond to primer-dimers. 1 kb DNA ladder (lane 1) was used to indicate the size of the PCR amplification products.

The PCR products of the first two primary amplifications were used as template DNA for the final fusion PCR amplification. The complementary DNA region that extended across 16 bp of the primary PCR products stabilised the formation of duplex template DNA. The oligonucleotide distal primers, 54gk3 and 54gk4 were used to PCR amplify the gene-flanking DNA as a continuous sequence containing an *EcoRV* cleavage site (Figure 4.1). High yields of fusion PCR product at the correct size of 940 bp were obtained for each of the reactions and no secondary PCR products were amplified (Figure 4.5). The PCR samples differed in the DNA: primer ratio and the NH_4Cl adjunct supplemented reactions 2, 4 and 6. Varying the reaction components in each PCR sample did not affect the yield of the fusion PCR amplification product (Figure 4.5).

The specificity of the highly sensitive fusion PCR technique indicated good primer design, especially for the proximal primers where sufficient overlap dictates PCR amplification of the desired product.

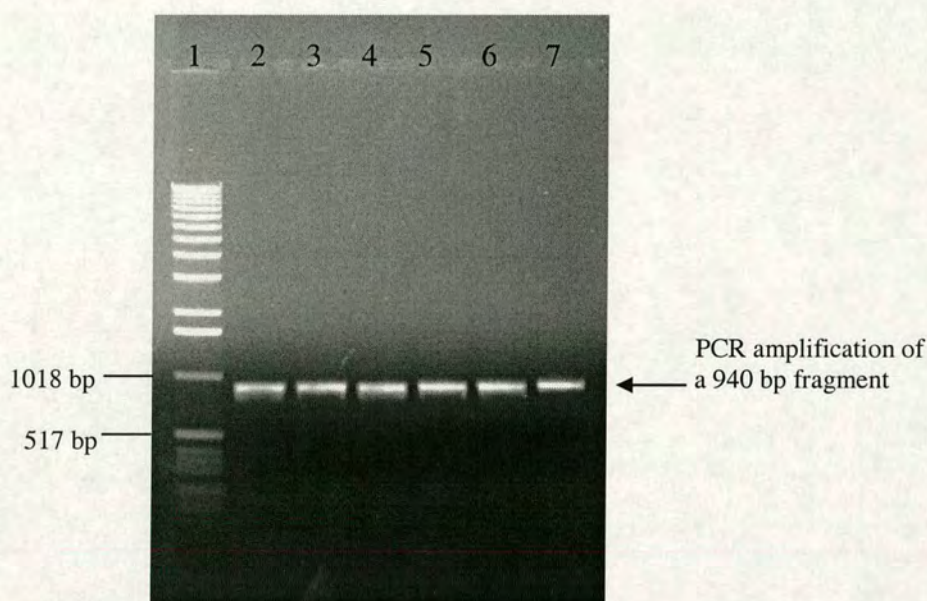


Figure 4.5: PCR amplification of the homologous template DNA

The distal primers, 54gk3 and 54gk4 initiated PCR fusion of the gene-flanking genomic DNA sequences as a contiguous fragment containing an *EcoRV* cleavage site. PCR amplification samples 1-6 were analysed using agarose gel electrophoresis (lanes 2-7, respectively). A specific PCR product corresponding to the size of the 940 bp homologous template DNA fragment was amplified for each of the samples. The samples differed in the DNA: primer ratio and NH_4Cl was added to reactions 2, 4 and 6 (lanes 3, 5 and 7). The variation in reaction components was not observed to affect the PCR product yield. 1 kb DNA ladder was used to show that the fusion PCR product was of the expected size.

4.2.3 Cloning the homologous template DNA in plasmid pUC19

The PCR amplified homologous template DNA generated by fusion PCR was inserted into pUC19, a high copy number *Escherichia coli* cloning plasmid (Yanisch-Perron *et al.*, 1985; Figure 4.6). There were several factors that dictated the use of pUC19 (2686 bp) as a convenient cloning plasmid. A unique *SmaI* cleavage site of pUC19 (Figure 4.6) was selected for insertion of the fusion PCR product by blunt-ended cloning necessitated by *PfuTurbo* PCR amplification.

Plasmid pUC19 does not contain an *EcoRV* cleavage site and was therefore suitable for mobilisation of the *EcoRV* kanamycin fragment without disruption of the remaining plasmid DNA. The restriction enzymes, *KpnI* and *XbaI* were selected as suitable endonucleases for excising the gene replacement fragment from pUC19 to the mobilisable plasmid. These restriction enzymes were identified not to cut in the homologous template DNA or the kanamycin cassette and were ultimately chosen due to unique cleavage sites for *KpnI* and *XbaI* in pUC19.

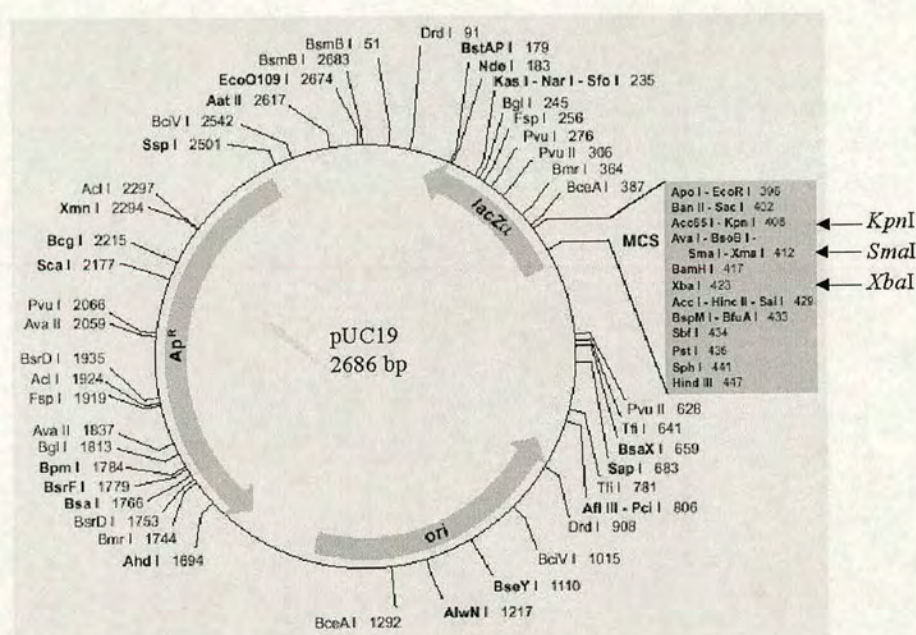


Figure 4.6: A map of the *E. coli* pUC19 cloning plasmid

A *SmaI* cleavage site that was used for insertion of the homologous template DNA PCR product is shown. The *KpnI* and *XbaI* cleavage sites used for transfer of the gene replacement fragment to pEP185.2 are also indicated. The pUC19 plasmid also contains a gene conferring ampicillin resistance (Yanisch-Perron *et al.*, 1985).

A sample of pUC19 plasmid DNA was cut with *Sma*I to generate blunt ends that were ligated to blunt ends of the fusion PCR product amplified using *Pfu*Turbo. Recombinant pUC19 containing the homologous template DNA fusion PCR product was transformed into *E. coli* DH5 α . The transformants were firstly screened for ampicillin resistance encoded on the plasmid DNA (Figure 4.6). There were zero colonies on the 'cells only' control plate that indicated the colonies on the transformation plates all contained pUC19 plasmid. There were approximately 200 ampicillin resistant colonies obtained from cells transformed with recombinant plasmid. However, a similar number of colonies were counted for the 'vector only' control. Plasmid DNA was isolated from 12 single ampicillin resistant colonies and *Eco*RV restriction digests were performed to identify those transformed with recombinant pUC19 plasmid. The formation of recombinant plasmid was detected by *Eco*RV digestion due to the fact that *Eco*RV does not cut in the parent pUC19 plasmid DNA. The cloned PCR product of recombinant pUC19 plasmid was cut with *Eco*RV to give a single restriction fragment at 3626 bp corresponding to pUC19 (2686 bp) and the inserted homologous template DNA (940 bp). The majority of the colonies screened were re-ligated pUC19 plasmid, as expected from the result of the 'vector only' control plate. The *Eco*RV restriction digests (Figure 4.7) revealed that 1 in 12 colonies contained recombinant pUC19 plasmid that was referred to as pMBGK9 (Figure 4.11).



Figure 4.7: Restriction digests to identify recombinant pUC19 plasmid

The homologous template DNA fragment was inserted in pUC19 using blunt-end cloning at a *Sma*I cleavage site. Recombinant pUC19 plasmid, named pMBGK9, was identified using *Eco*RV that cut the inserted homologous template DNA to give a single restriction fragment at 3626 bp (lane 3). *Eco*RV was used to identify recombinant plasmid due to the absence of an *Eco*RV cleavage site on the parent pUC19 plasmid DNA that remained undigested (lane 2). 1 kb DNA ladder (lane 1) was used to indicate the size of the restriction fragments.

4.2.4 Sequencing of the PCR product cloned in pMBGK9

The PCR product cloned in pMBGK9 was completely sequenced to check for any mutations incorporated during amplification by *PfuTurbo* DNA polymerase. The accuracy of the homologous template DNA sequence was essential to provide strict homology to endogenous genomic DNA of wild-type *S. oneidensis* MR-1. Sequencing primers, 54gk5 (forward primer) and 54gk6 (reverse primer), were designed to complement pUC19 plasmid DNA to sequence through the region where the PCR product was inserted in pMBGK9. The automated sequencing results revealed that no mutations occurred in the PCR product, corroborating the high fidelity of *PfuTurbo* DNA polymerase. The correctly amplified PCR product cloned into pMBGK9 was used for constructing the gene replacement fragment.

4.2.5 Construction of the gene replacement fragment

The kanamycin cassette from *E. coli* transposon Tn5 (Mazodier *et al.*, 1985) was provided as a 945 bp *EcoRV* fragment cloned in pGEM-T. The *EcoRV* cleavage sites flanking the 5' and 3' termini of the cassette were digested to release the *EcoRV* kanamycin fragment (939 bp) from pGEM-T. Recombinant pMBGK9 plasmid was digested with *EcoRV* to expose blunt ends of the cloned homologous template DNA. The generated *EcoRV* linear fragments were ligated to form a new recombinant plasmid that contained a kanamycin cassette disrupting the cloned homologous template DNA sequence. This plasmid carrying the kanamycin resistance gene replacement fragment was transformed into *E. coli* DH5 α and transformants were screened for ampicillin and kanamycin resistance. There were zero colonies apparent on the *E. coli* DH5 α 'cells only' control indicating good antibiotic selection. There was no growth on the 'vector only' control, strongly suggesting efficient blunt-ended ligation of 'vector and insert DNA'. The number of colonies obtained from cells transformed with recombinant plasmid generated from the blunt-ended ligation was very low. Following antibiotic selection, plasmid DNA was isolated from 4 single colonies and *EcoRV* restriction digests were used to identify insertion of the kanamycin cassette. Insertion of the kanamycin cassette in pMBGK9 as an *EcoRV* fragment would have restored *EcoRV* cleavage sites at both termini of the kanamycin cassette. Therefore, *EcoRV* restriction digests were used to verify insertion of the kanamycin cassette with release of a 939 bp *EcoRV* fragment from recombinant plasmid. It was confirmed that all four colonies selected for further screening were transformed with recombinant pMBGK2 plasmid (Figure 4.11) that contained the kanamycin resistance gene replacement fragment (Figure 4.8).

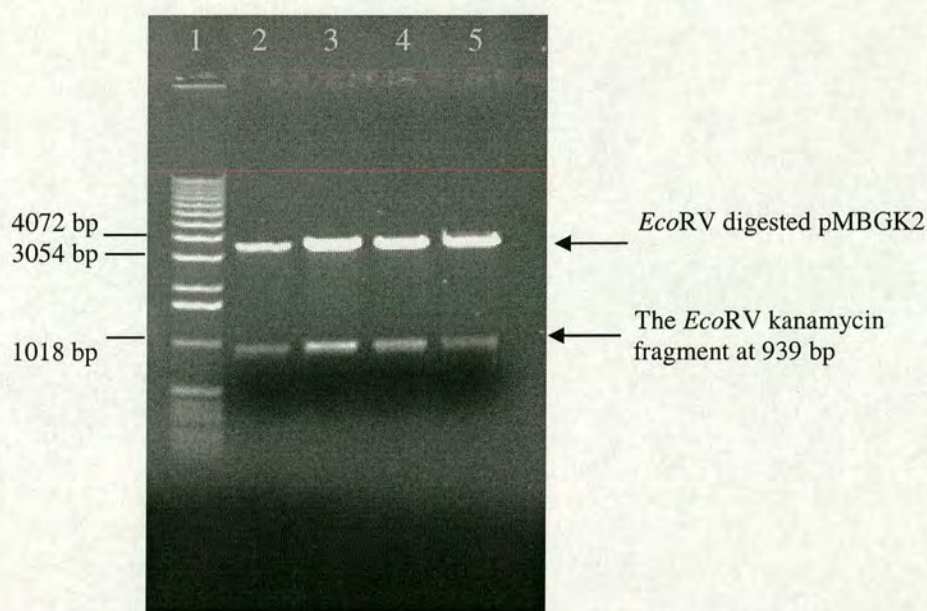


Figure 4.8: Restriction digests to identify formation of the gene replacement fragment

The *EcoRV* kanamycin cassette was inserted in the homologous template DNA of pMBGK9 to form a kanamycin resistance gene replacement fragment. Recombinant pMBGK9 plasmid containing the kanamycin cassette was referred to as pMBGK2. Insertion of the kanamycin cassette in pMBGK2 was verified using *EcoRV* restriction digests that excised the 939 bp *EcoRV* kanamycin cassette, as shown using agarose gel electrophoresis. The restriction fragments of pMBGK2 plasmid DNA isolated from colonies 1-4 are shown in lanes 2-5, respectively. 1 kb DNA ladder (lane 1) was used to indicate that the *EcoRV* restriction fragments were of the correct size.

4.2.6 Construction of a recombinant mobilisable plasmid

A prerequisite for constructing a gene replacement in the genome of *S. oneidensis* MR-1 involved transfer of the cloned gene replacement fragment to the mobilisable suicide plasmid named pEP185.2 (Pepe and Miller, 1993; Figure 4.9). The restriction enzymes, *KpnI* and *XbaI* were conveniently used to splice the gene replacement fragment from pMBGK2 to the mobilisable plasmid pEP185.2 (4275 bp). These restriction enzymes were chosen because they do not cut in the gene replacement fragment and cut at unique sites in plasmids, pMBGK2 (Figure 4.11) and pEP185.2 (Figure 4.9).

The gene replacement fragment was excised from pMBGK2 as a *KpnI/XbaI* 1898 bp fragment and ligated to complementary ends of pEP185.2, generated by digestion with *KpnI* and *XbaI*. The recombinant plasmid was transformed into *E. coli* S17 λ *pir* that contains the *pirR6K* gene required for initiation of pEP185.2 plasmid DNA replication. The pEP185.2 plasmid expresses chloramphenicol resistance encoded by the *cat* gene (Figure 4.9).

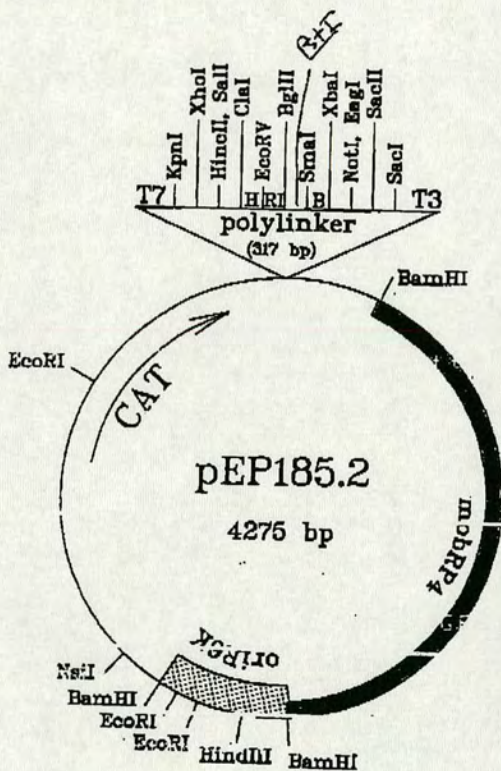


Figure 4.9: Map of pEP185.2 mobilisable plasmid
The *KpnI* and *XbaI* unique cleavage sites used for insertion of the gene replacement fragment are shown. The *cat* gene encoding chloramphenicol resistance is also shown (Pepe and Miller, 1993).

E. coli S17 λ pir cells transformed with recombinant pEP185.2 plasmid were selected for chloramphenicol and kanamycin resistance. There were zero colonies identified on the *E. coli* S17 λ pir ‘cells only’ control indicating that the antibiotic selection was implemented. No colonies were apparent for the ‘vector only’ control in which *E. coli* S17 λ pir cells were transformed with parent pEP185.2 plasmid. This result strongly suggested that the few colonies obtained from *E. coli* S17 λ pir cells transformed with ‘vector and insert DNA’, did indeed contain recombinant pEP185.2 expressing kanamycin resistance. Plasmid DNA was isolated from 2 single colonies and *KpnI/XbaI* double restriction digests were performed to identify recombinant plasmid. The isolation of recombinant plasmid, named pMBGK15 (Figure 4.11), was demonstrated by excision of a gene replacement fragment at 1898 bp upon cleavage with *KpnI* and *XbaI* (Figure 4.10).

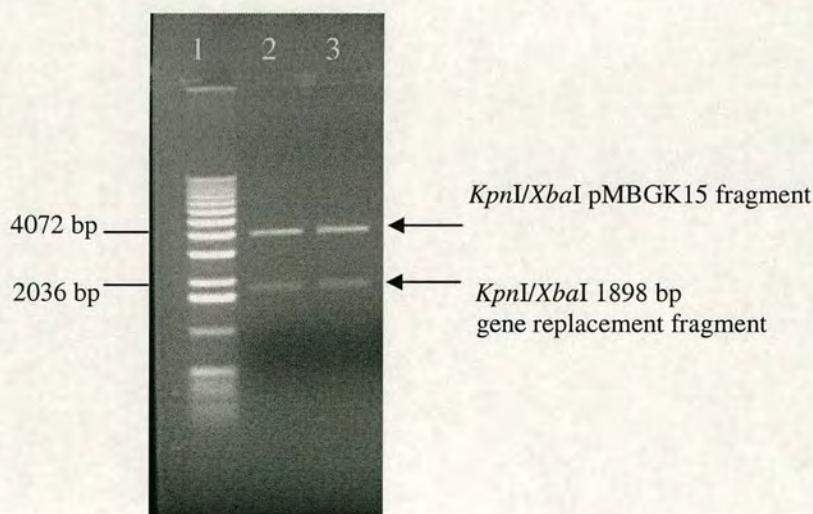


Figure 4.10: Restriction digests to verify construction of pMBGK15

The gene replacement fragment was transferred as a *KpnI/XbaI* fragment from pMBGK2 to the mobilisable pEP185.2 plasmid. Recombinant pEP185.2 plasmid, named pMBGK15 isolated from colonies 1 and 2 was digested with *KpnI* and *XbaI* (lanes 2 and 3, respectively). The results were analysed using agarose gel electrophoresis that showed excision of a *KpnI/XbaI* restriction fragment corresponding to the 1898 bp gene replacement fragment. 1 kb DNA ladder (lane 1) was used to indicate that the restriction fragments were of the correct size.

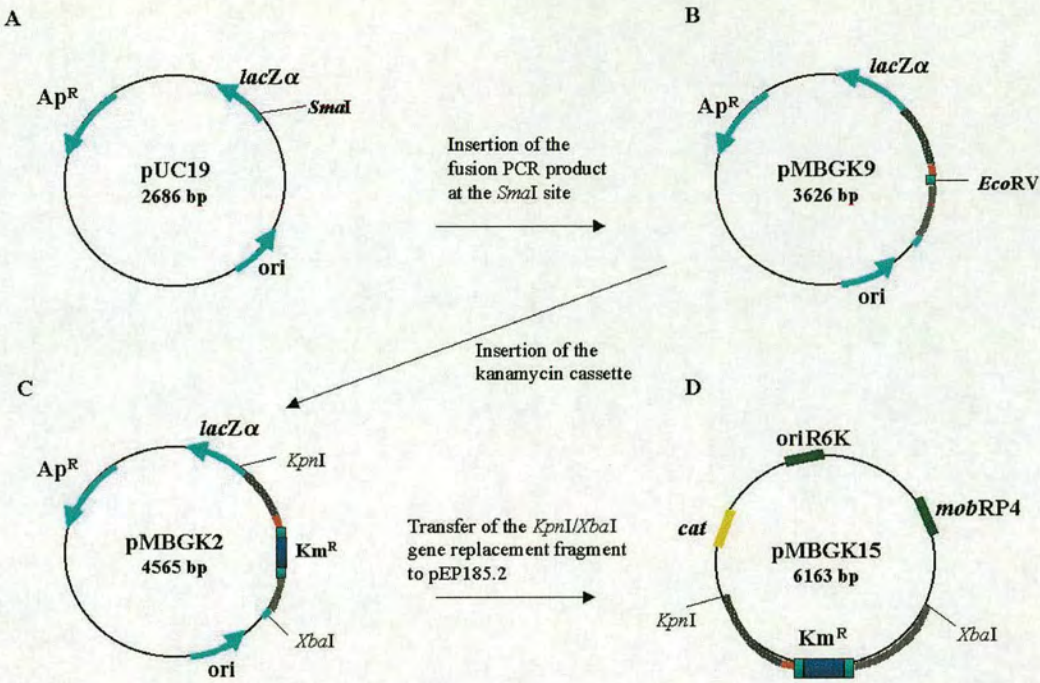


Figure 4.11: Plasmids constructed to generate the null mutant

The fusion PCR product comprising the homologous template DNA was inserted in the pUC19 cloning plasmid (A) to form pMBGK9 (B). The kanamycin cassette was inserted at the *EcoRV* site of the cloned fusion PCR product to form recombinant plasmid pMBGK2 (C). The kanamycin modified PCR product referred to as the gene replacement fragment was excised from pMBGK2 as a *KpnI/XbaI* fragment and inserted in the mobilisable pEP185.2 plasmid. The recombinant mobilisable plasmid, pMBGK15 (D), was introduced into *S. oneidensis* MR-1 *Rm^R* for homologous recombination to generate the null mutant.

4.2.7 Conjugative DNA transfer and antibiotic screening

The pMBGK15 plasmid DNA (Figure 4.11) carrying the gene replacement fragment was transferred from *E. coli* S17 λ pir into the spontaneous rifampicin resistant (Rm^R) strain of *S. oneidensis* MR-1 by bacterial conjugation. The pEP185.2 plasmid contains the *mob* site from the broad host range plasmid RP4 (Figure 4.9) that facilitates transfer from *E. coli* into a broad range of Gram-negative bacteria, including bacteria of the genus *Shewanella*. Attachment of *E. coli* S17 λ pir to recipient cells during conjugative mating was mediated by pili projecting from the cell surface of *E. coli* S17 λ pir.

The recombinant pMBGK15 plasmid was introduced into *S. oneidensis* MR-1 Rm^R to allow homologous recombination to occur between the cloned gene replacement fragment and homologous DNA of the bacterial chromosome. Following conjugative mating, transconjugants were firstly screened for kanamycin and rifampicin resistance that selected for *S. oneidensis* Rm^R strains containing the kanamycin cassette. The process of identifying the *fccA54* and *fccB54* gene replacement due to double recombination was then addressed over the single recombination event in which pMBGK15 is integrated into the chromosome. The pEP185.2 origin of replication can only operate in members of the *Enterobacteriaceae* and functions as a suicide plasmid in *Shewanella* species. This property was used to discriminate between double and single recombination events by means of chloramphenicol marker selection. The second antibiotic screen aimed to select for chloramphenicol sensitive transconjugants in which the double recombination event had led to loss of pMBGK15.

The first conjugation yielded 8 transconjugants (*S. oneidensis* MB541-MB548) that were kanamycin and rifampicin resistant. However, these transconjugants grew slowly in the presence of chloramphenicol, signifying a single crossover event and incorporation of pMBGK15 into the *S. oneidensis* MR-1 genome. There were zero colonies on the '*S. oneidensis* MR-1 Rm^R only' control indicating effective kanamycin selection. Low rifampicin resistance in the supplemented LB medium was suspected due to the appearance of three colonies on the '*E. coli* S17 λ pir only' control.

A similar result was obtained for the controls in conjugation II. From the second conjugation, 24 transconjugants grew which all displayed kanamycin and rifampicin resistance. To ascertain the occurrence of the double recombination event and the concomitant gene replacement, the 24 transconjugants were tested for their ability to grow in the presence of chloramphenicol. Eight transconjugants proved to be chloramphenicol sensitive suggesting a double-crossover event had occurred leading to deletion of the target genes. The control results provided supporting evidence that the chloramphenicol sensitivity was a true phenotype for 8 of the 24 transconjugants. The presence of chloramphenicol supported growth of the chloramphenicol resistant *S. oneidensis* MB541 control and inhibited growth of the *S. frigidimarina* EG301 chloramphenicol sensitive control. The antibiotic selection process for identifying the potential *fccA54* and *fccB54* null mutant formed the basis of further characterisation involving PCR to examine the genome of each chloramphenicol sensitive transconjugant.

4.2.8 PCR screening of transconjugants from conjugation II

PCR screening was used to scan the genomic DNA of chloramphenicol sensitive transconjugants for *fccA54* and *fccB54* gene replacement with the kanamycin cassette. The distal primers, 54gk3 and 54gk4 (Figure 4.1) were used to PCR amplify genomic DNA that comprised the region of endogenous homologous template DNA. A double crossover event that led to *fccA54* and *fccB54* gene replacement was confirmed with PCR amplification of the endogenous gene replacement fragment at 1879 bp (Figure 4.12). Amplification of two PCR products signified the occurrence of a single-crossover event in which the pMBGK15 plasmid was integrated in the genome of *S. oneidensis* MR-1. A 2814 bp PCR product corresponding to amplification of the *fccA54* and *fccB54* genes was amplified in addition to a 1879 bp PCR product corresponding to the integrated pMBGK15 gene replacement fragment (Figure 4.12).

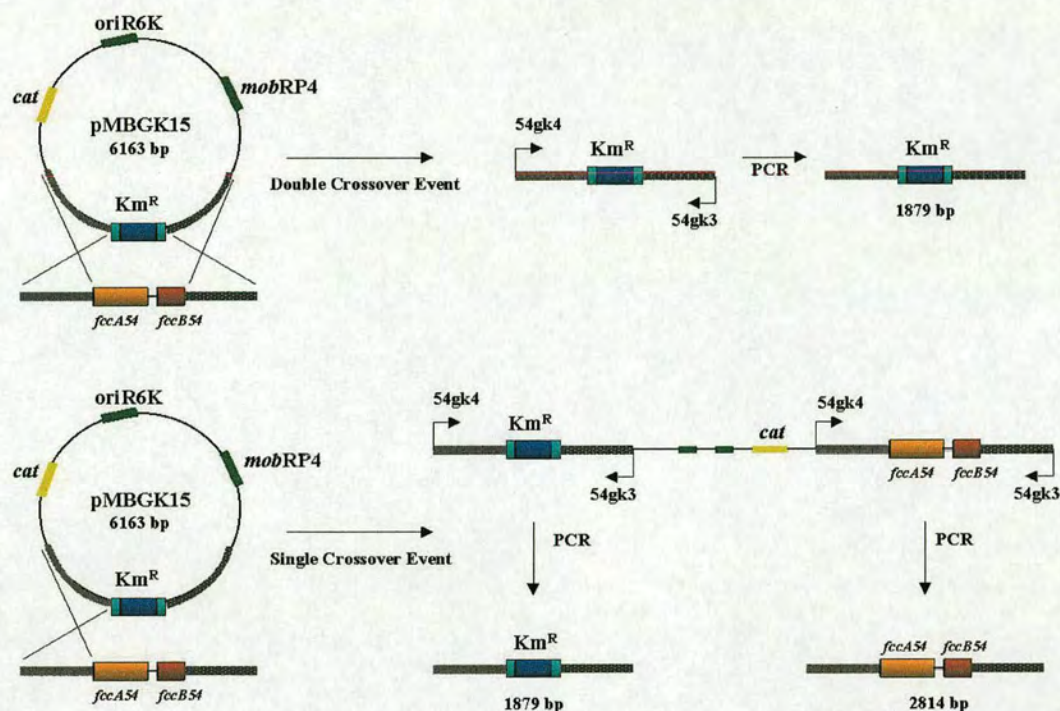


Figure 4.12: A schematic diagram to show PCR screening of transconjugants

PCR screening was used to analyse the genomic DNA of selected transconjugants to identify those containing the kanamycin cassette in position of the *fccA54* and *fccB54* genes. Primers 54gk3 and 54gk4 complementary to the homologous template DNA were used to PCR amplify the region of homologous recombination. The double crossover event was identified by amplification of a single PCR product at 1879 bp corresponding to insertion of the kanamycin cassette. The amplification of two PCR products using primers 54gk3 and 54gk4 indicated a single crossover event in which pMBGK15 plasmid DNA was integrated in the genome. A 2814 bp PCR product corresponding to the *fccA54* and *fccB54* genes was amplified in addition to the integrated pMBGK15 gene replacement fragment at 1879 bp. The diagram is not to scale.

4.2.9 Identification of an *fccA54* and *fccB54* null mutant

Primers 54gk3 and 54gk4 were successfully used to initiate PCR screening (Figure 4.12) of chloramphenicol sensitive transconjugants, named *S. oneidensis* MB5413 and *S. oneidensis* MB5415, obtained from conjugation II. The amplification products of four PCR samples that differed in the *S. oneidensis* MB5413 DNA: primer ratio were analysed using agarose gel electrophoresis (Figure 4.13). The amplification of two PCR products for reaction 2 (Figure 4.13) showed that *S. oneidensis* MB5413 was a chloramphenicol sensitive false positive transconjugant. A PCR product corresponding to the 1879 bp gene replacement fragment was amplified for *S. oneidensis* MB5413, as confirmed by comparison to the control PCR product amplified from the pMBGK15 template DNA (Figure 4.13). The *fccA54* and *fccB54* target genes were also PCR amplified from the genome of *S. oneidensis* MB5413, as shown by amplification of a 2814 bp product that was also apparent for the *S. oneidensis* MR-1 wild-type control (Figure 4.13). PCR screening of *S. oneidensis* MB5413 showed that the chloramphenicol sensitive phenotype was not due to *fccA54* and *fccB54* gene replacement and subsequent loss of the suicide plasmid pMBGK15. The chloramphenicol sensitive phenotype was perhaps attributed to a mutation in the *cat* gene of the pMBGK15 plasmid. An alternative explanation is that a non-specific double recombination event had occurred that led to insertion of the kanamycin cassette at an erroneous position in the *S. oneidensis* MB5413 genome. The imprecise gene replacement coupled to loss of the suicide plasmid pMBGK15 would produce transconjugants with a false positive chloramphenicol sensitive phenotype.

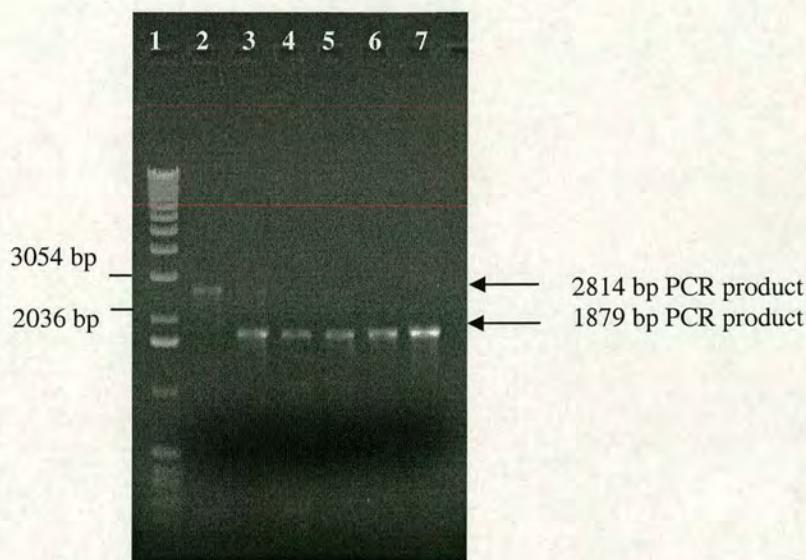


Figure 4.13: PCR screening of *S. oneidensis* MB5413

Primers 54gk3 and 54gk4 were used to initiate PCR screening of the *S. oneidensis* MB5413 genomic DNA. The products of four PCR samples that differed in the ratio of genomic DNA: primer were analysed using agarose gel electrophoresis (lanes 3-6). A PCR product was amplified for all four reactions (lanes 3-6) that corresponded to the 1879 bp gene replacement fragment amplified from the pMBGK15 control template DNA (lane 7). However, two PCR products were amplified for reaction 2 that was indicative of a single crossover event (lane 3). In addition to the 1879 bp PCR product, a second PCR product was amplified for *S. oneidensis* MB5413 (lane 3) that corresponded to the 2814 bp *fccA54* and *fccB54* PCR product of wild-type *S. oneidensis* MR-1 (lane 2). 1 kb DNA ladder (lane 1) was used to indicate the size of the PCR products.

Primers 54gk3 and 54gk4 successfully initiated PCR screening (Figure 4.12) of the chloramphenicol sensitive transconjugant *S. oneidensis* MB5415. The amplification products of four PCR samples that differed in the *S. oneidensis* MB5415 genomic DNA: primer ratio were analysed using agarose gel electrophoresis (Figure 4.14). A PCR amplification product for reactions 3 and 4 correlated to the 1879 bp gene replacement fragment amplified from the pMBGK15 control template DNA. A non-specific PCR product at approximately 1600 bp was amplified in addition to the 1879 bp PCR product (Figure 4.14). The 2814 bp *fccA54* and *fccB54* PCR product amplified from the genome of wild-type *S. oneidensis* MR-1 was not amplified for *S. oneidensis* MB5415 (Figure 4.14).

The PCR screening results generated using primers 54gk3 and 54gk4 led to the suggestion that a double crossover event had successfully occurred in *S. oneidensis* MB5415 to replace the *fccA54* and *fccB54* target genes (Figure 4.14).

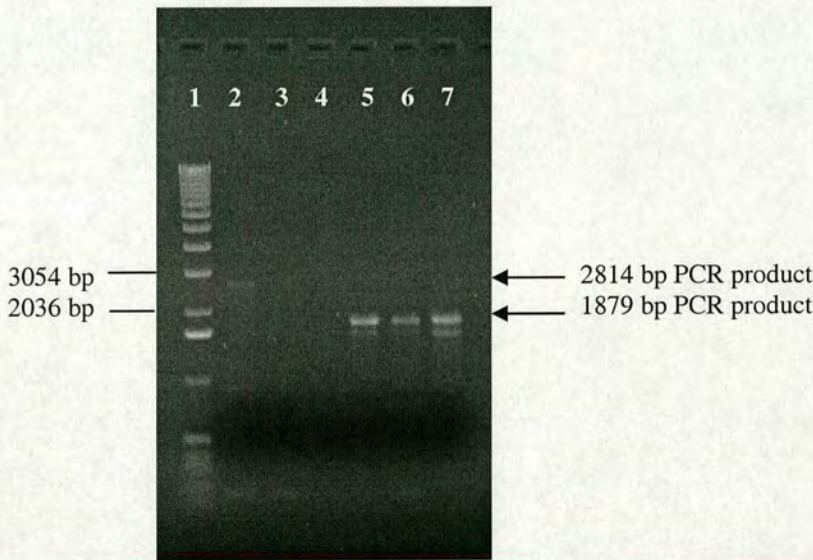


Figure 4.14: PCR screening of *S. oneidensis* MB5415

Primers 54gk3 and 54gk4 were used to initiate PCR screening of *S. oneidensis* MB5415 genomic DNA in order to determine *fccA54* and *fccB54* gene replacement with the kanamycin cassette. The products of four PCR samples that differed in the genomic DNA: primer ratio were analysed using agarose gel electrophoresis (lanes 3-6). A single PCR product was amplified for reactions 3 and 4 (lanes 5 and 6, respectively) that corresponded to the 1879 bp gene replacement fragment amplified from the control pMBGK15 template DNA (lane 7). The 2814 bp *fccA54* and *fccB54* PCR product amplified for the wild-type MR-1 control (lane 2) was not PCR amplified from the genome of *S. oneidensis* MB5415 (lanes 3-6). However, in addition to the 1879 bp PCR product, a PCR product at approximately 1600 bp was amplified due to non-specific priming of the template DNA (lanes 5-7). No PCR product was amplified for reactions 1 and 2 (lanes 3 and 4, respectively). 1 kb DNA ladder (lane 1) was used to indicate the size of the amplified PCR products.

PCR screening using primers 54F and 54RA that complement the *fccA54* gene was used to ascertain whether the target gene existed in the genomes of *S. oneidensis* MB5413 and *S. oneidensis* MB5415. The products of four PCR samples that differed in the *S. oneidensis* MB5413 genomic DNA: primer ratio were analysed using agarose gel electrophoresis. Primers 54F and 54RA successfully initiated PCR amplification of a product from the *S. oneidensis* MB5413 genome that was equivalent to the 1539 bp *fccA54* PCR product of wild-type *S. oneidensis* MR-1 (Figure 4.15a). However, one of the non-specific PCR products amplified from the pMBGK15 negative control template DNA corresponded to the size of the *fccA54* PCR product (Figure 4.15a). Sequencing of the 1539 bp PCR product of *S. oneidensis* MB5413 was used to confirm that this amplified product was indeed *fccA54*. Therefore, this PCR screen led to substantial evidence that *fccA54* and *fccB54* of the *S. oneidensis* MB5413 genome were not replaced with the kanamycin cassette.

The products of four PCR samples that differed in the *S. oneidensis* MB5415 genomic DNA: primer ratio were analysed using agarose gel electrophoresis. The *fccA54* 54FRA 1539 bp PCR product amplified from the genome of wild-type *S. oneidensis* MR-1 was not amplified from the genome of *S. oneidensis* MB5415 (Figure 4.15b). This result provided further evidence that a kanamycin cassette was inserted in the *S. oneidensis* MB5415 genome in place of the *fccA54* and *fccB54* genes (Figure 4.15b).

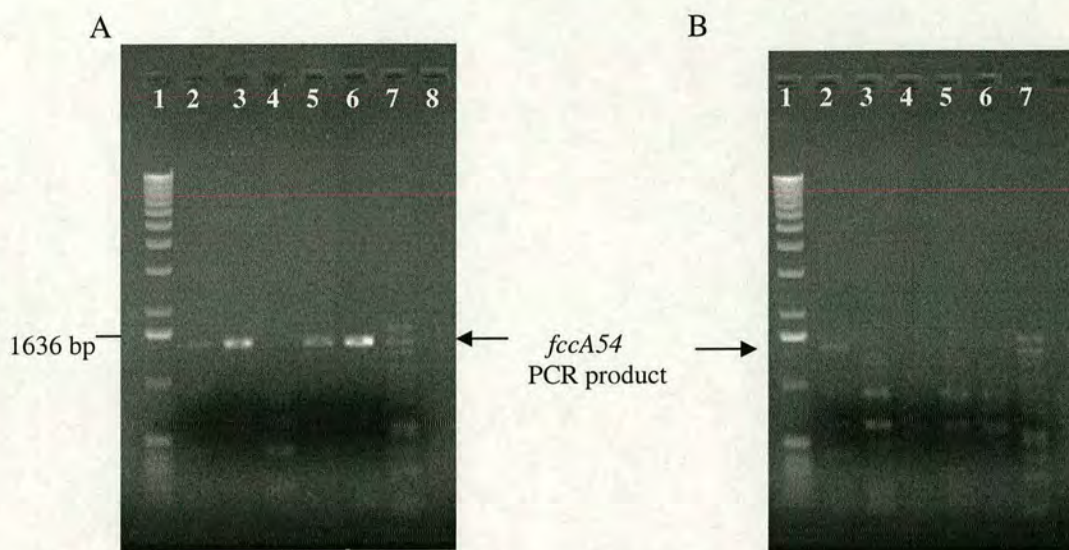


Figure 4.15: PCR screening of *S. oneidensis* MB5413 and *S. oneidensis* MB5415

A) PCR screening of the chloramphenicol sensitive *S. oneidensis* transconjugant MB5413 was initiated using primers 54F and 54RA that complement the *fccA54* gene. The products of four PCR samples that differed in the *S. oneidensis* MB5413 genomic DNA: primer ratio were analysed using agarose gel electrophoresis. The *fccA54* gene was amplified from the genome of wild-type *S. oneidensis* MR-1 as shown by the presence of a 1539 bp *fccA54* 54FRA product (lane 2). A PCR product corresponding to the size of the 1539 bp *fccA54* PCR product was also amplified from the *S. oneidensis* MB5413 genome (lanes 3, 5 and 6). Non-specific PCR products were amplified for the negative pMBGK15 control that does not contain *fccA54* (lane 7). 1 kb DNA ladder (lane 1) was used to indicate the size of the PCR products. **B)** PCR screening of the *S. oneidensis* MB5415 transconjugant was initiated using primers 54F and 54RA that hybridise to the *fccA54* target gene. The products of four samples that differed in the genomic DNA: primer ratio were analysed using agarose gel electrophoresis. A product corresponding to the *fccA54* 54FRA 1539 bp fragment was amplified from the genome of wild-type *S. oneidensis* MR-1 (lane 2). The *fccA54* gene was not amplified from the genome of *S. oneidensis* MB5415 (lanes 3-6). Non-specific PCR products were amplified for the negative pMBGK15 control that does not contain *fccA54* (lane 7). 1 kb DNA ladder (lane 1) was used to indicate the size of the PCR products.

Further PCR screening initiated with primers 54gk9 and 54gk10 (Figure 4.16) aimed to provide conclusive evidence that the kanamycin selectable marker was inserted in the *S. oneidensis* MB5415 genome in position of *fccA54* and *fccB54*. The 54gk9 and 54gk10 primers were designed to complement genomic DNA flanking the endogenous homologous template DNA sequence amplified using primers 54gk3 and 54gk4 (Figure 4.16).

The primers were designed to specifically explore the region of homologous recombination to verify that the kanamycin cassette had been inserted at the correct position in the *S. oneidensis* MB5415 genome. A double crossover event and insertion of the kanamycin cassette in position of the *fccA54* and *fccB54* genes was determined by PCR amplification of a 2091 bp PCR product. A crossover event that did not disrupt the endogenous *fccA54* and *fccB54* genes was characterised by PCR amplification of a 3024 bp product, corresponding to the wild-type genome (Figure 4.16).

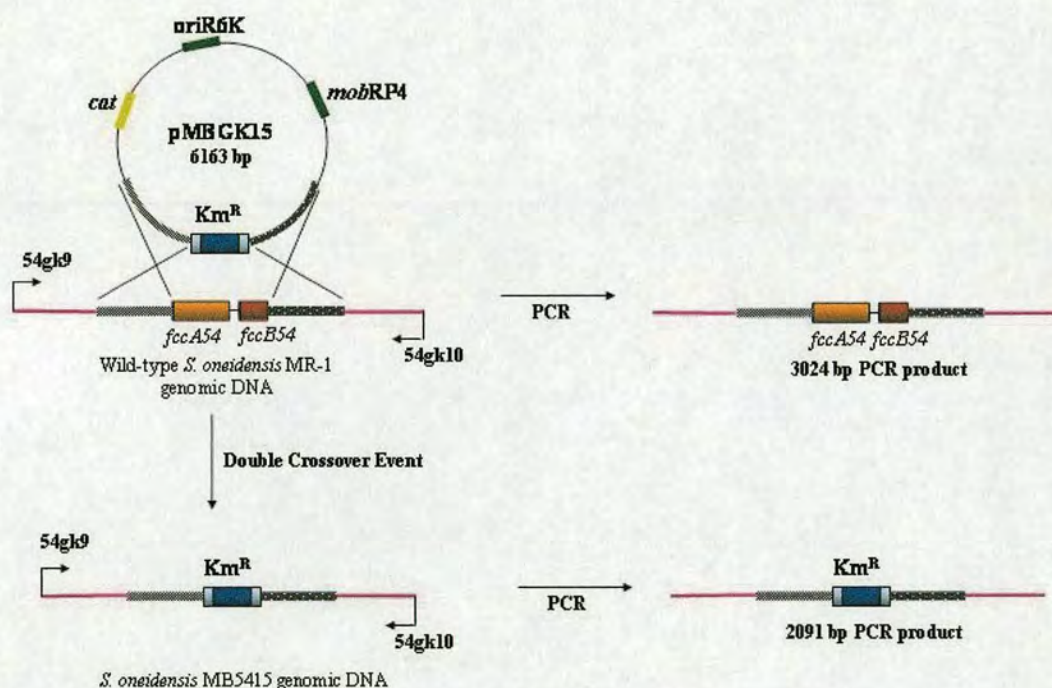


Figure 4.16: Schematic diagram to show PCR screening of *S. oneidensis* MB5415

Primers 54gk9 and 54gk10 were designed to initiate PCR screening of the *S. oneidensis* MB5415 genome. The primer positions and direction of synthesis are indicated. The 54gk9 and 54gk10 primers were designed to complement genomic DNA (purple line) that flanked the point of homologous recombination (grey and black lines). A double crossover event and insertion of the kanamycin cassette in position of the *fccA54* and *fccB54* genes was indicated by PCR amplification of a 2091 bp PCR product. The amplification of a 3024 bp PCR product corresponded to wild-type genomic DNA comprising the *fccA54* and *fccB54* genes within the homologous template DNA sequence. The diagram is not to scale.

Primers 54gk9 and 54gk10 were successfully used to initiate PCR screening of the *S. oneidensis* MB5415 genome. The products of four PCR samples that differed in the ratio of *S. oneidensis* MB5415 DNA: primer were analysed using agarose gel electrophoresis (Figure 4.17). It was clearly identified that the PCR products amplified from the *S. oneidensis* MB5415 genome were 2091 bp that corresponded to amplification of the kanamycin cassette. This result was substantiated by amplification of a 3024 bp PCR product from the wild-type *S. oneidensis* MR-1 genome that correlated to amplification of *fccA54* and *fccB54* (Figure 4.17). This PCR result provided evidence that the kanamycin cassette was inserted in the genome of *S. oneidensis* MB5415 at an equivalent position to *fccA54* and *fccB54* in the *S. oneidensis* MR-1 wild-type genome (Figure 4.17). Therefore, this PCR amplification indicated that *S. oneidensis* MB5415 is indeed an *fccA54* and *fccB54* null mutant.

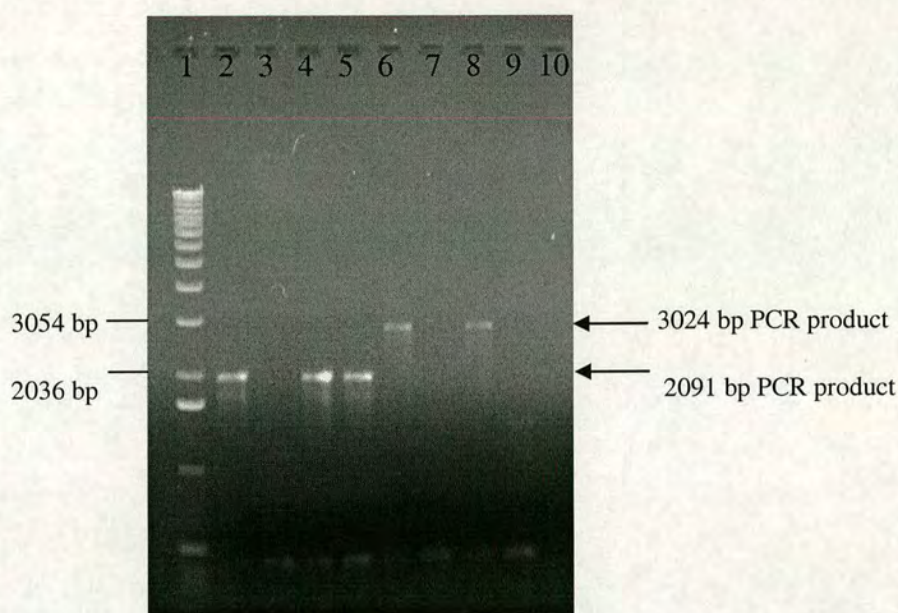


Figure 4.17: PCR screening of *S. oneidensis* MB5415

Primers 54gk9 and 54gk10 were used to initiate PCR screening of the *S. oneidensis* MB5415 genome to identify if the kanamycin cassette was inserted in position of the *fccA54* and *fccB54* genes. The products of four PCR samples that differed in the genomic DNA: primer ratio were analysed for *S. oneidensis* MB5415 (lanes 2-5) and wild-type *S. oneidensis* MR-1 (lanes 6-9) using agarose gel electrophoresis. PCR amplification of a 2091 bp PCR product from the *S. oneidensis* MB5415 genome (lanes 2, 4 and 5) indicated insertion of the kanamycin cassette in place of the *fccA54* and *fccB54* genes. This result was verified by amplification of a 3086 bp PCR product from the wild-type *S. oneidensis* MR-1 genome (lanes 6 and 8), corresponding to *fccA54* and *fccB54*. No PCR product was amplified for the negative control, pMBGK15 (lane 10). 1 kb DNA ladder was used to indicate the size of the PCR amplification products.

The 2091 bp PCR product of *S. oneidensis* MB5415 that was amplified using primers 54gk9 and 54gk10 was inserted in pGEM-T to form plasmid pMBGK41. Sequencing of the cloned PCR product was used to confirm that a kanamycin cassette in the genome of *S. oneidensis* MB5415 does indeed replace the *fccA54* and *fccB54* genes.

4.2.10 Phenotype analyses

4.2.10.1 Anaerobic growth on acrylate substrates

The molecular modelling studies led to the identification of acrylates as potential enzyme substrates of FccA54, FccA56 and FccA342 (3.2.3; Figure 3.17). The candidate substrates, including phenylacrylates were tested for their ability to sustain anaerobic growth of wild-type *S. oneidensis* MR-1. The aim was to identify substrates that supported growth of the wild-type strain in order to provide positive controls for direct comparison to growth of the *S. oneidensis* MB5415 mutant on each of the acrylates.

Minimal medium that contains nutrients required for sustaining growth of *S. oneidensis* MR-1 but no other components known to function as a carbon source or electron acceptor was selected as an ideal growth medium. The anaerobic growth patterns noted with addition of lactate and a particular electron acceptor were likely to be directly attributed to their specific addition to the minimal medium. Minimal medium that was supplemented with amino acids, trace elements and lactate (2.1.8) was dispensed into ½ oz bijou jars for anaerobic growth of *S. oneidensis* MR-1. Each of the candidate acrylates serving as the terminal electron acceptor was then added to the appropriate individual growth jar at a final concentration of 5.0 mM. The pH of the solubilised acrylates was adjusted to a neutral pH prior to supplementing the minimal media (pH 7.4) to achieve the native environmental pH (pH 7.5-8.2) that supports growth of *S. oneidensis* MR-1 (Myers and Nealson, 1988).

Anaerobic growth of *S. oneidensis* MR-1 with fumarate as terminal electron acceptor was used as a positive indicator of growth. Negative controls in which *S. oneidensis* MR-1 was grown in the absence of a carbon source and/or absence of fumarate as terminal electron acceptor were also included. Each of the anaerobic growth jars was inoculated with an overnight *S. oneidensis* MR-1 culture (200 µl) and incubated at room temperature for four weeks. The growth experiments were repeated several fold in an attempt to achieve unambiguous results. Colony counts were performed (2.1.9) in order to quantify anaerobic growth of *S. oneidensis* MR-1 on the various electron acceptors. The results are shown in Table 4.1.

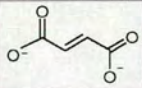
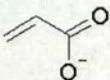
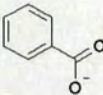
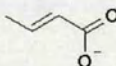
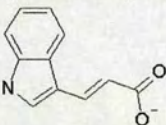
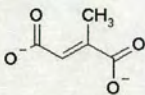
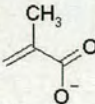
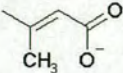
Electron Acceptor	Lactate Carbon Source	COLONY COUNT ($\times 10^4$ cells mL^{-1})				
		1	2	3	Mean	SD
Fumarate 	+	63	300	0	121	129.2
	-	600	0	0	200	282.8
-	+	182	464	39	228.3	176.6
-	-	0	0	40	13.3	18.9
Acrylate 	+	0	0	0	0	0
Benzoate 	+	166	629	124	306.3	228.8
Crotonate 	+	133	685	800	539.3	291.1
3-β-indoleacrylate 	+	306	-	-	-	-
Mesaconate 	+	1988	2139	0	1375.7	974.7
Methacrylate 	+	473	2100	0	857.7	899.4
Senecioate 	+	478	0	670	382.7	281.7

Table 4.1 continued overleaf

Table 4.1 continued.

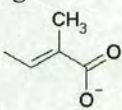
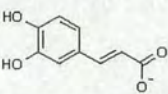
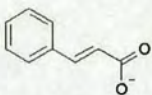
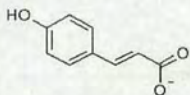
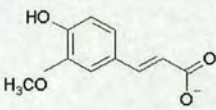
Electron Acceptor	Lactate <i>Carbon Source</i>	COLONY COUNT ($\times 10^4$ cells mL^{-1})				
		1	2	3	Mean	SD
Tiglate 	+	109	2332	0	813.7	1074.5
Caffeate 	+	107	1	0	36.0	50.2
Cinnamate 	+	114	0	20	44.7	49.7
Coumarate 	+	39	8	0	15.7	16.8
Ferulate 	+	139	0	0	46.3	65.5

Table 4.1: Growth of wild-type *S. oneidensis* MR-1 on acrylate electron acceptors

The colony counts for three individual anaerobic growth experiments (1-3) of wild-type *S. oneidensis* MR-1 on twelve different acrylate electron acceptors are shown (white). The colony counts for the positive control cultures containing lactate and fumarate are highlighted in grey. Control colony counts of *S. oneidensis* MR-1 grown in the absence of an electron acceptor and/or carbon source are also tabulated (grey). Acrylate is the only substrate that did not support anaerobic growth of wild-type *S. oneidensis* MR-1. However, growth of *S. oneidensis* MR-1 in the absence of fumarate (+ lactate) was similar to the positive control, which strongly suggests that the cultures were not strictly anaerobic. Therefore, the colony counts obtained for *S. oneidensis* MR-1 growth on each of the acrylates was not indicative of these substrates serving as the sole terminal electron acceptor due to the presence of oxygen. The tabulated colony counts represent $\times 10^4$ cells mL^{-1} of culture. The average colony count (red) obtained from the three cultures of *S. oneidensis* MR-1 grown on each acrylate and the standard deviation (SD) of the colony counts (green) were calculated and are also shown.

The anaerobic growth experiments of wild-type *S. oneidensis* MR-1 cultured in minimal media containing the appropriate supplements with addition of a candidate electron acceptor did not yield consistent results (Table 4.1). The relatively high standard deviation of the colony counts obtained for the anaerobic growth cultures of *S. oneidensis* MR-1 clearly show the variability in growth levels. *S. oneidensis* MR-1 grew anaerobically in the presence of lactate and fumarate, however, the mean colony count obtained for the positive control (121 colonies) was lower compared to those cultures containing lactate but no electron acceptor (228.3 colonies). This led to the conclusion that some growth cultures were not strictly anaerobic and oxygen served as the terminal electron acceptor in the control experiment containing lactate only. Although growth on each of the candidate terminal electron acceptors could not be attributed to anaerobic survival, growth levels similar to the positive control were observed on the following substrates: benzoate, crotonate, 3- β -indoleacrylate, mesaconate, methacrylate, senecioate and tiglate. Growth of *S. oneidensis* MR-1 occurred in the presence of phenylacrylates but was inhibited compared to growth in the presence of lactate and fumarate (positive control). The low growth levels of wild-type *S. oneidensis* MR-1 on fumarate may have been due to limiting concentrations of the substrate (5 mM). A higher concentration of fumarate (20 mM) is required to support robust growth of *S. oneidensis* MR-1 during anaerobic respiration (Maier and Myers, 2001).

Anaerobic growth of wild-type *S. oneidensis* MR-1 on a variety of substrates revealed that acrylate was the only substrate that consistently inhibited growth. Therefore, the anaerobic growth experiments led to the suggestion that benzoate, crotonate, 3- β -indoleacrylate, mesaconate, methacrylate, senecioate and tiglate and possibly cinnamate, coumarate, caffeate and ferulate support anaerobic growth of wild-type *S. oneidensis* MR-1.

4.2.10.2 Anaerobic growth of *S. oneidensis* MB5415

Several of the acrylates identified to support growth of *S. oneidensis* MR-1 were subsequently tested for their ability to support anaerobic growth of the *fccA54* and *fccB54* null mutant, *S. oneidensis* MB5415. An anaerobic growth defect of *S. oneidensis* MB5415 correlated to absence of FccA54 and FccB54 could be used to infer a possible catalytic function of the putative flavocytochrome in anaerobic metabolism of *S. oneidensis* MR-1. In order to indicate that a growth impairment of *S. oneidensis* MB5415 on a particular acrylate was linked to the absence of FccA54 and FccB54, the mutant was grown anaerobically in parallel with wild-type *S. oneidensis* MR-1.

The wild-type *S. oneidensis* MR-1 and *S. oneidensis* MB5415 strains were cultured in minimal media containing lactate, trace elements, amino acids and electron acceptor (2.1.8) dispensed into ½ oz bijou jars. Wild-type *S. oneidensis* MR-1 grown anaerobically in the presence of fumarate (20 mM) as terminal electron acceptor was used as a positive indicator of growth. The final concentration of the acrylates was also 20 mM, which is significantly higher than the previous concentration (5 mM) used for the wild-type growth experiments (4.2.10.1).

Each reaction was set up in duplicate for both strains tested. The growth jars were inoculated with the appropriate strain, either with a single colony of the *Shewanella* strain (experiment 1) or 100 µl of an overnight culture resuspended in minimal media (growth experiments 2-5). The growth jars were incubated in a static incubator at 23 °C for a period of four weeks. Colony counts (2.1.9) were used to quantify and compare growth of the wild-type and mutant strains from five individual growth experiments (Table 4.2).

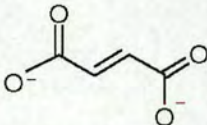
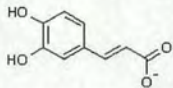
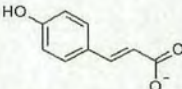
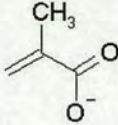
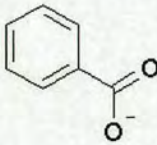
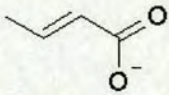
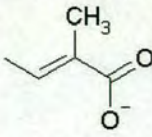
ELECTRON ACCEPTOR (EA)	+Lactate +EA				-Lactate +EA			
FUMARATE 	2	1	3	39	1	2	25	47
	202	39	235	187	40	30	76	105
	0	0	7	13	0	0	59	119
	0	0	200	225	0	0	37	68
	1	32	800	600	88	13	200	13
	27.7		230.9		17.4		74.9	
	57.0		254.8		27.2		52.3	
CAFFEATE 	0	0	0	0	-	-	-	-
	0	0	0	0	0	0	0	0
	0	0	0	0	0	0	0	0
	0	0	0	0	0	0	0	0
	0	0	0	0	0	0	0	0
	0		0		0		0	
	0		0		0		0	
COUMARATE 	18	0	0	0	-	-	-	-
	0	0	6	1	0	0	0	0
	0	0	0	0	0	0	0	0
	0	0	0	0	0	0	0	0
	0	0	0	2	0	0	0	0
	1.8		0.9		0		0	
	5.4		1.8		0		0	
METHACRYLATE 	0	1	4	23	-	-	-	-
	4	0	7	14	2	6	15	19
	0	0	13	75	0	0	36	48
	0	0	14	51	0	0	12	80
	6	35	0	1	3	0	12	38
	4.6		20.2		1.4		32.5	
	10.3		23.0		2.1		22.0	
BENZOATE 	0	0	0	0	-	-	-	-
	3	2	9	2	1	0	2	12
	0	0	1	0	0	0	9	297
	0	0	80	7	0	0	96	62
	0	0	1	0	0	0	0	0
	0.5		10		0.1		59.8	
	1.0		23.5		0.3		95.5	
CROTONATE 	3	0	0	12	-	-	-	-
	16	0	10	16	48	16	18	100
	0	0	219	9	0	0	190	270
	0	0	50	24	0	0	4	100
	1	0	19	5	0	0	0	60
	2.0		36.4		8.0		92.8	
	4.8		62.3		16.0		89.5	
TIGLATE 	44	150	17	34	-	-	-	-
	7	15	0	8	1	1	0	7
	0	0	32	56	0	0	27	11
	0	0	4	26	0	0	0	0
	1	2	0	1	0	2	1	8
	21.9		17.8		0.5		6.8	
	44.6		17.9		0.7		8.7	

Table 4.2 continued overleaf

Table 4.2 continued.

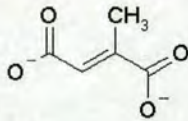
ELECTRON ACCEPTOR (EA)	+Lactate +EA				-Lactate +EA			
<div>MESACONATE</div> <div></div>	0	3	7	6	-	-	-	-
	3	6	¹¹⁸	1	29	26	41	31
	0	0	¹⁰²	12	0	0	66	44
	0	0	50	28	0	0	1	2
	5	5	19	3	4	6	16	37
	2.2		34.6		8.1		29.8	
	2.4		40.3		11.4		20.9	
CONTROLS MINUS EA	+Lactate -EA				-Lactate -EA			
	3	1	2	2	4	14	6	6
	0	0	¹³⁸	0	1	1	19	¹¹
	0	0	3	3	0	0	31	19
	0	0	16	5	0	0	16	9
	0	0	4	2	6	1	22	12
	0.4		17.5		2.7		15.1	
	0.9		40.4		4.2		7.5	

Table 4.2: Anaerobic growth of *S. oneidensis* MB5415 and *S. oneidensis* MR-1 on acrylates

Colony counts are listed for five individual growth experiments of wild-type *S. oneidensis* MR-1 (white) and *S. oneidensis* MB5415 (grey) grown anaerobically on 8 different acrylate substrates. Colony counts for duplicate cultures are shown in the same row. Both strains were grown in parallel in minimal media supplemented with lactate and an electron acceptor. Controls included in the experiment comprise growth of both strains in the absence of lactate and/or electron acceptor. Growth of wild-type *S. oneidensis* MR-1 in the presence of fumarate was used as a positive control of growth. The cell counts shown in the table represent $\times 10^4$ cells ml^{-1} . The average colony count (red) was calculated for each of the ten *S. oneidensis* MB5415 and wild-type *S. oneidensis* MR-1 cultures grown anaerobically on a specific acrylate under the various conditions. The standard deviation of the colony counts was also calculated and is shown in green.

The results obtained from the five anaerobic growth experiments were inconsistent between different growth experiments and duplicate cultures of the same experiment. The growth variability observed was exemplified by the relatively high standard deviation calculated for the colony counts obtained (Table 4.2). The following interpretation of the phenotype studies documents the most consistent colony count results that have a relatively low standard deviation. The variation in growth levels obtained on a particular substrate was probably due to a corresponding variation in anaerobic conditions in each individual growth jar.

A unique high colony number obtained for growth on a particular substrate was most likely due to the presence of oxygen serving as the preferred terminal electron acceptor.

The mean colony counts obtained for the positive control (230.9 colonies) showed that wild-type *S. oneidensis* MR-1 grew anaerobically in the presence of lactate and fumarate at much higher levels compared to the negative control in which lactate and fumarate were absent (15.1 colonies; Table 4.2). Growth of the wild-type strain was inhibited in the absence of fumarate (mean, 17.5 colonies) indicating that fumarate served as the sole terminal electron acceptor during anaerobic growth of *S. oneidensis* MR-1. Although at lower levels compared to the positive control, the wild-type strain grew anaerobically with fumarate in the absence of lactate (mean, 74.9 colonies; Table 4.2). This led to the suggestion that another factor in the media was acting as an alternative carbon source to lactate. Overall, the control results obtained for growth of *S. oneidensis* MR-1 on fumarate and/or lactate indicated that the cultures were anaerobic and the supplied substrate functioned as the terminal electron acceptor.

The quantitative colony counts of the anaerobic growth experiments revealed that *S. oneidensis* MR-1 grew well in the presence of fumarate as terminal electron acceptor during anaerobic respiration (Table 4.2). The level of growth on fumarate was further improved with inoculation of cultures with a bacterial suspension (experiments 2-5) rather than a single colony (experiment 1; Table 4.2).

Anaerobic growth of *S. oneidensis* MB5415 on lactate and fumarate (mean, 27.7 colonies) was significantly impaired compared to *S. oneidensis* MR-1 (mean, 230.9 colonies).

The colony counts obtained for *S. oneidensis* MB5415 on lactate and fumarate were similar to the negative *S. oneidensis* MB5415 control cultures in which lactate and/or fumarate were eliminated. This showed that the growth inhibition observed on fumarate was a true phenotype. This tentatively suggests that fumarate is a possible substrate of the flavocytochrome formed by association of FccA54 and FccB54.

The phenylacrylates, coumarate and caffeate did not sustain anaerobic growth of wild-type *S. oneidensis* MR-1 in the presence or absence of lactate. In the absence of these phenylacrylates, low, but significant growth levels of *S. oneidensis* MR-1 were observed indicating that the substrates were specifically inhibiting growth. This result was supported by the low standard deviation calculated for the colony counts obtained for these cultures. Coumarate and caffeate also inhibited growth of the *S. oneidensis* MB5415 mutant strain (Table 4.2). These data correlate with the inability of the related methacrylate reductase of *Geobacter sulfurreducens* to catalyse reduction of phenylacrylates such as ferulate and caffeate (Mikoulinskaia *et al.*, 1999).

The mean colony counts obtained for wild-type *S. oneidensis* MR-1 grown anaerobically in the presence of lactate and one of the following electron acceptors: methacrylate (20.2 colonies), benzoate (10 colonies), crotonate (36.4 colonies), tiglate (17.8 colonies) and mesaconate (34.6 colonies) was consistently low compared to growth in the presence of lactate and fumarate (230.9 colonies).

The low anaerobic growth levels of wild-type *S. oneidensis* MR-1 on each of the aforementioned acrylates were supported by the relatively low standard deviation data. Furthermore, the observed colony counts were similar to the control *S. oneidensis* MR-1 cultures grown in the absence of lactate and /or acrylate. Anaerobic growth of wild-type *S. oneidensis* MR-1 on crotonate was greater in the absence (mean, 92.8 colonies), rather than the presence of lactate (mean, 36.4 colonies). This result leads us to the suggestion that an alternative carbon source favours the terminal reduction of crotonate during anaerobic respiration of *S. oneidensis* MR-1. The mean colony counts obtained for anaerobic growth of *S. oneidensis* MB5415 on methacrylate (4.6 colonies), benzoate (0.5 colonies), crotonate (2.0 colonies), tiglate (21.9 colonies) and mesaconate (2.2 colonies), revealed low levels of growth, as found for wild-type *S. oneidensis* MR-1. The relatively low standard deviations calculated for the *S. oneidensis* MB5415 colony counts provided supporting data that the acrylates did not support growth of the mutant strain.

S. oneidensis MR-1 did not respire anaerobically in the presence of methacrylate, crotonate, benzoate, coumarate, caffeate, tiglate or mesaconate (Table 4.2). This growth defect was not due to poor inoculation of the growth jars with *S. oneidensis* MR-1 as the bacterium grew well in the presence of fumarate as terminal electron acceptor during anaerobic respiration. It is possible that inhibitory concentrations (20 mM) of each candidate acrylate were used in the growth experiment. It is therefore necessary to find the optimal concentration of each acrylate electron acceptor that is required to support growth of *S. oneidensis* MR-1. Further growth experiments are also required to obtain strict anaerobic conditions for growth of the wild-type and mutant strains on the range of acrylates. This would lead to the generation of consistent results where the acrylate is used as the sole terminal electron acceptor in the absence of oxygen. It may be possible to eliminate the presence of oxygen in the cultures by overlaying with mineral oil to form a tight seal. The exclusion of oxygen from the growth cultures could also be achieved by conducting the growth experiments in an anaerobic chamber.

Anaerobic growth experiments of *etrA* knockout strains (ETRA-153, ETRA1) on various electron acceptors showed that the mutations had no significant physiological effect on growth compared to wild-type *S. oneidensis* MR-1 (Maier and Myers, 2001; Beliaev *et al.*, 2002a). However, partial DNA microarrays were used to show that the *etrA* insertional mutation of ETRA1 had a significant effect on the mRNA levels of 69 genes involved in anaerobic metabolism under fumarate and nitrate reducing conditions.

For example, the *fccA* fumarate reductase gene encoding flavocytochrome c_3 was consistently repressed in ETRA1 indicating a role of EtrA in transcriptional activation of *fccA* under both fumarate and nitrate reducing conditions (Beliaev *et al.*, 2002a).

DNA microarrays could be used to compare the complete gene transcription profiles of *S. oneidensis* MR-1 and *S. oneidensis* MB5415 under acrylate-reducing conditions in order to examine the functional role of FccA54 and FccB54. A relative decrease in the mRNA levels of certain *S. oneidensis* MB5415 genes may indicate that these genes are involved in the respiratory pathway towards acrylate reduction catalysed by FccA54 and FccB54. It would also be of interest to observe if the *fccA54* and *fccB54* deletion caused an increase in mRNA levels of the related genes, *fccA56*, *fccB56*, *fccA342* and *fccB342*. An increase in mRNA levels of these related genes would indicate that the encoded proteins have a similar role to FccA54 and FccB54 during anaerobic metabolism. It would also be useful to compare the changes in mRNA levels of *S. oneidensis* MR-1 and *S. oneidensis* MB5415 during the switch from aerobic to anaerobic growth conditions to observe which genes are turned on or off.

Two-dimensional polyacrylamide gel electrophoresis (2-D PAGE) could also be used to analyse and compare protein expression of *S. oneidensis* MR-1 and *S. oneidensis* MB5415 under acrylate-reducing conditions. Mass spectrometry and N-terminal Edman sequencing could subsequently be used to characterise proteins that demonstrated significant changes in expression between the two strains.

The protein expression profiles could be used to complement the DNA microarray analyses to provide substantial information on the respiratory chain towards acrylate reduction.

DNA microarray and 2-D PAGE analyses have been successfully used to obtain mRNA and protein expression profiles, respectively of wild-type *S. oneidensis* MR-1 grown aerobically and anaerobically in the presence of fumarate, nitrate and Fe(III). It was shown that genes encoding cytochrome *c* and tricarboxylic acid cycle enzymes were repressed under anaerobic conditions. The expression of *cymA*, *ifcA* and *frdA* involved in anaerobic respiration, was specifically induced three to eight fold under fumarate reducing conditions. Other sets of genes induced during anaerobic respiration comprised those involved in cofactor biosynthesis, cofactor assembly and substrate transport (Beliaev *et al.*, 2002b).

4.3 CONCLUSION

This represents the first report of an *S. oneidensis* MR-1 mutant that lacks the entire gene coding sequences of an enzyme implicated in anaerobic respiration. A new fusion PCR technique was successfully used to synthesise the homologous template DNA sequence for *fccA54* and *fccB54* gene replacement in *S. oneidensis* MR-1. This method could be used to construct other gene replacements in bacteria of the genus *Shewanella* and indeed other Gram-negative bacteria. The double crossover event is reportedly more infrequent than single crossovers and this was found when constructing a gene replacement of *fccA54* and *fccB54* in *S. oneidensis* MR-1.

The occurrence of a double crossover event may be dependent on the sequence of the target gene or the homologous template DNA sequence. Some of the chloramphenicol sensitive transconjugants, such as *S. oneidensis* MB5413 were identified using PCR to contain the *fccA54* and *fccB54* genes. The chloramphenicol sensitivity of the false positives was attributed to a mutation in the *cat* gene or generation of non-specific homologous recombination. Perhaps increasing the length of the homologous template DNA would optimise homologous recombination at the correct position in the target genome. Automated DNA sequencing was used to confirm that the isolated *S. oneidensis* MB5415 mutant did indeed contain a kanamycin cassette in position of the endogenous *fccA54* and *fccB54* genes.

Anaerobic growth experiments of *S. oneidensis* MB5415 on various acrylates as terminal electron acceptor were directly compared to anaerobic growth of *S. oneidensis* MR-1. The *fccA54* and *fccB54* deletion had no detectable physiological effect on anaerobic growth of *S. oneidensis* MB5415 compared to wild-type. The anaerobic growth experiments could be improved by conducting the experiment in an anaerobic chamber. The function of FccA54 and FccB54 may be difficult to observe using anaerobic growth experiments as the function of the flavocytochrome may overlap with the related flavocytochromes. Alternatively, DNA microarrays and 2D-PAGE could be used to compare mRNA and protein expression profiles, respectively of *S. oneidensis* MR-1 and *S. oneidensis* MB5415. These methods could be used to identify the genes involved in acrylate reduction catalysed by FccA54 and FccB54 during anaerobic respiration of *S. oneidensis* MR-1.

Chapter 5

Overexpression and purification of a *Shewanella oneidensis* MR-1 flavoprotein

5.1 INTRODUCTION

5.1.1 Putative interaction of flavin and cytochrome subunits

The *fccA54* and *fccB54* genes that lie adjacent to one another on the same operon encode a putative flavoprotein subunit (FccA54) and a tetrahaem cytochrome *c* subunit (FccB54), respectively (1.8.1). The location of the genes in the same operon immediately led us to suggest that the encoded proteins have a common function. It was subsequently proposed that the FccA54 flavin-containing catalytic subunit associates with the FccB54 cytochrome *c* subunit to form a functional dimeric flavocytochrome. Furthermore, the cytochrome *c* subunit was proposed to function as the physiological electron donor to flavin embedded in the catalytic subunit. These conjectures led us to investigate the putative interaction between the flavin and cytochrome subunits. The aim was to specifically overexpress and purify FccA54 in order to test whether enzyme catalysis is dependent on association with the FccB54 electron transfer cytochrome subunit. A variety of substituted acrylates were selected as potential substrates to study enzyme catalysis of the purified FccA54 flavoprotein in order to identify the native substrate. The major objective was to obtain high yields of purified FccA54 protein to investigate the protein structure and function by X-ray crystallography and to undertake enzymological studies.

5.1.2 A strategy to overexpress and purify the FccA54 flavoprotein

The periplasmic methacrylate reductase from *Geobacter sulfurreducens* AM-1 comprises a flavoprotein subunit that is postulated to associate with a periplasmic cytochrome *c* subunit. The flavoprotein subunit was successfully purified from the periplasm as a stable protein in the absence of the associated tetrahaem cytochrome *c* (Mikoulinskaia *et al.*, 1999). The N-terminal sequence similarity observed between the methacrylate reductase and FccA54 led to the supposition that the related FccA54 protein could also be purified as a stable protein from the periplasm. However, it was anticipated that purification of FccA54 from the periplasm of *Shewanella* species might be problematic due to the endogenous expression of similar flavoproteins. Therefore, an FccA54 overexpression system was devised to preferentially overexpress and purify the FccA54 flavoprotein from an *Escherichia coli* host. Distinct variation in the Tat (*twin arginine translocation*) pathway machinery of *Shewanella* and *E. coli* strains might have led to poor recognition of the FccA54 preprotein signal peptide, impeding subsequent membrane translocation to the periplasm of *E. coli*. Therefore, cytoplasmic overexpression was selected to avoid heterogeneous expression of the FccA54 preprotein targeted to the periplasm of a foreign host cell. The overexpression system was designed to produce high yields of purified FccA54 protein that could be easily detected by measuring the UV-visible spectrum.

5.2 RESULTS AND DISCUSSION

5.2.1 PCR amplification of *fccA54* from the *S. oneidensis* MR-1 genome

Synthetic oligonucleotide primers, named 54FM and 54RA, were designed to initiate PCR amplification of the *fccA54* mature coding sequence. The extreme 5'-terminal *fccA54* coding sequence comprising 87 nucleotides was predicted to encode an N-terminal Tat signal peptide of 29 amino acid residues in length (Nielsen *et al.*, 1997; <http://www.cbs.dtu.dk/services/SignalP/>). The 5'-end of the 54FM forward primer complementary to the mature *fccA54* gene coding sequence was designed to begin 88 nucleotides downstream of the ATG start codon (Figure 5.1). To optimise the PCR specificity, the complementary sequence between the 54FM primer and genomic DNA template extended over a region of 18 nucleotides. The 54FM primer was engineered to contain a 5'-overhang that incorporated an ATG start codon positioned at the 5'-end of the complementary *fccA54* sequence (Figure 5.1). The 5'-end of the 54RA reverse primer sequence corresponded to the C-terminal *fccA54* TAA stop codon. The 16-nucleotide primer sequence of 54RA complementary to *fccA54* was lengthened to include a 5'-overhang sequence (Figure 5.1).

The engineered 5'-overhang sequences of each primer were designed to contain restriction endonuclease sites to produce a 1455 bp *Bam*HI/*Pst*I *fccA54* '54FMRA' PCR product. Inclusion of restriction sites in the *fccA54* 54FMRA PCR product intended to facilitate direct cloning of the PCR amplified product into the expression plasmid. The 54FM primer was designed to contain a *Bam*HI cleavage site (5'-GGATCC-3') and a *Pst*I cleavage site (5'-CTGCAG-3') was inserted in the 5'-overhang of primer 54RA. A triplet of extra nucleotides was introduced at the 5'-end of each engineered cleavage site to facilitate restriction enzyme digestion (Figure 5.1).

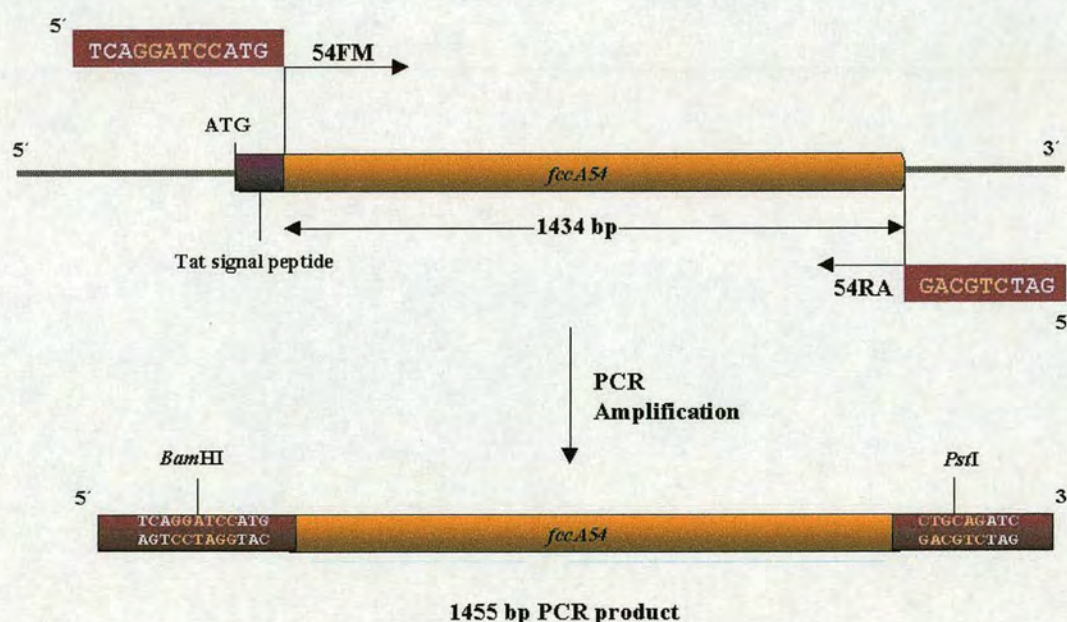


Figure 5.1: A schematic diagram to show PCR amplification of *fccA54*

Primers 54FM and 54RA were designed to amplify the *fccA54* gene sequence with exclusion of DNA sequence encoding the N-terminal Tat signal peptide. The *fccA54* gene was amplified as a 1455 bp *Bam*HI/*Pst*I 54FMRA fragment to facilitate cloning into the expression plasmid. The diagram is not to scale.

The restriction enzymes, *Bam*HI and *Pst*I were convenient for cloning the *fccA54* 54FMRA PCR product due to the absence of target sites within the *fccA54* gene coding sequence. Furthermore, unique cleavage sites for *Bam*HI and *Pst*I occur in expression plasmids, pJF118 (Fürste *et al.*, 1986) and pMMB503EH (Overbye Michel *et al.*, 1995), selected for overexpression of the flavoproteins. To maximise the success of PCR amplification, other standard considerations were met during primer design of 54FM and 54RA. The primer sequences were optimised in length and nucleotide content to obtain similar melting temperatures. The primer sequences complementary to *fccA54* did not contain polypurines or polypyrimidines thus preventing the formation of internal secondary structure. Complementary 3'-terminal sequences of the primer pair were avoided to prevent primer-dimer formation during PCR amplification.

Primers 54FM and 54RA successfully initiated PCR amplification of the *fccA54* gene sequence from the *S. oneidensis* MR-1 genome. The specific PCR amplification of a product corresponding to the size of the *fccA54* 1455 bp *Bam*HI/*Pst*I fragment (Figure 5.1) was observed by agarose gel electrophoresis (Figure 5.2). The quantity of PCR amplified product was approximately 0.045 µg DNA (Figure 5.2).

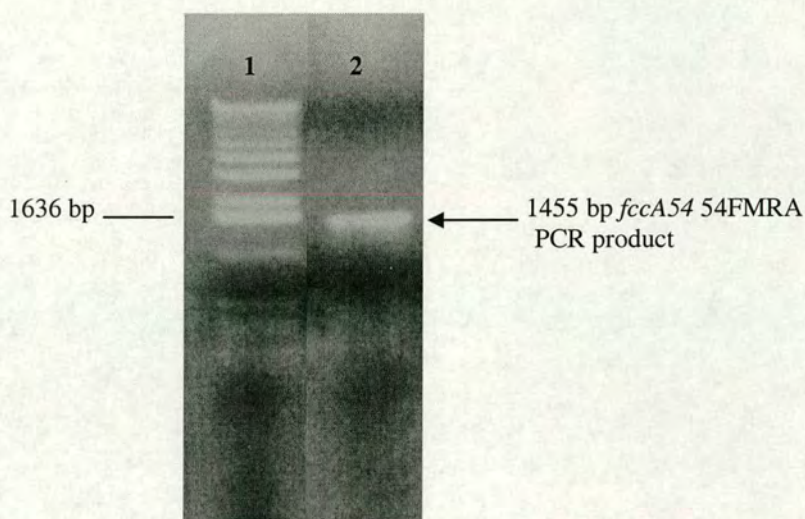


Figure 5.2: PCR amplification of *fccA54* mature coding sequence

The *fccA54* sequence encoding mature FccA54 flavoprotein was successfully PCR amplified from the *S. oneidensis* MR-1 genome. PCR amplification was analysed by agarose gel electrophoresis that showed amplification of a product corresponding to the size of the 1455 bp *fccA54* 54FMRA *Bam*HI/*Pst*I fragment (lane 2). 1 kb DNA ladder shown in lane 1 of the agarose gel indicated amplification of a PCR product at the correct size.

5.2.2 Cloning of the *fccA54* 54FMRA PCR product in pGEM-T

The 1455 bp *fccA54* PCR product was inserted into pGEM-T (Promega; Figure 5.3), a high copy number plasmid (3000 bp) to achieve multiple copies of the PCR product. PCR amplification catalysed by *Taq* thermostable DNA polymerase resulted in the non-template dependent addition of a single deoxyadenosine 5'-triphosphate to each 3'-end (Clark, 1988) of the *fccA54* PCR product. The 3'-adenine base overhangs served to ligate the *fccA54* PCR product into pGEM-T by complementary base pairing with each 3'-thymine base overhang of linearised pGEM-T DNA.

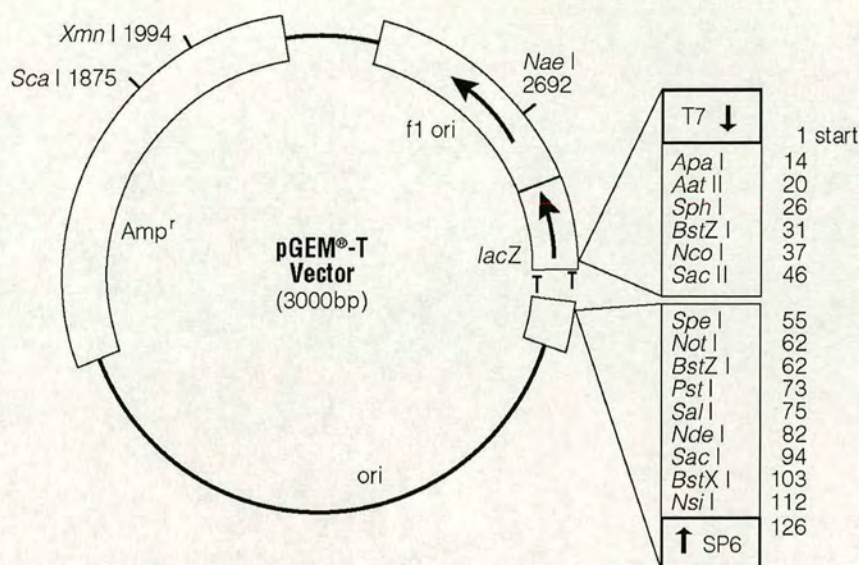


Figure 5.3: Map of pGEM-T (Promega) high copy number cloning plasmid

The 3' -thymine base overhangs that disrupt the *lacZ* gene are shown.

Recombinant pGEM-T plasmid was transformed into *E. coli* TG1 and positive transformants were identified using two selection procedures. Firstly, transformants were selected for ampicillin resistance encoded on the pGEM-T plasmid. Secondly, blue/white colony screening was used to differentiate between transformants containing re-ligated pGEM-T and those containing recombinant pGEM-T plasmid. A blue colony phenotype is due to the production of 5-bromo-4-chloro-indigo from the hydrolysis of X-gal (5-bromo-4-chloro-3-indolyl- β -D-galactoside) by β -galactosidase. The *lacZ* gene located in pGEM-T encodes β -galactosidase that is not expressed when *lacZ* is disrupted by insertion of a PCR product.

Seven white colonies indicative of *lacZ* gene disruption by the *fccA54* PCR product were randomly selected for further analysis. Plasmid DNA was isolated from the selected white colonies, numbered 3-1 to 3-7 and *Bam*HI/*Pst*I double digests were performed to verify insertion of the *fccA54* PCR product in pGEM-T. Only 2 of the 7 white colonies, named 3-1 and 3-4 contained recombinant plasmid, as shown by excision of a 1455 bp *Bam*HI/*Pst*I fragment corresponding to the *fccA54* PCR product (Figure 5.4). Recombinant pGEM-T plasmid containing the *fccA54* PCR product, isolated from colony 3-4 was named pMB3-4. This plasmid was used for further work to develop the FccA54 overexpression construct.

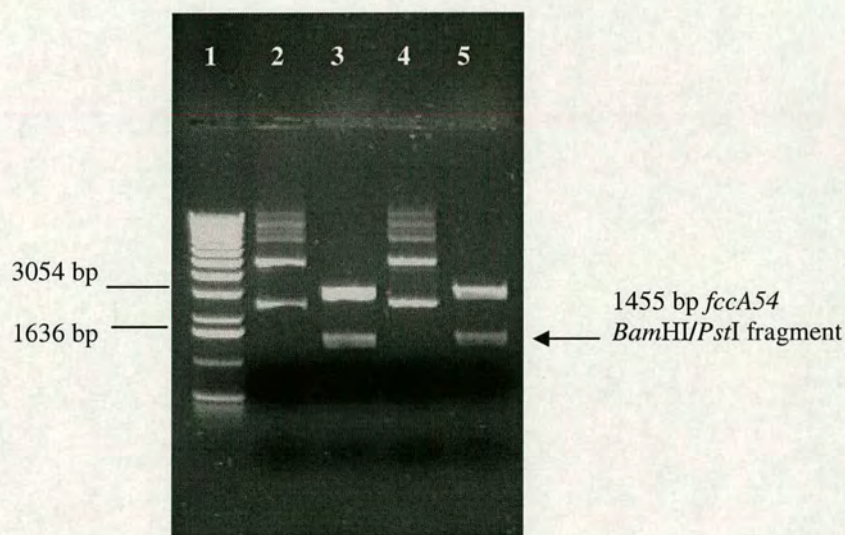


Figure 5.4: Cloning of the *fccA54* *Bam*HI/*Pst*I PCR product in pGEM-T

Recombinant pGEM-T plasmid DNA isolated from ampicillin resistant white colonies, 3-1 (lane 2) and 3-4 (lane 4) was analysed by agarose gel electrophoresis. Recombinant plasmid from colonies 3-1 and 3-4 was identified by the release of a 1455 bp *fccA54* 54FMRA fragment upon double digestion with *Bam*HI and *Pst*I (lanes 3 and 5, respectively). 1 kb DNA ladder was loaded in lane 1 of the agarose gel to show that the restriction fragments were of the correct size.

5.2.3 Sequencing the *fccA54* 54FMRA PCR product of pMB3-4

The *fccA54* 54FMRA PCR product was sequenced to check for possible mutations incorporated by the relatively low fidelity *Taq* DNA polymerase. Single-stranded DNA template was prepared from pMB3-4 and sequencing primers, 54P1, 54P2, 54P3 and 54P5 were designed to provide overlapping sequencing data of *fccA54*. Despite the lack of 3'-5'-exonuclease proofreading activity by *Taq* DNA polymerase, the *fccA54* sequence of pMB3-4 was correctly PCR amplified, as confirmed by automated sequencing. Comparison of the *fccA54* sequencing data to the *fccA54* sequence obtained from 'The Institute for Genomic Research' (TIGR; <http://www.tigr.org>) was used to confirm that the conserved proline residue in the fumarate reductase family (Pro366; Fcc₃ of *S. frigidimarina* NCIMB 400; Pealing *et al.*, 1992) is indeed substituted with histidine in FccA54 (Figure 3.4; 3.2.1).

5.2.4 Cloning of the *fccA54* 54FMRA PCR product in pMMB503EH

In the event that overexpression of FccA54 in *E. coli* was not achieved, a recombinant expression plasmid was constructed to suit FccA54 overexpression in a *Shewanella* strain. The *fccA54* 54FMRA PCR product was transferred into the broad host range plasmid, pMMB503EH (Overbye Michel *et al.*, 1995; Figure 5.5) to obtain a suitable construct for cytoplasmic overexpression in a *Shewanella* strain. The *fccA54* 54FMRA PCR product was cut from pMB3-4 as a *Bam*HI/*Pst*I 1455 bp fragment and ligated to complementary ends of pEX129 (Atanasiu, 2001) generated by digestion with *Bam*HI and *Pst*I. The recombinant plasmid was transformed into *E. coli* DH5 α and positive transformants were screened for streptomycin resistance encoded on pMMB503EH.

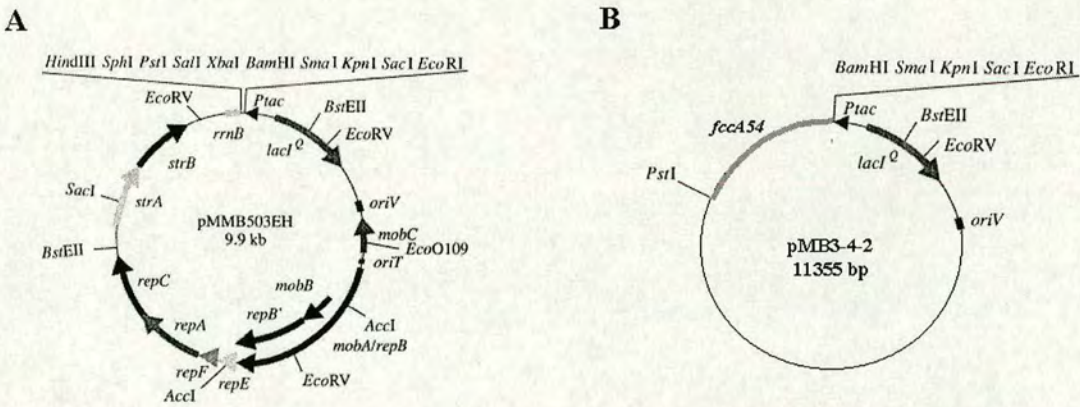


Figure 5.5: Construction of a plasmid for FccA54 overexpression in *Shewanella* species

(A) The parent pMMB503EH plasmid (Overbye Michel *et al.*, 1995) is shown.
(B) The *fccA54* gene from pMB3-4 was inserted in recombinant pMMB503EH expression plasmid pEX129 (Atanasiu, 2001), as a *Bam*HI/*Pst*I fragment to form pMB3-4-2. The position of the *Bam*HI, *Pst*I and *Eco*RI cloning sites are shown.

There were no colonies present on the ‘cells only’ control indicating reliable streptomycin selection. The absence of colonies on the ‘vector only’ control strongly suggested that the two streptomycin resistant transformants contained recombinant plasmid. Plasmid DNA was isolated from both colonies and digestion with *Bam*HI and *Pst*I released a 1455 bp fragment corresponding to *fccA54* (not shown). Recombinant pMMB503EH containing *fccA54* was named plasmid pMB3-4-2 (Figure 5.5). This plasmid DNA was subsequently used to generate an expression plasmid for FccA54 overexpression in *E. coli*.

5.2.5 Cloning of the *fccA54* 54FMRA PCR product in pJF118

To achieve overexpression of the FccA54 flavoprotein subunit in *E. coli*, the *fccA54* 54FMRA PCR product was introduced into pJF118 (5267 bp), an isopropylthiogalactoside (IPTG) inducible *E. coli* expression plasmid (Figure 5.6; Fürste *et al.*, 1986). The multiple cloning site of pJF118 contains an *EcoRI* cleavage site (5'-GAATTC-3') located 5 bp downstream of the plasmid ribosome-binding site (5'-AGGA-3'). To maximise protein overexpression levels, the ATG start codon of a cloned gene should ideally map within 13 nucleotides from a ribosome-binding site, reportedly at an optimal distance of 9 nucleotides (Wood *et al.*, 1984a). Therefore, the location of *EcoRI* as the first cleavage site closest to the ribosome-binding site makes pJF118 convenient for protein overexpression from a gene coding sequence cloned as an *EcoRI* fragment. The *BamHI* cleavage site of pJF118 maps 15 bp downstream of the plasmid ribosome-binding site. Therefore, cloning of *fccA54*, as a *BamHI/PstI* fragment in pJF118 would have unfavourably positioned the *fccA54* ATG start codon 21 bp from the ribosome-binding site. The endogenous ribosome-binding site upstream of *fccA54* in the genome was not PCR amplified; therefore, overexpression of FccA54 was dependent on the plasmid-borne ribosome-binding site. In order to construct an ideal plasmid for overexpression of FccA54 in *E. coli*, the pJF118 plasmid DNA sequence was altered to contain a *BamHI* cleavage site as the first cloning site adjacent to the ribosome-binding site.

An experimental procedure involving modifying enzymes was designed to alter the multiple cloning site of pJF118. This technique involved digesting recombinant pJF118 plasmid with *EcoRI* and removing the single-stranded DNA overhang in a reaction catalysed by mung bean nuclease. The intention was to create a blunt end containing the remaining *EcoRI* 5'-guanine base. The recombinant pJF118 plasmid DNA was subsequently digested with *BamHI* to generate a 5'-overhang that was end-filled in a reaction catalysed by the Klenow fragment of DNA polymerase I. This step was designed to form a blunt end comprising the sequence, 5'-GATCC-3'. The two modified blunt ends when re-ligated were designed to form a *BamHI* cleavage site (5'-GGATCC-3') located 5 bp downstream of the pJF118 plasmid ribosome-binding site.

It was identified that insertion of *fccA54* in pJF118 as a *BamHI/PstI* fragment would form a recombinant plasmid containing the *fccA54* N-terminal *BamHI* site 5 bp downstream from the *EcoRI* site. This short distance between cleavage sites may have prevented digestion with *EcoRI* and *BamHI* in consecutive reactions. To avoid this potential problem, the *fccA54* gene was inserted in pJF118 as an *EcoRI/PstI* 1476 bp fragment excised from pMB3-4-2 (Figure 5.5). This introduced 15 nucleotides of the pMB3-4-2 multiple cloning site upstream of the *fccA54 BamHI* site in order to lengthen the region between *EcoRI* and *BamHI* in pJF118 (Figure 5.6). Recombinant pJF118 plasmid containing *fccA54* was transformed into *E. coli* TG1 and positive transformants were firstly selected for ampicillin resistance encoded in the *bla* gene of pJF118 (Figure 5.6).

However, ampicillin selection on the plates was poor, as indicated by the appearance of 9 colonies on the 'cells only' control. There were approximately 100 colonies on the 'vector only' control plate, which were possibly due to the low ampicillin selection but did suggest a high probability of re-ligated vector for cells transformed with 'vector and insert' DNA. Compared to the 'vector only' background colony count, approximately 150 colonies grew from cells transformed with 'vector and insert' DNA. Following antibiotic selection, plasmid DNA was extracted from 16 putative ampicillin resistant colonies. Recombinant pJF118 plasmid containing *fccA54* was identified for 1 in 16 of the screened colonies, as shown by digestion with *EcoRI* and *PstI* and release of a 1476 bp fragment corresponding to *fccA54* (Figure 5.7). The recombinant pJF118 plasmid containing *fccA54* as an *EcoRI/PstI* 1476 bp fragment was referred to as pMB1 (Figure 5.6).

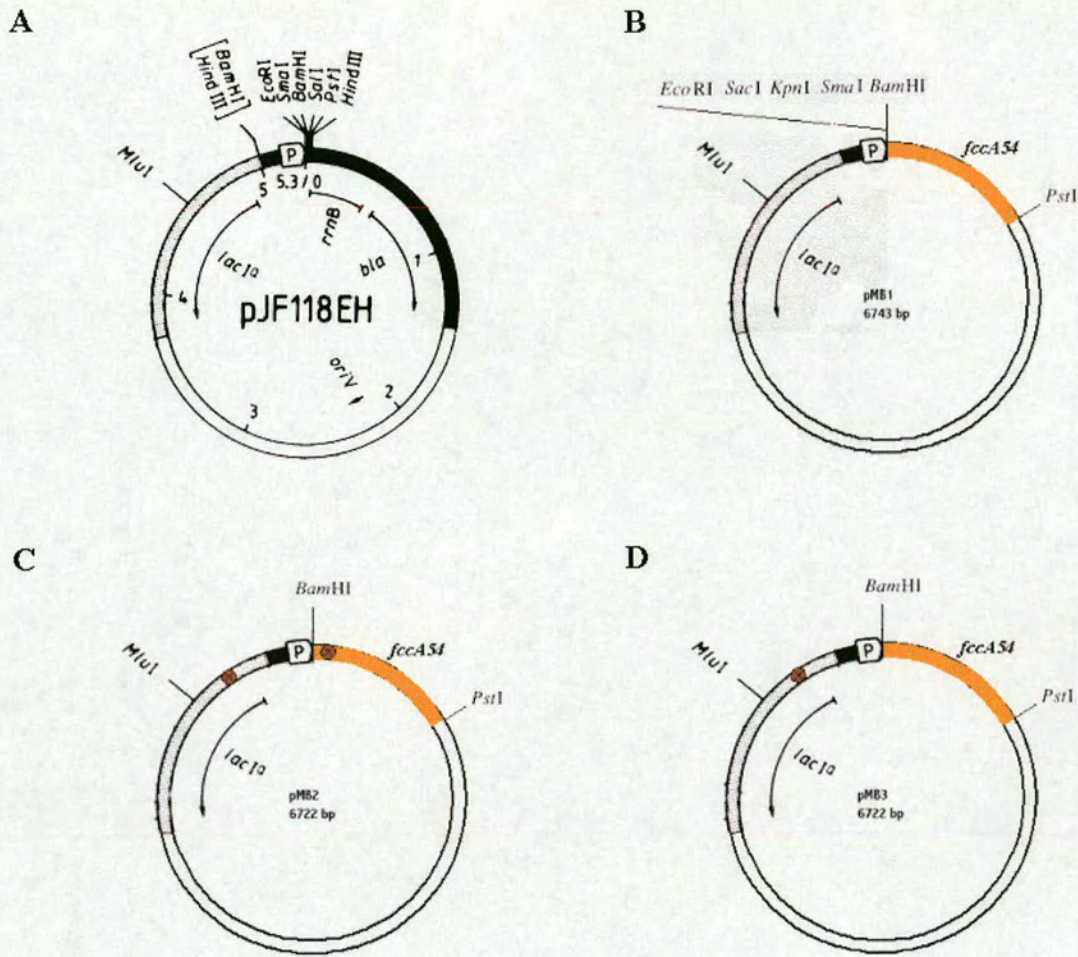


Figure 5.6: Construction of a modified pJF118 plasmid for FccA54 overexpression in *E. coli*
The *fccA54* 54FMRA PCR product cloned in pMB3-4-2 was transferred as an *EcoRI*/*PstI* fragment into pJF118 (Fürste *et al.*, 1986) (A) to generate pMB1 (B). This plasmid was modified using fusion PCR to form pMB2 that contained the N-terminal *fccA54* *BamHI* site adjacent to the ribosome-binding site (C). The deletion in the *fccA54* gene was corrected to form pMB3 (D). A red crossed circle represents a mutation.



Figure 5.7: Cloning of *fccA54* in pJF118 *E. coli* expression plasmid

The *fccA54* 54FMRA PCR product was transferred from pMB3-4-2 to pJF118 as a 1476 bp *EcoRI/PstI* fragment to form pMB1. An *EcoRI/PstI* double digest (lanes 3 and 4) of pMB1 plasmid DNA (lane 2) released a 1476 bp fragment corresponding to the size of *fccA54*. This result verified that pMB1 plasmid DNA (lane 2) was recombinant pJF118 plasmid containing *fccA54*. The results of the digests were analysed by agarose gel electrophoresis and 1kb DNA ladder (lane 1) was used to indicate the restriction fragments were of the correct size.

Plasmid DNA modification of pMB1 to obtain the N-terminal *fccA54* *Bam*HI site

5 bp from the plasmid ribosome-binding site was not achieved using modifying enzymes. This was attributed to the hyperactivity of mung bean nuclease that consistently degraded the pMB1 plasmid DNA under various conditions. An alternative approach to pMB1 plasmid DNA modification was implemented that used fusion PCR to generate a suitable *FccA54* overexpression plasmid.

5.2.6 Modification of pMB1 expression plasmid by fusion PCR

The ATG start codon of the *fccA54* gene inserted in pMB1 as an *EcoRI/PstI* 1476 bp fragment was positioned 32 nucleotides from the ribosome-binding site. Fusion PCR was designed to amplify an 'FccA54 overexpression fragment' that contained the *fccA54* N-terminal *BamHI* site 5 bp downstream of the plasmid ribosome-binding site. Substitution of the *EcoRI* site with *BamHI* intended to concomitantly position the *fccA54* start codon 11 nucleotides from the plasmid ribosome-binding site. The FccA54 overexpression fragment was PCR amplified to incorporate internal restriction cleavage sites that facilitated insertion of the fragment in pMB1. A new expression plasmid was formed that contained the FccA54 overexpression fragment specialised for obtaining maximal FccA54 overexpression levels.

5.2.6.1 Primer design and fusion PCR amplification

The FccA54 overexpression fragment was a chimeric sequence generated from fusion of parent pJF118 DNA and recombinant pMB1 plasmid DNA sequences. The primers distal to the point of plasmid sequence modification, namely, 54JF3 and 54JF4 were designed to initiate amplification of a 1396 bp fusion PCR product. The 5'-end of the forward primer 54JF4 was located in the pJF118 *lacI^Q* gene and precisely mapped to 779 bp upstream of the ribosome-binding site. The 3'-end of primer 54JF4 was positioned 34 bp from an integral *MluI* site (5'-ACGCGT-3') selected for cloning the fusion PCR product (Figure 5.8). The reverse distal primer 54JF3 was designed to complement *fccA54* 54FMRA insert DNA of pMB1. The 5'-end of 54JF3 was positioned 604 bp downstream of the integrated ATG start codon of *fccA54*.

The 3'-end of 54JF3 was positioned 14 bp from a cleavage site specific to *Bgl*II, a restriction enzyme convenient for cloning the fusion PCR product (Figure 5.8). The restriction enzymes, *Bgl*II and *Mlu*I were ideally suited for cloning the fusion PCR product due to the absence of target sites within the *fccA54* gene coding sequence and presence of unique sites in pJF118.

The central primers, 54JF1 and 54JF2 were designed to contain the desired plasmid DNA sequence in which the *fccA54* N-terminal *Bam*HI site lies adjacent to the ribosome-binding site. This effectively positioned the *fccA54* ATG start codon 11 nucleotides from the ribosome-binding site. The central forward primer 54JF1 was complementary to pMB1 plasmid DNA and extended over a region of 17 bp comprising the *Bam*HI site and the N-terminal nucleotides of *fccA54*. A 5'-overhang sequence of 54JF1 introduced the ribosome-binding site of the plasmid next to the *Bam*HI cleavage site (Figure 5.8). The reverse central primer 54JF2 was complementary to 15 nucleotides of pJF118 plasmid DNA that included the ribosome-binding site of the plasmid. A 5'-overhang sequence of 54JF2 incorporated the *Bam*HI site next to the ribosome-binding site (Figure 5.8). The central primers were designed to be complementary over 16 nucleotides spanning the critical region of modified plasmid DNA. The primary fusion PCR products annealed to one another to provide template DNA sequence for the final fusion PCR step in which a 1396 bp FccA54 overexpression fragment was synthesised (Figure 5.8).

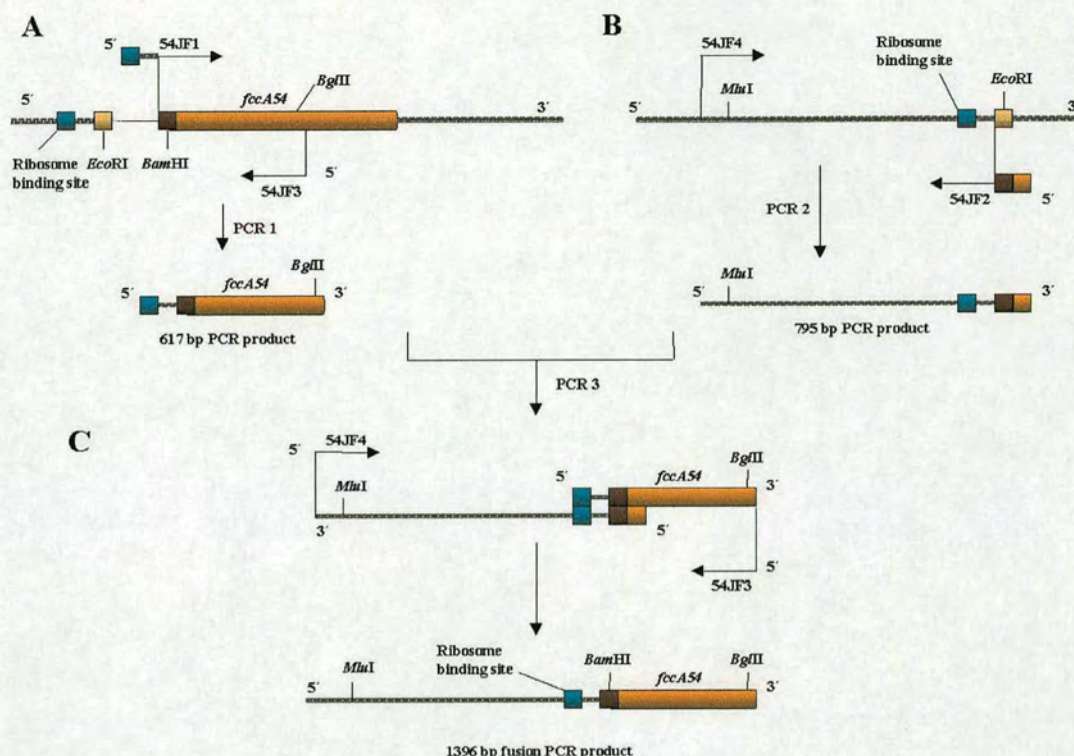


Figure 5.8: A schematic diagram of the fusion PCR procedure

The three PCR steps of fusion PCR are shown for synthesis of an FccA54 overexpression fragment. Arrows indicate the primer positions and direction of synthesis. In the final fusion PCR (C), the modified pMB1 product (A) was fused to the modified pJF118 product (B) to form the FccA54 overexpression fragment (C). The diagram is not to scale.

Primers 54JF1 and 54JF3 were used to successfully PCR amplify a fragment from pMB1 plasmid DNA (Figure 5.9). The amplified PCR product was 617 bp in length (Figure 5.9) and contained the *fccA54* N-terminal *Bam*HI site contiguous to the ribosome-binding site (Figure 5.8). PCR reactions differed in the DNA: primer ratio and NH_4Cl was added to reaction 2. There was no variation in the quantity of product amplified in the presence or absence of the NH_4Cl adjunct. For both reactions, a 617 bp fragment was successfully amplified at a high yield of 0.04 μg DNA (Figure 5.9).

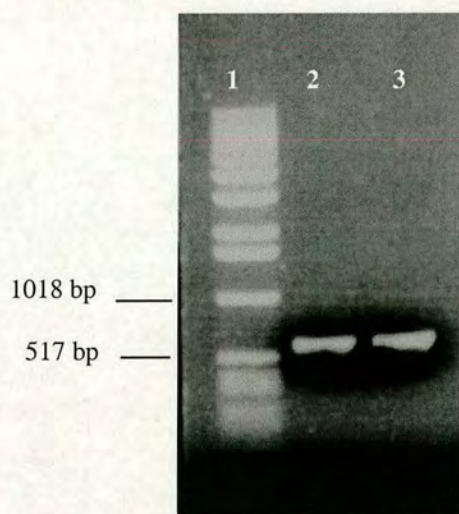


Figure 5.9: PCR amplification of modified pMB1 plasmid DNA

As shown by agarose gel electrophoresis, primers 54JF1 and 54JF3 specifically amplified a 617 bp PCR product from pMB1 plasmid DNA (lanes 2 and 3). This PCR product corresponded to *fccA54* 54FMRA insert DNA containing an N-terminal *Bam*HI site 5 bp from the ribosome-binding site. Reactions 1 and 2 (lanes 2 and 3, respectively) differed in the ratio of DNA: primer with the addition of NH_4Cl to reaction 2. The variation in reaction components did not alter the product yield, approximately 0.045 μg DNA was amplified for both reactions. 1 kb DNA ladder was loaded in lane 1 to indicate amplification of PCR product at the expected size.

Primers 54JF2 and 54JF4 initiated amplification of a 795 bp pJF118 plasmid DNA fragment that included the integral ribosome-binding site (Figure 5.10). The pJF118 template DNA was modified to produce a PCR product that contained the *fccA54* ATG start codon and the N-terminal *Bam*HI site adjacent to the ribosome-binding site (Figure 5.8). A PCR product at the expected size of 795 bp was amplified for both reactions that differed only in the addition of NH_4Cl to reaction 2. There was no change in the quantity of product by addition of NH_4Cl . A high concentration of product was amplified for both reactions, at approximately 0.05 μg (Figure 5.10).

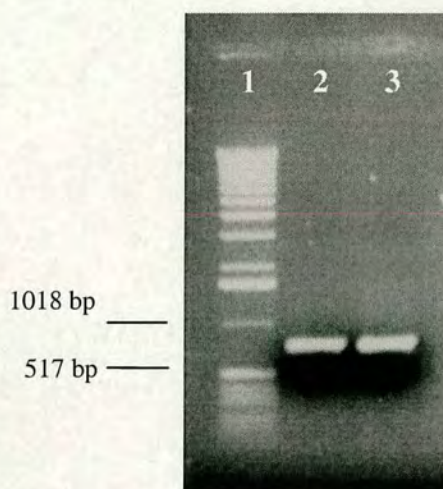


Figure 5.10: PCR amplification of modified pJF118 plasmid DNA

Primers 54JF2 and 54JF4 specifically initiated PCR amplification of a 795 bp fragment from pJF118 plasmid DNA, as shown by agarose gel electrophoresis (lanes 2 and 3). This PCR product corresponded to pJF118 plasmid DNA manipulated to contain the *fccA54* start codon and the N-terminal *Bam*HI site juxtaposed with the plasmid ribosome-binding site. Reactions 1 and 2 (lanes 2 and 3, respectively) differed in the DNA: primer ratio and addition of NH_4Cl to reaction 2. The quantity of PCR product amplified for both reactions was similar at approximately 0.05 μg DNA. 1 kb DNA ladder was loaded in lane 1 of the agarose gel to indicate that the amplified PCR product was of the expected size.

The primary amplification PCR products provided template DNA for fusion PCR to generate an FccA54 overexpression fragment (Figure 5.8). The distal primers 54JF3 and 54JF4 successfully initiated PCR amplification of a 1396 bp FccA54 overexpression fragment (Figure 5.11). This PCR product contained the ribosome-binding site of pJF118 fused to the *Bam*HI site at the N-terminus of *fccA54* from pMB1 (Figure 5.8). Six reactions were performed that differed in the DNA: primer ratio and NH_4Cl addition to reactions 2, 4 and 6 (Figure 5.11). A PCR product at the expected size of 1396 bp was amplified for all reactions at approximately 0.06 μg DNA. However, secondary PCR products were amplified in addition to the desired product (Figure 5.11). The range of fusion PCR amplification products was probably due to insufficient stabilisation of the two complementary primary PCR products as a single DNA template.

PCR sample 1 was run on a preparative agarose gel and the desired band corresponding to the FccA54 overexpression fragment was excised and purified to high quantity at approximately 0.05 μ g DNA.

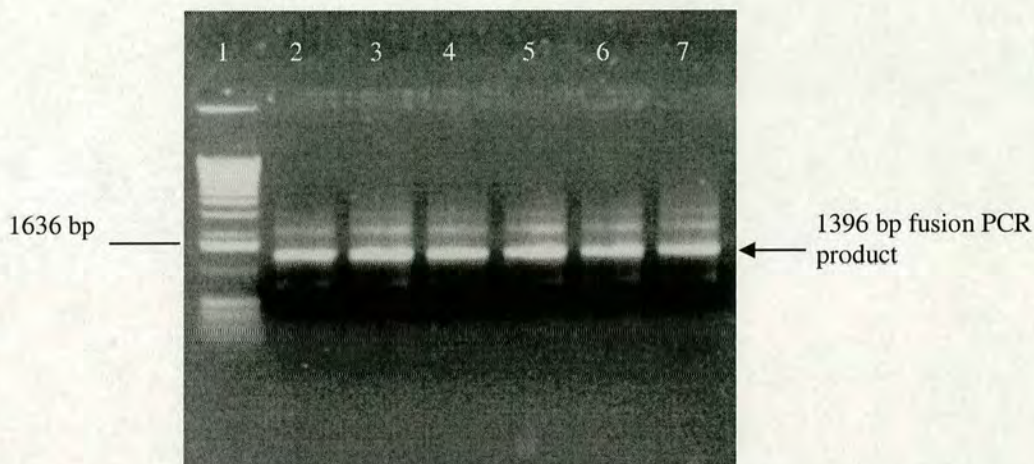


Figure 5.11: Fusion PCR amplification of the FccA54 overexpression fragment

The distal primers 54JF3 and 54JF4 successfully initiated PCR amplification of the 1396 bp fusion PCR product from the primary amplification template DNA, as shown by agarose gel electrophoresis (lanes 2-7). The FccA54 overexpression fragment was a contiguous sequence that contained the *fccA54* sequence and the N-terminal *Bam*HI site from pMB1 adjacent to the pJF118 ribosome-binding site. Six reactions were performed that varied in the DNA: primer ratio and the addition of NH_4Cl to reactions 2, 4 and 6 (lanes 3, 5 and 7, respectively). A similar quantity of the 1396 bp fragment was amplified for all six reactions at approximately 0.06 μ g DNA. In addition to the desired fragment, several other non-specific PCR products were amplified. 1 kb DNA ladder in lane 1 was used to indicate that the desired fragment was amplified at the expected size.

5.2.6.2 Sequencing of the FccA54 overexpression fragment

The FccA54 overexpression fragment was inserted into pGEM-T (Figure 5.3) to provide multiple copies of the fragment and to obtain sequencing information. The fusion PCR product was amplified using *Taq* DNA polymerase and was therefore inserted in pGEM-T by ligation of the complementary single base overhangs, as previously described (5.2.2). The recombinant plasmid was transformed into *E. coli* TG1 and positive transformants were selected using blue/white colony screening and ampicillin resistance. No colonies were apparent on the 'cells only' control indicating antibiotic selection of transformants.

A lawn of colonies was apparent for cells transformed with ‘vector and insert’ DNA. Plasmid DNA was prepared from five ampicillin resistant white colonies. In order to identify colonies transformed with recombinant plasmid, double *Bgl*III/*Mlu*I restriction digests were performed to release the 1396 bp fusion PCR product. Colonies numbered 1, 2 and 4 were shown to contain recombinant pGEM-T plasmid DNA, as shown by release of the *Bgl*III/*Mlu*I FccA54 overexpression fragment at 1396 bp (Figure 5.12). Colony 3 was shown to contain re-ligated pGEM-T only and plasmid DNA isolated from colony 5 contained a *Bgl*III/*Mlu*I fragment at a lower molecular weight than expected. This erroneous insert DNA most probably corresponded to a secondary fusion PCR amplification product (Figure 5.12).

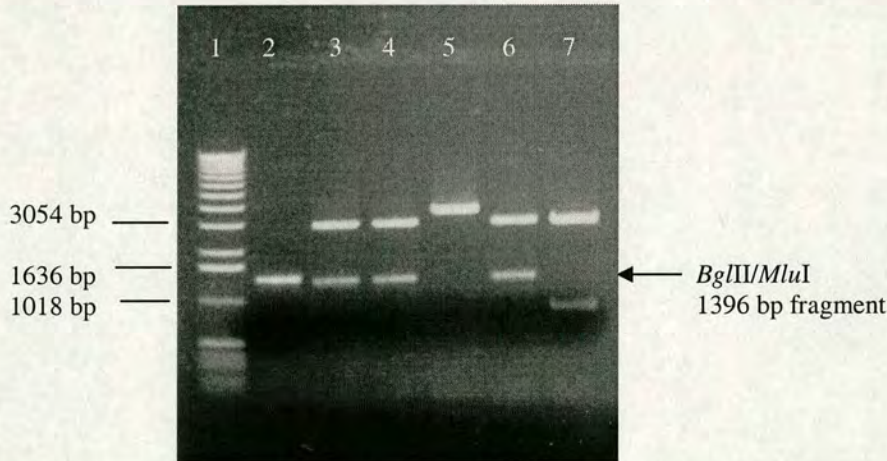


Figure 5.12: Cloning of the fusion PCR product in pGEM-T

Five ampicillin resistant white colonies were screened for insertion of the 1396 bp fusion PCR product (lane 2) in pGEM-T plasmid. Recombinant plasmid was isolated from colonies 1, 2 and 4 as verified by double *Bgl*III/*Mlu*I digestion and release of a 1396 bp fragment corresponding to the fusion PCR product (lanes 3, 4 and 6, respectively). Plasmid DNA isolated from colony 3 was shown to be re-ligated plasmid (lane 5). Double *Bgl*III/*Mlu*I digestion of plasmid DNA isolated from colony 5 released an erroneous fragment that did not correspond to the fusion PCR product (lane 7). 1 kb DNA ladder (lane 1) was used to indicate the size of the restriction fragments.

Recombinant pGEM-T plasmid extracted from colony 2 was used as template DNA for sequencing the fusion PCR product. An *MluI* restriction digest of plasmid DNA was used to determine the orientation of insert DNA in pGEM-T. A unique *MluI* cleavage site occurs at position 99 of the pGEM-T multiple cloning sequence downstream of the insert DNA. The reverse orientation of insert DNA in pGEM-T was clearly shown by the production of one *MluI* digest product at 4396 bp indicating that the 5'-*MluI* site of the insert DNA was proximal to the downstream *MluI* site of the plasmid. The forward orientation would have potentially separated the two *MluI* sites over a distance of 1486 bp generating two *MluI* digest products at 1486 bp and 2910 bp.

The reverse primer 54RP4 complementary to *fccA54* was used to sequence across the modified junction of the FccA54 overexpression fragment. Interpretation of the automated sequencing result confirmed that fusion PCR had successfully omitted *EcoRI* and replaced this cleavage site with the *fccA54* N-terminal *BamHI* site. The ATG start codon of *fccA54* was shown to map 11 nucleotides from the ribosome-binding site. Therefore, the FccA54 overexpression fragment amplified by fusion PCR contained the desired sequence for FccA54 overexpression. However, upon closer inspection of the sequencing result, a secondary mutation introduced by *Taq* DNA polymerase was identified. A single 5'-adenine base was deleted 6 nucleotides downstream of the *fccA54* ATG start codon causing a frameshift in the *fccA54* gene coding sequence.

Primers 54JF5 and 54JF6 were designed to complement pJF118 plasmid DNA in order to scan the fusion PCR product for secondary mutations upstream of the ribosome-binding site. The FccA54 overexpression fragment was completely sequenced and was found to also contain a single base mutation in the *lac* repressor gene *lacI^Q*. A 5'-guanine base 140 bp downstream of the *lacI^Q* start codon substituted a 5'-adenine base. It was inferred that the mutated sequence led to the conversion of Ile48 to Thr48 in the *lac* repressor protein. Residue 48 was identified in a loop of the repressor protein that projected away from the protein-DNA interface. Therefore, mutation of this residue was not expected to interfere with repressor function and so the single base substitution in the *lacI^Q* gene was not corrected. Sequencing of the fusion PCR construct identified a mutation in pJF118 that was not reported in the literature. The mutation consisted of a 4 bp insertion, 5'-GATG-3', located 32 nucleotides upstream of the remaining *Bam*HI site used in construction of pJF118 (Fürste *et al.*, 1986). Sequencing of the parent pJF118 plasmid was used to validate the inherent nature of the 4 bp mutation that was introduced into the fusion PCR construct.

5.2.6.3 Cloning of the FccA54 overexpression fragment

The sequenced FccA54 overexpression fragment was introduced into plasmid pMB1 to form a modified pJF118 expression plasmid ideally suited to FccA54 overexpression. The FccA54 overexpression fragment was released from pGEM-T plasmid as an *MluI*/*Bgl*III 1396 bp fragment. The recombinant pJF118 plasmid, pMB1 was digested with *MluI* and *Bgl*III to excise the equivalent region that contained the original pJF118 plasmid sequence. The *MluI* and *Bgl*III staggered ends of the FccA54 overexpression fragment were ligated to complementary ends of pMB1 to generate the new recombinant pJF118 expression plasmid. The modified plasmid was transformed into *E. coli* TG1 and positive transformants were selected on the basis of ampicillin resistance. The absence of colonies on the 'cells only' control indicated that the ampicillin resistance was implemented. The absence of colonies on the 'vector only' control indicated a low probability of re-ligated vector for the 100 ampicillin resistant colonies transformed with 'vector and insert' DNA. Three ampicillin resistant colonies were randomly selected and putative recombinant plasmid DNA was isolated for further screening. Recombinant plasmid DNA isolated from the selected colonies was shown to contain the FccA54 overexpression fragment.

An *MluI/BglII* double restriction digest of plasmid DNA released an *MluI/BglII* product corresponding to the 1396 bp *FccA54* overexpression fragment (Figure 5.13). Further restriction digests were performed to ensure that the *fccA54* gene coding sequence was recreated by efficient ligation at the internal *BglII* cleavage site. *BamHI/PstI* double restriction digests of modified plasmid DNA excised a fragment corresponding to the 1455 bp *fccA54 BamHI/PstI* fragment (Figure 5.13). Therefore, the reconstructed recombinant plasmid was shown to contain the complete *fccA54* gene coding sequence. The results generated by restriction digests of plasmid DNA (Figure 5.13) were used to verify formation of a recombinant pJF118 expression plasmid that contained the *fccA54* start codon 11 nucleotides from the ribosome-binding site. This modified expression plasmid containing the *fccA54* 54FMRA *BamHI/PstI* construct was referred to as pMB2 (Figure 5.6).

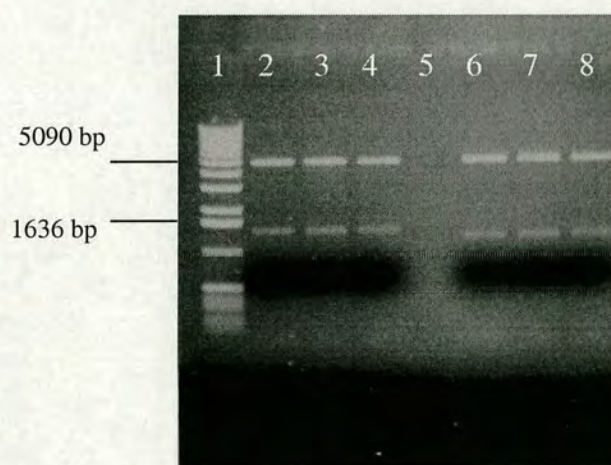


Figure 5.13: Cloning of the *FccA54* overexpression fragment in pMB1

Plasmid DNA isolated from 3 ampicillin resistant colonies was screened for insertion of the *FccA54* overexpression fragment. Double *MluI/BglII* restriction digests of plasmid DNA from colonies 1-3 released a product corresponding to the 1396 bp *FccA54* overexpression fragment (lanes 6-8, respectively). Double *BamHI/PstI* restriction digests were performed to ensure that the *fccA54* gene sequence was recreated upon insertion of the *FccA54* overexpression fragment. The *BamHI/PstI* restriction digests of plasmid DNA from colonies 1-3 released a product corresponding to the 1455 bp *BamHI/PstI fccA54* construct (lanes 2-4, respectively). 1 kb DNA ladder in lane 1 was used to indicate that the restriction fragments analysed by agarose gel electrophoresis were of the correct size.

5.2.6.4 Formation of the FccA54 overexpression plasmid

The modified recombinant plasmid pMB2 contained an *fccA54* mutated coding sequence (Figure 5.6). This mutation was corrected to form a modified recombinant expression plasmid suitable for FccA54 overexpression. The mutated *fccA54* sequence comprising a base pair deletion was removed from pMB2 as a 1455 bp *Bam*HI/*Pst*I fragment. The remaining *Bam*HI and *Pst*I sticky ends of pMB2 plasmid DNA were ligated to complementary ends of a correctly amplified *fccA54* sequence derived from pMB1. The recombinant modified plasmid containing the correct sequence of *fccA54* was transformed into *E. coli* TG1 and positive transformants were selected for ampicillin resistance. A successful transformation was indicated by the absence of colonies on the ‘cells only’ control and the ‘vector only’ control. A lawn of ampicillin resistant colonies was produced from cells transformed with ‘vector and insert’ DNA. Plasmid DNA was prepared from two ampicillin resistant colonies and *Bam*HI/*Pst*I double restriction digests were used to confirm *fccA54* insertion. A 1455 bp product corresponding to *fccA54* was released from plasmid DNA upon digestion with *Bam*HI and *Pst*I (Figure 5.14). Therefore, the accurate *fccA54* sequence was inserted in the modified pJF118 expression plasmid. This recombinant plasmid prepared for FccA54 overexpression was named pMB3 (Figure 5.6).

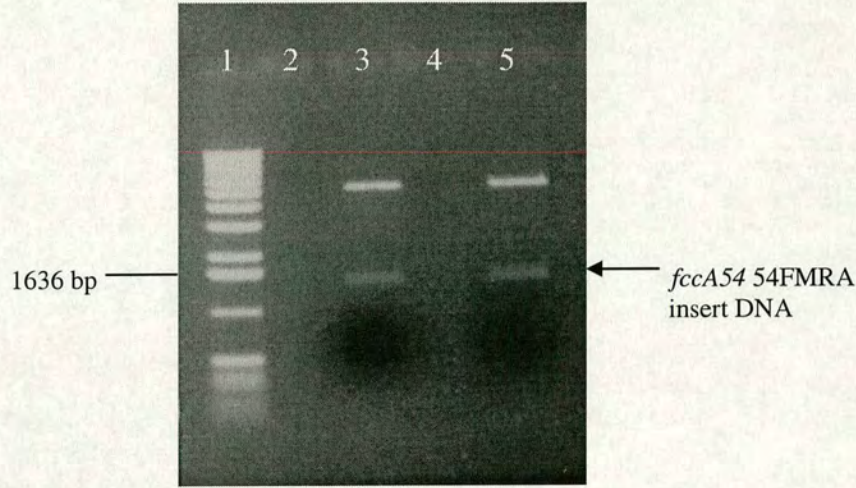


Figure 5.14: Correction of the *fccA54* mutated sequence in pMB2

The correct sequence of *fccA54* was transferred as a 1455 bp *Bam*HI/*Pst*I fragment from pMB1 to pMB2. Two ampicillin resistant colonies were selected and putative recombinant plasmid DNA was isolated. Double *Bam*HI/*Pst*I restriction digests were performed to show insertion of the correct *fccA54* 54FMRA *Bam*HI/*Pst*I fragment in pMB2 to form pMB3. A 1455 bp fragment corresponding to *fccA54* was released from plasmid DNA isolated from colonies 1 and 2, as shown by agarose gel electrophoresis (lanes 3 and 5, respectively). 1 kb DNA ladder shown in lane 1 indicated that the digested products were of the correct size.

5.2.7 Cytoplasmic overexpression of FccA54 in *E. coli* TG1

The recombinant pMB3 plasmid transformed in *E. coli* TG1 was induced with IPTG to obtain high levels of FccA54 overexpressed protein. A time course experiment was used to identify the optimal duration of induction for FccA54 overexpression in *E. coli* TG1. Recombinant *E. coli* TG1 containing pMB3 was induced with IPTG and grown for a period of 2 hours, 4 hours and 16 hours. A sample was also extracted immediately after IPTG induction and was referred to as '0 hours'. Control cultures of non-recombinant *E. coli* TG1 and uninduced recombinant *E. coli* TG1 were grown in parallel and the results were analysed by SDS-PAGE (Figure 5.15).

An overexpressed protein was identified for recombinant *E. coli* TG1 that was clearly absent in the non-recombinant *E. coli* TG1 control. However, the molecular weight of the overexpressed protein was approximately 45 kDa (Figure 5.15), inconsistent with the predicted mass of the FccA54 holoenzyme at 53,025 Da (52,178 Da for apoenzyme and 847 Da for FAD). Therefore, the overexpressed protein in recombinant *E. coli* TG1 was tentatively linked to FccA54.

To monitor IPTG induction, uninduced recombinant *E. coli* TG1 controls were included in the time course experiment. The putative FccA54 protein was overexpressed in the uninduced controls, indicating that the flavoprotein was non IPTG-inducible (Figure 5.15). The ineffective regulation of protein overexpression was presumably caused by the *lacI*^Q mutation in pMB3 (5.2.6.2) that severely affected activity of the *lac* repressor protein.

The time course experiment showed maximal overexpression of a non IPTG-inducible protein from recombinant *E. coli* TG1 cultures grown over a period of 16 hours (Figure 5.15).

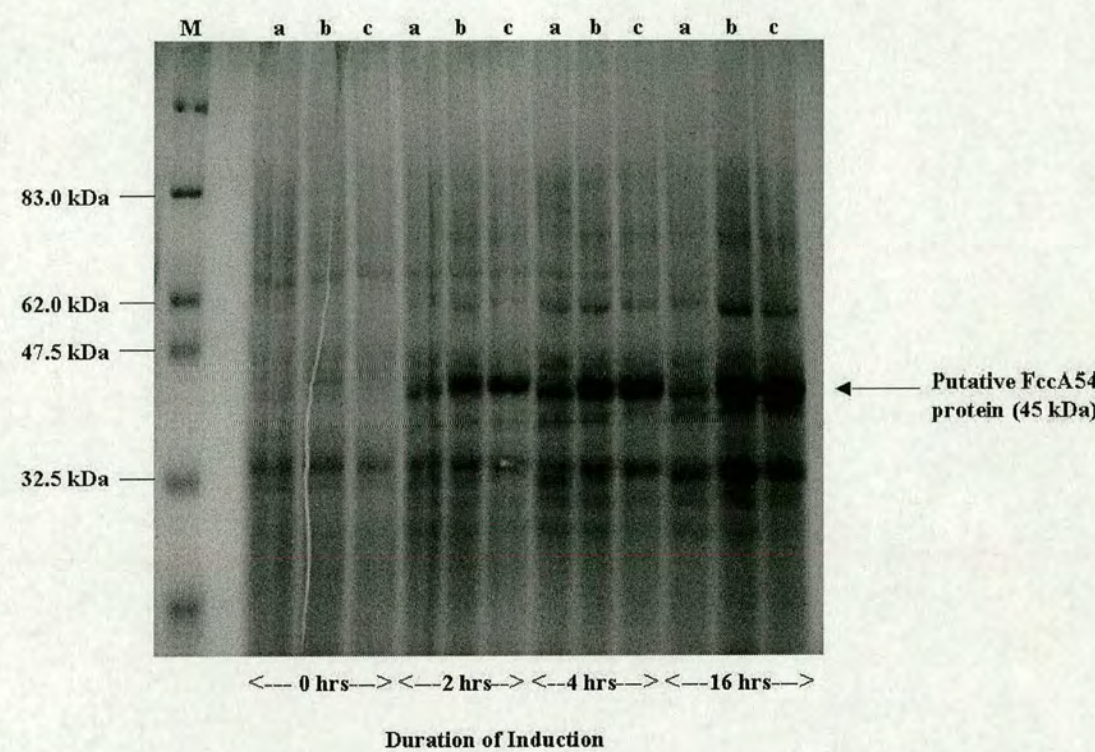


Figure 5.15: Time course of FccA54 overexpression in *E. coli* TG1
A time course experiment was used to identify the optimal duration of IPTG induction for FccA54 overexpression. Recombinant *E. coli* TG1 containing pMB3 was induced with 1 mM IPTG and grown for a period of 0 hours, 2 hours, 4 hours and 16 hours. For each time slot, non-recombinant *E. coli* TG1 (a) and uninduced recombinant *E. coli* TG1 (b) were grown in parallel with IPTG induced recombinant *E. coli* TG1 (c). Samples from each stage were analysed by SDS-PAGE. A high yield of putative overexpressed FccA54 protein was produced when recombinant *E. coli* TG1 cells were grown for 16 hours. Molecular weight marker (M) was loaded in lane 1 to accurately determine the size of the putative overexpressed FccA54 protein.

Recombinant *E. coli* TG1 samples induced with IPTG and grown for 16 hours were analysed using a 4-12 % precast SDS-PAGE gel (Figure 5.16). The migration of the putative overexpressed FccA54 protein corresponded to a 49 kDa protein, closer to the expected size of FccA54 at 53, 025 Da. The observed size discrepancy of the putative overexpressed FccA54 protein was therefore consistent with a migration anomaly on SDS-PAGE. This strongly suggested that the overexpressed protein from *E. coli* TG1 did correspond to the FccA54 flavoprotein. Furthermore, the overexpressed protein was detected in samples of cell free extract, confirming the expected soluble nature of the FccA54 flavoprotein.

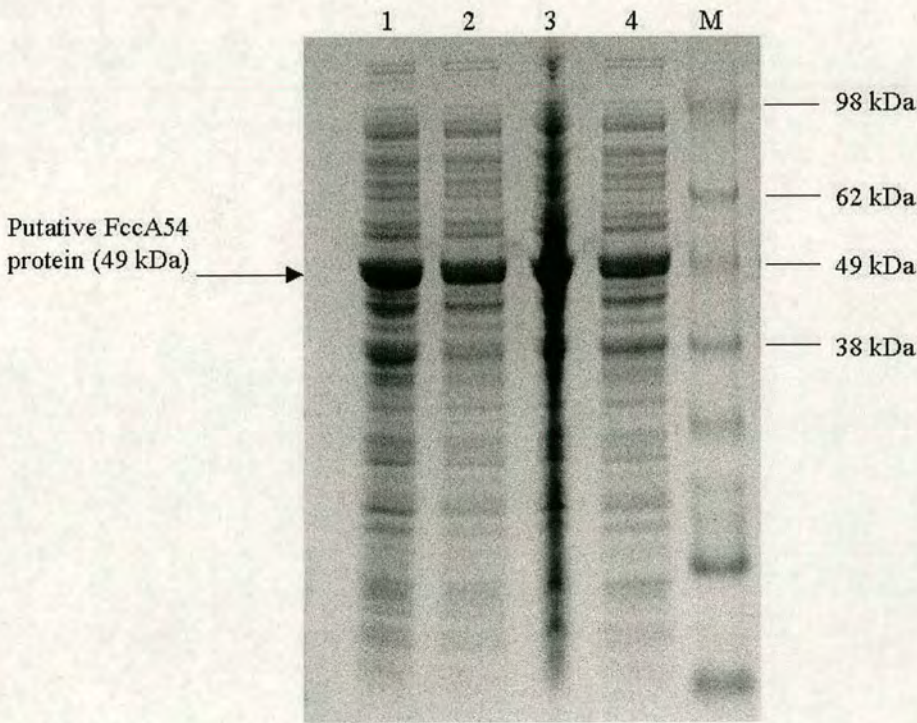


Figure 5.16: FccA54 flavoprotein is located in the soluble cell fraction

The putative overexpressed FccA54 protein appears to have a migration anomaly on SDS-PAGE. The protein migrated to approximately 49 kDa on a precast SDS-PAGE gel, closer to the predicted molecular weight of 53 kDa. Whole cell fractions of recombinant *E. coli* TG1, resuspended in 10 mM CAPS buffer, pH 10.5 and 10 mM Tris buffer, pH 7.5 are shown in lanes 1 and 3, respectively, of the 4-12 % agarose gel. FccA54 was also detected in the soluble cell fraction of recombinant *E. coli* TG1. Cell free extract isolated from recombinant *E. coli* TG1, resuspended in 10 mM CAPS buffer, pH 10.5 and 10 mM Tris buffer, pH 7.5 is shown in lanes 2 and 4, respectively, of the precast gel. Molecular weight marker (M) was used to indicate the approximate size of overexpressed FccA54 protein.

To ascertain that the 49 kDa overexpressed protein was FccA54 that displayed a migration anomaly on SDS-PAGE; the molecular mass of the protein was determined by electrospray mass spectrometry. The cell free extract of recombinant *E. coli* TG1 in 10 mM Tris buffer pH 7.5 (Figure 5.16) was used as the sample for determining the total mass of the overexpressed protein. The nominal molecular mass of FccA54 was determined using mass spectrometry to be 52550.0 Da, close to the predicted mass of 53,025 Da (52,178 Da for apoenzyme and 847 Da for FAD; Figure 5.17). This result provided substantial evidence that the overexpressed protein analysed by SDS-PAGE was indeed FccA54.

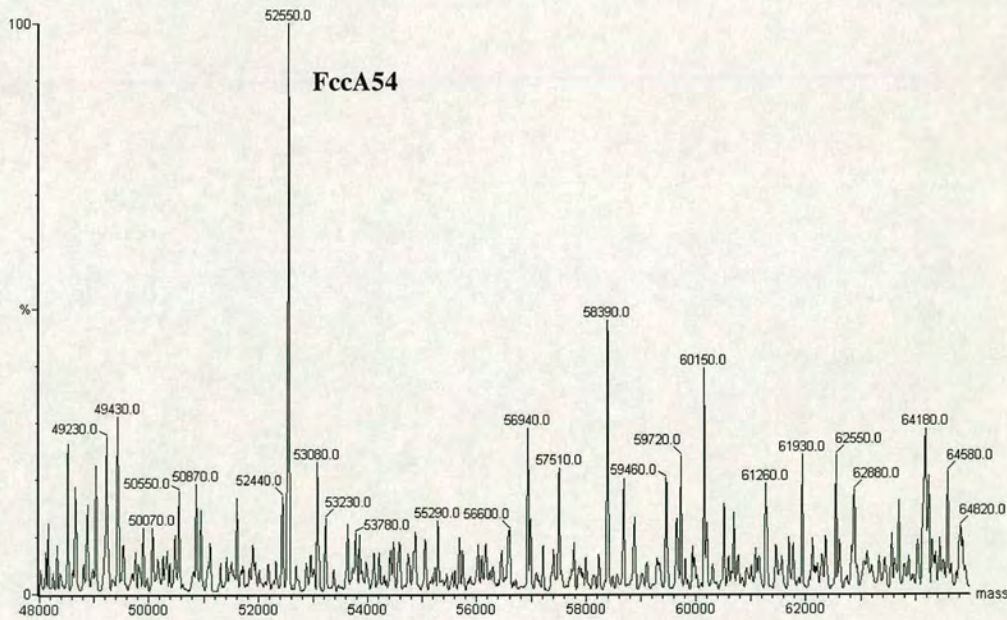


Figure 5.17: Mass spectrometry of FccA54
The molecular mass of FccA54 was determined to be 52550.0 Da using positive electrospray ionisation.

5.2.8 FccA54 protein purification

The recombinant *E. coli* TG1 growth conditions that produced high yields of overexpressed FccA54 were used to obtain purified FccA54 flavoprotein. The FccA54 protein with an estimated isoelectric point (pI) of 8.34 (<http://www.expasy.org/tools/protparam.html>) was purified using a Q Sepharose anion exchanger equilibrated with 10 mM Tris buffer at pH 8.0. The FccA54 protein was purified from the soluble fraction of recombinant *E. coli* TG1 cells resuspended in 10 mM Tris buffer at pH 8.0. A NaCl salt gradient was used to elute protein bound to the strong anion-exchange column.

Column fractions A1-C1 contained protein that did not bind to the positively charged matrix of the column. This was consistent with the slightly positive charge of the FccA54 protein at pH 8.0. Column fractions C2-H8 contained protein with a net negative charge that bound to the column and were eluted during the NaCl gradient. The concentration of proteins in the individual fractions was measured by UV absorption at 280 nm (Figure 5.18a and 5.18b). The yellow fractions indicative of flavin-containing proteins were selected for further analyses using 4-12 % precast SDS-PAGE gels. Purified FccA54 that did not bind to the column at pH 8.0 was produced in fractions A12 to B4. The quantity of purified FccA54 protein in these eluted fractions was lower compared to column fractions C10 and C11 (Figures 5.19a and 5.19b). The fractions C10 and C11 contained purified FccA54 protein that bound to the column and was eluted during the NaCl gradient at approximately 15 % NaCl. A high concentration of FccA54 suitable for crystallisation was obtained from fractions C10 and C11 (Figures 5.19a and 5.19b).

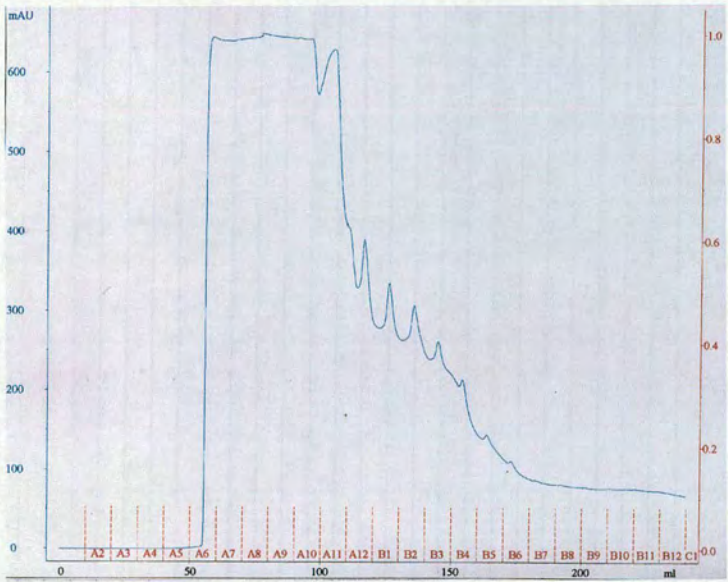


Figure 5.18a: UV absorption spectra of FccA54 column fractions
The blue line represents the UV-visible absorption spectra for fractions eluted from the Q Sepharose column before the NaCl gradient. The fraction numbers are shown in red. Yellow fractions A11, A12 and B1-B5 were analysed using SDS-PAGE.

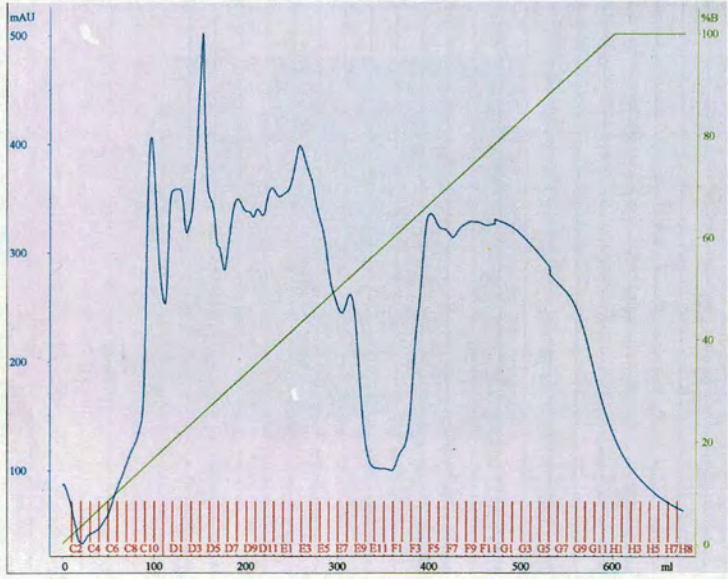


Figure 5.18b: UV absorption spectra of FccA54 column fractions
The UV-visible absorption spectra (blue line) for fractions collected during the NaCl salt gradient (green line) is shown. '% B' represents the concentration of 10 mM Tris buffer pH 8.0 containing 1M NaCl. Yellow fractions C9, C10-C12 and D1-D4 were analysed using SDS-PAGE.

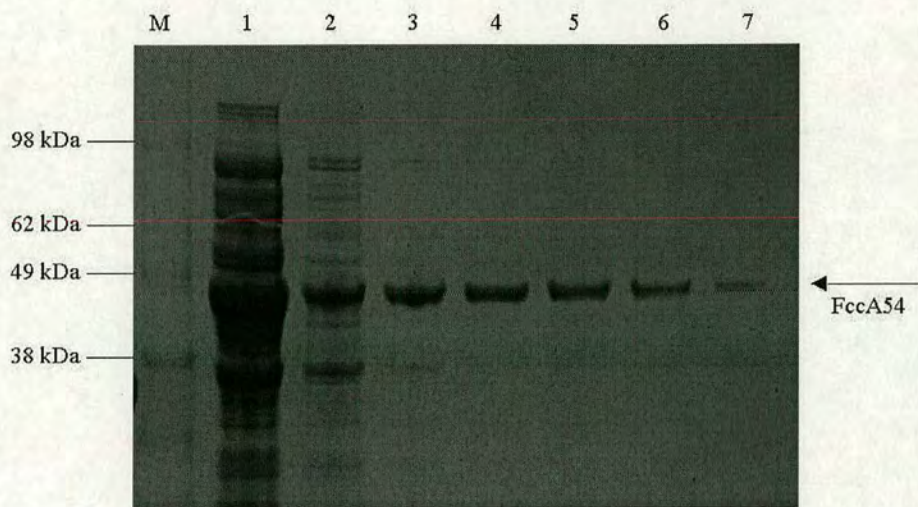


Figure 5.19a: FccA54 protein purification

FccA54 was purified from the soluble cell free extract of recombinant *E. coli* TG1 using a Q Sepharose column at pH 8.0. Fractions A11, A12 and B1-B4 collected from the flow through of the column were analysed by SDS-PAGE (lanes 2-7, respectively). Purified FccA54 was apparent in fractions B1-B4. A sample of cell free extract was loaded in lane 1 of the SDS-PAGE gel to indicate the overexpressed FccA54 protein. A standard molecular marker (M) was also used to determine the size of the purified protein.

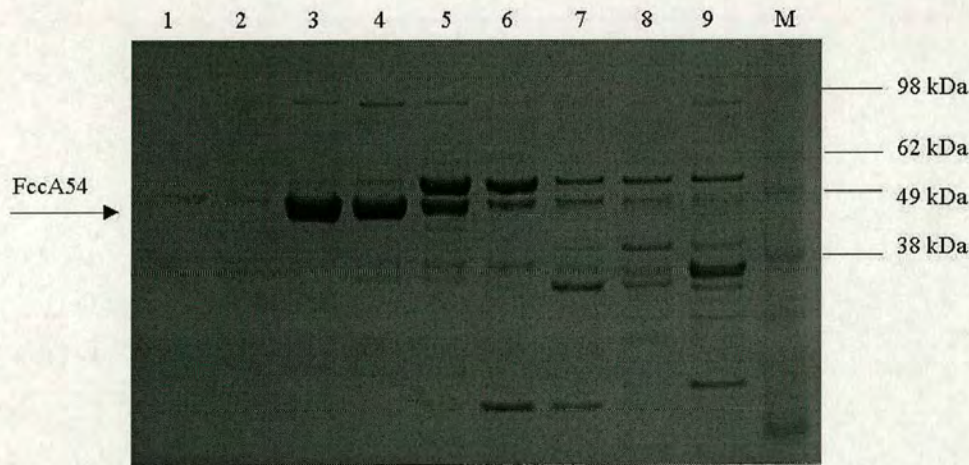


Figure 5.19b: FccA54 protein purification

Protein from fractions C9 to D4 bound to the positively charged column and was eluted during the NaCl gradient. Fraction B5 was eluted before the gradient. A high yield of pure FccA54 protein was produced in fraction C10 and C11 (lanes 3 and 4) as shown by SDS-PAGE. Purified FccA54 protein was also apparent for samples B5 and C9 (lanes 1 and 2) at a lower concentration. Fractions C12 to D4 (lanes 5-9) did not contain pure FccA54. Molecular weight marker (M) was used to indicate the size of the proteins collected in the column fractions.

Flavin spectra were measured for the purified FccA54 fractions and were characteristic of flavin bound to protein (Figure 5.20; Munro and Noble, 1999).

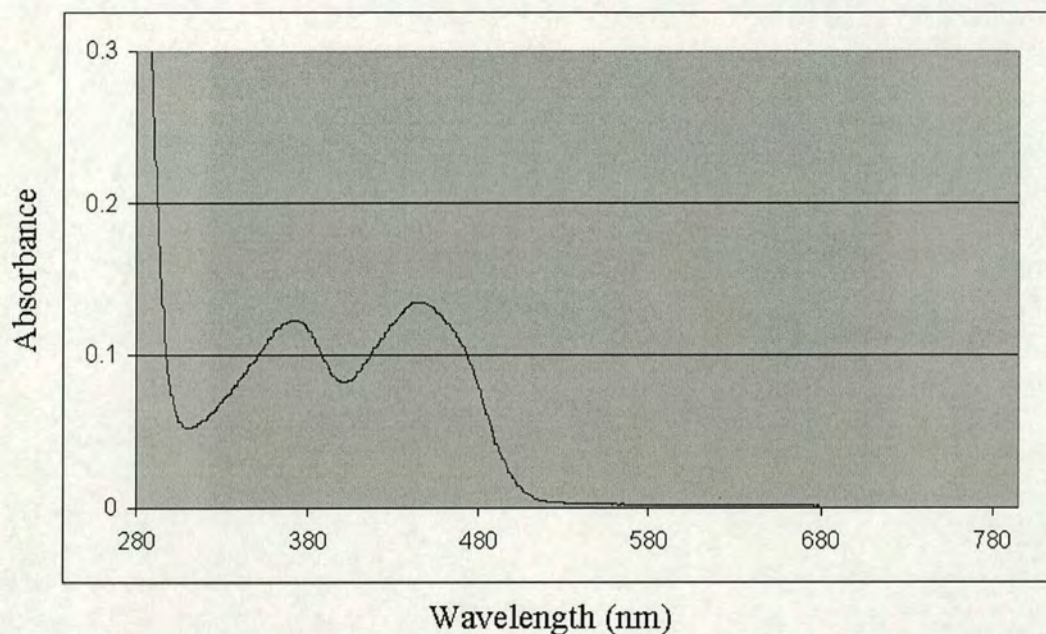


Figure 5.20: UV/visible absorbance spectrum of the purified FccA54 flavoprotein

The purified protein showed two absorption maxima characteristic of flavins.

5.2.9 Characterisation of the FccA54 flavoprotein

N-terminal sequencing was used to provide conclusive evidence that the purified 52.6 kDa protein was FccA54. The purified FccA54 protein indicated in Figures 5.19a and 5.19b was sequenced using Edman degradation of an FccA54 Western blot sample. The first five N-terminal residues were identified to be Thr, Glu, Xaa, Ala and Ser that correlated with FccA54 sequence information from TIGR (<http://www.tigr.org>). The residue that remained unidentified by N-terminal sequencing was cysteine. The first five N-terminal residues correspond to the beginning of the FccA54 mature protein sequence encoded by the *fccA54* 54FMRA PCR product with removal of the initiating methionine residue.

The FccA54 flavoprotein was tested for fumarate reductase activity and succinate oxidation activity. Samples for the enzyme assays were obtained from partially purified FccA54 fractions eluted from a Q Sepharose column at pH 7.5. The FccA54 protein was the most intense protein in the samples tested. The enzyme assays did not reveal any activity for fumarate reduction or succinate oxidation by FccA54. The fractions were yellow, indicative of flavin and were tested for enzyme activity shortly after elution from the purification column. Therefore, the lack of FccA54 enzyme activity was unlikely due to loss of flavin. The FccB54 partner cytochrome subunit is perhaps required to deliver electrons from reduced methyl viologen to the flavin cofactor of FccA54. Over a short duration, the non-covalently bound FAD dissociated from the FccA54 flavin subunit, suggesting that the FccB54 cytochrome subunit acts to cap the FccA54 FAD binding site, forming a stable heterodimer.

5.3 CONCLUSION

In this project an expression plasmid was constructed based upon pJF118 to optimise FccA54 overexpression levels. Fusion PCR was successfully used to generate an FccA54 overexpression fragment containing the *fccA54* ATG start codon 11 bp from the ribosome-binding site within the required distance for protein overexpression (Wood *et al.*, 1984a). Ideally, the 5'-overhang sequence of primer 54FM used in the original PCR amplification of the *fccA54* mature coding sequence should have incorporated an *EcoRI* site instead of a *BamHI* site. PCR amplification of an *EcoRI/PstI fccA54* product would have eliminated the need for pJF118 plasmid DNA modification. Various primers were designed for PCR amplification of a set of several genes encoding flavoproteins (Chapter 7).

Cleavage sites for restriction enzymes *Bam*HI and *Pst*I were incorporated into the 5'-overhang sequence of each primer pair. A target site for *Eco*RI occurred in the *fccA342* flavoprotein gene sequence. Therefore, the *Eco*RI target site was not incorporated into primers used in PCR amplification of the set of genes that included *fccA54*.

The FccA54 holoenzyme was purified to high purity using a Q Sepharose column at pH 8.0. However, over a short duration, the purified FccA54 fractions were bleached, indicating loss of the FAD cofactor. This strongly suggested that the flavin was non-covalently bound to FccA54 as predicted from sequence alignments. From this observation it was concluded that non-covalently bound flavin was unstable in the absence of an associated cytochrome subunit. From comparison to the flavocytochrome *c*₃ structure (Taylor *et al.*, 1999), it was postulated that the FccB54 cytochrome subunit associates with the FccA54 flavin subunit to cap the FAD binding site. The loss of flavin from purified FccA54 rendered the protein inactive and unsuitable for studying enzyme kinetics.

The FccA54 flavoprotein did not catalyse fumarate reduction, however perhaps this was due to the conditions of the experiment used. To test fumarate reduction of FccA54 it will be necessary to repeat the experiment using Fcc₃ as a positive control for fumarate reduction to ascertain the optimal conditions, including pH and enzyme and substrate concentrations. The inability of the purified FccA54 holoenzyme to catalyse fumarate reduction also suggested that haem groups of the cytochrome subunit were required to transfer electrons from reduced methyl viologen to flavin.

The results generated led to the conjecture that the flavin subunit does not function in *S. oneidensis* MR-1 as a single entity and associates with the cytochrome subunit to function as a flavocytochrome. This is supported by similar evidence generated from studies of the methacrylate reductase flavoprotein from *G. sulfurreducens*. The purified flavoprotein subunit catalysed the reduction of methacrylate with reduced benzyl viologen at a rate of 0.4 U.mg^{-1} . The activity increased with addition of the associated cytochrome *c* to a maximal specific rate of $\sim 50 \text{ U.mg}^{-1}$ indicating that the cytochrome haem groups were necessary for electron transfer from reduced benzyl viologen (Mikoulińska *et al.*, 1999). In comparison to the basal level of methacrylate reduction catalysed by the flavoprotein, there was absolutely no fumarate reduction catalysed by the FccA54 flavoprotein. However, FccA54 was purified in the absence of the associated cytochrome subunit whereas the methacrylate reductase flavoprotein preparation contained residual amounts of cytochrome *c*. The flavoprotein and tetrahaem cytochrome *c* protein are both required for methacrylate reduction (Mikoulińska *et al.*, 1999). Furthermore, overexpression of the Fcc₃ flavin domain in the Fcc₃ deletion strain '*S. frigidimarina* EG301' did not restore the ability of this mutant to respire with fumarate suggesting that both the flavin and cytochrome domains are essential for enzyme catalysis in Fcc₃ (Gordon *et al.*, 1998). From the results presented here it appears probable that the FccA54 flavin and FccB54 cytochrome subunits also associate to form a functional flavocytochrome. To further investigate the nature of this association and identify the native substrate of the flavocytochrome, the FccA54 and FccB54 subunits were co-expressed to form the dimeric flavocytochrome (Chapter 6).

Chapter 6

Overexpression and purification trials of novel *Shewanella oneidensis* MR-1 flavocytochromes

6.1 INTRODUCTION

A single PCR fragment comprising *fccA54* and *fccB54* was amplified to obtain co-expression of the FccA54 flavin subunit and FccB54 cytochrome subunit in the periplasm of *S. frigidimarina* EG301. PCR amplification of the contiguous genes, *fccA342* and *fccB342* as a single PCR product also aimed to achieve periplasmic co-expression of the encoded protein subunits. The intention was to co-express and purify the subunits comprising the putative dimeric flavocytochromes in order to analyse their redox, catalytic and structural properties. Moreover, purification of the flavocytochromes putatively formed by association of distinct flavin and cytochrome subunits aimed to produce stable proteins that contained non-covalently bound FAD. Purification of each flavocytochrome intended to allow the study of enzyme catalysis with electron transfer from methyl viologen to flavin mediated by the cytochrome haem groups.

6.2 RESULTS AND DISCUSSION

6.2.1 Primer design and PCR amplification of *fccAB54*

The *fccA54* and *fccB54* genes are located in the same operon with only 3 bp separating the upstream *fccA54* stop codon from the ATG start codon of *fccB54* (Figure 6.1). In order to co-express the FccA54 and FccB54 subunits, two oligonucleotide primers, denoted 54F and 54RB were designed to initiate PCR amplification of *fccA54* and *fccB54* as a contiguous sequence (Figure 6.1). The *fccB54* gene sequence determined by 'The Institute for Genomic Research' (TIGR; <http://www.tigr.org>) was interpreted to encode a hydrophobic N-terminal signal sequence characteristic of proteins targeted to the periplasm by the Sec-dependent pathway (von Heijne and Abrahmsén, 1989). Therefore, to allow co-expression of the flavin and cytochrome subunits in the periplasm, PCR amplification was designed to include the N-terminal sequence of *fccA54* that encodes the predicted Tat (*twin arginine translocation*) signal peptide required for targeting preproteins to the periplasm (Berks, 1996). The 5'-end of the 54F forward primer was designed to complement the *fccA54* ATG start codon to initiate amplification of the FccA54 preprotein encoding sequence (Figure 6.1). The 54F primer sequence corresponding to *fccA54* was 17 nucleotides in length to ensure specific annealing of primer and template DNA during PCR amplification. The 5'-end of the 54RB reverse primer sequence precisely mapped to the TAA stop codon of *fccB54* encoding the FccB54 cytochrome subunit. The 54RB primer was 20 nucleotides in length to promote specific binding to *fccB54* template DNA.

The nucleotide sequences of the 54F and 54RB primers were checked for the absence of complementary sequence at the 3'-end and adjusted in length to possess similar melting temperatures to promote specific PCR amplification. The 54F and 54RB primers were engineered to contain 5'-overhang restriction endonuclease sites to facilitate direct cloning of the *fccAB54* PCR product. A *Bam*HI cleavage site (5'-GGATCC-3') was introduced into the 5'-overhang sequence of primer 54F and a *Pst*I cleavage site (5'-CTGCAG-3') was inserted in primer 54RB (Figure 6.1). The restriction enzymes *Bam*HI and *Pst*I were selected to facilitate cloning of the *fccAB54* PCR product due to the absence of target sites within *fccA54* and *fccB54*. In addition, unique target sites for *Bam*HI and *Pst*I occur in the expression plasmid pMMB503EH (Overbye Michel *et al.*, 1995; Figure 5.5), selected for co-expression of FccA54 and FccB54. A triplet of nucleotides was positioned upstream of the engineered cleavage sites to enable restriction enzyme digestion. The manipulation of template DNA sequence led to PCR amplification of *fccA54* and *fccB54* as a contiguous 1914 bp *Bam*HI/*Pst*I *fccAB54* '54FRB' fragment (Figure 6.1).

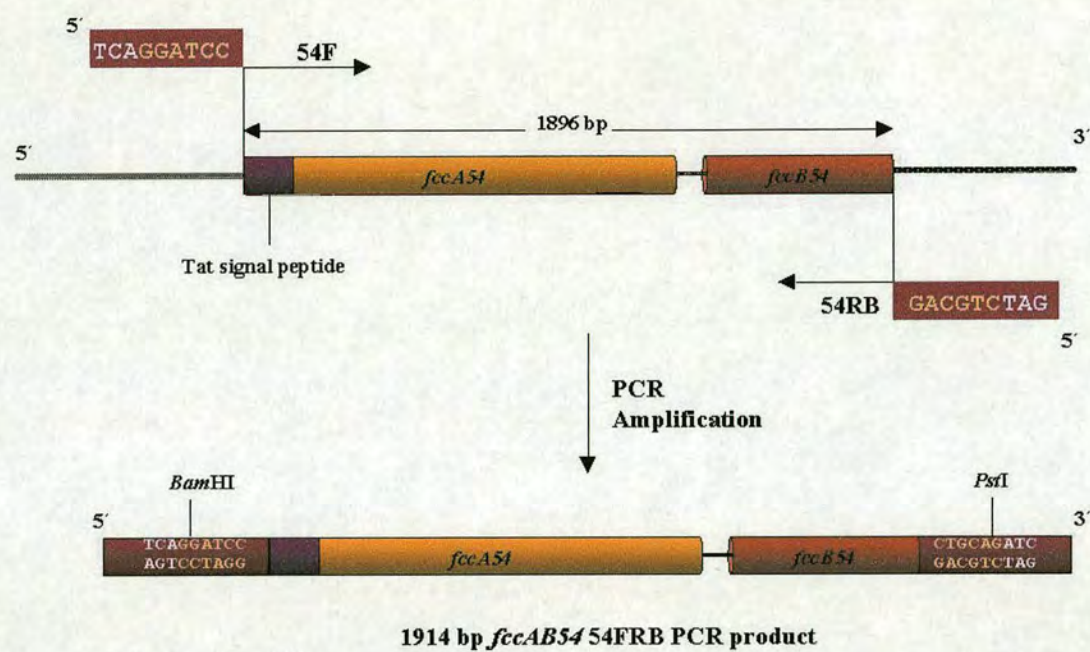


Figure 6.1: A schematic diagram of the *fccAB54* PCR amplification
The *fccA54* and *fccB54* contiguous genes were amplified as a single PCR fragment from the *Shewanella oneidensis* MR-1 genome. Arrows indicate the forward ‘54F’ and reverse ‘54RB’ primer positions and the direction of PCR amplification. The 54F primer was specifically designed to include amplification of sequence encoding the Tat signal peptide. The red-boxed sequences represent the 5'-overhang primer sequences containing the restriction enzyme cleavage sites for *Bam*HI and *Pst*I. The final 1914 bp *Bam*HI/*Pst*I *fccAB54* 54FRB PCR product is shown. The diagram is not to scale.

The *fccAB54* continuous sequence was successfully PCR amplified from the *S. oneidensis* MR-1 genome using primers 54F and 54RB. A PCR product correlating to the expected size of the 1914 bp *Bam*HI/*Pst*I *fccAB54* 54FRB fragment (Figure 6.1) was observed using agarose gel electrophoresis (Figure 6.2). A PCR product was specifically amplified for each of the six reactions that differed in the DNA: primer ratio and the addition of NH_4Cl to reactions 2, 4 and 6. The greatest yield of PCR product at approximately 0.05-0.06 μg DNA was produced for reactions 1-4 that contained a lower concentration of DNA template compared to reactions 5 and 6. The product yield was further improved with addition of NH_4Cl to reactions 2 and 4 (Figure 6.2).

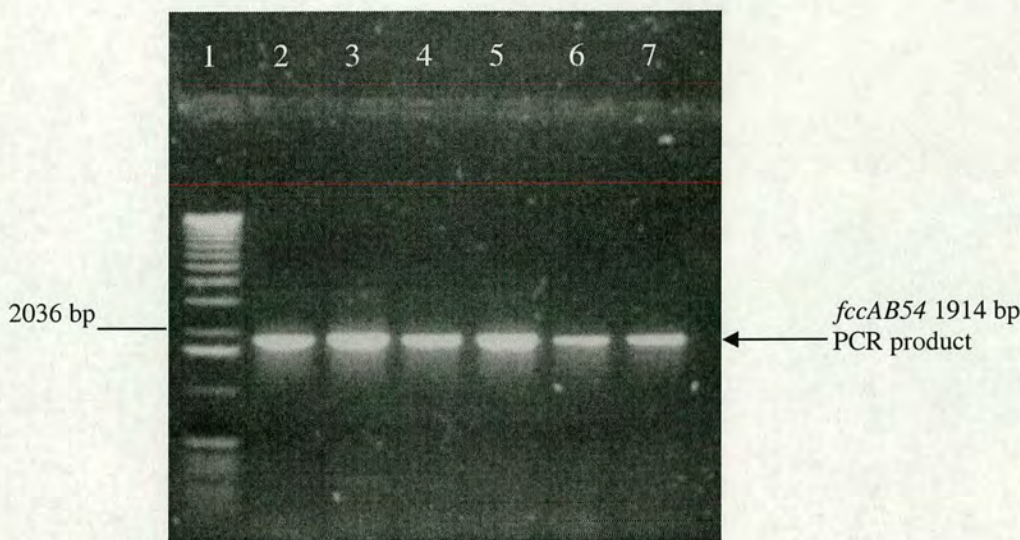


Figure 6.2: PCR amplification of the *fccAB54* 54FRB fragment

Primers 54F and 54RB successfully PCR amplified the *fccAB54* 54FRB fragment from the *S. oneidensis* MR-1 genome. The PCR results for reactions 1 to 6 (lanes 2-7, respectively) were analysed using agarose gel electrophoresis that revealed a product corresponding to the 1914 bp *Bam*HI/*Pst*I fragment. The quantity of PCR product was significantly greater for reactions 1-4 that contained a lower concentration of DNA template compared to reactions 5 and 6. The addition of NH_4Cl to reactions 2 (2 mM) and 4 (4 mM) improved the yield of the *fccAB54* 54FRB PCR product. 1 kb DNA ladder (lane 1) was used to indicate the size of the PCR products.

6.2.2 Cloning of the *fccAB54* 54FRB PCR product in pGEM-T

The *fccAB54* 54FRB 1914 bp PCR product was transferred into the pGEM-T cloning plasmid (Figure 5.3) to achieve multiple copies of the product. In addition, recombinant pGEM-T plasmid was constructed to provide a suitable template for sequencing the *fccAB54* 54FRB PCR product for potential errors incorporated by *Taq* DNA polymerase. The *fccAB54* 54FRB PCR product was inserted in pGEM-T using the 3'-adenine base overhangs (5.2.2). This insertion intended to interrupt the *lacZ* gene to impede β -galactosidase activity detected by blue/white colony screening (5.2.2).

Six white ampicillin resistant transformants, referred to as 2-1 to 2-6 were selected and further screened for recombinant pGEM-T plasmid. Two of the six selected colonies, named 2-1 and 2-5 were identified using restriction enzyme digests to contain recombinant pGEM-T plasmid carrying the *fccAB54* *Bam*HI/*Pst*I fragment. The *fccAB54* 54FRB PCR product was released as a 1914 bp restriction fragment upon double digestion with *Bam*HI and *Pst*I, as detected by agarose gel electrophoresis. Recombinant pGEM-T plasmid named pMB2-1 contained the *fccAB54* 54FRB sequence that was used to construct an FccA54 and FccB54 co-expression plasmid.

6.2.3 Sequencing of the *fccAB54* 54FRB PCR product in pMB2-1

The *fccAB54* 54FRB PCR product of plasmid pMB2-1 was sequenced for mutations introduced during PCR amplification catalysed by the low fidelity *Taq* DNA polymerase. Primers 54RP1, 54RP2, 54RP3 and 54RP4 were designed to complement the *fccAB54* sequence to provide overlapping sequencing information. The results generated from automated sequencing of pMB2-1 single-stranded DNA revealed six point mutations in the *fccAB54* 54FRB PCR product. The six mutations were randomly positioned in the *fccAB54* 54FRB 1914 bp PCR product. A silent point mutation that retained an Aspartate codon (GAC → GAT) was identified 426 bp downstream of the *fccA54* ATG start codon. This mutation was not corrected. The other five point mutations, consisting of transitions and transversions, altered the amino acid sequence composition of the encoded protein. One of these point mutations occurred in the *fccB54* gene and the other four mutations were intermittently dispersed in the *fccA54* gene, downstream of the silent mutation.

A correctly PCR amplified *fccAB54* '54FMRB' sequence from plasmid pMB4-11 (7.2.2 and 7.2.3) was used to correct the mutated *fccAB54* 54FRB sequence cloned in pMB2-1. The variant *fccAB54* sequence of pMB4-11 was amplified using primers 54FM and 54RB that precluded amplification of the N-terminal sequence encoding the Tat signal peptide of the FccA54 flavin subunit (7.2.2). The automated sequencing result generated for *fccAB54* of pMB4-11 matched the correct sequences of *fccA54* and *fccB54* (<http://www.tigr.org>) except for one silent point mutation located 12 bp downstream of the *fccB54* ATG start codon (7.2.4).

The region of mutated *fccAB54* 54FRB DNA sequence spanning 800 bp was removed from pMB2-1 as an *AvaI*/*Bsu36I* 1293 bp fragment. The pMB2-1 *fccAB54* 54FRB sequence was repaired by ligation to correctly amplified *fccAB54* 54FMRB sequence cut from pMB4-11 as a 1293 bp *AvaI*/*Bsu36I* fragment. The restriction enzymes, *AvaI* and *Bsu36I* were selected to mobilise the *fccAB54* DNA due to the location of unique cleavage sites flanking the mutated region in pMB2-1. Furthermore, *AvaI* and *Bsu36I* restriction enzymes do not cut in pGEM-T therefore the enzymes specifically spliced the mutated region of cloned *fccAB54* DNA. Recombinant pGEM-T plasmid containing the correct sequence of *fccAB54* 54FRB was transformed into *E. coli* TG1 and positive transformants were selected for ampicillin resistance encoded on the pGEM-T plasmid. No colonies were apparent on the 'cells only' control indicating that the antibiotic selection was implemented. A lawn of ampicillin resistant transformants was produced and two colonies were selected for further analysis.

Double *Bam*HI/*Pst*I restriction digests were used to verify repair of *fccAB54* 54FRB in pMB2-1. A *Bam*HI/*Pst*I restriction fragment corresponding to the size of *fccAB54* 54FRB was excised from restored pMB2-1 plasmids isolated from both selected colonies (Figure 6.3). The recombinant pGEM-T plasmid containing the correctly amplified *fccAB54* 54FRB sequence was named pMB2-1-4 (Figure 6.5). Sequencing of the regenerated *fccAB54* 54FRB sequence in pMB2-1-4 was used to provide absolute confirmation that the correct sequence of *fccAB54* 54FRB was indeed obtained.

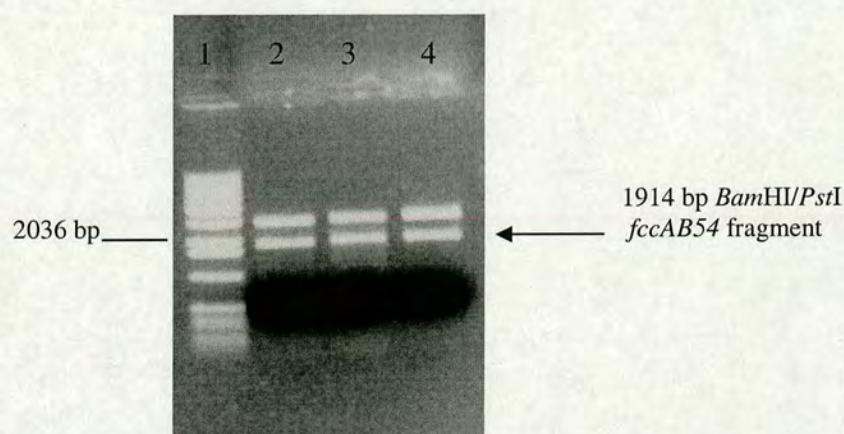


Figure 6.3: Correction of the mutated *fccAB54* 54FRB DNA sequence

The mutated *fccAB54* 54FRB DNA sequence in pMB2-1 was excised as a 1293 bp *Ava*I/*Bsu*36I fragment and replaced with the correct *Ava*I/*Bsu*36I *fccAB54* sequence from pMB4-11. The correct *fccAB54* 54FRB sequence was generated in pMB2-1 to form recombinant plasmid named pMB2-1-4, isolated from two ampicillin resistant colonies. *Bam*HI/*Pst*I double restriction digests were used to verify formation of the correct *fccAB54* 54FRB sequence in pMB2-1-4. The results of the digests were analysed using agarose gel electrophoresis and clearly showed excision of a restriction fragment corresponding to the 1914 bp *fccAB54* 54FRB fragment (lanes 2 and 3). A *Bam*HI/*Pst*I restriction digest of pMB2-1 (lane 4) was used as a control to indicate the restriction fragment from pMB2-1-4 corresponded to *fccAB54*. 1 kb DNA ladder (lane 1) was also used to indicate the restriction fragments were of the expected size.

6.2.4 FccA54 and FccB54 co-expression in *S. frigidimarina* EG301

The aim was to co-express FccA54 and FccB54 in the Fcc₃ deletion strain of *Shewanella frigidimarina* designated EG301. This host strain was selected for overexpression and purification of the predicted 66,636 Da FccA54 (53,025 Da) and FccB54 (13,611 Da) heterodimer due to the absence of Fcc₃ at 64 kDa that might have obscured detection of the desired protein. The overexpression and purification strategy was based upon the assumption that the putative interactions between FccA54 and FccB54 would remain stable during purification.

The strategy designed to obtain FccA54 and FccB54 periplasmic co-expression involved insertion of the *fccAB54* 54FRB PCR product in the pMMB503EH expression plasmid. This plasmid is a broad host range plasmid that is suited to protein overexpression in *Shewanella* species (Overbye Michel *et al.*, 1995; Figure 5.5). However, insertion of the *fccAB54* 54FRB *Bam*HI/*Pst*I fragment in pMMB503EH would have unsuitably positioned the ATG start codon 32 bp from the plasmid-borne ribosome-binding site. Therefore, to initialise maximal levels of FccA54 and FccB54 co-expression using pMMB503EH, the pMMB503EH plasmid was modified to contain the N-terminal *fccAB54* *Bam*HI site 5 bp from the plasmid ribosome-binding site. This modification concomitantly positioned the *fccA54* ATG start codon 11 bp from the ribosome-binding site. It was identified that the sequence upstream of the ribosome-binding site that comprises the *lacI*^Q gene of pMMB503EH was exactly the same as that of the *E. coli* expression plasmid pJF118 (Fürste *et al.*, 1986; Figure 5.6).

Therefore, the process of constructing a modified pMMB503EH plasmid involved excising the modified segment from pMB3 (Figure 5.6) that contained a *Bam*HI site 5 bp from the ribosome-binding site and transferring this sequence to pMMB503EH. It was noted that the plasmid DNA transfer to pMMB503EH would introduce the *lacI*^Q mutation of pMB3 (5.2.6.2) that appeared to render the FccA54 protein non-IPTG inducible (5.2.7).

6.2.5 Insertion of the *fccAB54* 54FRB PCR product in pMB3

The *fccAB54* 54FRB PCR product from pMB2-1-4 was transferred into the modified pJF118 plasmid pMB3 to form an *fccAB54* overexpression fragment for transfer to pMMB503EH (Figure 6.5). The *fccAB54* 54FRB PCR product was excised from pMB2-1-4 as a *Bam*HI/*Pst*I 1914 bp restriction fragment and ligated to complementary sticky ends of pMB3. The recombinant plasmid was transferred into *E. coli* TG1 and positive transformants were selected using ampicillin resistance. Four ampicillin resistant colonies were selected for further screening using double *Bam*HI/*Pst*I digests to verify transformation with recombinant plasmid. A *Bam*HI/*Pst*I 1914 bp *fccAB54* restriction fragment was generated upon digestion of recombinant plasmid named pMB4 (Figure 6.4). Therefore, the pMB4 expression plasmid was identified to contain the *fccAB54* overexpression fragment comprising the N-terminal *fccAB54* 54FRB *Bam*HI cleavage site 5 bp from the plasmid ribosome-binding site.

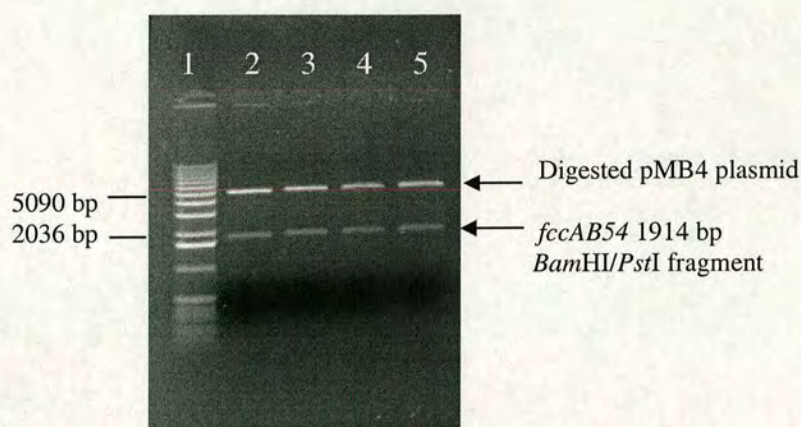


Figure 6.4: Restriction digests to confirm insertion of *fccAB54* in pMB3 to form pMB4

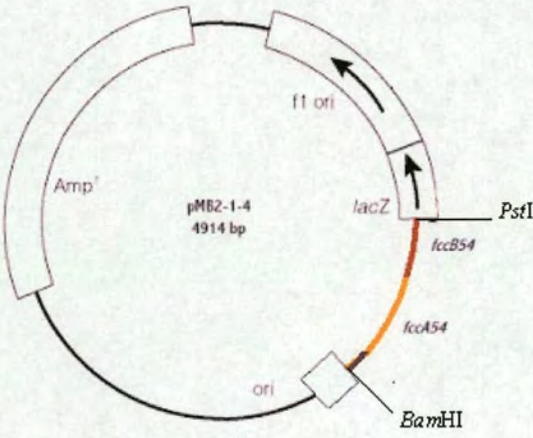
The *fccAB54* PCR product was transferred from pMB2-1-4 to pMB3 as a 1914 bp *Bam*HI/*Pst*I fragment. The recombinant pJF118 plasmid formed was referred to as pMB4 and was isolated from ampicillin resistant colonies 1-4. Recombinant plasmid was identified using double *Bam*HI/*Pst*I restriction digests that released a restriction fragment corresponding to the length of the 1914 bp *fccAB54* 54FRB *Bam*HI/*Pst*I PCR product (lanes 2-5, respectively). 1 kb DNA ladder (lane 1) was used to indicate that the restriction fragments analysed using agarose gel electrophoresis were of the expected size.

6.2.6 Insertion of the *fccAB54* overexpression fragment in pMMB503EH

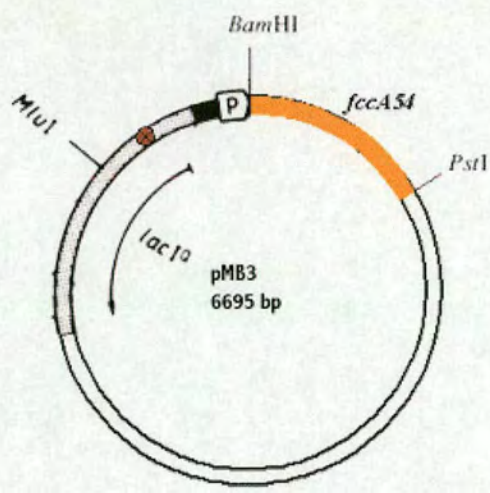
In order to form an ideal pMMB503EH expression plasmid for FccA54 and FccB54 co-expression in *S. frigidimarina* EG301, the *fccAB54* overexpression fragment was transferred from pMB4 to pMMB503EH on a 2650 bp *Mlu*I/*Pst*I fragment. This sequence contained the *lacI*^Q gene and the *fccAB54* 54FRB insert DNA of pMB4 (Figure 6.5). The *fccAB54* overexpression fragment was transferred into the pMMB503EH expression plasmid by ligation of complementary *Mlu*I and *Pst*I sticky ends. This cloning step produced a modified pMMB503EH expression plasmid that contained a *Bam*HI cleavage site adjacent to the ribosome-binding site, ideally suited for cloning and expression of *Bam*HI fragments. The recombinant pMMB503EH expression plasmid was transformed into *E. coli* DH5 α and positive transformants were selected on the basis of streptomycin resistance.

Double *MluI/PstI* restriction digests were used to confirm that the *fccAB54* overexpression fragment was inserted in pMMB503EH. An *MluI/PstI* restriction fragment corresponding to the 2650 bp *fccAB54* overexpression fragment was excised upon digestion of recombinant plasmid named pMB5 (not shown). The suitable expression plasmid pMB5 (Figure 6.5) was transferred from *E. coli* DH5 α to *E. coli* SM10 for subsequent conjugative transfer to *S. frigidimarina* EG301 (Km^R, Rm^R). Positive *S. frigidimarina* EG301 transformants that were kanamycin, rifampicin and streptomycin resistant were selected to test co-expression of FccA54 and FccB54 in the periplasm of the host strain.

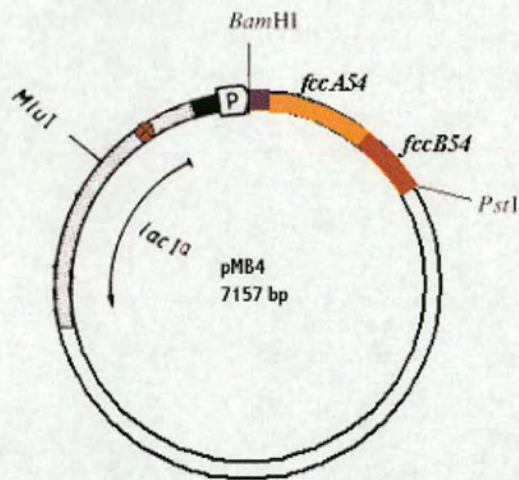
A



B



C



D

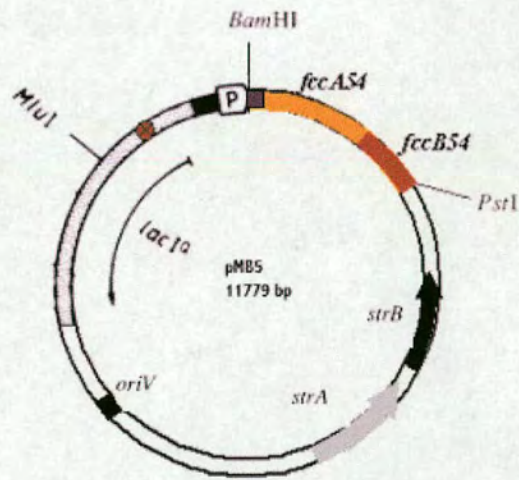


Figure 6.5: Construction of the recombinant pMB5 expression plasmid

The *fccAB54* 54FRB PCR product was excised as a *Bam*HI/*Pst*I 1914 bp fragment from pMB2-1-4 recombinant pGEM-T plasmid (A) and ligated to complementary ends of pMB3 (B) to form plasmid pMB4 (C). The modified plasmid DNA of pMB4 comprising a *Bam*HI site next to the ribosome-binding site and the *fccAB54* PCR product were transferred to pMMB503EH as an *Mlu*I/*Pst*I *fccAB54* overexpression fragment to form pMB5 (D). This modified pMMB503EH plasmid containing *fccAB54* 54FRB was introduced into *S. frigidimarina* EG301 for periplasmic co-expression of the encoded flavin and cytochrome subunits.

6.2.7 Overexpression of FccA54 and FccB54 in *S. frigidimarina* EG301

A time course experiment was performed to identify the optimal induction conditions for co-expression of the FccA54 and FccB54 subunits in *S. frigidimarina* EG301. Recombinant *S. frigidimarina* EG301 containing pMB5 was grown to an OD₆₀₀ of 0.6, induced with isopropylthiogalactoside (IPTG) and grown for 1 hour, 2 hours, 4 hours and 16 hours. Cultures were also extracted for protein analysis at the time of IPTG induction (referred to as 0 hours). Uninduced recombinant *S. frigidimarina* EG301 containing pMB5 was included as a control in the time course experiment to assess the specificity of induction by IPTG. Non-recombinant *S. frigidimarina* EG301 was also included as a control to show that the overexpressed protein was specific to the *Shewanella* strain bearing the pMB5 expression plasmid. The protein content of each sample was analysed using SDS-PAGE that was haem stained to selectively detect cytochrome proteins (Figures 6.6a and 6.6b) and Coomassie stained to reveal all proteins. Following haem staining of the gel, an overexpressed cytochrome protein with an approximate molecular mass of 11 kDa was observed. The absence of the protein in non-recombinant *S. frigidimarina* EG301 indicated that the protein corresponded to the FccB54 tetrahaem cytochrome protein with a predicted molecular mass of 13,611 Da (11,145 Da for apoprotein and 2466 Da for 4 haem groups). The putative overexpressed FccB54 protein was also present in the uninduced samples indicating that the protein was non IPTG-inducible (Figures 6.6a and 6.6b). This was most probably caused by the transfer to pMB5 of a *lacI*^Q mutation in pMB3 (6.2.4) that was postulated to affect the *lac* repressor protein activity (5.2.7). The greatest quantity of the putative FccB54 protein was produced after growth of recombinant *S. frigidimarina* EG301 for 16 hours (Figure 6.6b).

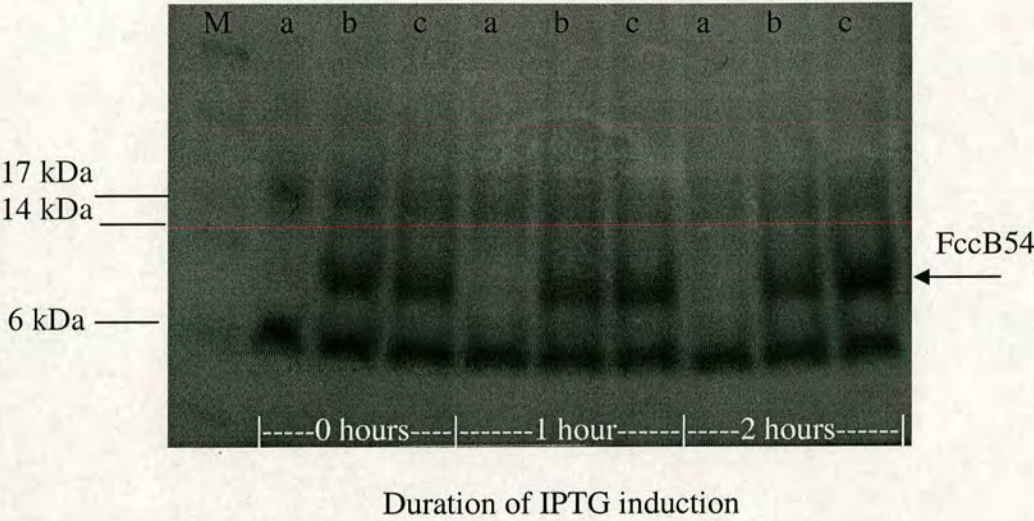


Figure 6.6a: Time course overexpression of FccB54
Recombinant *S. frigidimarina* EG301 containing pMB5 induced with IPTG (c) was grown for a period of 1 hour and 2 hours to monitor the optimal conditions of induction. Samples were also analysed immediately following IPTG induction (0 hours). The results were analysed using SDS-PAGE haem stained to observe cytochrome proteins. An overexpressed protein at 11 kDa, close to the predicted mass of FccB54 (13.6 kDa) was detected (c) that also appeared in the uninduced recombinant *S. frigidimarina* EG301 strain containing pMB5 (b). The overexpressed protein was clearly absent in the non-recombinant *S. frigidimarina* EG301 strain (a). Molecular marker (M) was used to indicate the size of the overexpressed protein.

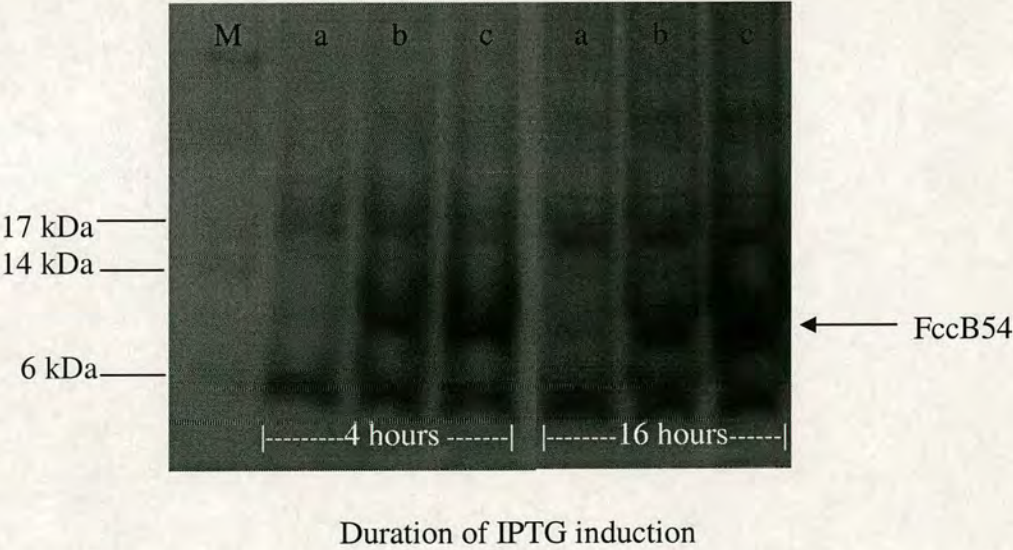


Figure 6.6b: Time course overexpression of FccB54
Recombinant *S. frigidimarina* EG301 containing pMB5 (c) was induced with IPTG and grown for a period of 4 hours and 16 hours. The results were analysed using SDS-PAGE haem stained for the detection of cytochrome proteins. Growth of recombinant *S. frigidimarina* EG301 containing pMB5 over a period of 16 hours produced the highest quantity of the putatively overexpressed FccB54 protein. There was no difference in FccB54 expression when comparing uninduced recombinant *S. frigidimarina* EG301 (b) to induced recombinant *S. frigidimarina* EG301 (c). The overexpressed protein corresponding to the size of FccB54 clearly did not occur in non-recombinant *S. frigidimarina* EG301 (a). Molecular marker (M) was used to indicate the size of the overexpressed protein.

Following haem staining of the SDS-PAGE gel, Coomassie Blue staining was used to observe overexpression of the FccA54 flavoprotein. However, over the time course of IPTG induction, overexpression of the FccA54 flavoprotein at the known molecular mass of 52.6 kDa was not observed. The cloned *fccAB54* 54FRB PCR product of pMB5 was oriented to position the *fccA54* gene closest to the plasmid ribosome-binding site. Therefore, the observed putative overexpression of FccB54 (Figures 6.6a and 6.6b) encoded by the *fccB54* gene cloned distal to the plasmid ribosome-binding site must be coupled to overexpression of FccA54. The inability to detect the overexpressed FccA54 flavoprotein targeted to the periplasm of *S. frigidimarina* EG301 was most probably due to the poor sensitivity of Coomassie staining combined with the vast number of flavoproteins in *S. frigidimarina* EG301. To try and significantly reduce the total number of isolated proteins, the periplasm was extracted from recombinant *S. frigidimarina* EG301 containing pMB5 induced with IPTG for a period of 16 hours. A sample of the periplasmic extract was analysed for FccA54 overexpression using SDS-PAGE stained with Coomassie Blue (Figure 6.7). Two proteins of approximately 50 kDa were evident at the expected position of FccA54 (52.6 kDa) that was previously identified to display a migration anomaly on SDS-PAGE (5.2.7). However, these proteins were also apparent in non-recombinant *S. frigidimarina* EG301 at the same concentration as for recombinant *S. frigidimarina* EG301 induced for protein expression (Figure 6.7). These proteins may correspond to similar proteins of FccA54 found in *S. frigidimarina* EG301. Periplasmic isolation of recombinant *S. frigidimarina* EG301 did not improve detection of FccA54 overexpressed in *S. frigidimarina* EG301 (Figure 6.7).

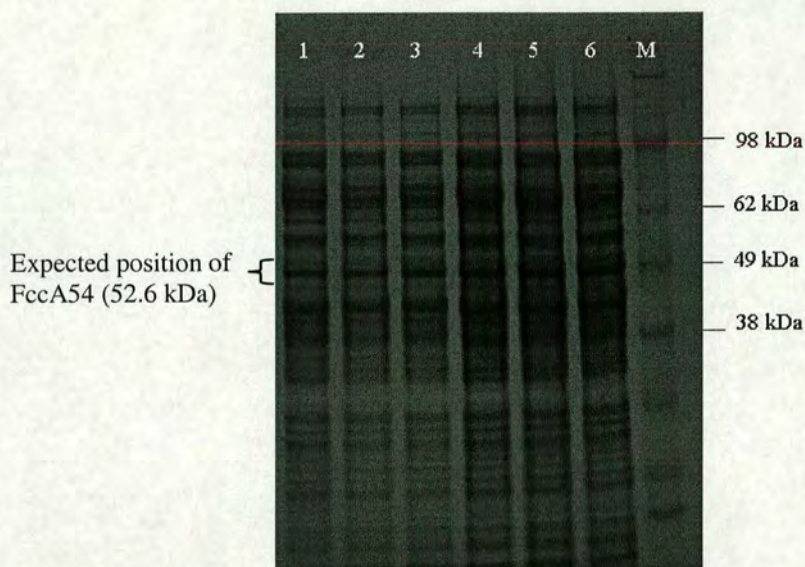


Figure 6.7: Periplasmic extraction to identify FccA54 overexpression

The samples obtained from the periplasm of non-recombinant *S. frigidimarina* EG301 (lanes 1 and 4), uninduced recombinant EG301 containing pMB5 (lanes 2 and 5) and recombinant *S. frigidimarina* EG301 containing pMB5 induced with ITPG (lanes 3 and 6) were analysed using SDS-PAGE Coomassie stained for protein. A higher sample concentration was sequentially loaded in lanes 4-6. Molecular marker (M) was used to indicate the expected position of the FccA54 flavoprotein. The expected position of the FccA54 protein at 52.6 kDa that displays a migration anomaly on SDS-PAGE is shown. The results show that there is no detectable periplasmic overexpression of the flavoprotein.

Following periplasmic extraction, cytochromes targeted to the periplasm of induced recombinant *S. frigidimarina* EG301 containing pMB5 were specifically analysed using SDS-PAGE. Haem staining of the SDS-PAGE gel revealed that the putative overexpressed FccB54 protein was indeed targeted to the periplasm of recombinant *S. frigidimarina* EG301 (Figure 6.8). It was also observed that a small cytochrome of approximately 6 kDa prevalent in *S. frigidimarina* EG301 was less abundant in recombinant *S. frigidimarina* EG301 containing pMB5 (Figure 6.8). This observation led to the hypothesis that gene expression of the unknown ‘Lower protein’ and FccB54 is controlled via a common regulatory pathway. This proposed regulatory mechanism of gene expression is perhaps linked to a shared function of the proteins.

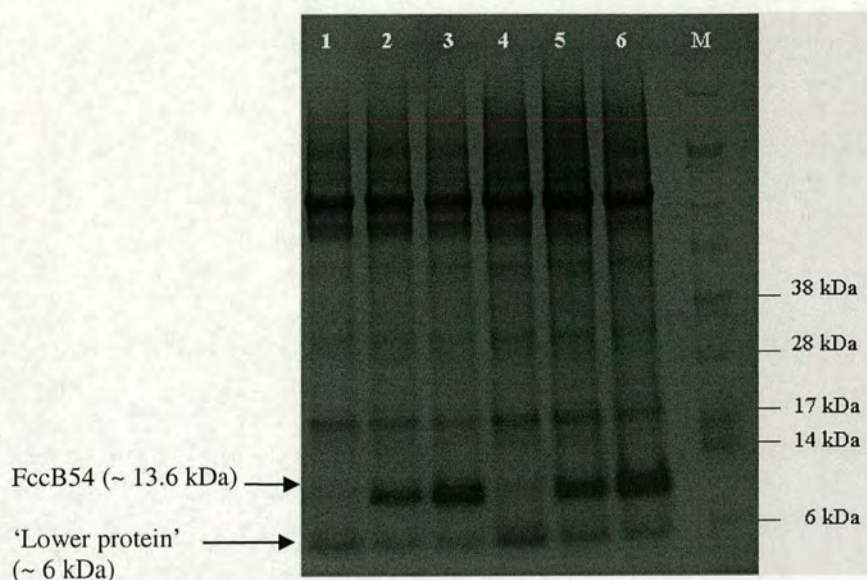


Figure 6.8: Periplasmic extraction to identify FccB54

The samples obtained from the periplasm of *S. frigidimarina* EG301 (lanes 1 and 4), uninduced recombinant *S. frigidimarina* EG301 (lanes 2 and 5) and recombinant *S. frigidimarina* EG301 induced with IPTG (lanes 3 and 6) were analysed using SDS-PAGE haem stained for cytochrome proteins. A higher sample concentration was sequentially loaded in lanes 4-6. Molecular marker (M) was used to indicate the expected position of the FccB54 cytochrome. An arrow indicates the position of overexpressed protein correlating to the predicted size of FccB54 at 13.6 kDa. The 'Lower protein' of *S. frigidimarina* EG301 at approximately 6 kDa (1 and 4) was less abundant in the presence of overexpressed FccB54 (lanes 2-3 and 5-6).

6.2.8 Characterisation of the putative overexpressed FccB54 protein

The molecular mass of the putative overexpressed FccB54 protein was determined using mass spectrometry to be 13.6 kDa (Figure 6.9) that correlated with the predicted mass of FccB54 at 13,611 Da (11,145 Da for apoprotein and 2466 Da for 4 haem groups). The putative FccB54 protein was sequenced using mass spectrometry of an SDS-PAGE gel piece containing FccB54 digested with trypsin. The digested fragments that contained a haem-binding motif were not identified using mass spectrometry. However, a peak corresponding to an FccB54 trypsin fragment (1112.6 Da) comprising the sequence 'Leu79-Ala-Ile-Pro-Glu-Ala-His-Pro-His-Lys88' of the FccB54 preprotein sequence (Figure 1.14) was identified.

The sequencing data therefore provided some evidence that the overexpressed cytochrome protein is FccB54.

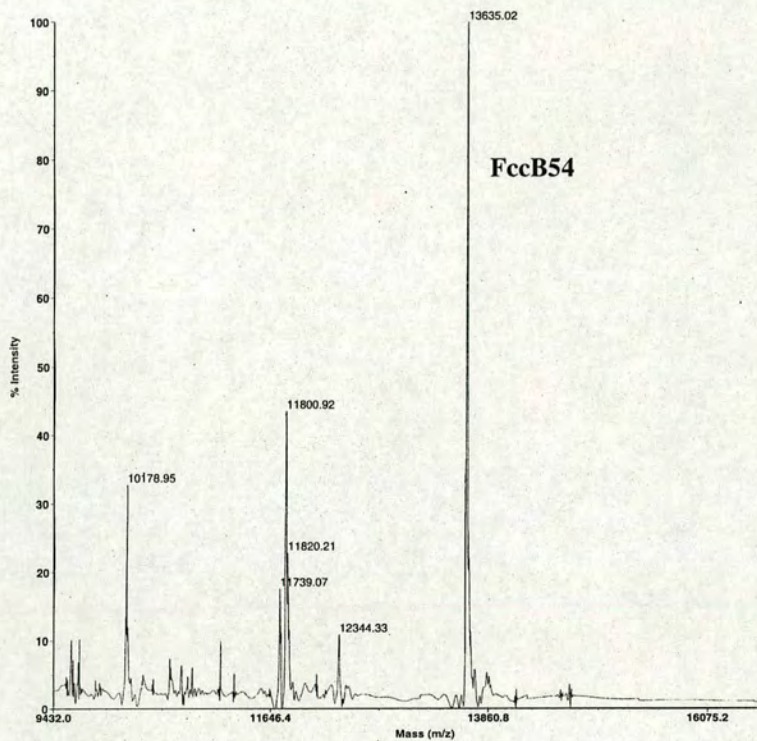


Figure 6.9: Mass spectrometry of FccB54

The total mass of the putative overexpressed FccB54 tetrahaem cytochrome was identified using MALDI mass spectrometry to be 13635.02 Da.

The molecular mass of the 'Lower protein' (Figure 6.8) was identified using mass spectrometry to be 7.4 kDa (Figure 6.10). The unknown *S. frigidimarina* EG301 cytochrome was sequenced using mass spectrometry of an SDS-PAGE gel piece containing the 'lower protein' digested with trypsin. However, no N-terminal sequencing result was obtained.

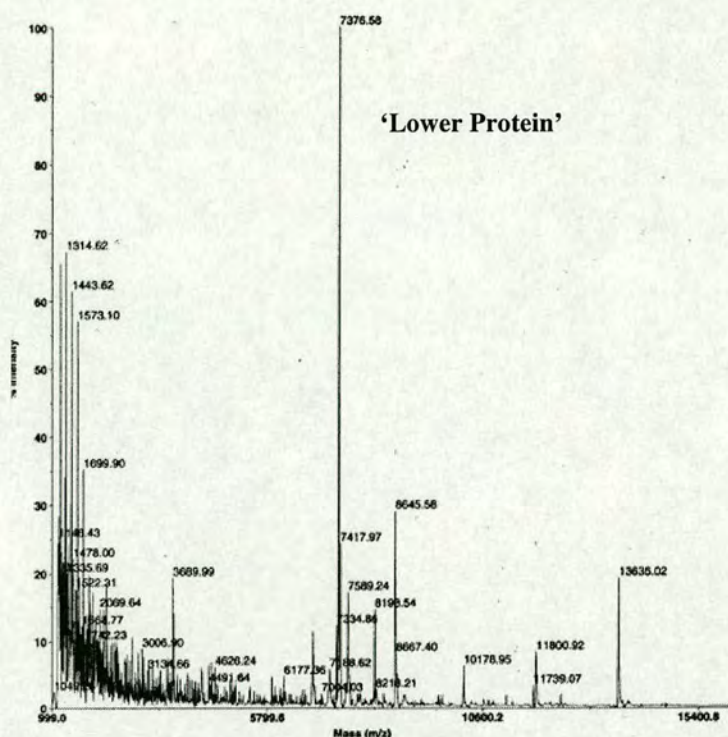


Figure 6.10: Mass spectrometry of the 'lower protein'

The total molecular mass of the unknown *S. frigidimarina* EG301 'lower protein' was identified using MALDI mass spectrometry to be 7.4 kDa.

6.2.9 Purification trials of the FccA54 and FccB54 subunits

Overexpression of the FccA54 flavin subunit in *S. frigidimarina* EG301 remained undetected during analysis of the time course experiment, nevertheless, subsequent purification steps were undertaken to achieve co-purification of the FccA54 and FccB54 subunits. A large-scale culture of recombinant *S. frigidimarina* EG301 containing pMB5 was grown to an OD_{600} of 0.6 and induced with 1 mM IPTG for the optimal duration of 16 hours. The induced cells were subsequently harvested and the soluble fraction was isolated to ensure that the purification sample did indeed contain soluble FccA54 and FccB54. A cell free extract sample and whole cell sample were both analysed using an SDS-PAGE gel haem stained to identify the FccB54 cytochrome protein.

The majority of the FccB54 cytochrome was isolated in the soluble cell fraction (Figure 6.11) therefore isolation of this fraction was used as the first step during purification. Isolation of the periplasm did not appear to significantly reduce the total number of proteins; therefore this additional step was omitted from the purification strategy. Coomassie staining of the SDS-PAGE gel did not reveal the presence of FccA54, however, the presence of the flavoprotein subunit in the soluble cell fraction was previously identified during overexpression and purification of the FccA54 subunit from *E. coli* TG1 (5.2.7). Therefore, it was assumed that the FccA54 flavoprotein subunit putatively associated with FccB54 was also present in the soluble fraction of the purification sample.

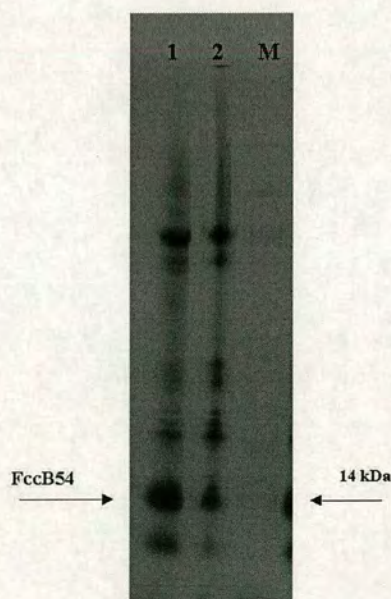


Figure 6.11: Isolation of FccB54 from the soluble cell fraction

The cell free extract (lane 1) and whole cell sample (lane 2) of recombinant *S. frigidimarina* EG301 containing pMB5 were analysed using SDS-PAGE haem stained to identify the FccB54 cytochrome. As anticipated, the FccB54 subunit was identified in the soluble fraction of the purification sample.

The flavocytochrome formed by association of FccA54 and FccB54 was estimated to have a neutral isoelectric point (pI) of 7.28, calculated from a contiguous sequence of FccA54 and FccB54 (<http://www.expasy.org/tools/protparam.html>). Ion exchange columns of the BioCAD system were used to ascertain the optimal conditions for purification of the flavocytochrome heterodimer. Initially, an HQ anion exchanger equilibrated with 10 mM Tris buffer at pH 8.4 was used to provide a positively charged matrix for binding of the net negatively charged heterodimer. The soluble fraction of recombinant *S. frigidimarina* EG301 adjusted to pH 8.4 was applied to the purification column and proteins that adsorbed to the column were eluted during a NaCl gradient. A UV-visible spectrum was measured as a means of determining the concentration of proteins collected in the column fractions.

The fractions that displayed a high UV absorbance at 280 nm were analysed using SDS-PAGE that was haem stained to observe cytochrome proteins and silver stained to identify all proteins. As an alternative method to Coomassie staining, a highly sensitive silver staining technique was used to try and detect FccA54. Protein separation of the FccA54 and FccB54 subunits from other *S. frigidimarina* EG301 proteins was not achieved using the anion exchanger at pH 8.4. Extremely low levels of the FccB54 cytochrome protein were recovered from the purification column and many other lower molecular weight cytochrome proteins were also present. Due to the presence of many other *S. frigidimarina* EG301 proteins at approximately 50 kDa, the FccA54 flavoprotein remained unidentified.

Therefore, to further investigate the conditions required for purification of the putative heterodimer, an HS cation exchanger was tested. The column was equilibrated to pH 7.0 to produce a system in which the FccA54 and FccB54 protein complex was slightly positive (pH 7.28) relative to the column resin. Therefore, it was predicted that the protein complex would adsorb to the column matrix and elute during a NaCl salt gradient. The soluble cell fraction of recombinant *S. frigidimarina* EG301 containing the putative FccA54 and FccB54 heterodimer was applied to the cation exchanger at pH 7.0. A UV-visible spectrum was used to monitor the concentration of proteins that were collected in the individual column fractions. Fractions 12-14 displayed a high UV absorbance at 280 nm indicative of containing protein. These colourless fractions were eluted at a salt concentration of 0.5 M NaCl (Figure 6.12).

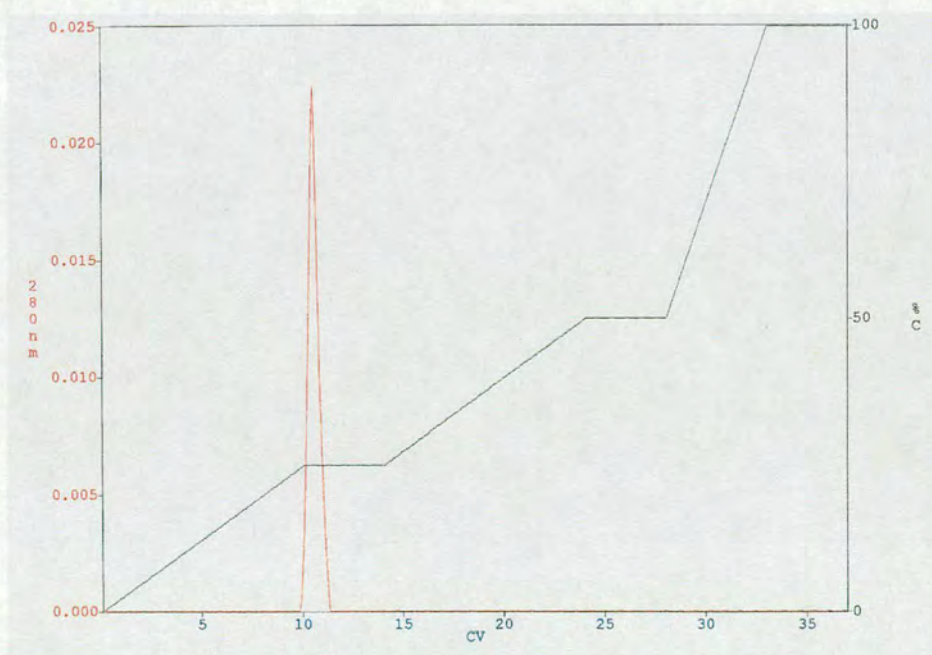


Figure 6.12: A chromatogram of the HS cation exchanger fractions

Fractions 12-14 collected from the HS cation exchanger displayed a UV absorbance peak at 280 nm indicative of containing protein (red). The proteins in these fractions were eluted at a salt concentration of 0.5 M NaCl (green).

The three fractions were analysed using SDS-PAGE that was haem stained to identify FccB54 and subsequently silver stained to identify FccA54. A protein corresponding to the size of FccB54 was the most concentrated cytochrome protein collected in each of the fractions. The other cytochromes present in each of the fractions consisted of high molecular weight proteins. Therefore, purification using the cation exchanger was particularly successful in separating the FccB54 protein from other low molecular weight cytochromes (Figure 6.13).

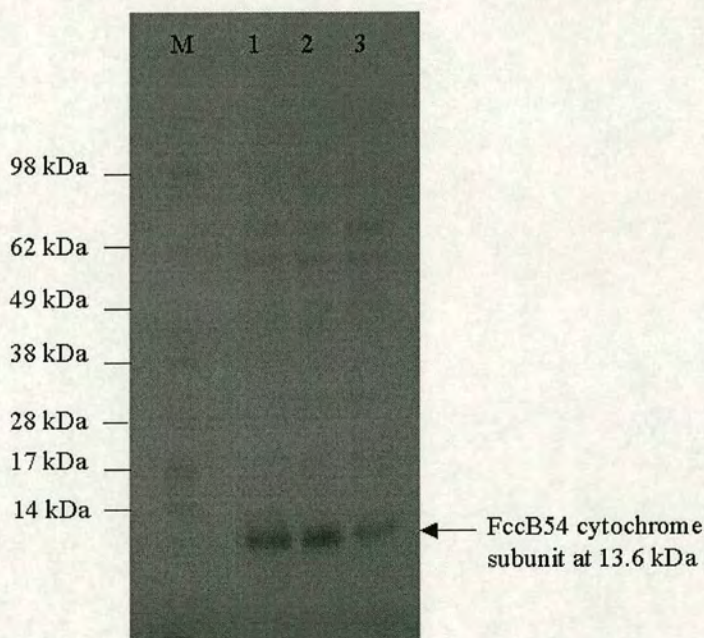


Figure 6.13: Haem staining analysis of fractions collected from the HS cation exchanger

The fractions collected from the HS cation exchanger were analysed using SDS-PAGE haem stained to identify the FccB54 protein. A putative FccB54 protein was identified in fractions 12-14 (lanes 1-3, respectively). Molecular marker was used to identify the size of the proteins collected in the column fractions.

A low separation of all proteins eluted from the cation exchanger was identified upon silver staining of the SDS-PAGE gel. It was therefore not possible to distinguish FccA54 from the many other high molecular weight proteins of approximately 50 kDa (Figure 6.14). A low molecular weight protein putatively corresponding to FccB54 displayed a different migration position (Figure 6.14) compared to the haem stained SDS-PAGE gel (Figure 6.13). The different staining procedures may affect the observed protein migration pattern on SDS-PAGE.

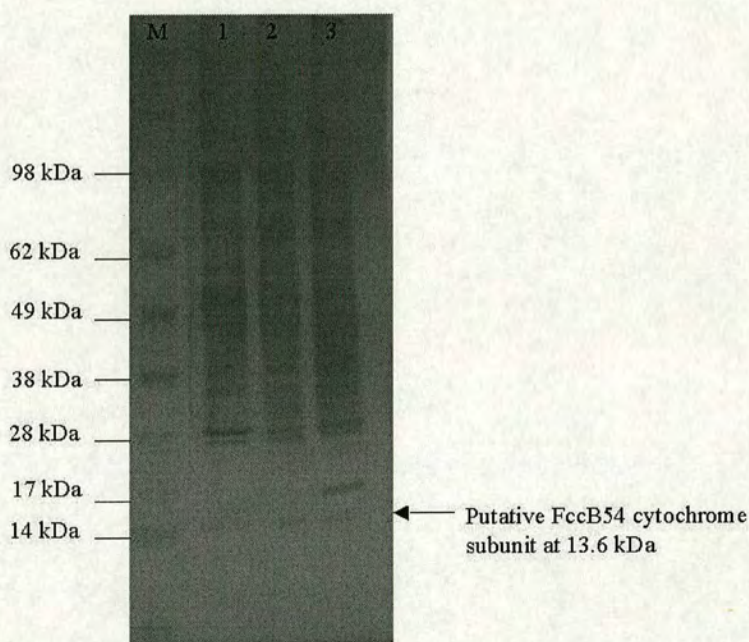


Figure 6.14: Silver staining analysis of fractions collected from the HS cation exchanger

Fractions 12-14 collected from the HS cation exchanger were analysed using SDS-PAGE that was silver stained for total proteins. A putative FccB54 protein was identified (lanes 1-3). A band corresponding to FccA54 flavoprotein was not identified. Molecular marker (M) was used to show the approximate size of the proteins collected from the column.

6.2.10 Overexpression and purification of FccA54 and FccB54

A recombinant plasmid containing the *fccAB54* 54FRB PCR product was constructed for overexpression of the encoded subunits in the periplasm of *S. frigidimarina* EG301. High levels of overexpressed FccB54 protein were identified in the periplasm of the host strain. Conversely, overexpression of the putatively associated FccA54 subunit was not detected when analysed using SDS-PAGE. Nevertheless, purification of the putative heterodimer was attempted by closely monitoring the FccB54 cytochrome subunit, analysed using SDS-PAGE. The purification fractions could be alternatively analysed using a native polyacrylamide gel to test if the FccA54 flavin subunit was associated with FccB54 to form the 66.6 kDa flavocytochrome. Should the subunits be dissociated it would be possible to purify the FccB54 cytochrome subunit and combine this with the purified FccA54 flavin subunit (5.2.8) to form the flavocytochrome. The small-scale purification trials of the flavocytochrome led to identification of possible methods for purification of the FccB54 cytochrome subunit. Purification using an HS cation exchanger gave good separation of FccB54 from other low molecular weight cytochromes present in the sample. Several high molecular weight cytochromes were also present at a low concentration compared to FccB54. Following cation exchange chromatography; the higher molecular weight cytochrome proteins could be separated from FccB54 on the basis of size using a gel filtration column. Further purification trials are required for purification of the putative heterodimer, which may involve exploring various pH conditions, different buffers and cation exchange columns to find the optimal conditions.

6.2.11 Primer design and PCR amplification of *fccAB342*

The *fccA342* and *fccB342* genes of *S. oneidensis* MR-1 are located in the same operon and share a similar gene arrangement to *fccA54* and *fccB54* (Figure 1.11). The *fccA342* gene that encodes a flavoprotein subunit maps 11 bp upstream of *fccB342* encoding a tetrahaem cytochrome *c*. The encoded flavin and cytochrome subunits were hypothesised to associate in the periplasm to form a functional flavocytochrome. In order to achieve co-expression of the individual subunits, PCR amplification was designed to amplify the contiguous *fccA342* and *fccB342* genes of *S. oneidensis* MR-1 as a single PCR product.

Primers were designed to initiate amplification of a PCR product that when cloned would direct periplasmic expression of both the flavoprotein and cytochrome subunits. The forward 342F primer was positioned to include amplification of the *fccA342* Tat-signal peptide coding sequence necessary for targeting the encoded FccA342 preprotein to the periplasm (Figure 6.15). The 5'-end of the 342RB reverse primer sequence was designed to complement the TAG stop codon of *fccB342*. PCR amplification of the contiguous genes therefore included the *fccB342* N-terminal sequence encoding the FccB342 Sec-dependent signal sequence required for targeting to the periplasm. The primer sequences were approximately 20 nucleotides in length to promote specific annealing to the *fccA342* and *fccB342* target genes. The primer pair was also designed to lack complementary sequence at the 3' terminus to prevent primer-dimer formation. The primer sequences did not contain continuous runs of polypurines or polypyrimidines thus avoiding the possible formation of internal secondary structure.

The 5'-end of each primer sequence was modified to contain a restriction endonuclease site to facilitate subsequent cloning of the PCR product. A *Bam*HI cleavage site was incorporated in the 5'-overhang of primer 342F and a *Pst*I cleavage site was inserted in the 5'-overhang of primer 342RB. The primers were designed to initiate PCR amplification of *fccA342* and *fccB342* as a contiguous *Bam*HI/*Pst*I 1864 bp fragment (Figure 6.15).

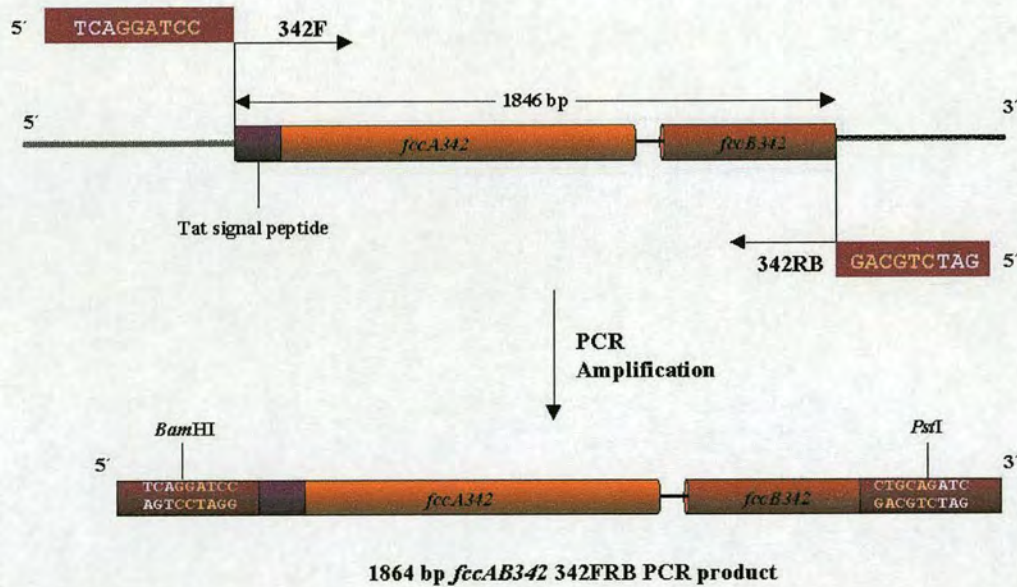


Figure 6.15: PCR amplification of *fccAB342*

PCR amplification was designed to amplify the contiguous *fccA342* and *fccB342* genes as a single PCR fragment. Primer 342F was specifically designed to initiate amplification of the *fccA342* Tat signal peptide coding sequence to direct periplasmic expression of the encoded flavoprotein. The reverse 342RB primer was designed to complement the extreme 3' terminus of the *fccB342* gene. Arrows indicate the primer positions and the direction of PCR amplification. *Bam*HI and *Pst*I cleavage sites were incorporated in 5' overhang sequences of the primers (red-boxed sequences). The final *Bam*HI/*Pst*I *fccAB342* 342FRB PCR amplified product was 1864 bp in length. The diagram is not to scale.

Primers 342F and 342RB successfully initiated PCR amplification of a fragment comprising the *fccA342* and *fccB342* genes from the *S. oneidensis* MR-1 genome. The results of PCR were analysed using agarose gel electrophoresis that showed a PCR product at approximately 0.06 μ g DNA that corresponded to the *fccAB342* 342FRB 1864 bp *Bam*HI/*Pst*I fragment. In addition to the desired fragment, a 700 bp PCR product at approximately 0.02 μ g DNA was PCR amplified, indicative of non-specific PCR amplification (Figure 6.16).

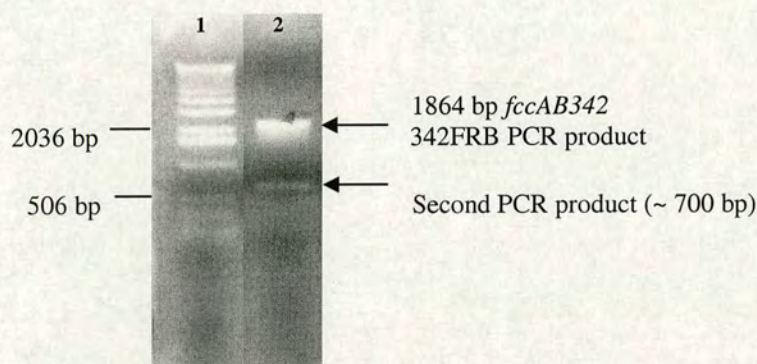


Figure 6.16: PCR amplification of *fccAB342*

Primers 342F and 342RB initiated PCR amplification of the *fccA342* and *fccB342* genes from the *S. oneidensis* MR-1 genome. The results of PCR were analysed using agarose gel electrophoresis that revealed a PCR product correlating to the size of the 1864 bp *Bam*HI/*Pst*I *fccAB342* 342FRB fragment (lane 2). A second PCR product at approximately 700 bp was also PCR amplified due to non-specific priming of the genomic template DNA (lane 2). 1 kb DNA ladder (lane 1) was used to indicate that the PCR products were of the correct size.

6.2.12 Cloning of the *fccAB342* 342FRB PCR product in pGEM-T

The *fccAB342* 342FRB 1864 bp *Bam*HI/*Pst*I fragment was cloned into pGEM-T to obtain multiple copies of the PCR product. The specific PCR product at the correct size of 1864 bp was amplified at a higher concentration than the non-specific PCR product. This suggested that insertion of the desired PCR product in pGEM-T would occur preferentially, preventing the need for purification of the two PCR products. Recombinant pGEM-T plasmid was transformed in *E. coli* TG1 and positive transformants were selected using blue/white colony screening and ampicillin resistance. Sixteen colonies with the required phenotype were selected for further screening to ensure they contained recombinant pGEM-T plasmid containing the correct insert DNA. The isolated plasmid DNA was cut with *Bam*HI and *Pst*I to excise insert DNA cloned as a *Bam*HI/*Pst*I fragment. Only 2 of the 16 colonies were identified to contain the *fccAB342* 342FRB PCR product (Figure 6.17). Six of the colonies contained the non-specific 700 bp PCR product and the remaining colonies contained non-recombinant plasmid. The recombinant pGEM-T plasmid containing the desired *fccAB342* PCR product cloned as a *Bam*HI/*Pst*I 1864 bp fragment was referred to as plasmid pMB6-14 (Figure 6.17).

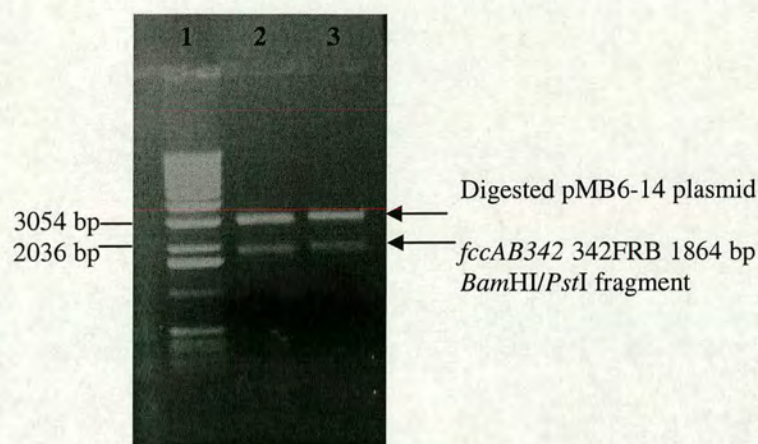


Figure 6.17: Restriction digests to show isolation of recombinant pGEM-T

Recombinant pGEM-T plasmid, named pMB6-14 was isolated from two ampicillin resistant white colonies. Double *Bam*HI/*Pst*I restriction digests were used to reveal excision of the cloned 1864 bp *fccAB342* 342FRB PCR product from pMB6-14, isolated from colonies 1 (lane 2) and 2 (lane 3). 1 kb DNA ladder (lane 1) was used to indicate that the restriction fragments were of the correct size.

6.2.13 Sequencing of the *fccAB342* PCR product in pMB6-14

The *fccAB342* 342FRB PCR product cloned in pMB6-14 was checked for possible sequence errors introduced by the low fidelity *Taq* DNA polymerase. Sequencing primers, 342P1, 342P2, 342P3, 342P4 and 342P5 were designed to complement the *fccAB342* PCR product at intervals of approximately 400 bp to provide overlapping sequencing data. The sequencing results obtained were compared to the known sequences of *fccA342* and *fccB342* (<http://www.tigr.org>). Interpretation of the results showed that the *fccAB342* 342FRB PCR product cloned in pMB6-14 was accurately PCR amplified.

6.2.14 Cloning of the *fccAB342* PCR product in pMB5

The pMB5 expression plasmid comprising the *fccAB54* *Bam*HI/*Pst*I fragment (6.2.6; Figure 6.5) was successfully used to obtain high levels of overexpressed FccB54 (6.2.7). As a modified version of the parent pMMB503EH plasmid, a *Bam*HI site resides 5 bp from the ribosome-binding site of pMB5 (6.2.6). The pMB5 plasmid can be utilized to express inserts cloned as *Bam*HI fragments that contain the start codon 11 bp from the ribosome-binding site. The pMB5 plasmid was therefore selected as a suitable expression plasmid for cloning of the 1864 bp *fccAB342* *Bam*HI/*Pst*I fragment. The aim was to transfer the recombinant expression plasmid into *S. frigidimarina* EG301 to obtain periplasmic co-expression of the FccA342 and FccB342 subunits.

The *fccAB342* correctly amplified PCR product was excised from pMB6-14 as a *Bam*HI/*Pst*I fragment and ligated to complementary ends of the pMB5 expression plasmid to form plasmid pMB6 (Figure 6.18). Recombinant plasmid was transformed into *E. coli* DH5 α and five positive transformants were selected on the basis of streptomycin resistance encoded on the pMMB503EH plasmid. Recombinant pMB6 plasmid DNA isolated from each colony was identified using double *Bam*HI/*Pst*I restriction digests. A *Bam*HI/*Pst*I restriction fragment corresponding to the 1864 bp *fccAB342* PCR product was released upon digestion of recombinant plasmid (not shown). The isolated pMB6 plasmid was identified as a suitable recombinant pMMB503EH expression construct for co-expression of FccA342 and FccB342 in the periplasm of *S. frigidimarina* EG301.

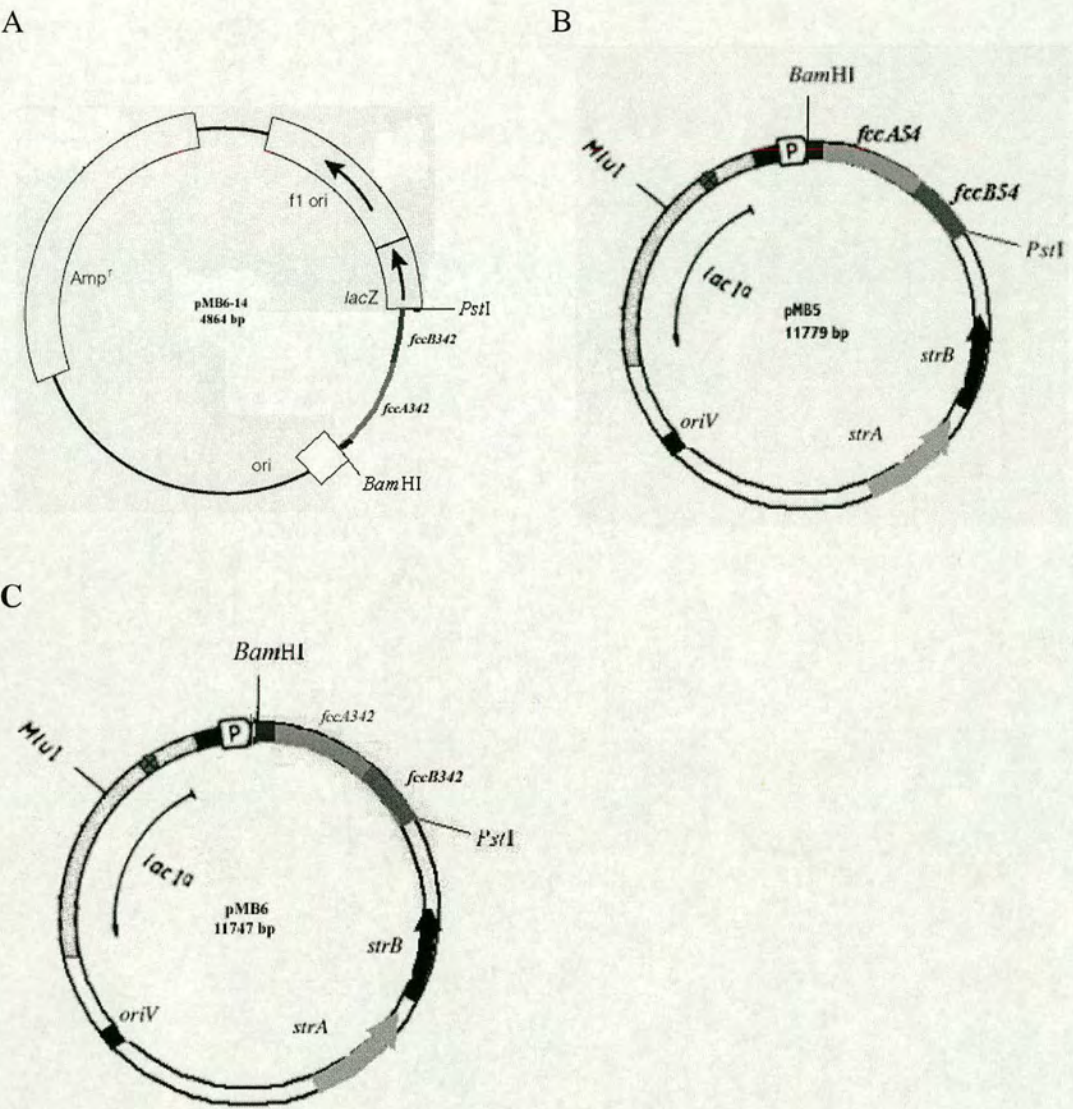


Figure 6.18: Construction of the pMB6 expression plasmid
The *fccAB342* 342FRB PCR product was transferred from pMB6-14 (A) as a *BamHI/PstI* fragment to pMB5 (B), digested with *BamHI* and *PstI*, to form the pMB6 plasmid (C) for overexpression of the FccA342 and FccB342 subunits.

The pMB6 expression plasmid containing the *fccAB342* 342FRB PCR product was transferred from *E. coli* DH5 α to the conjugative *E. coli* SM10 strain. The expression plasmid was subsequently introduced by conjugative transfer to *S. frigidimarina* EG301 (Km^R, Rm^R) for co-expression of the encoded flavin and cytochrome subunits. Positive *S. frigidimarina* EG301 transformants exhibiting kanamycin, rifampicin and streptomycin resistance were selected to test co-expression of FccA342 and FccB342 in the periplasm of the host strain.

6.2.15 Flavocytochrome overexpression in *S. frigidimarina* EG301

A time course induction experiment was used to identify the optimal conditions for overexpression of FccA342 and FccB342 in *S. frigidimarina* EG301. Recombinant *S. frigidimarina* EG301 containing the pMB6 expression plasmid was grown to an OD₆₀₀ of 0.6 and induced with 1 mM of IPTG for 1 hour, 2 hours, 4 hours and 16 hours. Samples were also extracted immediately after IPTG induction. A non-recombinant *S. frigidimarina* EG301 control was included in parallel to show that any overexpressed protein identified in the *S. frigidimarina* EG301 recombinant strain was due to the presence of the pMB6 plasmid. An uninduced recombinant *S. frigidimarina* EG301 control was also included to monitor the regulation of protein expression. The samples were analysed using 4-12 % precast SDS-PAGE gels that were haem stained to specifically observe cytochrome proteins and Coomassie stained to identify all proteins.

Upon haem staining of the SDS-PAGE gels, no overexpressed FccB342 protein at the predicted molecular mass of 13,247 Da (10,781 Da for apoprotein and 2466 Da for 4 haem groups) was observed (Figure 6.19). A protein of approximately 12 kDa was apparent but was not specific to recombinant *S. frigidimarina* EG301 containing pMB6. An increase in the duration of IPTG induction (4 hours and 16 hours) did not produce overexpression of the FccB342 cytochrome (not shown). The putatively associated FccA342 flavoprotein was not observed upon Coomassie staining of the SDS-PAGE gel.

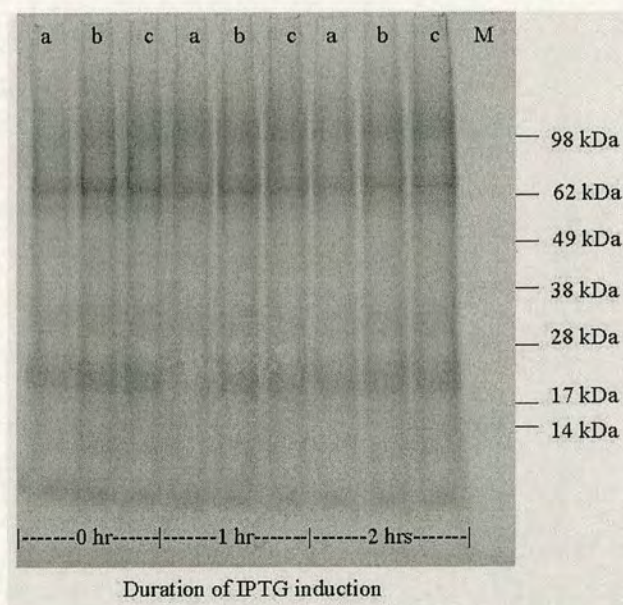


Figure 6.19: Time course overexpression of FccB342

A time course induction experiment was used to identify the optimal duration of IPTG induction for FccA342 and FccB342 co-expression. The results were analysed using SDS-PAGE haem stained to identify FccB342. Recombinant *S. frigidimarina* EG301 containing pMB6 (c) was induced with IPTG and grown for 1 hour and 2 hours. A sample was also extracted immediately following IPTG induction. A recombinant uninduced *S. frigidimarina* EG301 control (b) and non-recombinant *S. frigidimarina* EG301 (a) were included in the time course experiment. No overexpressed protein was identified corresponding to the predicted mass of FccB342 at 13.2 kDa. Molecular marker (M) was used to indicate the size of the isolated proteins.

Overexpression of the FccA342 and FccB342 proteins was not detected during the IPTG induction time course. PCR amplification of *fccA342* and *fccB342* was designed to include sequence encoding the N-terminal signal peptides for targeting to the periplasm. Therefore, the time course induction experiment could be altered to include periplasmic isolation following IPTG induction. This procedure may improve detection of the co-expressed proteins targeted to the periplasm. Other parameters such as IPTG concentration could be changed to analyse the effect on protein overexpression.

Chapter 7

PCR amplification constructs for flavoprotein overexpression

7.1 INTRODUCTION

An optimal overexpression system comprising the host strain, expression plasmid and cellular location of expression was unknown for each of the novel flavoproteins. In order to try different cellular overexpression conditions, four distinct PCR products were amplified for each gene sequence encoding a novel *Shewanella oneidensis* MR-1 flavocytochrome (FccA54:FccB54 and FccA342:FccB342). Primers were designed to specifically amplify the target *fccA* gene with or without the N-terminal Tat (*twin arginine translocation*) signal peptide coding sequence. The two forms of the *fccA* gene sequence were also optionally PCR amplified with the downstream *fccB* gene sequence. The assortment of PCR products was designed to provide expression constructs that would generate periplasmic or cytoplasmic overexpression of the flavoprotein subunit, optionally co-expressed with the partner cytochrome subunit. Therefore, in addition to the PCR constructs that were primarily used for flavoprotein overexpression (Figures 5.1, 6.1 and 6.15), other PCR products were synthesised for each target gene. PCR amplification of the putative iron-induced flavocytochrome named IfcA-1 of *S. oneidensis* MR-1 was also achieved.

7.2 RESULTS AND DISCUSSION

7.2.1 PCR amplification of the *fccA54* preprotein coding sequence

The *fccA54* PCR amplification product encoding mature FccA54 protein that was cloned in pMB3 (Figure 5.6) led to overexpression of FccA54 in the cytoplasm of *E. coli* TG1 (5.2.7). PCR amplification was also designed to amplify an *fccA54* fragment that would confer periplasmic overexpression of the FccA54 flavin subunit (Figure 7.1). The N-terminal Tat signal peptide coding sequence was included in PCR amplification of *fccA54* to target the synthesised protein to the periplasm. The 5'-end of the 17-nucleotide primer '54F' was specifically designed to hybridise at the N-terminal ATG start codon of *fccA54*. To facilitate cloning of the PCR product, a 5'-overhang sequence incorporating a *Bam*HI cleavage site was added upstream of the 54F primer sequence that corresponded to *fccA54*. A random sequence of three nucleotides was included upstream of the *Bam*HI cleavage site to facilitate restriction enzyme digestion. The 54F forward primer was used in combination with the reverse 54RA primer to PCR amplify the *fccA54* gene encoding the FccA54 preprotein as a 1539 bp *Bam*HI/*Pst*I '54FRA' fragment.

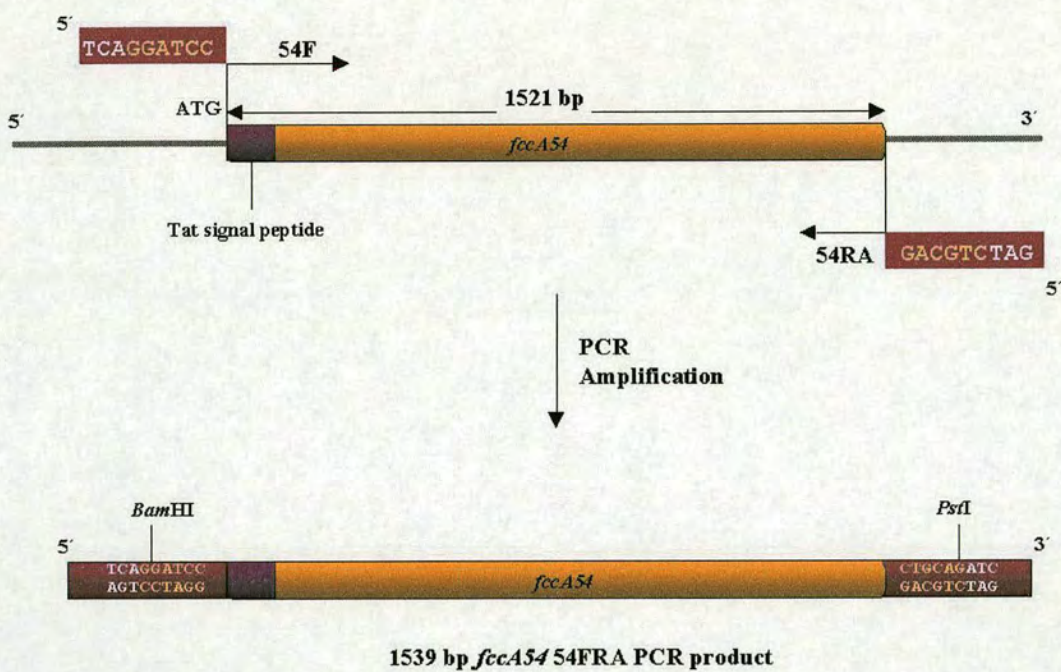


Figure 7.1: PCR amplification of the *fccA54* preprotein coding sequence
A schematic diagram (not to scale) shows the primer positions of 54F and 54RA that initiated PCR amplification of the *fccA54* gene as a *Bam*HI/*Pst*II 54FRA 1539 bp fragment. The 54F primer position was designed to include PCR amplification of the extreme N-terminal *fccA54* sequence encoding the Tat signal peptide.

Primers 54F and 54RA specifically initiated PCR amplification of the 1539 bp *fccA54* 54FRA preprotein coding sequence from the *S. oneidensis* MR-1 genome. However, a very low quantity of PCR product was synthesised, at approximately 0.01 µg DNA, as observed by agarose gel electrophoresis (gel photo not shown).

7.2.2 PCR amplification of an *fccAB54* co-expression fragment

The *fccAB54* 54FRB PCR amplification product was designed to direct periplasmic co-expression of FccA54 and FccB54 in *Shewanella frigidimarina* EG301 (Figure 6.1). It was considered that both protein subunits targeted to the periplasm to form the flavocytochrome might dissociate during purification preventing isolation of the intact heterodimer. Therefore, a second *fccAB54* PCR product was synthesised that did not contain the *fccA54* N-terminal Tat signal peptide coding sequence. This intended to produce a cloned *fccAB54* PCR product for overexpression of the FccA54 flavin subunit in the cytoplasm of the selected host strain. The N-terminal sequence encoding the hydrophobic signal sequence of FccB54 was PCR amplified to direct the co-expressed cytochrome subunit to the periplasm. Overexpression of the flavin and cytochrome subunits in distinct cellular locations intended to facilitate separate purification of the subunits for subsequent *in vitro* assembly of the flavocytochrome. The alternative *fccAB54* 54FMRB PCR product was synthesised using primers 54FM and 54RB as a *Bam*HI/*Pst*I 1830 bp PCR product (Figure 7.2).

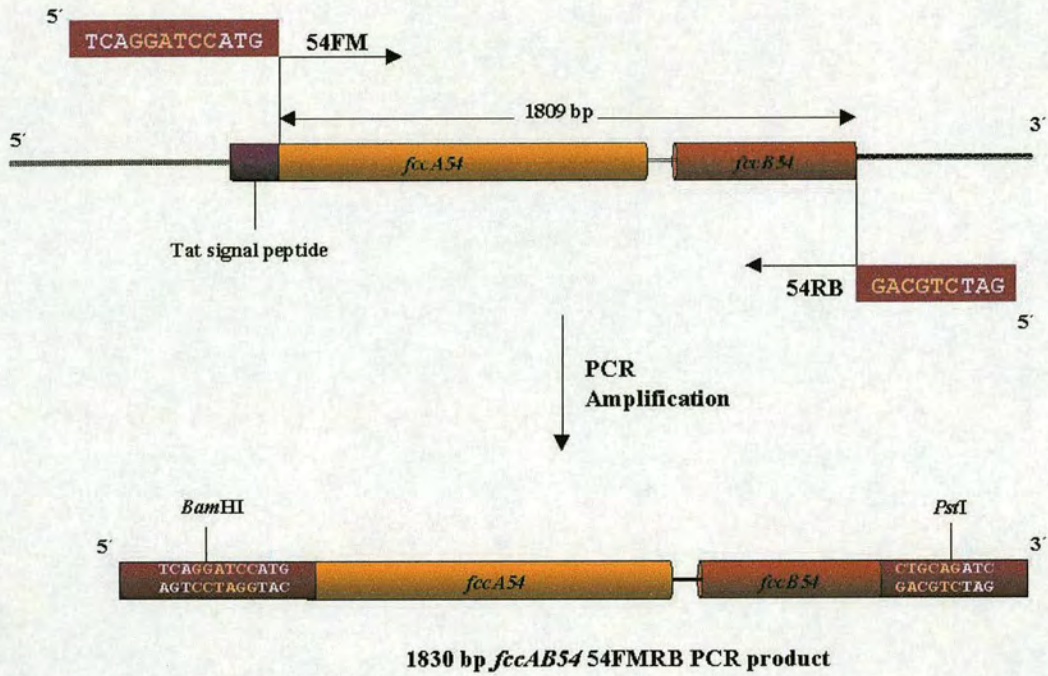


Figure 7.2: A schematic diagram of *fccAB54* PCR amplification
Primers 54FM and 54RB were used to initiate PCR amplification of *fccA54* and *fccB54*. The forward primer 54FM was positioned downstream of the *fccA54* N-terminal Tat signal peptide. The *fccAB54* 54FMRB PCR product was amplified as a *Bam*HI/*Pst*II 1830 bp fragment.

Primers 54FM and 54RB successfully initiated PCR amplification of *fccA54* and *fccB54* as a single 1830 bp 54FMRB fragment from the *S. oneidensis* MR-1 genome. The PCR result was analysed by agarose gel electrophoresis that revealed a single PCR product of the correct size, at approximately 0.06 µg DNA (Figure 7.3).

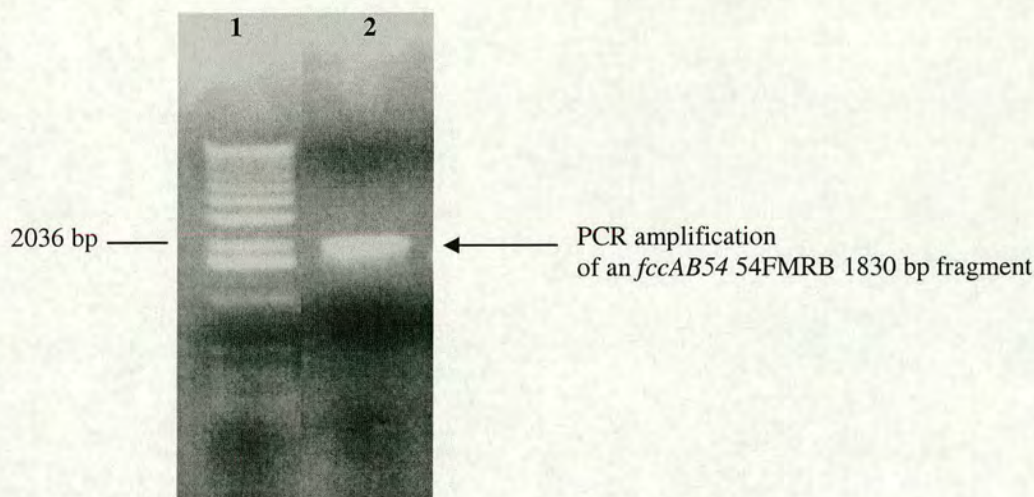


Figure 7.3: PCR amplification of *fccA54* and *fccB54* as a single product

PCR amplification of *fccA54* and *fccB54* as a single 1830 bp fragment was analysed by agarose gel electrophoresis. A single PCR product was observed (lane 2) that corresponded to the expected size of the 1830 bp *Bam*HI/*Pst*I 54FMRB *fccAB54* fragment. 1 kb DNA marker (lane 1) was used to indicate the PCR product amplified using primers 54FM and 54RB was of the correct size.

7.2.3 Cloning of the PCR products in pGEM-T

The *fccA54* 54FRA and *fccAB54* 54FMRB PCR products were cloned into pGEM-T (Figure 5.3) and transformed into *E. coli* TG1. Positive transformants were selected using ampicillin resistance and blue/white colony screening (5.2.2). White ampicillin resistant colonies were selected and further screened for recombinant plasmid using double *Bam*HI/*Pst*I restriction digests. A *Bam*HI/*Pst*I fragment corresponding to the size of the 1539 bp *fccA54* 54FRA PCR product was excised from recombinant pGEM-T plasmid referred to as pMB1-2. The *Bam*HI/*Pst*I restriction digest produced a fragment corresponding to the size of the 1830 bp *fccAB54* 54FMRB PCR product from recombinant pGEM-T plasmid named pMB4-11 (Figure 7.4).

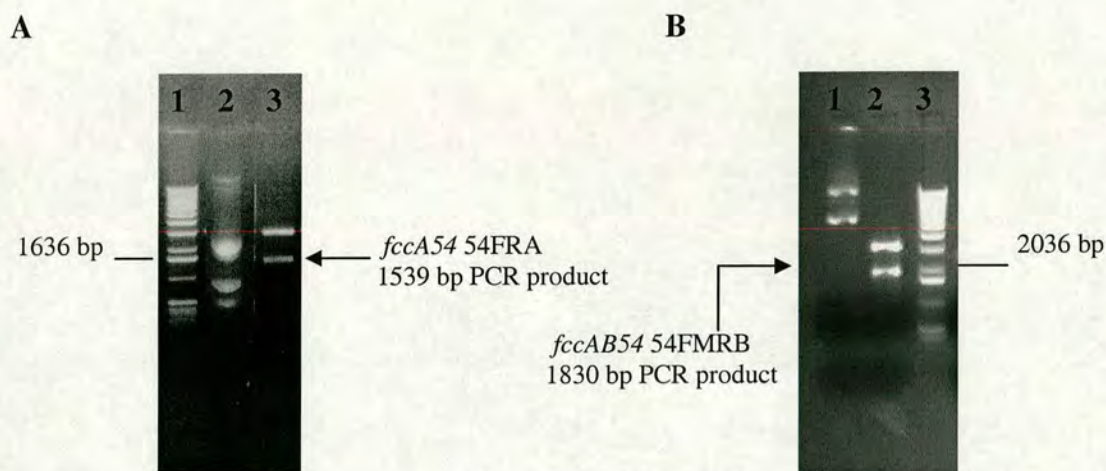


Figure 7.4: Cloning of the alternative *fccA54* and *fccAB54* PCR products in pGEM-T

A) Recombinant pGEM-T plasmid named pMB1-2 (lane 2) was isolated from ampicillin resistant white colonies. A restriction digest analysed by agarose gel electrophoresis was used to show formation of recombinant pGEM-T by excision of the *Bam*HI/*Pst*I PCR product. Plasmid pMB1-2 digested with *Bam*HI and *Pst*I produced a restriction fragment that corresponded to the *fccA54* 54FRA 1539 bp PCR product (lane 3). 1 kb DNA ladder (lane 1) was used to indicate the restriction fragments were of the expected size.

B) Plasmid pMB4-11 (lane 1) isolated from ampicillin resistant white colonies was shown to be recombinant plasmid DNA. A double *Bam*HI/*Pst*I restriction digest, analysed by agarose gel electrophoresis revealed excision of a *Bam*HI/*Pst*I fragment corresponding to the size of the *fccAB54* 54FMRB 1830 bp PCR product (lane 2). 1 kb DNA ladder (lane 3) was used to indicate that the restriction fragments were of the correct size.

7.2.4 Sequencing of the *fccA54* and *fccAB54* PCR products

The PCR amplified nucleotide sequences of *fccA54* 54FRA and *fccAB54* 54FMRB were checked for possible mutations incorporated by *Taq* DNA polymerase. Single-stranded DNA sequencing template was prepared from plasmids pMB1-2 and pMB4-11. The M13 primer (-20) complementary to pGEM-T and primers 54P1, 54P2, 54P3, 54P4 and 54P5 were designed to provide overlapping sequencing data of the entire PCR amplified sequences. Accurate PCR amplification of the *fccA54* 54FRA PCR product of pMB1-2 was shown from interpretation of the automated sequencing result. The *fccAB54* 54FMRB PCR product of pMB4-11 was identified to contain a silent mutation that retained a Leucine codon (TTA → TTG), located 12 nucleotides downstream of the *fccB54* ATG start codon.

7.2.5 Future cloning of the *fccA54* and *fccAB54* PCR products

A suitable expression system was developed (5.2.6) for overexpression of the FccA54 flavin subunit in the cytoplasm of *E. coli* TG1 (5.2.7). This established FccA54 flavoprotein overexpression system could be conveniently used to obtain periplasmic overexpression of FccA54. The strategy would involve excision of the correctly amplified *fccA54* 54FRA PCR product from pMB1-2 as a 1539 bp *Bam*HI/*Pst*II fragment. Ligation of the *fccA54* restriction fragment sticky ends to complementary ends of digested pMB3 plasmid would generate an expression plasmid suitable for periplasmic FccA54 overexpression. To specifically examine FccA54 overexpression levels in the periplasm of *E. coli* TG1, it would be necessary to isolate the periplasm following IPTG induction and monitor FccA54 overexpression using SDS-PAGE.

A modified pMMB503EH expression plasmid, named pMB5 was specifically constructed for co-expression of FccA54 and FccB54 in the periplasm of *S. frigidimarina* EG301 (Figure 6.5). Periplasmic overexpression of the FccA54 flavoprotein was not detected when using the *fccAB54* 54FRB PCR product of pMB5 introduced into *S. frigidimarina* EG301. This was attributed to the vast number of flavoproteins in *S. frigidimarina* EG301 combined with the low sensitivity of Coomassie blue staining (6.2.7). During purification of the FccA54 and FccB54 subunits targeted to the periplasm, the flavin subunit was not detected which suggested possible separation of the subunits (6.2.9). The type of interaction that occurs between the FccA54 and FccB54 subunits is not known.

It would therefore be advantageous to purify the subunits separately which could be achieved using the cloned *fccAB54* 54FMRB PCR product to direct overexpression. Following purification it would be possible to combine the purified subunits to form the functional flavocytochrome.

The constructed pMB5 expression plasmid could be used to obtain overexpression of the FccA54 and FccB54 subunits in the cytoplasm and periplasm, respectively. This would involve digestion of pMB4-11 and removal of the cloned *fccAB54* 54FMRB PCR product as an 1830 bp *Bam*HI/*Pst*I fragment. Subsequent ligation of the *Bam*HI/*Pst*I *fccAB54* restriction fragment to complementary sticky ends of digested plasmid pMB5 would generate a suitable expression plasmid. Conjugative transfer of the recombinant expression plasmid into *S. frigidimarina* EG301 would provide a suitable system to test co-expression of the FccA54 flavin subunit in the cytoplasm and FccB54 in the periplasm. Overexpression of the FccB54 protein could be specifically monitored by isolation of the periplasm prior to protein analysis using SDS-PAGE.

7.2.6 PCR amplification of the *fccA342* flavoprotein encoding sequence

PCR amplification of *fccA342* was designed to favour amplification of two products that differed in their N-terminal sequence. PCR amplification of the *fccA342* N-terminal Tat signal peptide coding sequence was determined by the forward primer position. Variation of the *fccA342* PCR products aimed to provide cloned fragments that would direct cytoplasmic or periplasmic overexpression of FccA342 in *E. coli* TG1. The 5'-end of the 21-nucleotide forward primer '342F' was specifically designed to complement the *fccA342* ATG start codon. The 342F primer was ideally positioned to initiate PCR amplification of the *fccA342* N-terminal sequence encoding the Tat signal peptide. The 5'-end of the 21-nucleotide forward primer '342FM' mapped directly downstream of the predicted peptidase cleavage point to generate specific amplification of *fccA342* sequence encoding mature flavoprotein. The forward primers, 342F and 342FM were both extended to incorporate a 5'-overhang *Bam*HI cleavage site to facilitate cloning into the expression plasmid. The 5'-end of the 20-nucleotide reverse primer sequence '342RA' was designed to complement the C-terminal TAG stop codon of *fccA342*. The 342RA primer sequence complementary to *fccA342* was modified to contain a *Pst*I cleavage site incorporated as a 5'-overhang sequence. PCR amplification of the *fccA342* 342FRA sequence encoding the FccA342 preprotein was designed to synthesise a 1503 bp *Bam*HI/*Pst*I fragment. Primers 342FM and 342RA were designed to amplify the *fccA342* sequence encoding mature FccA342 protein as a 1443 bp *Bam*HI/*Pst*I 342FMRA fragment (Figure 7.5).

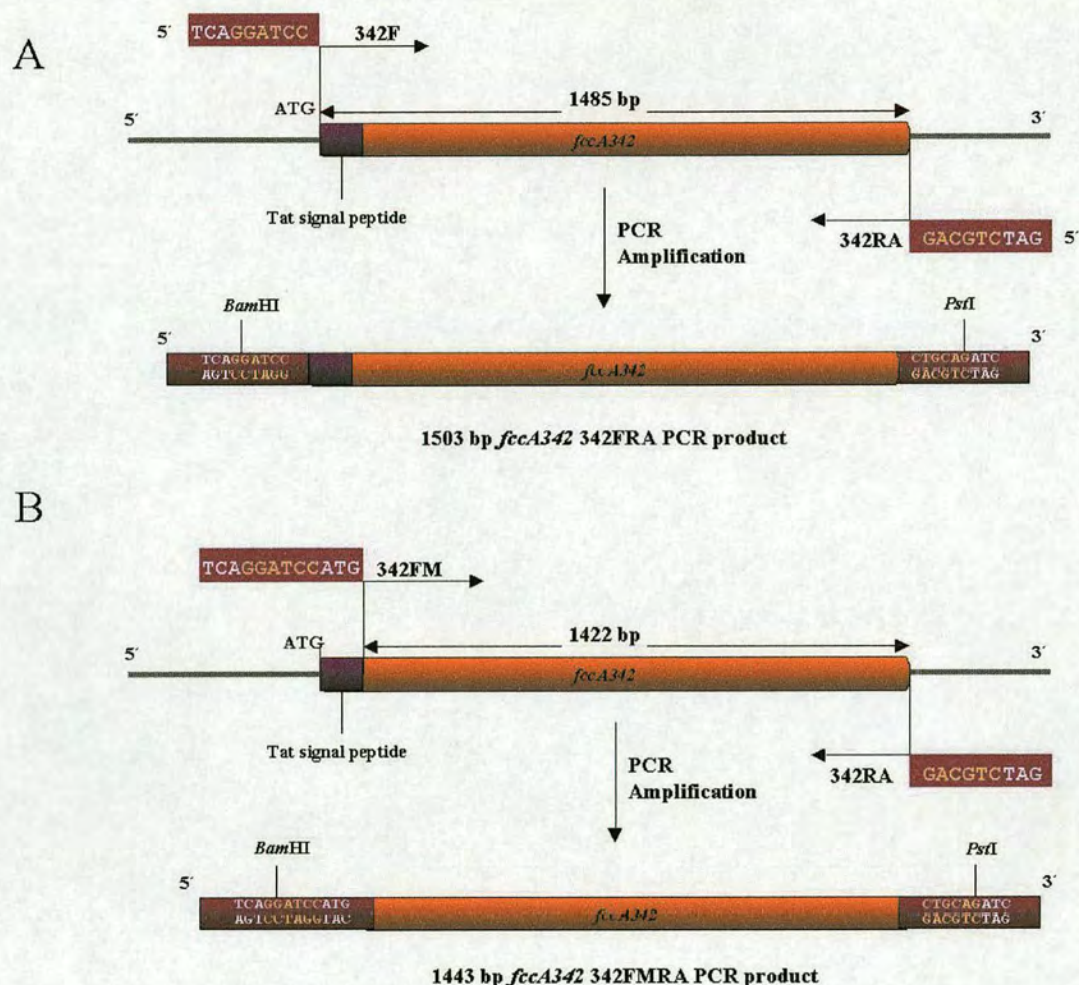


Figure 7.5: A schematic diagram of *fccA342* PCR amplification

(A) The diagram shows the primer positions of 342F and 342RA that were designed to initiate PCR amplification of *fccA342* preprotein coding sequence as a 1503 bp *Bam*HI/*Pst*I fragment.

(B) The 342FM primer was positioned downstream of sequence encoding the N-terminal Tat signal peptide to initiate amplification of the *fccA342* mature protein coding sequence as a 1443 bp *Bam*HI/*Pst*I fragment.

The two distinct forms of *fccA342* encoding preprotein and mature protein were successfully PCR amplified from the *S. oneidensis* MR-1 genome. The PCR results analysed by agarose gel electrophoresis revealed a high yield of specific PCR amplification products at the expected size (Figure 7.6).

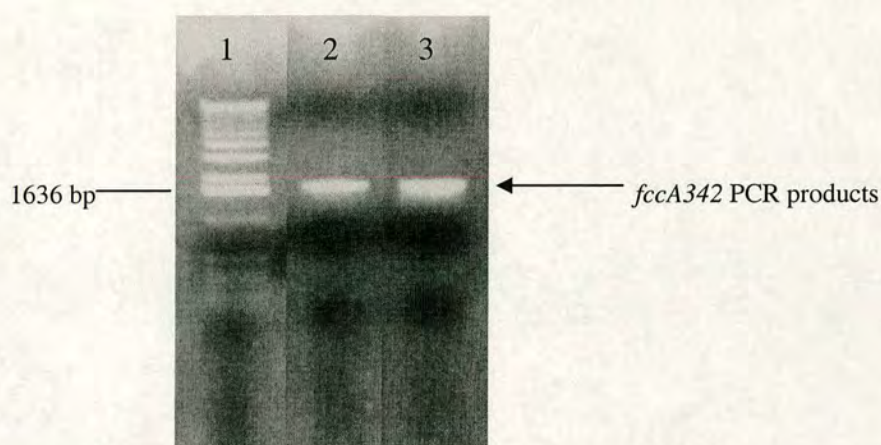


Figure 7.6: PCR amplification of *fccA342* from the *S. oneidensis* MR-1 genome

Primers 342F and 342RA initiated PCR amplification of *fccA342* preprotein coding sequence as a 1503 bp *Bam*HI/*Pst*I 342FRA PCR product. Analysis of the results by agarose gel electrophoresis showed that approximately 0.05 µg DNA was amplified (lane 2). The *fccA342* mature protein coding sequence was amplified from the *S. oneidensis* MR-1 genome using primers 342FM and 342RA (lane 3). A specific *fccA342* 342FMRA PCR product at the expected size of 1443 bp was amplified at approximately 0.06 µg DNA (lane 3). 1 kb DNA ladder (lane 1) was used to indicate that the PCR products were of the expected length.

7.2.7 Cloning of the *fccA342* PCR products in pGEM-T

The *fccA342* PCR products were inserted into pGEM-T and transformed into *E. coli* TG1. Positive transformants were selected using ampicillin resistance and blue/white colony screening. Recombinant pGEM-T plasmid was identified by isolation of plasmid DNA and digestion with *Bam*HI and *Pst*I. A fragment corresponding to the 1503 bp *fccA342* 342FRA PCR product was excised from recombinant pGEM-T named pMB5-4. Recombinant plasmid, named pMB7A-1 was shown to contain the 1443 bp *fccA342* 342FMRA PCR product, excised as a *Bam*HI/*Pst*I fragment (Figure 7.7). Single-stranded DNA was prepared from plasmids pMB5-4 and pMB7A-1 to provide DNA sequencing template. The PCR products were primarily sequenced using the M13 (-20) primer complementary to pGEM-T plasmid to yield sequence information that proved the *fccA342* gene was specifically amplified from the *S. oneidensis* MR-1 genome.

The PCR product sequences amplified using the low fidelity *Taq* DNA polymerase were not completely checked for possible mutations.

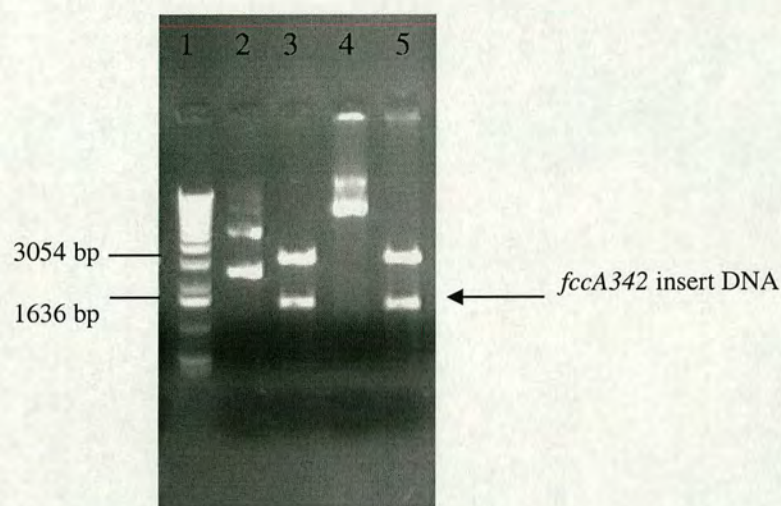


Figure 7.7: Cloning of the *fccA342* PCR products in pGEM-T

Recombinant pGEM-T plasmid DNA containing *fccA342* was isolated from ampicillin resistant white colonies. Plasmid pMB5-4 (lane 2) was shown using double *Bam*HI/*Pst*I restriction digests to contain the *fccA342* 342FRA PCR product, excised as a 1503 bp *Bam*HI/*Pst*I fragment (lane 3). Recombinant pMB7A-1 (lane 4) digested with *Bam*HI and *Pst*I released a restriction fragment corresponding to the 1443 bp *fccA342* 342FMRA PCR product (lane 5). 1 kb DNA ladder (lane 1) was used to indicate the restriction fragments analysed by agarose gel electrophoresis were of the correct size.

7.2.8 PCR amplification of *fccAB342* from *S. oneidensis* MR-1

The *fccAB342* 342FRB fragment (6.2.11) of pMB6 (Figure 6.18) introduced into *S. frigidimarina* EG301 was used preferentially to generate high levels of overexpressed flavocytochrome in the periplasm. In addition to the *fccAB342* 342FRB PCR product specifically synthesised for periplasmic overexpression, a second *fccAB342* PCR product was amplified. An *fccAB342* 342FMRB overexpression fragment was PCR amplified without the N-terminal Tat signal peptide coding sequence of *fccA342*. This *fccA342* mature protein coding sequence was fused to PCR amplification of *fccB342* containing sequence encoding the N-terminal Sec-dependent signal sequence.

The cloned *fccAB342* fragment was designed to generate overexpression of the FccA342 subunit in the cytoplasm and the FccB342 cytochrome subunit in the periplasm. The production of overexpressed protein in different cellular locations aimed to allow separate purification of the subunits. The forward 342FM primer was designed to initiate PCR amplification of *fccA342* mature protein coding sequence. This primer was used in combination with the reverse 19-nucleotide 342RB primer sequence, complementary to the C-terminal coding sequence of *fccB342*. The 342RB primer sequence that annealed to *fccB342* was extended to contain a 5'-overhang sequence incorporating a *Pst*I cleavage site. PCR amplification using primers 342FM and 342RB was designed to initiate amplification of *fccAB342* as a *Bam*HI/*Pst*I 1804 bp fragment (Figure 7.8).

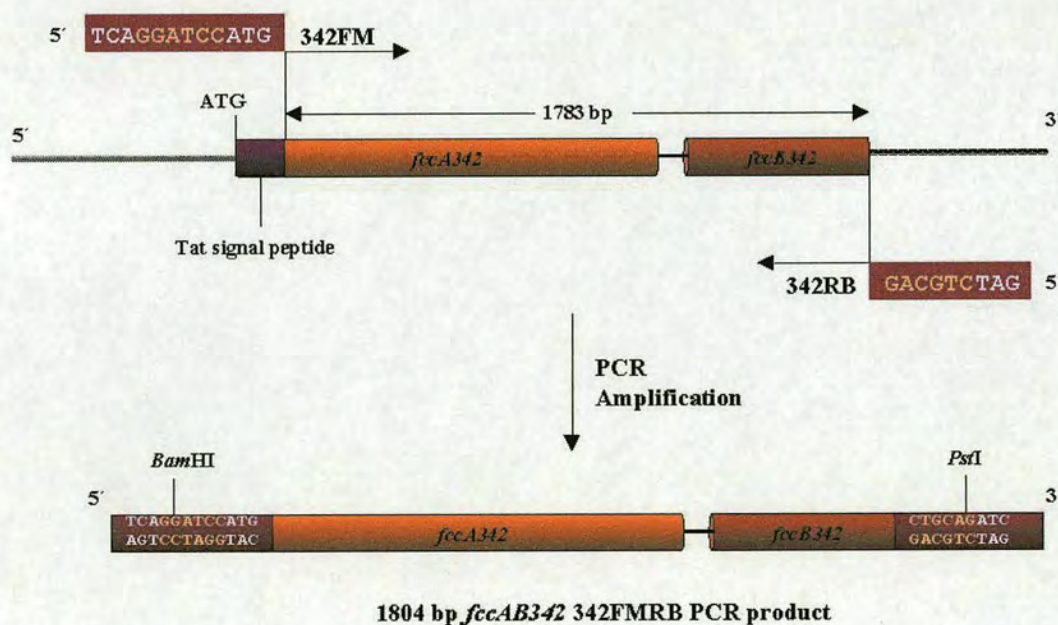


Figure 7.8: PCR amplification of *fccA342* and *fccB342*

A schematic diagram (not to scale) shows the position of primers used to amplify the *fccAB342* fragment from the *S. oneidensis* MR-1 genome. The forward primer 342FM was suitably positioned to initiate PCR amplification of the *fccA342* mature protein coding sequence downstream of the encoded N-terminal Tat signal peptide. The reverse primer sequence 342RB was complementary to the extreme C-terminal coding sequence of *fccB342*. The primers 342FM and 342RB initiated PCR amplification of *fccAB342* as a *Bam*HI/*Pst*I 1804 bp PCR product.

PCR amplification of the *fccAB342* co-expression fragment was successfully PCR amplified from the genome of *S. oneidensis* MR-1. The PCR result analysed using agarose gel electrophoresis revealed a specific PCR product corresponding to the 1804 bp *fccAB342* PCR product. Approximately 0.06 µg DNA was PCR amplified (Figure 7.9).

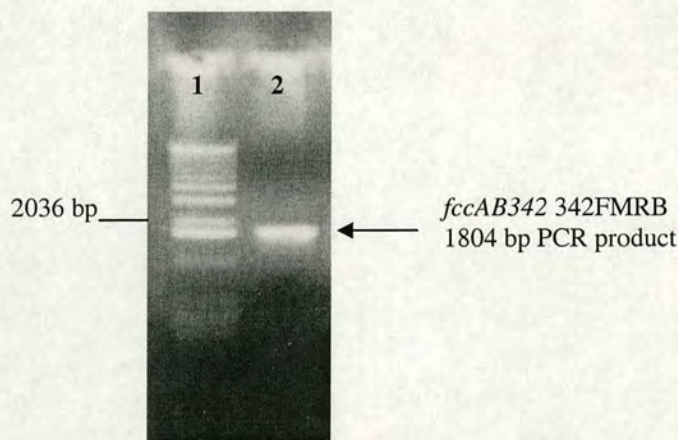


Figure 7.9: PCR amplification of *fccAB342* from *S. oneidensis* MR-1

The *fccAB342* 342FMRB co-expression fragment was specifically PCR amplified from the genome of *S. oneidensis* MR-1 using primers 342FM and 342RB. The PCR result was analysed by agarose gel electrophoresis and revealed a product corresponding to the length of the 1804 bp *fccAB342* fragment (lane 2). 1 kb DNA ladder (lane 1) was used to analyse the size of the PCR product.

7.2.9 Cloning of the *fccAB342* PCR product in pGEM-T

The amplified *fccAB342* 342FMRB fragment was cloned into pGEM-T to provide multiple copies of the product. Following ampicillin selection and blue/white colony screening, white ampicillin resistant colonies were selected and screened for recombinant plasmid. An isolated recombinant plasmid referred to as pMB8-3 was shown using *Bam*HI and *Pst*I restriction digests to contain the *fccAB342* 342FMRB PCR product. The *fccAB342* product was excised from pMB8-3 as a *Bam*HI/*Pst*I 1804 bp fragment as shown by agarose gel electrophoresis (Figure 7.10).

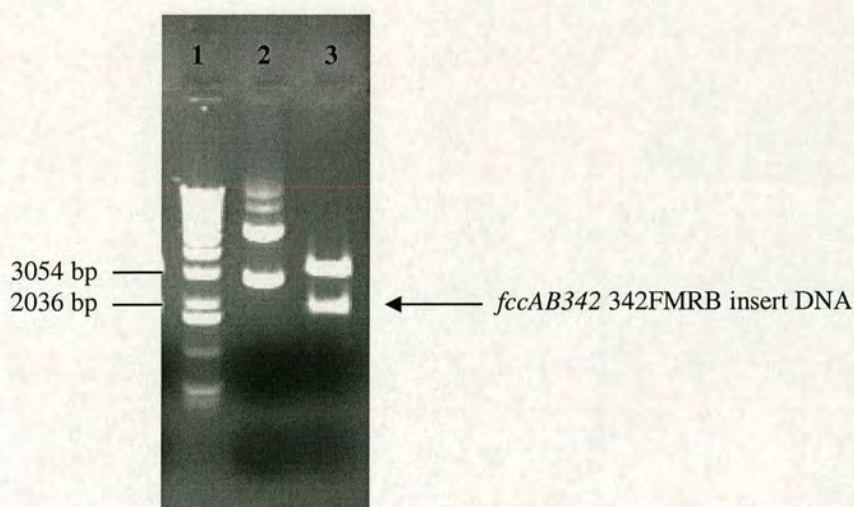


Figure 7.10: Cloning of the *fccAB342* PCR product in pGEM-T

The *fccAB342* 342FMRB PCR product was inserted in pGEM-T to form recombinant plasmid named pMB8-3 (lane 2). Double *Bam*HI/*Pst*I restriction digests of pMB8-3 analysed using agarose gel electrophoresis were used to verify recombinant plasmid was formed. A restriction fragment corresponding to the 1804 bp *fccA342* 342FMRB fragment was produced upon digestion of pMB8-3 with *Bam*HI and *Pst*I (lane 3). 1 kb DNA ladder (lane 1) was used to analyse the size of the restriction fragments using agarose gel electrophoresis.

7.2.10 Sequencing of the *fccAB342* PCR product of pMB8-3

The *fccAB342* 342FMRB sequence was amplified from the *S. oneidensis* MR-1 genome using *Taq* DNA polymerase. The cloned sequence of pMB8-3 was therefore checked for nucleotide sequence errors introduced by the low fidelity enzyme. The M13 primer (-20) complementary to pGEM-T plasmid was primarily used to verify, by automated sequencing, that the correct *fccA342* and *fccB342* target genes were amplified. Primers 342RP1, 342RP2, 342RP3 and 342RP4 were designed to complement the *fccA342* and *fccB342* genes to provide overlapping sequencing data. The *fccB342* amplified nucleotide sequence of pMB8-3 was shown from interpretation of the sequencing results to consist of the correct sequence. The *fccA342* sequence of pMB8-3 requires further sequencing to check that the correct sequence was PCR amplified.

7.2.11 Future overexpression work of FccA342

In order to try overexpression of FccA342 it will be necessary to completely sequence the *fccA342* PCR products cloned in pMB5-4 and pMB7A-1. A suitable overexpression system involving plasmid pMB3 was constructed to produce high levels of FccA54 flavoprotein in the cytoplasm of *E. coli* (5.2.7). The pMB3 plasmid altered to contain an *fccA342* PCR product would provide an ideal system to try overexpression of FccA342 in *E. coli*. To test periplasmic overexpression of FccA342 it would be convenient to cut the *fccA342* 342FRB PCR product from pMB5-4 as a *Bam*HI/*Pst*I 1503 bp fragment. Insertion of the fragment in pMB3 by ligation of complementary *Bam*HI and *Pst*I ends would form an ideal expression plasmid to direct periplasmic expression. Following IPTG induction of recombinant *E. coli* and isolation of the periplasm, the levels of FccA342 periplasmic expression could be analysed using SDS-PAGE. The N-terminal Tat signal peptide of FccA342 does not contain the twin arginine residues that are essential for recognition and targeting to the periplasm via the Tat pathway (Figure 1.12). Therefore, targeting of the FccA342 preprotein to the periplasm of *E. coli* might be problematic and lead to low levels of periplasmic expression. To improve the FccA342 overexpression levels, insertion of the *fccA342* 342FMRA PCR product in pMB3 would conveniently provide a construct to direct cytoplasmic overexpression. This overexpression strategy would involve excision of the *fccA342* 342FMRA *Bam*HI/*Pst*I fragment from pMB7A-1 and insertion into pMB3 cut with *Bam*HI and *Pst*I. Subsequent to IPTG induction of recombinant *E. coli*, cytoplasmic FccA54 overexpression analysed using SDS-PAGE would provide a means of determining the optimal overexpression conditions.

7.2.12 Future co-expression work of FccA342 and FccB342

The *fccAB342* 342FRB co-expression fragment comprising sequence to direct periplasmic co-expression of the flavin and cytochrome subunits was cloned in pMB6 and transferred into *S. frigidimarina* EG301. However, under the expression conditions tested, no overexpression of the flavocytochrome was induced in the periplasm of *S. frigidimarina* EG301 (6.2.15). The *fccAB342* 342FMRB fragment could be alternatively used to produce high levels of the target proteins in *S. frigidimarina* EG301. In order to develop a suitable expression plasmid for *fccAB342* 342FMRB, it would be necessary to cut the *fccAB342* insert DNA from pMB8-3 as a *Bam*HI/*Pst*I 1804 bp fragment. The *fccAB342* restriction fragment ligated to complementary sticky ends of pMB6 would form the desired expression plasmid. Conjugative transfer of the recombinant expression plasmid from *E. coli* to *S. frigidimarina* EG301 would provide a suitable expression system for testing FccA342 overexpression in the cytoplasm and FccB342 overexpression in the periplasm. Following induction with IPTG, isolation of the periplasm contents would enable specific detection of FccB54 overexpressed in the periplasm. The flavin and cytochrome subunits could subsequently be purified in two distinct steps and combined to form the flavocytochrome.

7.2.13 A putative iron-induced flavocytochrome of *S. oneidensis* MR-1

Sequencing of the *S. oneidensis* MR-1 genome (<http://www.tigr.org> and Heidelberg *et al.*, 2002) led to the identification of a gene sequence *ifcA-1* (ORF number: SO1421; Table 7.1) encoding a putative monomeric flavocytochrome comprising an N-terminal tetrahaem *c*-type cytochrome domain and a C-terminal flavin domain (Figure 7.11). The predicted amino acid sequence of IfcA-1 was identified to share striking amino acid sequence identity to Fcc₃ (40 %) and the iron-induced flavocytochrome Ifc₃ (41 %) of *S. frigidimarina* NCIMB 400 (Dobbin *et al.*, 1999; <http://www.ncbi.nlm.nih.gov/blast/bl2seq/bl2.html>). The N-terminal sequence of IfcA-1 constituting the cytochrome domain was shown to contain four CxxCH motifs for haem attachment (where x is any amino acid residue; Figure 7.11) that aligned with those of the related flavocytochromes, leading us to the hypothesis that IfcA-1 is also a tetrahaem *c*-type cytochrome. Furthermore, a histidine residue of Fcc₃ that serves as the sixth ligand to form *c*₃-haems (Pealing *et al.*, 1995) is conserved in IfcA-1 and Ifc₃ (Figure 7.11). The N-terminal flavoprotein sequence of IfcA-1 contains the conserved FAD adenine binding motif that appears to provide a non-covalent attachment site, as shown by the conserved substitution of the essential histidyl residue required for covalent attachment (Weiner and Dickie, 1979; Cole, 1982) with asparagine (Figure 7.11). The extreme N-terminal sequence of IfcA-1 was identified to comprise a signal sequence of 22 amino acid residues (<http://www.cbs.dtu.dk/services/SignalP/>; Nielsen *et al.*, 1997) that is characteristic of proteins targeted to the periplasm via the Sec-dependent pathway (Figure 7.11; von Heijne and Abrahmsén, 1989).

Protein name	Gene name	ORF number	Protein length (aa)		Molecular weight (Da)		pI
			Preprotein	Mature	Preprotein	Mature	
IfcA-1	<i>ifcA-1</i>	SO1421	589	567	63,025	60,590	7.72

Table 7.1: Predicted properties of a putative iron-induced flavocytochrome

The open reading frame (ORF) number corresponding to *ifcA-1* (<http://www.tigr.org>) encoding the putative iron-induced flavocytochrome, IfcA-1 of *S. oneidensis* MR-1, is shown. The amino acid (aa) sequence lengths of the preprotein and mature protein are also shown. The preprotein length was calculated using SignalP (<http://www.cbs.dtu.dk/services/SignalP/>; Nielsen *et al.*, 1997). The estimated molecular weight of the apoprotein (preprotein and mature protein) and isoelectric point (pI) for the mature protein (<http://www.expasy.org/tools/protparam.html>) are also shown.

The catalytic and substrate-binding residues of Fcc₃ that are conserved in the family of fumarate reductases; Arg402, His504, and Arg544 (*S. frigidimarina* NCIMB 400 Fcc₃ numbering; Pealing *et al.*, 1992) are strictly conserved in the flavin domain of IfcA-1 and Ifc₃ (Figure 7.11). An arginine residue equivalent to Arg381 of Fcc₃ that forms the proton delivery pathway to reprotonate the Arg402 active site acid (Doherty *et al.*, 2000) was also identified in IfcA-1 and Ifc₃. However, Glu378 of Fcc₃, another residue of the proton delivery pathway (Doherty *et al.*, 2000) is not conserved in IfcA-1 (Figure 7.11), which leads to the suggestion that an alternative proton pathway operates in IfcA-1. Furthermore, His365 of Fcc₃ that is a key substrate-binding residue of the active site (Taylor *et al.*, 1999) is not conserved in IfcA-1 and is substituted with Phenylalanine (Figure 7.11). Thr377 is the second key substrate-binding residue of Fcc₃ that is located in the clamp domain and is conservatively substituted with Serine in both isozymes (Figure 7.11).



Figure 7.11: 'ClustalW' multiple sequence alignment of IfcA-1 and related proteins

The preprotein sequence of IfcA (*S. oneidensis* MR-1; IfcSO) was aligned with Ifc₃ (*S. frigidimarina* NCIMB 400; IfcSF) and Fcc₃ of *S. frigidimarina* NCIMB 400 (FccSF) using 'ClustalW' (Thompson *et al.*, 1994). The predicted signal sequence for targeting to the periplasm is shown in red (Nielsen *et al.*, 1997; <http://www.cbs.dtu.dk/services/SignalP/>). The CxxCH motifs that are characteristic of *c*-type cytochromes are shown in yellow and histidine residues that may provide the sixth ligand to the haems are also shown (green). The FAD binding site and asparagine (bold, black) indicate that IfcA-1 also binds to FAD non-covalently. The active site residues that are conserved in the related enzymes (magenta) and the residues that are not conserved (cyan) are shown. The active site residues are numbered according to Fcc₃ (*S. frigidimarina* NCIMB 400).

The data interpreted from the multiple sequence alignment of IfcA-1 against Fcc₃ and Ifc₃ of *S. frigidimarina* NCIMB 400 leads us to the conjecture that IfcA-1 of *S. oneidensis* MR-1 is also a tetrahaem flavocytochrome *c*₃. The particularly high sequence identity of IfcA-1 with Ifc₃ combined with the apparent presence of two fumarate reductases in *S. oneidensis* MR-1 (<http://www.tigr.org>), tentatively suggests that IfcA-1 is not a fumarate reductase but rather is induced by iron respiration and shares an *in vivo* function similar to Ifc₃. However, the *in vitro* fumarate reductase catalytic activity of Ifc₃ (Dobbin *et al.*, 1999) may not be a conserved feature of the related IfcA-1 flavocytochrome due to the substitution of His365→Phe365, which may impede binding of fumarate due to steric constraints.

To investigate the cellular expression and catalytic activity of the unusual IfcA-1 flavocytochrome, the *ifcA-1* gene was PCR amplified from the *S. oneidensis* MR-1 genome. This intended to provide a suitable DNA template for insertion into an appropriate expression plasmid for overexpression, purification and characterisation.

7.2.14 PCR amplification and cloning of *ifcA-1*

Primers were designed to specifically amplify the putative iron-induced flavocytochrome from the *S. oneidensis* MR-1 genome. The 5'-end of the forward 23-nucleotide primer 'IFC3F' was designed to hybridise at the ATG start codon of the gene that encoded the cytochrome domain. The 24-nucleotide reverse primer 'IFC3R' was designed to complement the extreme C-terminal coding sequence of the flavin domain. The 5' forward primer sequence complementary to *ifcA-1* was modified to contain a *Bam*HI cleavage site and a *Pst*I cleavage site was incorporated at the 5'-end of the reverse primer to allow direct cloning of the PCR product. The primers were designed to initiate PCR amplification of *ifcA-1* as a 1788 bp *Bam*HI/*Pst*I fragment (Figure 7.12).

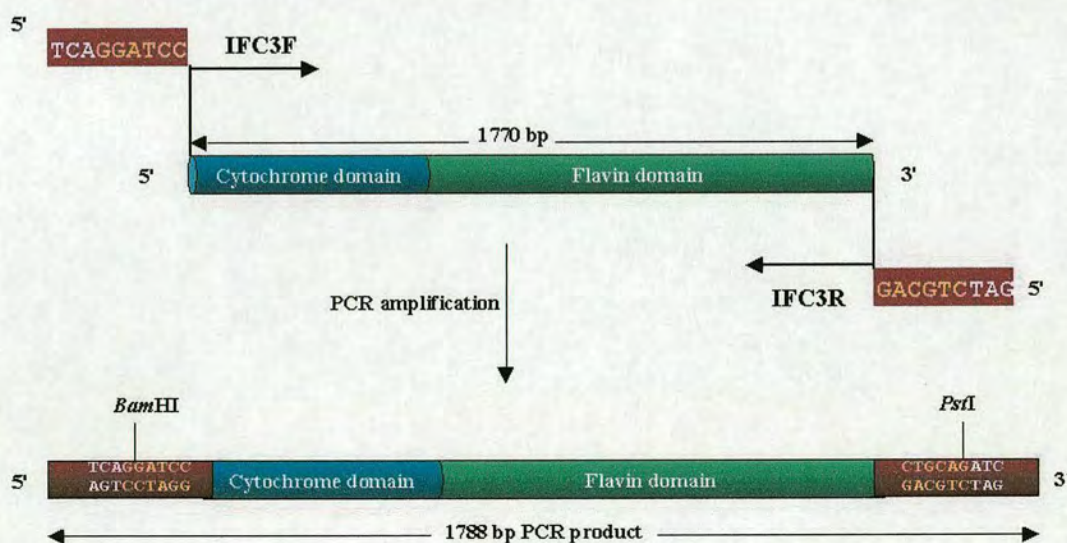


Figure 7.12: PCR amplification of *ifcA-1* from *S. oneidensis* MR-1

A schematic diagram (not to scale) shows the forward and reverse primer positions used to initiate amplification of *ifcA-1*. The primer sequences were modified to contain *Bam*HI and *Pst*I cleavage sites for direct cloning of the *ifcA-1* PCR product amplified as a 1788 bp fragment.

PCR amplification using primers IFC3F and IFC3R specifically amplified a PCR product from the *S. oneidensis* MR-1 genome that corresponded to the expected size of *ifcA-1*. The PCR result was analysed by agarose gel electrophoresis that revealed a single PCR product correlating to the 1788 bp *ifcA-1* PCR product at approximately 0.06 µg DNA (Figure 7.13).

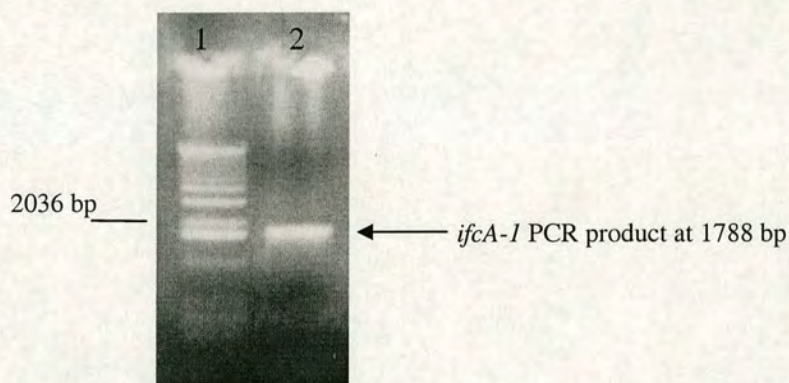


Figure 7.13: PCR amplification of *ifcA-1* from the *S. oneidensis* MR-1 genome

Primers IFC3F and IFC3R initiated PCR amplification of the *ifcA-1* gene from the *S. oneidensis* MR-1 genome. A single PCR product corresponding to the *ifcA-1* 1788 bp *Bam*HI/*Pst*I fragment (lane 2) was shown using agarose gel electrophoresis. 1 kb DNA ladder (lane 1) was used to indicate the PCR product was of the correct size.

The *ifcA-1* PCR product was cloned into the high copy number pGEM-T plasmid and transformed into *E. coli* TG1. Recombinant pMB9-5 plasmid was isolated from a positive transformant that was initially identified using ampicillin resistance and blue/white colony screening. The recombinant pMB9-5 plasmid was identified using double *Bam*HI/*Pst*I restriction digests that were subsequently analysed using agarose gel electrophoresis. A restriction fragment corresponding to the length of the *ifcA-1* PCR product was produced upon digestion of pMB9-5 with *Bam*HI and *Pst*I (Figure 7.14).

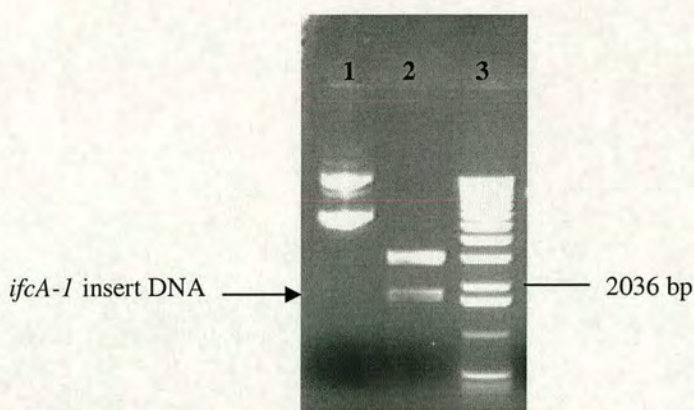


Figure 7.14: Cloning of the *ifcA-1* PCR product in pGEM-T

Recombinant pMB9-5 plasmid (lane 1) was isolated from a white ampicillin resistant colony and was shown to be recombinant using double *Bam*HI/*Pst*I restriction enzyme digests. A *Bam*HI/*Pst*I restriction fragment corresponding to the 1788 bp *ifcA-1* PCR product was excised from pMB9-5 (lane 2). 1 kb DNA ladder (lane 3) was used to indicate the size of the restriction fragments using agarose gel electrophoresis.

7.2.15 Future overexpression work of IfcA-1

The *ifcA-1* fragment cloned in pGEM-T to form pMB9-5 was primarily sequenced to identify that the correct target gene was amplified from the *S. oneidensis* MR-1 genome. Single-stranded template DNA was prepared from pMB9-5 and the M13 (-20) primer complementary to pGEM-T was used to identify that the correct gene was amplified. For overexpression purposes, it will be necessary to completely sequence the cloned *ifcA-1* PCR product for potential errors incorporated by *Taq* DNA polymerase. The modified pMMB503EH plasmid, pMB5, could be conveniently used for overexpression of IfcA-1. Formation of the *ifcA-1* recombinant expression plasmid would involve digestion of plasmid pMB9-5 with *Bam*HI and *Pst*I to release *ifcA-1* as a *Bam*HI/*Pst*I 1788 bp overexpression fragment. Ligation of the *ifcA-1* restriction fragment to complementary sticky ends of pMB5 would generate an expression plasmid specific to IfcA-1 overexpression.

Conjugative transfer of the recombinant expression plasmid into *S. frigidimarina* EG301 would provide a suitable system to test overexpression of IfcA-1.

7.2.16 Summary

A variety of PCR products were amplified to achieve protein overexpression of FccA54 and FccA342 as separate flavin subunits and for co-expression with the putative partner cytochrome subunit. In addition to the *fccA54* 54FMRA PCR construct synthesised for cytoplasmic overexpression of FccA54 (Chapter 5), a second *fccA54* 54FRA PCR product was amplified. However, high yields of overexpressed FccA54 flavoprotein were obtained from the cloned *fccA54* 54FMRA product. Therefore, FccA54 overexpression in the periplasm of *E. coli* was unnecessary and the cloned *fccA54* 54FRA product was not required.

The findings obtained from overexpression (5.2.7) and purification (5.2.8) of the FccA54 flavin subunit led to the suggestion that these novel flavoenzymes only function with the partner cytochrome subunit. Therefore, further cloning of the *fccA342* fragments and overexpression of the FccA342 flavin subunit in the cytoplasm or periplasm was not attempted. However, purification of the flavin subunit in *E. coli* may provide the best means of obtaining the flavoprotein subunit, which could subsequently be combined with the independently purified partner cytochrome subunit. Alternatively, cloning of the other PCR products, *fccAB54* 54FMRB and *fccAB342* 342FMRB in pMB5 to direct expression of the subunits in distinct cellular locations may provide a suitable method to facilitate purification of the co-expressed subunits.

Chapter 8

Conclusion

S. oneidensis MR-1 is a respiratory versatile bacterium that can couple anaerobic growth to the reduction of many substrates and consequently has received considerable interest due its potential role in bioremediation. The completely sequenced *S. oneidensis* MR-1 genome (<http://www.tigr.org>; Heidelberg *et al.*, 2002) has recently provided us with the fundamental tool for identifying and exploring the role of respiratory proteins involved in the complex anaerobic respiratory pathways. Inclusive of the 39 *c*-type cytochromes that were identified from genome sequencing, four novel putative flavocytochromes of *S. oneidensis* MR-1 were identified and selected for further study in this thesis.

8.1 Molecular modelling

The four novel flavocytochromes comprise separately encoded flavin (FccA) and cytochrome (FccB) subunits that were identified to share striking sequence identity to Fcc₃ of *Shewanella*, suggesting that the novel flavoproteins are also periplasmic, tetrahaem flavocytochrome *c*₃ enzymes containing non-covalently bound FAD. The active sites of the novel flavoproteins have been identified to contain only one set of substrate binding residues required for binding the dicarboxylate groups of fumarate in Fcc₃. This finding leads us to the theory that the related flavoenzymes bind to acrylate-like substrates that contain one carboxylate group. Molecular models of the novel flavoenzymes have been constructed based upon the known X-ray crystal structure of Fcc₃ (Taylor *et al.*, 1999), to provide a three-dimensional insight into the architecture of each enzyme active site.

The molecular models predict a putative spatial arrangement of residues in each enzyme active site and have shown that the structural topology and orientation of active site residues are conserved in the flavin domains but less well conserved in the clamp domains, consistent with the findings obtained from sequence analyses. The molecular models have been used as structural templates for screening enzyme substrates of the novel flavoproteins. A wide variety of acrylates have been identified as potential, biologically relevant substrates, including methacrylate, crotonate, and tiglate. One of the novel flavoproteins (FccA56) has been shown to accommodate phenylacrylates such as cinnamate produced from degradation of phenylalanine. A number of these candidate substrates have been identified to support anaerobic growth of wild-type *S. oneidensis* MR-1.

8.2 A mutant strain of *S. oneidensis* MR-1

A knockout strain of *S. oneidensis* MR-1 deficient in expressing one of the novel flavocytochromes (FccA54; FccB54) has been constructed and named *S. oneidensis* MB5415. This represents the first report of an *S. oneidensis* MR-1 mutant that lacks the entire gene-coding sequences of an enzyme implicated in anaerobic respiration. *S. oneidensis* MB5415 has been used to test which of the acrylates fails to support growth of this mutant strain in comparison to wild-type *S. oneidensis* MR-1. This approach was used as a means of identifying the target protein function, where a growth defect of the null mutant on a particular acrylate is associated with absence of the novel flavocytochrome.

Deletion of the genes encoding the novel flavocytochrome had no detectable physiological effect on anaerobic growth of *S. oneidensis* MB5415 compared to the wild-type strain. However, the anaerobic growth experiments need to be improved, particularly, the oxygen levels in the growth jars need to be consistent and this could be achieved with higher accuracy by conducting the experiment in an anaerobic growth chamber. It would also be advantageous to examine the effect of the substrate concentration on anaerobic growth of *S. oneidensis* MR-1 to ascertain the optimal acrylate concentration that supports growth. Obtaining strictly anaerobic growth cultures of *S. oneidensis* MR-1 supplemented with the optimal concentration of acrylate would provide an accurate control for comparing growth of the null mutant strain.

The related novel flavocytochromes may have similar functions *in vivo* and deletion of genes encoding one flavocytochrome is perhaps negated by the presence of the other flavocytochromes. Therefore, it may be unfeasible to determine the biological function of these novel flavocytochromes by constructing gene knockouts and conducting anaerobic growth experiments of a mutant strain compared to wild-type *S. oneidensis* MR-1. Alternatively, *S. oneidensis* MB5415 and *S. oneidensis* MR-1 grown under acrylate reducing conditions could be subjected to DNA microarray analyses in order to examine and compare the complete gene transcription profiles. A relative decrease in the mRNA levels of certain *S. oneidensis* MB5415 genes compared to *S. oneidensis* MR-1 may indicate that these genes are involved in the respiratory pathway towards acrylate reduction catalysed by the target flavocytochrome.

Two-dimensional polyacrylamide gel electrophoresis (2-D-PAGE) could also be used to analyse and compare the protein expression profiles of the null mutant and wild-type strains under acrylate reducing conditions to complement the findings of the microarray analyses.

The growth conditions of *S. oneidensis* MR-1 that induce expression of the novel flavocytochromes could be determined by using Northern blotting. It would be necessary to isolate total RNA from wild-type *S. oneidensis* MR-1 grown anaerobically with various acrylates as terminal electron acceptor and use RNA isolated from aerobically grown cells as a control. Following electrophoresis of the isolated RNA, hybridisation of a labelled DNA probe specific for each novel flavocytochrome would signify the presence of the protein under the conditions tested.

The *S. oneidensis* MB5415 null mutant constructed in this work has further potential to be used as a host organism for future expression of site-directed mutant forms of the novel flavocytochrome not expressed in this deletion strain.

8.3 Protein overexpression and purification

The genes encoding two of the novel flavocytochromes (FccA54; FccB54 and FccA342; FccB342) have been PCR amplified from the *S. oneidensis* MR-1 genome. A variety of PCR products have been amplified to allow periplasmic or cytoplasmic expression of the flavin subunits (FccA) and optional co-expression with the partner cytochrome subunits (FccB). The gene encoding a putative iron-induced flavocytochrome has also been PCR amplified from the *S. oneidensis* MR-1 genome. An expression plasmid has been constructed for maximising overexpression of the novel flavin subunits in *E. coli*. A novel flavoprotein subunit (FccA54) has been overexpressed in *E. coli* TG1 and the holoenzyme has been purified to high purity.

Purification of the FccA54 flavin-containing subunit followed by gradual conversion to the apoform has shown that the flavoprotein is unstable in the absence of the partner cytochrome subunit. Therefore, it has been postulated that the cytochrome subunit associates with the flavin subunit to cap the FAD binding site. It was anticipated that the novel flavoprotein would be able to turnover fumarate (Atanasiu, 2001), however, the inability of the purified holoenzyme to catalyse fumarate reduction has led to the suggestion that haem groups of the cytochrome subunit are essential for electron transfer from reduced methyl viologen to flavin. The results presented here have provided supporting evidence that the separately encoded flavin and cytochrome subunits do indeed associate to form a flavocytochrome, where the flavin subunit is dependent on association with the cytochrome subunit for catalysis.

To further test the requirement of the cytochrome subunit for electron transfer, it would be necessary to supplement the inactive apoenzyme with FAD and monitor reduction of acrylates, e.g. methacrylate, that may serve as the native substrate.

To overexpress and purify a novel flavocytochrome, a recombinant expression plasmid has been constructed for co-expression of the flavin and cytochrome subunits in the periplasm of *S. frigidimarina* EG301. High periplasmic expression levels of the FccB54 cytochrome subunit have been attained, however, the putatively associated FccA54 flavin subunit was not detected. Detection of the co-expressed flavin and cytochrome subunits could be improved by using native polyacrylamide gel electrophoresis to avoid dissociation into the respective protein subunits. Suitable conditions have been tested for purification of the overexpressed FccB54 cytochrome subunit and a protein at the expected size has been detected at each stage. It will be necessary to confirm by N-terminal sequencing that the cytochrome protein detected is indeed FccB54. Further purification trials are required to attain optimal purification conditions for the cytochrome subunit. It would be most convenient to purify the FccB54 cytochrome subunit and combine this with the previously purified FccA54 flavin subunit to produce the functional flavocytochrome for further analysis.

This work aimed to overexpress and purify one of the novel flavocytochromes to ultimately determine the enzyme structure and function by means of X-ray crystallography and kinetic analysis. In this work, purification of the FccA54 flavoprotein has been achieved and molecular models of the flavoprotein subunit have provided a three-dimensional insight into possible enzyme substrates. Overexpression and purification conditions have been established for purification of the partner FccB54 cytochrome subunit. It is anticipated that the separately purified flavin and cytochrome subunits can be successfully combined to produce the desired flavocytochrome. Therefore, this work has overcome the challenges involved in overexpressing and purifying a novel dimeric flavocytochrome and has provided the working foundations for producing a novel *S. oneidensis* MR-1 flavocytochrome for future analyses. Furthermore, a null mutant of a novel flavocytochrome (FccA54; FccB54) has been constructed which is fundamentally important for further genetic analysis linked to identifying the protein function.

Bibliography

- Arikawa, Y., Enomoto, K., Muratsubaki, H., Okazaki, M (1998) Soluble fumarate reductase isoenzymes from *Saccharomyces cerevisiae* are required for anaerobic growth. *FEMS Microbiol. Lett.* **165**: 111-116.
- Atanasiu, D (2001) Respiratory enzymes from *Shewanella* MR-1. PhD thesis. *The University of Edinburgh*.
- Bamford, V., Dobbin, P.S., Richardson, D.J., Hemmings, A.M (1999) Open conformation of a flavocytochrome c_3 fumarate reductase. *Nat. Struct. Biol.* **6**(12): 1104-1107.
- Barberio, C., Pagliai, L., Cavalieri, D., Fani, R (2001) Biodiversity and horizontal gene transfer in culturable bacteria isolated from activated sludge enriched in nonylphenol ethoxylates. *Res. Microbiol.* **152**: 105-112.
- Bates, D.M., Popescu, C.V., Khoroshilova, N., Vogt, K., Beinert, H., Münck, E., Kiley, P.J (2000) Substitution of leucine 28 with histidine in the *Escherichia coli* transcription factor FNR results in increased stability of the $[4\text{Fe-4S}]^{2+}$ cluster to oxygen. *J. Biochem.* **275**(9): 6234-6240.
- Beliaev, A.S., Saffarini, D.A (1998) *Shewanella putrefaciens mtrB* encodes an outer membrane protein required for Fe(III) and Mn(IV) reduction. *J. Bacteriol.* **180**(23): 6292-6297.
- Beliaev, A.S., Saffarini, D.A., McLaughlin, J.L., Hunnicutt, D (2001) MtrC, an outer membrane decahaem c cytochrome required for metal reduction in *Shewanella putrefaciens* MR-1. *Mol. Microbiol.* **39**: 722-730.
- Beliaev, A.S., Thompson, D.K., Fields, M.W., Wu, L., Lies, D.P., Nealson, K.H., Zhou, J (2002a) Microarray transcription profiling of a *Shewanella oneidensis etrA* mutant. *J. Bacteriol.* **184**(16): 4612-4616.
- Beliaev, A.S., Thompson, D.K., Khare, T., Lim, H., Brandt, C.C., Li, G., Murray, A.E., Heidelberg, J.F., Giometti, C.S., Yates III, J., Nealson, K.H., Tiedje, J.M., Zhou, J (2002b) Gene and protein expression profiles of *Shewanella oneidensis* during anaerobic growth with different electron acceptors. *J. Int. Biol.* **6**(1): 39-60.
- Berks, B.C (1996) A common export pathway for proteins binding complex redox cofactors? *Mol. Microbiol.* **22**(3): 393-404.
- Berks, B.C., Richardson, D.J., Reilly, A., Willis, A.C., Ferguson, S.J (1995) The *napEDABC* gene cluster encoding the periplasmic nitrate reductase system of *Thiosphaera pantotropha*. *Biochem. J.* **309**: 983-992.

Blundell T., Carney D., Gardner S., Hayes F., Howlin B., Hubbard T., Overington J., Singh A.D., Sibanda L.B., Sutcliffe M (1988) Knowledge-based protein modelling and design. *Eur. J. Biochem.* **172**: 513-520.

Bowman, J.P., McCammon, S.A., Nichols, D.S., Skerratt, J.H., Rea, S.M., Nichols, P.D., McMeekin, T.A (1997) *Shewanella gelidimarina* sp. nov. and *Shewanella frigidimarina* sp. nov., novel Antarctic species with the ability to produce eicosapentaenoic acid (20:5 ω 3) and grow anaerobically by dissimilatory Fe(III) reduction. *Int. J. Syst. Bacteriol.* **47**(4): 1040-1047.

Burnes, B.S., Mulberry, M.J., Dichristina, T.J (1998) Design and application of two rapid screening techniques for isolation of Mn(IV) reduction-deficient mutants of *Shewanella putrefaciens*. *Appl. Environ. Microbiol.* **64**(7): 2716-2720.

Cecchini, G., Ackrell, B.A.C., Deshler, J.O., Gunsalus, R.P (1986) Reconstitution of quinone reduction and characterization of *Escherichia coli* fumarate reductase activity. *J. Biol. Chem.* **261**: 1808-1814.

Chen, Z., Koh, M., Van Driessche, G., Van Beeumen, J.J., Bartsch, R.G., Meyer, T.E., Cusanovich, M.A., Mathews, F.S (1994) The structure of flavocytochrome *c* sulfide dehydrogenase from a purple phototrophic bacterium. *Science* **266**: 430-432.

Clark, J.M (1988) Novel non-templated nucleotide addition reactions catalysed by procaryotic and eucaryotic DNA polymerases. *Nucl. Acids. Res.* **16**: 9677-9686.

Cole, S.T (1982) Nucleotide sequence coding for the flavoprotein subunit of the fumarate reductase of *Escherichia coli*. *Eur. J. Biochem.* **122**: 479-484.

Cole, S.T (1987) Nucleotide sequence and comparative analysis of the *frd* operon encoding the fumarate reductase of *Proteus vulgaris*. *Eur. J. Biochem.* **167**: 481-488.

Cole, S.T., Grundström, T., Jaurin, B., Robinson, J.J., Weiner, J.H (1982) Location and nucleotide sequence of *frdB*, the gene coding for the iron-sulphur protein subunit of the fumarate reductase of *Escherichia coli*. *Eur. J. Biochem.* **126**: 211-216.

Darlison, M.G., Guest, J.R (1984) Nucleotide sequence encoding the iron-sulphur protein subunit of the succinate dehydrogenase of *Escherichia coli*. *Biochem J.* **223**:507-517.

Derby, H.A., Hammer, B.W (1931) Bacteriology of butter. IV. Bacteriological studies on surface taint butter. *Iowa. Agric. Exp. Stn. Res. Bull.* **145**: 389-416.

Dichristina, T.J., Delong, E. F (1994) Isolation of anaerobic respiratory mutants of *Shewanella putrefaciens* and genetic analysis of mutants deficient in anaerobic growth on Fe³⁺. *J. Bacteriol.* **176**(5): 1468-1474.

- Dobbin, P.S., Butt, J.N., Powell, A.K., Reid, G.A., Richardson, D.J (1999) Characterization of a flavocytochrome that is induced during the anaerobic respiration of Fe^{3+} by *Shewanella frigidimarina* NCIMB 400. *Biochem. J.* **342**: 439-448.
- Doherty, M.K., Pealing, S.L., Miles, C.S., Moysey, R., Taylor, P., Walkinshaw, M.D., Reid, G.A., Chapman, S.K (2000) Identification of the active site acid/base catalyst in a bacterial fumarate reductase: A kinetic and crystallographic study. *Biochemistry* **39**: 10695-10701.
- Eiglmeier, K., Honoré, N., Luchi, S., Lin, E.C.C., Cole, S.T (1989) Molecular genetic analysis of FNR-dependent promoters. *Mol. Microbiol.* **3**(7): 869-878.
- Eschbach, M., Möbitz, H., Rompf, A., Jahn, D (2003) Members of the genus *Arthrobacter* grow anaerobically using nitrate ammonification and fermentative processes: anaerobic adaptation of aerobic bacteria abundant in soil. *FEMS Microbiol. Letts.* **223**: 227-230.
- Field, S.J., Dobbin, P.S., Cheesman, M.R., Watmough, N.J., Thomson, A.J., Richardson, D.J (2000) Purification and magneto-optical spectroscopic characterization of cytoplasmic membrane and outer membrane multiheme *c*-type cytochromes from *Shewanella frigidimarina* NCIMB400. *J. Biol. Chem.* **275** (12): 8515-8522.
- Fürste, J.P., Pansegrau, W., Frank, R., Blöcker, H., Scholz, P., Bagdasarian, M., Lanka, E (1986) Molecular cloning of the plasmid RP4 primase region in a multi-host-range *tacP* expression vector. *Gene* **48**: 119-131.
- Gordon, E.H.J (1996) The physiological role of a novel flavocytochrome *c* from *Shewanella putrefaciens*. PhD thesis. *The University of Edinburgh*.
- Gordon, E.H.J., Pealing, S.L., Chapman, S.K., Ward, F.B., Reid, G.A (1998) Physiological function and regulation of flavocytochrome *c*₃, the soluble fumarate reductase from *Shewanella putrefaciens* NCIMB 400. *Microbiology* **144**: 937-945.
- Gordon, E.H.J., Pike, A.D., Hill, A.E., Cuthbertson, P.M., Chapman, S.K., Reid, G.A (2000) Identification and characterization of a novel cytochrome *c*₃ from *Shewanella frigidimarina* that is involved in Fe(III) respiration. *Biochem. J.* **349**:153-158.
- Gross, R., Simon, J., Kröger, A (2001) Periplasmic methacrylate reductase activity in *Wolinella succinogenes*. *Arch. Microbiol.* **176**: 310-313.
- Grundström, T., Jaurin, B (1982) Overlap between *ampC* and *frd* operons on the *Escherichia coli* chromosome. *Proc. Natl. Acad. Sci. USA* **79**:1111-1115.
- Hamilton, W.A (1988) Energy transduction in anaerobic bacteria. In *Bacterial energy transduction* (ed. Anthony, C), pp. 83-149. Academic Press. London.

Heidelberg, J.F., Paulsen, I.T., Nelson, K.E., Gaidos, E.J., Nelson, W.C., Read, T.D., Eisen, J.A., Seshadri, R., Ward, N., Methe, B., Clayton, R.A., Meyer, T., Tsapin, A., Scott, J., Beanan, M., Brinkac, L., Daugherty, S., DeBoy, R.T., Dodson, R.J., Durkin, A.S., Haft, D.H., Kolonay, J.F., Madupu, R., Peterson, J.D., Umayam, L.A., White, O., Wolf, A.M., Vamathevan, J., Weidman, J., Impraim, M., Lee, K., Berry, K., Lee, C., Mueller, J., Khouri, H., Gill, J., Utterback, T.R., McDonald, L.A., Feldblyum, T.V., Smith, H.O., Venter, J.C., Neilson, K.H., Fraser, C.M (2002) Genome sequence of the dissimilatory metal ion-reducing bacterium *Shewanella oneidensis*. *Nat. Biotechnol.* **20**: 1118-1123.

von Heijne, G., Abrahmsén, L (1989) Species-specific variation in signal peptide design: implications for protein secretion in foreign hosts. *FEBS letts.* **244**(2): 439-446.

Iverson, T.M., Luna-Chavez, C., Cecchini, G., Rees, D.C (1999) Structure of the *Escherichia coli* fumarate reductase respiratory complex. *Science* **284**: 1961-1966.

Jones, C.W (1988) Membrane-associated energy conservation in bacteria: a general introduction. In *Bacterial energy transduction* (ed. Anthony, C), pp. 1-82. Academic Press. London.

Jones, H.M., Gunsalus, R.P (1985) Transcription of the *Escherichia coli* fumarate reductase genes (*frdABCD*) and their coordinate regulation by oxygen, nitrate and fumarate. *J. Bacteriol.* **164**(3): 1100-1109.

Jones, H.M., Gunsalus, R.P (1987) Regulation of *Escherichia coli* fumarate reductase (*frdABCD*) operon expression by respiratory electron acceptors and the *fnr* gene product. *J. Bacteriol.* **169**(7): 3340-3349.

Jørgensen, B.R., Huss, H.H (1989) Growth and activity of *Shewanella putrefaciens* isolated from spoiling fish. *Int. J. Food. Microbiol.* **9**: 51-62.

Jormakka, M., Törnroth, S., Byrne, B., Iwata, S (2002) Molecular basis of proton motive force generation: Structure of formate dehydrogenase-N. *Science* **295**:1863-1868.

Jüngst, A., Wakabayashi, S., Matsubara, H., Zumft, W.G (1991) The *nirSTBM* region coding for cytochrome *cd₁*-dependent nitrite respiration of *Pseudomonas stutzeri* consists of a cluster of mono-, di- and tetraheme proteins. *FEBS letters.* **279**(2): 205-209.

Kenney, W.C., Kröger, A (1977) The covalently bound flavin of *Vibrio succinogenes* succinate dehydrogenase. *FEBS lett.* **73**(2): 239-243.

Khashe, S., Janda, J.M (1998) Biochemical and pathogenic properties of *Shewanella alga* and *Shewanella putrefaciens*. *J. Clin. Microbiol.* **36**(3): 783-787.

- Körtner, C., Lauterbach, F., Tripier, D., Unden, G., Kröger, A (1990) *Wolinella succinogenes* fumarate reductase contains a dihaem cytochrome *b*. *Mol. Microbiol.* **4**(5): 855-860.
- Lancaster, C. R. D., Gross, R., Haas, A., Ritter, M., Mäntele, W., Simon, J., Kröger, A (2000) Essential role of Glu-C66 for menaquinol oxidation indicates transmembrane electrochemical potential generation by *Wolinella succinogenes* fumarate reductase. *Proc. Natl. Acad. Sci. USA* **97**: 13051-13056.
- Lancaster, C. R. D., Gross, R., Simon, J (2001) A third crystal form of *Wolinella succinogenes* quinol:fumarate reductase reveals domain closure at the site of fumarate reduction. *Eur. J. Biochem.* **268**: 1820-1827.
- Lancaster, C.R.D., Kröger, A., Auer, M., Michel, H (1999) Structure of fumarate reductase from *Wolinella succinogenes* at 2.2 Å resolution. *Nature* **402**: 377-385.
- Lancaster, C. R. D., Simon, J (2002) Succinate:quinone oxidoreductases from ϵ -proteobacteria. *Biochim. Biophys. Acta* **1553**: 84-101.
- Lee, J.V., Gibson, D.M., Shewan, J.M (1977) A numerical taxonomic study of some *Pseudomonas*-like marine bacteria. *J. Gen. Microbiol.* **98**: 439-451.
- Leys, D., Meyer, T.E., Tsapin, A.S., Nealson, K.H., Cusanovich, M.A., Van Beeumen, J.J (2002) Crystal structures at atomic resolution reveal the novel concept of "electron-harvesting" as a role for the small tetrahaem cytochrome *c*. *J. Biol. Chem.* **277**(38): 35703-35711.
- Leys, D., Tsapin, A.S., Nealson, K.H., Meyer, T.E., Cusanovich, M.A., Van Beeumen, J.J (1999) Structure and mechanism of the flavocytochrome *c* fumarate reductase of *Shewanella putrefaciens* MR-1. *Nat. Struct. Biol.* **6**(12): 1113-1117.
- Lloyd, J.R., Leang, C., Hodges-Myerson, A.L., Coppi, M.V., Cuifo, S., Methe, B., Sandler, S.J., Lovley, D.R (2003) Biochemical and genetic characterisation of PpcA, a periplasmic *c*-type cytochrome in *Geobacter sulfurreducens*. *Biochem. J.* **369**: 153-161.
- Lower, S.K., Hochella Jr., M.F., Beveridge, T.J (2001) Bacterial recognition of mineral surfaces: nanoscale interactions between *Shewanella* and α -FeOOH. *Science* **292**: 1360-1363.
- Magnuson, T.S., Isoyama, N., Hodges-Myerson, A.L., Davidson, G., Maroney, M.J., Geesey, G.G., Lovley, D.R (2001) Isolation, characterization and gene sequence analysis of a membrane-associated 89 kDa Fe(III) reducing cytochrome *c* from *Geobacter sulfurreducens*. *Biochem. J.* **359**: 147-152.
- Maier, T.M., Myers, C.R (2001) Isolation and characterization of a *Shewanella putrefaciens* MR-1 electron transport regulator *etrA* mutant: Reassessment of the role of EtrA. *J. Bacteriol.* **183**(16): 4918-4926.

- Makemson, J.C., Fulayfil, N.R., Landry, W., Van Ert, L.M., Wimpee, C.F., Widder, E.A., Case, J.F (1997) *Shewanella woodyi* sp. nov., an exclusively respiratory luminous bacterium isolated from the Alboran Sea. *Int. J. Syst. Bacteriol.* **47**: 1034-1039.
- Maklashina, E., Berthold, D.A., Cecchini, G (1998) Anaerobic expression of *Escherichia coli* succinate dehydrogenase: functional replacement of fumarate reductase in the respiratory chain during anaerobic growth. *J. Bacteriol.* **180**(22): 5989-5996.
- Manodori, A., Cecchini, G., Schröder, I., Gunsalus, R.P., Werth, M.T., Johnson, M.K (1992) [3Fe-4S] to [4Fe-4S] cluster conversion in *Escherichia coli* fumarate reductase by site directed mutagenesis. *Biochemistry* **31**: 2703-2712.
- Mattevi, A., Obmolova, G., Kalk, K.H., Van Berkel, W.J.H., Hol, W.G.J (1993) Three-dimensional structure of lipoamide dehydrogenase from *Pseudomonas fluorescens* at 2.8 Å resolution. *J. Mol. Biol.* **230**:1200-1215.
- Mattevi, A., Tedeschi, G., Bacchella, L., Coda, A., Negri, A., Ronchi, S (1999) Structure of L-aspartate oxidase: implications for the succinate dehydrogenase/fumarate reductase oxidoreductase family. *Structure* **7**: 745-756.
- Mazodier, P., Cossart, P., Giraud, E., Gasser, F (1985) Completion of the nucleotide sequence of the central region of Tn5 confirms the presence of three resistance genes. *Nucleic Acids Res.* **13**(1): 195-205.
- Méjean, V., Iobbi-Nivol, C., Lepelletier, M., Giordano, G., Chippaux, M., Pascal, M.C (1994) TMAO anaerobic respiration in *Escherichia coli*: involvement of the *tor* operon. *Mol. Microbiol.* **11**: 1169-1179.
- Mikoulinskaia, O., Akimenko, V., Galouchko, A., Thauer, R.K., Hedderich, R (1999) Cytochrome *c*-dependent methacrylate reductase from *Geobacter sulfurreducens* AM-1, *Eur. J. Biochem.* **263**: 346-352.
- Misoph, M., Daniel, S.L., Drake, H.L (1996) Bidirectional usage of ferulate by the acetogen *Peptostreptococcus productus* U-1: CO₂ and aromatic acrylate groups as competing electron acceptors. *Microbiology* **142**: 1983-1988.
- Mitchell, P (1961) Coupling of phosphorylation to electron and hydrogen transfer by a chemi-osmotic type of mechanism. *Nature* **191**: 144-148.
- Mittl, P.R.E., Schulz, G.E (1994) Structure of glutathione-reductase from *Escherichia coli* at 1.86 angstrom resolution– comparison with the enzyme from human erythrocytes. *Protein Sci.* **3**(5): 799-809.
- Mori, H., Summer, E.J., Ma, X., Cline, K (1999) Component specificity for the thylakoidal Sec and Delta pH-dependent protein transport pathways. *J. Cell Biol.* **146**(1): 45-55.

- Morris, C.J (1987) The *c*-type cytochromes of *Shewanella putrefaciens*. PhD thesis. The University of Edinburgh.
- Morris, C.J., Black, A.C., Pealing, S.L., Manson, F.D.C., Chapman, S.K., Reid, G.A., Gibson, D.M., Ward, F.B (1994) Purification and properties of a novel cytochrome: flavocytochrome *c* from *Shewanella putrefaciens*. *Biochem. J.* **302**: 587-593.
- Moser, D. P., Nealson, K.H (1996) Growth of the facultative anaerobe *Shewanella putrefaciens* by elemental sulfur reduction. *Appl. Environ. Microbiol.* **62**(6): 2100-2105.
- Mowat, C.G., Moysey, R., Miles, C.S., Leys, D., Doherty, M.K., Taylor, P., Walkinshaw, M.D., Reid, G.A., Chapman, S.K (2001) Kinetic and crystallographic analysis of the key active site acid/base arginine in a soluble fumarate reductase. *Biochemistry* **40**: 12292-12298.
- Mracek, J., Snyder, S.J., Chavez, U.B., Turrens, J.F (1991) A soluble fumarate reductase in *Trypanosoma brucei* procyclic trypomastigotes. *J. Protozool.* **38**(6): 554-558.
- Munro, A.W., Noble, M.A (1999) Fluorescence analysis of flavoproteins. In *Methods in Molecular Biology, Flavoprotein protocols* vol. 131 (eds. Chapman, S.K and Reid, G.A) pp. 25-48. Humana Press, Totowa, NJ.
- Murakamia, H., Kitab, K., Oyab, H., Anrakua, Y (1985) The *Escherichia coli* cytochrome b556 gene, *cybA*, is assignable as *sdhC* in the succinate dehydrogenase gene cluster. *FEMS Microbiol. Lett.* **30**: 307-311.
- Murray, A.E., Lies, D., Li, G., Nealson, K., Zhou, J., Tiedje, J.M (2001) DNA/DNA hybridisation to microarrays reveals gene-specific differences between closely related microbial genomes. *Proc. Natl. Acad. Sci. USA* **98**(17): 9853-9858.
- Myers, C.R., Carstens, B.P., Antholine, W.E., Myers, J.M (2000) Chromium(VI) reductase activity is associated with the cytoplasmic membrane of anaerobically grown *Shewanella putrefaciens* MR-1. *J. Appl. Microbiol.* **88**: 98-106.
- Myers, C.R., Myers, J.M (1992) Localisation of cytochromes to the outer membrane of anaerobically grown *Shewanella putrefaciens* MR-1. *J. Bacteriol.* **174**(11): 3429-3438.
- Myers, C.R., Myers, J.M (1993) Role of menaquinone in the reduction of fumarate, nitrate, iron(III) and manganese(IV) by *Shewanella putrefaciens* MR-1. *FEMS Microbiol. Lett.* **114**: 215-222.
- Myers, C.R., Myers, J.M (1997a) Outer membrane cytochromes of *Shewanella putrefaciens* MR-1: spectral analysis and purification of the 83-kDa *c*-type cytochrome. *Biochim. Biophys. Acta* **1326**: 307-318.

- Myers, C.R., Myers, J.M (1997b) Cloning and sequence of *cymA*, a gene encoding a tetraheme cytochrome *c* required for reduction of iron(III), fumarate and nitrate by *Shewanella putrefaciens* MR-1. *J. Bacteriol.* **179**(4): 1143-1152.
- Myers, C.R., Myers, J.M (1997c) Isolation and characterization of a transposon mutant of *Shewanella putrefaciens* MR-1 deficient in fumarate reductase. *Lett. Appl. Microbiol.* **25**: 162-168.
- Myers, C.R., Myers, J.M (2002) MtrB is required for proper incorporation of the cytochromes OmcA and OmcB into the outer membrane of *Shewanella putrefaciens* MR-1. *Appl. Environ. Microbiol.* **68**(11): 5585-5594.
- Myers, C.R., Nealson, K. H (1988) Bacterial manganese reduction and growth with manganese oxide as the sole electron acceptor. *Science* **240**: 1319-1321.
- Myers, C.R., Nealson, K.H (1990) Respiration-linked proton translocation coupled to anaerobic reduction of manganese(IV) and iron(III) in *Shewanella putrefaciens* MR-1. *J. Bacteriol.* **172**(11): 6232-6238.
- Myers, J.M., Myers, C.R (1998) Isolation and sequence of *omcA*, a gene encoding a decaheme outer membrane cytochrome *c* of *Shewanella putrefaciens* MR-1 and detection of *omcA* homologs in other strains of *S. putrefaciens*. *Biochim. Biophys. Acta* **1373**:237-251.
- Myers, J.M., Myers, C.R (2000) Role of the tetraheme cytochrome CymA in anaerobic electron transport in cells of *Shewanella putrefaciens* MR-1 with normal levels of menaquinone. *J. Bacteriol.* **182**(1): 67-75.
- Myers, J.M., Myers, C.R (2001) Role for outer membrane cytochromes omcA and omcB of *Shewanella putrefaciens* MR-1 in reduction of manganese dioxide. *Appl. Environ. Microbiol.* **67**(1): 260-269.
- Nealson, K. H., Moser, D.P., Saffarini, D.A (1995) Anaerobic electron acceptor chemotaxis in *Shewanella putrefaciens*. *Appl. Environ. Microbiol.* **61**(4): 1551-1554.
- Newman, D.K., Kolter, R (2000) A role for excreted quinones in extracellular electron transfer. *Nature* **405**: 94-97.
- Nicholls, D.G., Ferguson, S.J (2002) *Bioenergetics 3*. Academic Press, London.
- Nielsen, H., Engelbrecht, J., Brunak, S., Von Heijne, G (1997) Identification of prokaryotic and eukaryotic signal peptides and prediction of their cleavage sites. *Protein Eng.* **10**(1): 1-6.
- Nogi, Y., Kato, C (1999) Taxonomic studies of extremely barophilic bacteria isolated from the Mariana Trench and description of *Moritella yayanosii* sp. nov., a new barophilic bacterial isolate. *Extremophiles* **3**: 71-77.

Ohnishi, T., King, T.E., Salerno, J.C., Blum, H., Bowyer, J.R and Maida, T (1981) Thermodynamic and electron paramagnetic resonance characterization of flavin in succinate dehydrogenase. *J. Biol. Chem.* **256**: 5577-5582.

Overbye Michel, L., Sandkvist, M., Bagdasarian, M (1995) Specificity of the protein secretory apparatus: secretion of the heat-labile enterotoxin B subunit pentamers by different species of Gram⁻ bacteria. *Gene* **152**: 41-45.

Oyedotun, K.S., Lemire, B.D (2001) The quinone-binding sites of the *Saccharomyces cerevisiae* succinate-ubiquinone oxidoreductase. *J. Biol. Chem.* **276**(20): 16936-16943.

Pealing, S.L., Black, A.C., Manson, F.D.C., Ward, F.B., Chapman, S.K., Reid, G.A (1992) Sequence of the gene encoding flavocytochrome *c* from *Shewanella putrefaciens* : A tetraheme flavoenzyme that is a soluble fumarate reductase related to the membrane-bound enzymes from other bacteria. *Biochemistry* **31**: 12132-12140.

Pealing, S.L., Cheesman, M.R., Reid, G.A., Thomson, A.J., Ward, F.B., Chapman, S.K (1995) Spectroscopic and kinetic studies of the tetraheme flavocytochrome *c* from *Shewanella putrefaciens* NCIMB 400. *Biochemistry* **34**: 6153-6158.

Pepe, J.C., Miller, V.L (1993) *Yersinia-enterocolitica* invasion- a primary role in the initiation of infection. *Proc. Natl. Acad. Sci. USA* **90**(14): 6473-6477.

Pessanha, M., Brennan, L., Xavier, A.V., Cuthbertson, P.M., Reid, G.A., Chapman, S.K., Turner, D.L., Salgueiro, C.A (2001) NMR structure of the haem core of a novel tetrahaem cytochrome isolated from *Shewanella frigidimarina*: identification of the haem-specific axial ligands and order of oxidation. *FEBS lett.* **489**: 8-13.

Pessanha, M., Louro, R.O., Correia, L.J., Rothery, E.L., Pankhurst, K.L., Reid, G.A., Chapman, S.K., Turner, D.L., Salgueiro, C.A (2003) Thermodynamic characterization of a tetrahaem cytochrome isolated from a facultative aerobic bacterium, *Shewanella frigidimarina*: a putative redox model for flavocytochrome *c*₃. *Biochem. J.* **370**: 489-495.

Philips, M.K., Hederstedt, L., Hasnain, S., Rutberg, L., Guest, J.R (1987) Nucleotide sequence encoding the flavoprotein and iron-sulfur protein subunits of the *Bacillus subtilis* PY79 succinate dehydrogenase complex. *J Bacteriol.* **169**(2): 864-873.

Reid, G.A., Gordon, E.H.J (1999) Phylogeny of marine and freshwater *Shewanella*: reclassification of *Shewanella putrefaciens* NCIMB400 as *Shewanella frigidimarina*. *Int. J. Syst. Bacteriol.* **49**: 189-191.

Saffarini, D.A., Blumberman, S.L., Mansoorabadi, K.J (2002) Role of menaquinones in Fe(III) reduction by membrane fractions of *Shewanella putrefaciens*. *J. Bacteriol.* **184**(3): 846-848.

- Saffarini, D.A., Nealson, K.H (1993) Sequence and genetic characterization of *etrA*, an *fnr* analog that regulates anaerobic respiration in *Shewanella putrefaciens* MR-1. *J. Bacteriol.* **175**(24): 7938-7944.
- Sargent, F., Boggsch, E.G, Stanley, N.R., Wexler, M., Robinson, C., Berks, B.C., Palmer, T (1998) Overlapping functions of components of a bacterial Sec-independent protein export pathway. *EMBO J.* **17**(13): 3640-3650.
- Schröder, I., Gunsalus, R.P., Ackrell, B.A.C., Cochran, B., Cecchini, G (1991) Identification of active site residues of *Escherichia coli* fumarate reductase by site-directed mutagenesis. *J. Biol. Chem.* **266**(21): 13572-13579.
- Schwalb, C., Chapman, S.K., Reid, G.A (2002) The membrane-bound tetrahaem *c*-type cytochrome CymA interacts directly with the soluble fumarate reductase in *Shewanella*. *Biochem. Soc. Trans.* **30**: 658-662.
- Schwede, T.F., Rétey, J., Schulz, G.E (1999) Crystal structure of histidine ammonia-lyase revealing a novel polypeptide modification as the catalytic electrophile. *Biochemistry* **38**: 5355-5361.
- Semple, K.M., Westlake, D.W.S (1987) Characterization of iron reducing *Alteromonas putrefaciens* strains from oil field fluids. *Can. J. Microbiol.* **33**: 366-371.
- Simon, J., Gross, R., Klimmek, O., Ringel, M., Kröger, A (1998) A periplasmic flavoprotein in *Wolinella succinogenes* resembling the fumarate reductase of *Shewanella putrefaciens*. *Arch. Microbiol.* **169**(5): 424-433.
- Stanley, N.R., Palmer, T., Berks, B.C (2000) The twin arginine consensus motif of Tat signal peptides is involved in Sec-independent protein targeting in *Escherichia coli*. *J. Biol. Chem.* **275**(16): 11591-11596.
- Sucheta, A., Cammack, R., Weiner, J., Armstrong, F.A (1993) Reversible electrochemistry of fumarate reductase immobilized on an electrode surface. Direct voltammetric observations of redox centers and their participation in rapid catalytic electron transport. *Biochemistry* **32**(20): 5455-5465.
- Taylor, P., Pealing, S.L., Reid, G.A., Chapman, S.K., Walkinshaw, M.D (1999) Structural and mechanistic mapping of a unique fumarate reductase. *Nat. Struct. Biol.* **6**(12): 1108-1112.
- Tedeschi, G., Negri, A., Mortarino, M., Cecilian, F., Simonic, T., Faotto, L., Ronchi, S (1996) L-Aspartate oxidase from *Escherichia coli*. II. Interaction with C4 dicarboxylic acids and identification of a novel L-aspartate: fumarate oxidoreductase activity. *Eur. J. Biochem.* **239**(2): 427-433.

- Tedeschi, G., Ronchi, S., Simonic, T., Treu, C., Mattevi, A., Negri, A (2001) Probing the active site of L-Aspartate oxidase by site-directed mutagenesis: Role of basic residues in fumarate reduction. *Biochemistry* **40**: 4738-4744.
- Tedeschi, G., Zetta, L., Negri, A., Mortarino, M., Ceciliani, F., Ronchi, S (1997) Redox potentials and quinone reductase activity of L-aspartate oxidase from *Escherichia coli*. *Biochemistry* **36**: 16221-16230.
- Thompson, D.K., Beliaev, A.S., Giometti, C.S., Tollaksen, S.L., Khare, T., Lies, D.P., Nealson, K.H., Lim, H., Yates III, J., Brandt, C.C., Tiedje, J.M., Zhou, J (2002) Transcriptional and proteomic analysis of a ferric uptake regulator (Fur) mutant of *Shewanella oneidensis*: Possible involvement of Fur in energy metabolism, transcriptional regulation and oxidative stress. *Appl. Environ. Microbiol.* **68**(2): 881-892.
- Thompson, J.D., Higgins, D.G., Gibson, T.J (1994) ClustalW: improving the sensitivity of progressive multiple sequence alignment through sequence weighting, position-specific gap penalties and weight matrix choice. *Nucleic Acids Res.* **22**(22): 4673-4680.
- Tsapin, A.I., Vandenberghe, I., Nealson, K.H., Scott, J.H., Meyer, T.E., Cusanovich, M.A., Harada, E., Kaizu, T., Akutsu, H., Leys, D., Van Beeumen, J.J (2001) Identification of a small tetraheme cytochrome *c* and a flavocytochrome *c* as two of the principle soluble cytochromes *c* in *Shewanella oneidensis* strain MR-1. *Appl. Environ. Microbiol.* **67**(7): 3236-3244.
- Tsukihara, T., Aoyama, H., Yamashita, E., Tomizaki, T., Yamaguchi, H., Shinzawa-Itoh, K., Nakashima, R., Yaono, R., Yoshikawa, S (1996) The whole structure of the 13-subunit oxidized cytochrome *c* oxidase at 2.8 Å. *Science* **272**:1136-1144.
- Turner, K.L., Doherty, M.K., Heering, H.A., Armstrong, F.A., Reid, G.A., Chapman, S.K (1999) Redox properties of flavocytochrome *c*₃ from *Shewanella frigidimarina* NCIMB 400. *Biochemistry* **38**: 3302-3309.
- Turner, K.L., Doherty, M.K., Heering, H.A., Armstrong, F.A., Reid, G.A., Chapman, S.K (1999) Redox properties of flavocytochrome *c*₃ from *Shewanella frigidimarina* NCIMB 400. *Biochemistry* **38**: 3302-3309.
- Venkateswaran, K., Dollhopf, M.E., Aller, R., Stackebrandt, E., Nealson, K.H (1998) *Shewanella amazonensis* sp. nov., a novel metal-reducing facultative anaerobe from Amazonian shelf muds. *Int. J. Syst. Bacteriol.* **48**: 965-972.
- Venkateswaran, K., Moser, D.P., Dollhopf, M.E., Lies, D.P., Saffarini, D.A., MacGregor, B.J., Ringelberg, D.B., White, D.C., Nishijima, M., Sano, H., Burghardt, J., Stackebrandt, E., Nealson, K.H (1999) Polyphasic taxonomy of the genus *Shewanella* and description of *Shewanella oneidensis* sp. nov. *Int. J. Syst. Bacteriol.* **49**: 705-724.

Wallace, G., Fry, S.C (1994) Phenolic components of the plant cell wall. *Int. Rev. Cytol.* **151**: 229-267.

Wang, H-L., Postier, B.L., Burnap, R.L (2002) Optimization of fusion PCR for *in vitro* construction of gene knockout fragments. *BioTechniques* **33**: 26-32.

Weiner, J.H., Dickie, P (1979) Fumarate reductase of *Escherichia coli*. *J. Biol. Chem.* **254**(17): 8590-8593.

Westenberg, D.J., Gunsalus, R.P., Ackrell, B.A.C., Cecchini, G (1990) Electron transfer from menaquinol to fumarate. *J. Biol. Chem.* **265**: 19560-19567.

Widmer, A (1999) WITNOTP (Novartis A.G., Basel, Switzerland).

Wood, C.R., Boss, M.A., Patel, T.P., Emtage, J.S (1984a) The influence of messenger RNA secondary structure on expression of an immunoglobulin heavy chain in *Escherichia coli*. *Nucl. Acids. Res.* **12**(9): 3937-3950.

Wood, D., Darlison, M.G., Wilde, R.J., Guest, J.R (1984b) Nucleotide sequence encoding the flavoprotein and hydrophobic subunits of the succinate dehydrogenase of *Escherichia coli*. *Biochem J.* **222**: 519-534.

Yanisch-Perron, C., Vieira, J., Messing, J (1985) Improved M13 phage cloning vectors and host strains: nucleotide sequences of the M13mp18 and pUC19 vectors. *Gene* **33**: 103-119.

Zhang, Z., Huang, L., Shulmeister, V.M., Chi, Y-I., Kim, K.K., Hung, L-W., Crofts, A.R., Berry, E.A., Kim, S-H (1998) Electron transfer by domain movement in cytochrome *bc₁*. *Nature* **392**: 677-684.

Website references:

<http://www.expasy.org/tools/protparam.html>

Protparam, a tool for estimating protein properties, including molecular weight and isoelectric point

http://www.icmb.ed.ac.uk/sss_align/sss_align.html

sss_align: Sequence and secondary structure alignment website

<http://www.tigr.org>

The Institute for Genomic Research website

<http://www.cbs.dtu.dk/services/SignalP/>

SignalP signal peptide prediction website

<http://www.ncbi.nlm.nih.gov/blast/bl2seq/bl2.html>

Blast 2 sequences, tool for alignment of two given sequences

Appendix 1

Presentations

This work was presented in the form of poster presentations at the following conferences and meetings:

1. **'14th International Symposium on Flavins and Flavoproteins'** (2002) *University of Cambridge.*
2. **'The Biochemical Society 676th Meeting'** (2002) *Heriot-Watt University, Edinburgh.*
3. **'The Physiology, Regulation and Biochemistry of Electron Transfer in Microbial Catabolism'** (2001) *Isle of Terschelling, The Netherlands.*
4. **'The Institute of Cell and Molecular Biology Second Year Poster Presentations'** (2001) *University of Edinburgh.*

Conference Publications

Bilsland, M., Walkinshaw, M.D., Reid, G.A (2002) Novel respiratory flavocytochromes of *Shewanella oneidensis* MR-1. In Flavins and Flavoproteins (eds. Chapman, S.K., Perham, R., Scrutton, N). pp. 767-772. Rudolf Weber, agency for scientific publications, Berlin.